REPORT NO. FAA-RD-78-47

AIRCRAFT WAKE VORTEX CHARACTERISTICS FROM DATA MEASURED AT JOHN F. KENNEDY INTERNATIONAL AIRPORT

W.R. Eberle
M.R. Brashears
A.D. Zalay
K.R. Shrider
D.A. Love

LOCKHEED MISSILES & SPACE COMPANY, INC.
HUNTSVILLE RESEARCH & ENGINEERING CENTER
4800 Bradford Drive
Huntsville AL 35807

MARCH 1978
FINAL REPORT

Prepared for

U.S. DEPARTMENT OF TRANSPORTATION
FEDERAL AVIATION ADMINISTRATION
Systems Research and Development Service
Washington DC 20591

NOTICE

This document is disseminated under the sponsorship of the Department of Transportation in the interest of information exchange. The United States Government assumes no liability for its contents or use thereof.

NOTICE

The United States Government does not endorse products or manufacturers. Trade or manufacturers' names appear herein solely because they are considered essential to the object of this report.

Technical Report Documentation Page

1. Report No.	2. Government Accession No.	3. Recipient's Catalog No
FAA-RD-78-47		

4. Title and Subtitle	5. Report Date
AIRCRAFT WAKE VORTEX CHARACTERISTICS FROM DATA MEASURED AT JOHN F. KENNEDY INTERNATIONAL AIRPORT	March 1978
	6. Performing Organization Code
7. Author(s): W.R. Eberle, M.R. Brashears, A.D. Zalay, K.R. Shrider, D.A. Love	8. Performing Organization Report No. DOT-TSC-FAA-78-5 LMSC-HREC-TR D568181
9. Performing Organization Name and Address Lockheed Missiles & Space Company, Inc.* Huntsville Research & Engineering Center 4800 Bradford Drive Huntsville AL 35807	10. Work Unit No. (TRAIS) FA805/R8106 11. Contract or Grant No. DOT-TSC-1023
12. Sponsoring Agency Name and Address U.S. Department of Transportation Federal Aviation Administration Systems Research and Development Service Washington DC 20591	13. Type of Report and Period Covered Final Report June 1975-June 1977 14. Sponsoring Agency Code

15. Supplementary Notes

*Under contract to: U.S. Department of Transportation
Transportation Systems Center
Kendall Square
Cambridge MA 02142

16. Abstract

Data from 1320 aircraft flybys at Kennedy International Airport, Jamaica, New York, in 1975 were processed and stored in a computerized vortex data management system. The data were selectively recalled to determine vortex characteristics pertinent to the design of an effective wake vortex avoidance system. Vortex and meteorological characteristics which are relevant to the design of an effective wake wortex avoidance system are discussed from an analytical viewpoint as well as from an analysis of the data. Several formulations for feedback of vortex sensor information to provide vortex prediction are presented. Several wake vortex avoidance system designs are shown.

17. Key Words	18. Distribution Statement
Vortices Wake Vortices Kalman Filtering Meteorological Effects	DOCUMENT IS AVAILABLE TO THE U.S. PUBLIC THROUGH THE NATIONAL TECHNICAL INFORMATION SERVICE, SPRINGFIELD, VIRGINIA 22161

19. Security Classif. (of this report)	20. Security Classif. (of this page)	21. No. of Pages	22. Price
Unclassified	Unclassified	264	

Form DOT F 1700.7 (8-72) Reproduction of completed page authorized

PREFACE

One of the primary causes of aircraft delay at major airports which are operating near their capacity is aircraft longitudinal separation constraints imposed by wake vortex considerations. The importance of the problem has increased in recent years because of the increased fraction of wide-body aircraft in the airline fleets. For this reason, the U.S. Department of Transportation initiated a wake vortex research program in the early 1970s. Initially, the research program was directed toward an understanding of vortex phenomena — vortex roll-up and formation, vortex structure, vortex transport, vortex demise, and vortex-aircraft interaction for a following aircraft. Experimental data from individual flybys were carefully examined to aid in the understanding of vortex phenomena.

The end objective of the vortex-related research and development is an effective wake vortex avoidance system which could be implemented at airports. It has long been known that a vortex hazard exists for a very small fraction of airport operating time. However, because absolute safety is a requirement, long aircraft separations are used under radar control even though such separations are not necessary most of the time. The purpose of the wake vortex avoidance system is the identification of the times for which long aircraft separation times are necessary and identification of the times for which short aircraft separation times may be used.

Research oriented toward the understanding of vortex phenomena is certainly necessary for the design of an effective wake vortex avoidance system. However, a study of vortex characteristics in an operational environment is also necessary for the design of an effective wake vortex avoidance system. Thus, the questions to be answered are: What are the vortex characteristics which are relevant to the design of an effective wake vortex

avoidance system? How is a wake vortex avoidance system likely to operate? What are the limitations which will be imposed upon an operational wake vortex avoidance system? From the study of vortex behavior in an operational environment, what should the design of an operational wake vortex avoidance system be?

From the beginning of the wake vortex program, it has been assumed that one of the elements of a wake vortex avoidance system would be vortex sensing. The sensing of vortex residence time would be used as feedback for the prediction of future vortex behavior. However, no definitive concept of how such feedback should be accomplished has been formulated.

The authors gratefully express their appreciation to James N. Hallock of the Transportation Systems Center for his help and advice during the study.

TABLE OF CONTENTS

TABLE OF CONTENTS (Continued)

LIST OF ILLUSTRATIONS

LIST OF ILLUSTRATIONS (Continued)

LIST OF ILLUSTRATIONS (Continued)

LIST OF ILLUSTRATIONS (Continued)

LIST OF ILLUSTRATIONS (Continued)

LIST OF TABLES

LIST OF TABLES (Concluded)

METRIC CONVERSION FACTORS

Approximate Conversions to Metric Measures

Symbol	When You Know	Multiply by	To Find	Symbol
	LENGTH			
in	inches	2.5	centimeters	cm
ft	feet	30	centimeters	cm
yd	yards	0.9	meters	m
mi	miles	1.6	kilometers	km
	AREA			
in^2	square inches	6.5	square centimeters	cm^2
ft^2	square feet	0.09	square meters	m^2
yd^2	square yards	0.8	square meters	m^2
mi^2	square miles	2.6	square kilometers	km^2
	acres	0.4	hectares	ha
	MASS (weight)			
oz	ounces	28	grams	g
lb	pounds	0.45	kilograms	kg
	short tons (2000 lb)	0.9	tonnes	t
	VOLUME			
tsp	teaspoons	5	milliliters	ml
Tbsp	tablespoons	15	milliliters	ml
fl oz	fluid ounces	30	milliliters	ml
c	cups	0.24	liters	l
pt	pints	0.47	liters	l
qt	quarts	0.95	liters	l
gal	gallons	3.8	liters	l
ft^3	cubic feet	0.03	cubic meters	m^3
yd^3	cubic yards	0.76	cubic meters	m^3
	TEMPERATURE (exact)			
°F	Fahrenheit temperature	5/9 (after subtracting 32)	Celsius temperature	°C

Approximate Conversions from Metric Measures

Symbol	When You Know	Multiply by	To Find	Symbol
	LENGTH			
mm	millimeters	0.04	inches	in
cm	centimeters	0.4	inches	in
m	meters	3.3	feet	ft
m	meters	1.1	yards	yd
km	kilometers	0.6	miles	mi
	AREA			
cm^2	square centimeters	0.16	square inches	in^2
m^2	square meters	1.2	square yards	yd^2
km^2	square kilometers	0.4	square miles	mi^2
ha	hectares (10,000 m^2)	2.5	acres	
	MASS (weight)			
g	grams	0.035	ounces	oz
kg	kilograms	2.2	pounds	lb
t	tonnes (1000 kg)	1.1	short tons	
	VOLUME			
ml	milliliters	0.03	fluid ounces	fl oz
l	liters	2.1	pints	pt
l	liters	1.06	quarts	qt
l	liters	0.26	gallons	gal
m^3	cubic meters	35	cubic feet	ft^3
m^3	cubic meters	1.3	cubic yards	yd^3
	TEMPERATURE (exact)			
°C	Celsius temperature	9/5 (then add 32)	Fahrenheit temperature	°F

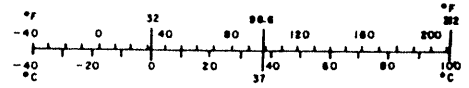

1. INTRODUCTION

One of the primary causes of aircraft delays at major airports which are operating near their capacity is aircraft longitudinal separation constraints imposed by wake vortex considerations. Based on projected increases in the number of aircraft operations (Ref. 1), increased traffic delay will occur unless the landing and takeoff capacity of major airports is increased. Delay is a nonlinear function of aircraft demand and increases very rapidly as demand approaches theoretical runway capability. Although the physical expansion of existing air terminals is limited by environmental constraints, economic constraints, and available land (with consideration given to 5000-ft separation between independent parallel ILS runways); increased numbers of aircraft operations can be achieved by decreasing the longitudinal aircraft spacing between successive operations. In order to maintain safe aircraft operations while achieving minimum delays, a Wake Vortex Avoidance System (WVAS) is under development by the U.S. Department of Transportation for minimizing the constraint on aircraft separation imposed by the presence of wake vortices near the runway threshold.

The purpose of the work described in this report was an analysis of wake vortex data collected at Kennedy International Airport (JFK) during 1975. The analysis was intended to evaluate the design options and to determine the operational characteristics of a WVAS in an operational environment. To provide a background for the results of the analysis to be presented in the later sections of this report, an overview of vortex behavior and wave vortex avoidance systems is presented in this section.

1.1 BACKGROUND OF THE UNITED STATES WAKE VORTEX PROGRAM

Although the phenomenon of aircraft wake vortices has been known since the beginnings of powered flight, it is only recently that operational problems associated with the phenomenon have been experienced. All aircraft generate trailing wake vortices as a result of generating lift; however, the potential danger of encountering these wake vortices has only recently become apparent. Aircraft wake vortices now constitute one of the major problems confronting the air traffic control system.

Before 1970, landing aircraft maintained 3-nautical-mile separations under Instrument Flight Rule (IFR) operations. The separation standard was based primarily on radar operating limits and to a lesser extent on runway occupancy limitations. There were no separation standards imposed because of vortex considerations.

With the introduction of the wide-body jets (B-747, DC-10, and L-1011) and the increasing number of aircraft operations at the major airports, the wake vortex problem has taken on increasing significance. The vortices from heavy aircraft can present a severe hazard to smaller aircraft which inadvertently encounter the vortices; the following aircraft can be subjected to rolling moments which exceed the aircraft roll control authority, to a dangerous loss of altitude, and to a possible structural failure. The probability of a vortex encounter is greatest in the terminal area where light and heavy aircraft operate on the same flight paths in close proximity and where recovery from an upset may not be possible because of the low aircraft altitude.

Accordingly, the solution implemented by the Federal Aviation Administration (FAA) in March 1970 was to increase the separation standards behind the heavy jets (a heavy jet has a maximum certificated takeoff weight of at least 300,000 lb) to 4 nautical miles for a following heavy aircraft and to 5 nautical miles for a following non-heavy aircraft. The United Kingdom took similar measures, and in April 1975 implemented a 6-nautical-mile spacing for non-heavy aircraft following a wide-body jet. The United States revised the separation standards in November 1975 by requiring the addition of an extra nautical-mile separation for following aircraft with a maximum certificated takeoff weight less than 12,500 lb. However, these increased separations led to additional delays and decreased the capacity and efficiency of the airport system through reduced runway utilization rates and increased fuel consumption.

The FAA has a broad objective to increase the airport and airway system capacity by 1980 and to increase current capacity five-fold by 1995. Potential

capacity relief through construction of more air carrier airports or additional runways at existing airports is not economically feasible. The need to increase the capacity of the nation's airports and to increase protection against accidents has led to a program by the FAA to develop an Upgraded Third Generation air traffic control system for the 1980s (Ref. 2).

The success of this system is dependent upon the development of techniques for reducing the longitudinal separations required to avoid the hazard from trailing wake vortices, particularly behind heavy aircraft during approach and landing. It appears that airports can achieve a two-fold capacity increase with the Upgraded Third Generation improvements, such as dual runways, improved landing aids and data acquisition systems, reduced separation to 2500 ft between parallel runways, and reduced longitudinal separations. Today, the technology exists to develop the necessary hardware/software which will substantially increase runway capacity; but the wake vortex problem must be solved before these advanced systems can be used to their full potential.

An excellent summary of the current state-of-the-art understanding of the aircraft wake vortex phenomenon and the results of the United States program to minimize the restrictions caused by aircraft wake vortices in the terminal environment is presented in Ref. 3. The reader is referred to that document for a background to the work presented in this report. Summaries of the important topics in Refs. 4 through 18 as cited in the remainder of this section are contained in Ref. 3.

In the early 1970s, vortex work centered on vortex formation and vortex structure. Particularly significant was the analytical model of the vortex roll-up process by Donaldson et al. (Ref. 4), which augmented the earlier work by Betz (Ref. 5). The Donaldson model clearly showed the effect of aircraft and flight parameters on vortex roll-up and vortex strength. Criteria for the generation of multiple vortices were derived. During the same time period (early 1970s), the National Aviation Facilities Experimental Center (NAFEC) conducted a series of measurements of vortex structure using tower-mounted

anemometers and colored smoke for photographic records (e.g., Refs. 6, 7, and 8). Vortex structure (i.e., vortex tangential velocity as a function of the radial coordinate) was measured for different configurations (i.e., flap and power settings) and different values of vortex age. Also in the early 1970s, Crow presented his model of mutual annihilation of the vortex pair due to an instability triggered and driven by atmospheric turbulence (Ref. 9).

In the mid 1970s, much attention was given to an understanding of vortex transport. Brashears and Hallock (Ref. 10) developed a model of vortex transport which included the effects of ambient wind, wind shear, and buoyancy on vortex transport. The influence of the various meteorological parameters upon vortex transport was derived (Ref. 11).

In addition to the activity related to the study of vortex phenomena described above, three other parallel efforts occurred in the early and mid 1970s. The first was the development of vortex sensors. Several candidate systems were evaluated and tested to determine their feasibility as vortex sensors. The most significant of the candidates (in terms of the ability to make meaningful vortex measurements and have some potential for operational implementation) were the Ground Wind Vortex Sensing System (GWVSS, Ref. 12), the Doppler Acoustic Vortex Sensing System (DAVSS, Ref. 13), the Monostatic Acoustic Vortex Sensing System (MAVSS, Ref. 14), and the Laser Doppler Velocimeter (LDV, Ref. 15). These systems were developed to the point at which their feasibility was determined and their salient operating characteristics were defined. The second effort was a hazard definition effort (Refs. 16 and 17) which attempted to define the minimum safe separation between an aircraft and a vortex. The third effort was aerodynamic minimization, which was an attempt to decrease the strength of vortices or induce early vortex break-up by aerodynamic modifications to the generating aircraft. Reference 18 contains a summary of aerodynamic minimization techniques which have been tested.

The elements of the wake vortex program described above have been conducted in a research environment. The conducting of these elements in a research environment has been based upon the axioms: (1) an increased understanding of vortex phenomena and vortex behavior will lead to better methods of avoiding the hazardous effects of wake vortices; (2) analytic models of vortex behavior and the calculated results of such analytic models developed in a research environment will be directly useful for the avoidance of wake vortices in an operational environment; and (3) some of the instruments developed for measuring vortex characteristics in a research environment can be developed into operational vortex detectors, and the research vortex measurements will provide an indication of the capabilities of various vortex measurement devices.

The purpose of the test series which is the subject of this report is effecting the transition between the research environment in which the previous elements of the wake vortex program have been conducted and the implementation of a preprototype Wake Vortex Avoidance System. The intent of the test series was to collect a large quantity of data which are similar to data which would be obtained in an operational environment. A study of the data would then indicate which parameters would be most useful in an operational environment, in what form the parameters should be presented in an operational environment, the degree of sophistication of analytic and predictive models which would be appropriate in an operational environment, and how the various vortex sensors could be expected to perform in an operational environment.

1.2 DEFINITIONS

The definition of several terms is deemed appropriate for the clear understanding of the principles discussed in this report.

1.2.1 Vortex-protected Corridor

If there is no vortex in a region near the ILS,* there is no vortex hazard to following aircraft. The vortex-protected corridor (or vortex corridor) is defined as the airspace for which the absence of vortices is a sufficient condition for safe passage by a following aircraft. For the purposes of this report, the vortex corridor is defined as a corridor which extends 150 ft laterally on each side of the localizer centerline from the middle marker to the runway touchdown zone. The altitude of the vortex corridor extends upward from the surface. The 150-ft criterion is based upon the standard deviation of lateral aircraft position about the localizer centerline (3σ = 50 ft, Ref. 19) at the middle marker and the lateral distance above which a vortex cannot significantly affect aircraft motion (100 ft, Ref. 20). Since the primary focus of this report is vortex behavior in ground effect, vortex behavior when the aircraft is inbound from the middle marker is of primary concern.

1.2.2 Significant Times Related to Vortex Behavior

There are three significant times related to vortex behavior. These are: (1) vortex transport time, which is the time (measured from the time of aircraft passage) required for both vortices to be transported out of the vortex corridor; (2) vortex life time, which is the time from aircraft passage until both vortices disintegrate or decay sufficiently to be innocuous to following aircraft, regardless of the position of the vortices relative to the vortex corridor; and (3) vortex residence time, which is the time (measured from aircraft passage) during which a vortex is active in the vortex corridor.

*In the context of this report, the Instrument Landing System (ILS) refers to the path defined by the intersection of the centerline of the localizer and the centerline of the glideslope from the outer marker to the runway touchdown zone.

For vortex transport, the downwind vortex almost always exits the vortex corridor before the upwind vortex. Therefore, the vortex transport time is almost always the time at which the upwind vortex exits from the vortex corridor. If the vortex disintegrates before it leaves the vortex corridor, the transport time is the time that the vortex would have left the vortex corridor if it had not disintegrated. Vortex life time is the time at which vortex demise occurs. There are three mechanisms by which vortex demise may occur. The first and second mechanisms are vortex bursting (Ref. 3) and mutual annihilation by Crow Instability (Ref. 9). "Vortex disintegration" is the term used for vortex demise by either of these two mechanisms. The third mechanism is viscous decay by which the strength of the vortex decreases sufficiently so that it will not be hazardous to following aircraft. "Vortex decay" is the term used for vortex demise by viscous decay. The term "vortex demise" is a general term which implies vortex disintegration or vortex decay.

Vortex residence time is the time at which vortex life in the vortex corridor ceases. It is the lesser of vortex transport time and vortex life time.

1.2.3 Vortex Models

This report refers to three types of models of vortex behavior. These are: (1) analytic models (deterministic and probabilistic), (2) empirical models, and (3) predictive models.

Analytic models of vortex behavior are based on the physics of fluid mechanics. Thus, analytical models may also be termed theoretical models. The degree of sophistication of various analytic models may vary. The models may be either deterministic or probabilistic. Deterministic analytic models are used primarily for research. They answer the question: "Given values for all independent parameters affecting vortex behavior, what is the behavior (i.e., values of dependent parameters) of the vortex pair?" The development and validation (by experimental means) of deterministic analytic

models is extremely important. Such a model may be used for identification of the important mechanisms and parameters of vortex behavior and determination of the limit to which calculated vortex parameters will agree with actual vortex parameters. In addition, a good deterministic analytical model is required for probabilistic models and predictive models. The role of such a deterministic model in probabilistic models and predictive models is discussed in the following paragraphs.

In an operational environment, values for all of the independent parameters necessary to calculate vortex behavior may not be available. Examples are exact aircraft weight, exact aircraft position relative to the ILS, spanwise loading distribution, etc. In general, these parameters may vary from flight to flight for the same aircraft type. Therefore, the dependent vortex parameters may be determined probabilistically, depending on the probability distribution functions of the various independent parameters. If the probability distribution functions of the independent parameters are known, the deterministic analytic model may be used to generate the probability distribution functions of the dependent vortex parameters.

For the analytical models of vortex behavior (both deterministic and probabilistic) the values of the dependent parameters are based upon concurrent values of the independent parameters.

In this report, the term "predictive model" refers to any model which forecasts vortex behavior. The model may calculate vortex behavior based on forecast meteorological parameters or may forecast vortex behavior based on previous history of vortex behavior. It is noted that previous literature on vortex behavior (e.g., Refs. 10 and 11) have used the term "predictive model" to describe vortex behavior based on concurrent values of independent parameters. However, in this report "predictive" is synonymous with forecasting.

Since predictive models always imply forecasting, predictive models are always probabilistic. Future events can never be forecast with absolute certainty.

1.3 ANALYTIC TRANSPORT MODEL

1.3.1 Evolution of the Analytic Transport Model

The development of an analytic vortex transport model has encompassed four stages: (1) the formulation of a model of vortex behavior using aerodynamic principles to calculate vortex strength and initial descent rate and using fluid mechanic principles to calculate vortex transport by mutual induction; (2) a comparison of vortex trajectories calculated from the analytic model with measured vortex trajectories from a series of controlled flight tests; (3) refinement of the model to account for deviations between the simple model and the flight test data; and (4) verification of the analytic transport model under operational conditions.

The early analytic transport model consisted of calculation of vortex transport by mutual induction. Image vortices below the ground level were used to account for ground effect. Vortex transport by mutual induction is discussed in Section 3.1 of this report. The model also included the effect of viscous vortex decay on vortex transport. The inclusion of vortex decay is based on classical hydrodynamics (Ref. 21). A laminar solution for an isolated vortex is obtained from the momentum equation written in terms of the vorticity. Replacing the kinematic viscosity ν with the sum of an eddy and kinematic viscosity, the circumferential velocity is

$$v = \frac{\Gamma}{2\pi r}\left[1 - e^{-r^2/4(\nu+\epsilon)t}\right] . \qquad (1)$$

This equation is used in the model to calculate decay using a value of the eddy viscosity obtained from Owen (Ref. 22).

A series of flight tests was conducted to verify the model using B-747, B-707, CV-880, and DC-6 aircraft (over 400 flybys). Both the motion of the vortices and the meteorological conditions were recorded. The tests were performed at the National Aviation Facilities Experimental Center (NAFEC) in 1972.

Vortex tracks were recorded photographically and by ground wind sensors. NAFEC has a 140-ft tower instrumented with hot-film anemometers, colored smoke dispensers at 20-ft intervals, and meteorological instrumentation at five levels. Smoke was used to visualize the vortices. A 35-mm camera was positioned 2000 ft from the tower on a line nearly normal to the prevailing wind direction. Photographs were taken every second, and the vortex tracks were obtained by examining each photo and locating the vortices by scaling photographic distances with known distances. Gill single-axis propeller anemometers were arrayed on a baseline near the 140-ft tower to measure the wind component perpendicular to the aircraft flight path. As a vortex moved through the anemometer system, it produced a distinctive signature superimposed upon the background wind.

Figure 1 shows a typical cross-sectional vortex track compared with a calculated track (Ref. 23). The wind was determined by a least-square polynomial fit to the mean wind averaged for 2 min before the aircraft passage. Figure 2 shows the ground wind track for three calculated vortex tracks: two linear interpolations of the five tower-measured average wind speeds ("before" denotes the mean for the two minutes prior to the aircraft flyby and "after" denotes the two minutes after the flyby), and a power law profile fit as used in Fig. 1. A power-law fit to the mean wind consistently produced the best agreement with the vortex tracks. After about 90 sec the upwind calculated track often lagged behind the data, and this is attributed to the rising of the upwind vortex or to a decrease in the circulation of the vortex. The differences between calculated and measured vortex tracks consistently fell within the computed uncertainty in the transport due to random fluctuations in the wind (Ref. 23).

When comparing the calculated time for a vortex to strike the tower with the actual time, the calculated time is often less than the observed time, especially for older vortices; calculated sink rates based upon elliptical loading assumptions are less than measured rates. At least two mechanisms have been suggested as the cause of the discrepancy: deviations from a clean wing configuration and buoyancy effects leading to decreases in the rolled-up initial vortex separations (Ref. 23).

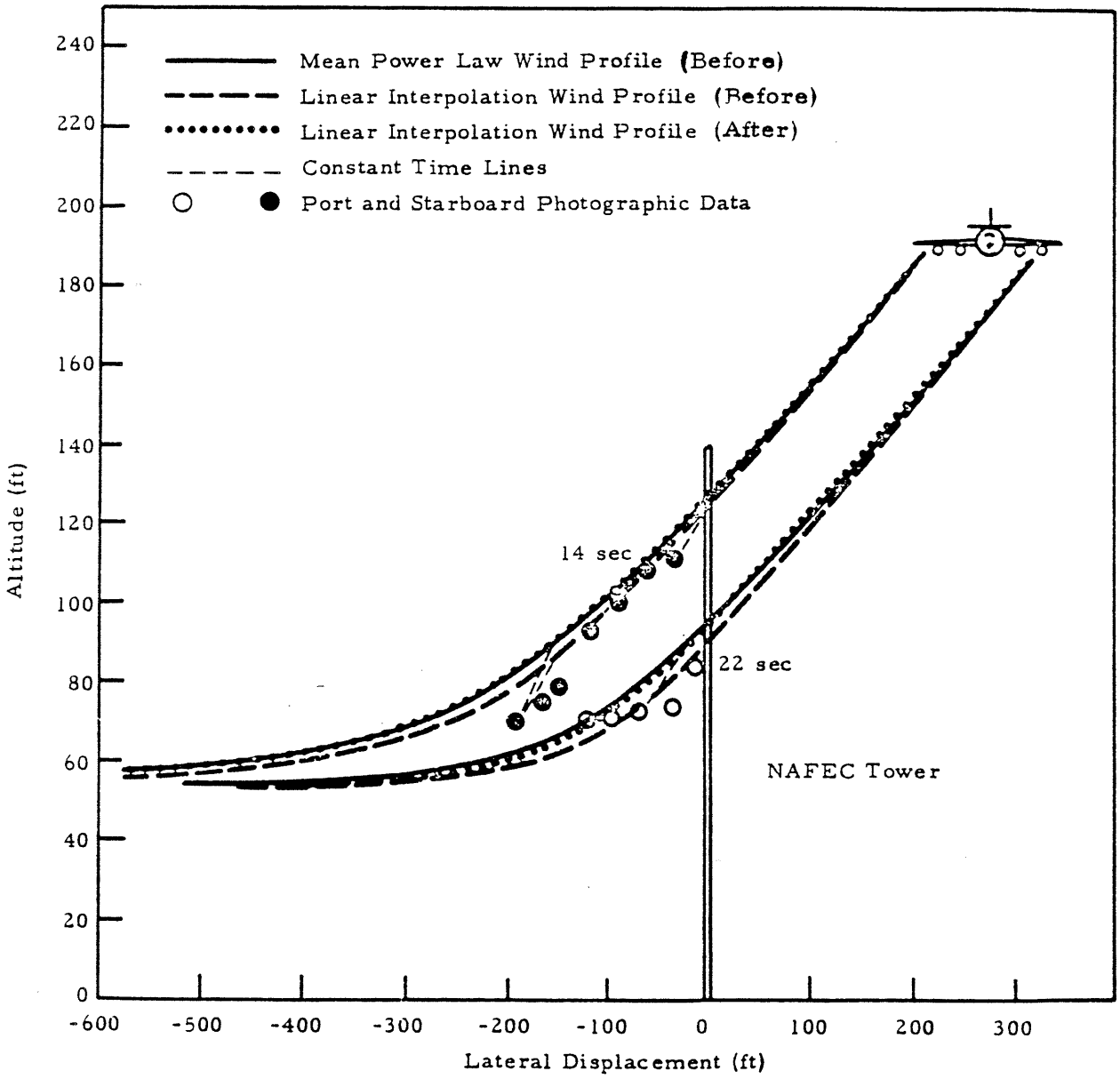

FIGURE 1. COMPARISON OF CALCULATED VORTEX TRAJECTORIES WITH PHOTOGRAPHIC DATA FOR A B-707

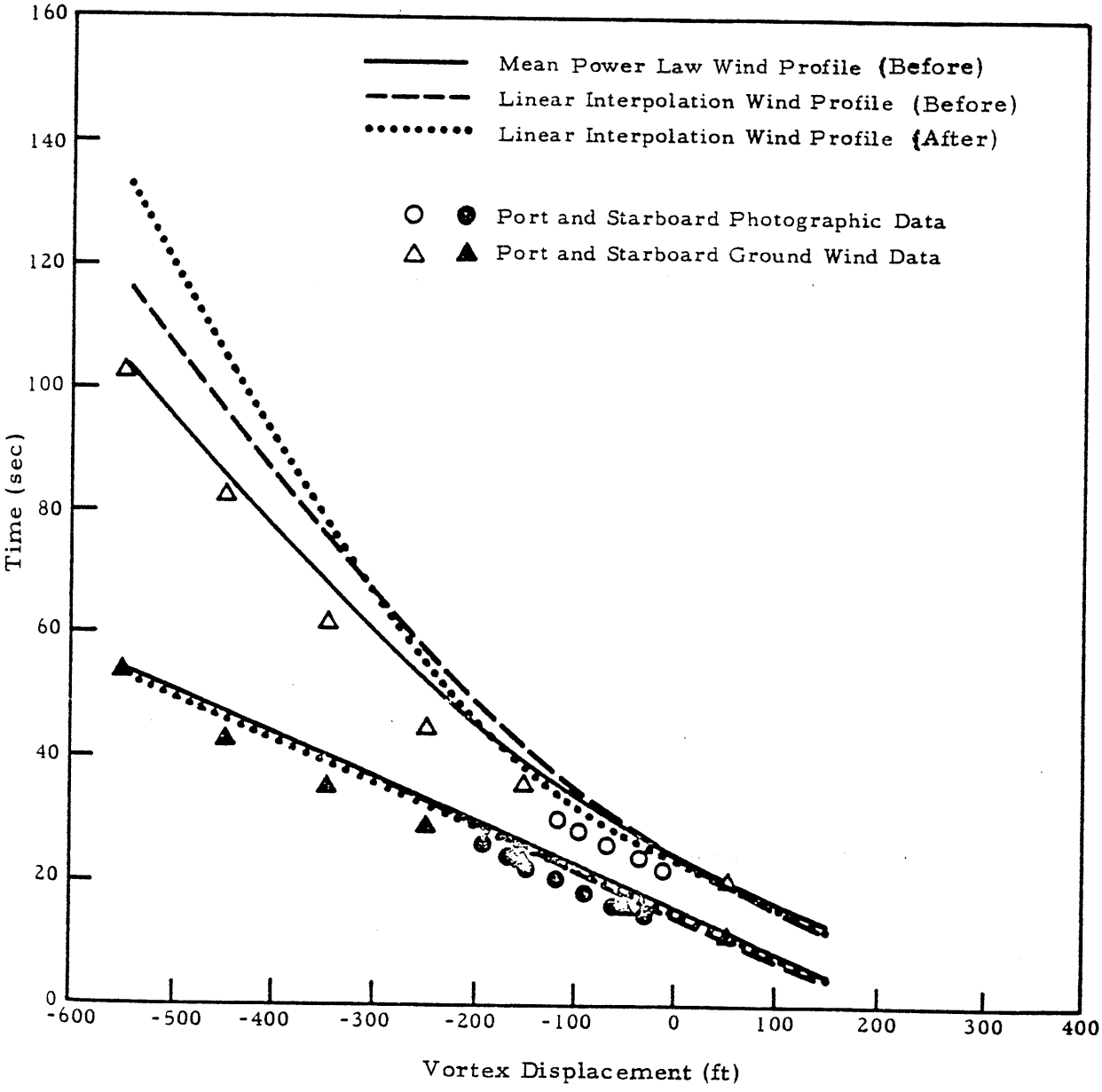

FIGURE 2. COMPARISON OF CALCULATED VORTEX TRAJECTORIES WITH MEASURED TRAJECTORIES FOR A B-707

The vortex sink rate for a wing having an arbitrary spanwise loading distribution is given from momentum conservation for a wing of span, b, by

$$dZ/dt = \frac{-C_L U_\infty}{4\pi K^2 \text{AR}} \qquad (2)$$

where C_L is the lift coefficient, U_∞ is the flight speed, K is the wing spanwise loading coefficient, and AR is the aspect ratio. For wings with inboard flaps, the root sections tend to be more heavily loaded; K is less, and hence the vortex sink rate is higher.

An analysis was performed (Ref. 24) to determine the streamlines associated with the presence of a vortex pair near a ground plane acted upon by a wind shear. The NAFEC data produced a definite trend in which the upwind vortex was at a higher altitude for large shears and the downwind vortex higher in light shears. In a light shear, the upper stagnation point rises as the wake oval descends toward the ground. In a strong shear the upper stagnation point moves closer to the ground.

Ground proximity tends to draw both the stagnation points toward the ground in a strong shear. Ground plane tends to "open up" a region between the two cells and causes a sweeping motion of the external stream around the cells. The downwind cell gets smaller as wind shear and ground proximity increase. The upwind cell increases in area as wind shear and altitude increase.

The downwind vortex cell shrinkage with increasing wind shear may give rise to an increased detrainment of the vorticity, as the increasing core size will encounter the inviscid cell boundary quicker than in the upwind case. This would cause the upwind vortex to rise due to the decreased induced velocity by the downwind vortex. The sweeping motion might cause upwind cell detrainment, thus causing the downwind vortex to rise.

The vertical descent of the vortex wake varies as a function of atmospheric conditions. The driving force for buoyancy is the difference in density

encountered during the descent of the vortex pair through a stratified fluid. Even for the case of no initial density difference (no engine exhaust entrainment), a difference is produced by the low density in the vortex core as a result of centrifugal motion of the air. An additional density difference can occur if the nearly adiabatic compression of the wake oval is different from the stratification of the atmosphere. Buoyancy generated in this manner alters the circulation through the Bjerkness relation; however, the manner of alteration is controversial as discussed by Tombach (Ref. 25). The models chosen to represent the effect of buoyancy in the transport model are Tombach's (Ref. 25) and Scorer and Davenport's (Ref. 26). These two theories contain a representation of the full spectrum of events.

The verification of the analytic transport model under operational conditions was one of the purposes of the test which is the subject of this report.

1.3.2 Role of Analytic and Predictive Models in a Wake Vortex Avoidance System

Both analytic models of vortex behavior (which yield calculated values of behavior) and predictive models have value in a WVAS. There are several purposes for the analytic model. First, there are many meteorological conditions for which vortex considerations do not constrain aircraft separations. An accurate analytic model allows identification of those meteorological conditions. The analytical model provides a theoretical basis for certification of spacings used. The model may be used in conjunction with empirically derived data. Certification criteria which are based on theoretical considerations and supported by empirical data have a greater credibility than criteria based on empirical data alone.

Second, in an operational WVAS, an analytic model is necessary for the selection of optimal spacing standards, based on current or forecast meteorological parameters. The Vortex Advisory System (VAS, Ref. 27 and discussed further in Section 1.4.3) allows either uniform 3-nautical-

mile spacing or 3/4/5/6-nautical-mile spacing (defined in Section 1.4.1), but no intermediate spacing standards. An accurate analytic model would allow an intermediate spacing standard to be used.

Third, certification of aircraft spacing must provide protection from anomalous vortex behavior. Therefore, both theoretical and experimental approaches to vortex behavior are appropriate to identify the conditions under which extremely long vortex life can occur. An analytic model can be used to identify conditions of anomalous vortex behavior which may not be identified by experimental results alone because the anomalous conditions may not occur during the experiments.

The purpose of the predictive model in the Wake Vortex Avoidance System is to forecast wake vortex residence times and safe aircraft separation distances based on known aircraft parameters and meteorological conditions. The aircraft separation distances given by the predictive model serve to eliminate hazardous wake vortex encounters and at the same time increase the current runway capacity and minimize aircraft delays. The functional relationship of the predictive model to the overall Wake Vortex Avoidance System is sketched in Fig. 3. The predictive model uses prevailing weather conditions and aircraft parameters to compute and forecast the safe aircraft separation distances. Vortex sensors provide a feedback on the calculated and predicted values of wake vortex transport time and life time and serve as a check on the integrity of the system. The safe separation distance provided by the predictive model and by vortex sensors is used by air traffic controllers and pilots for maintaining safe and efficient terminal area operations. The spacing information can also serve as an important input to the ARTS-3 air traffic control system.

Since the predictive model plays a dominant role in the WVAS, it is essential that the reliability, accuracy, and operational characteristics of the predictive model be established. The need to evaluate and to improve the wave vortex transport and decay model (upon which a predictive model is based) and to postulate a feasible predictive model was the motivation for the present research effort.

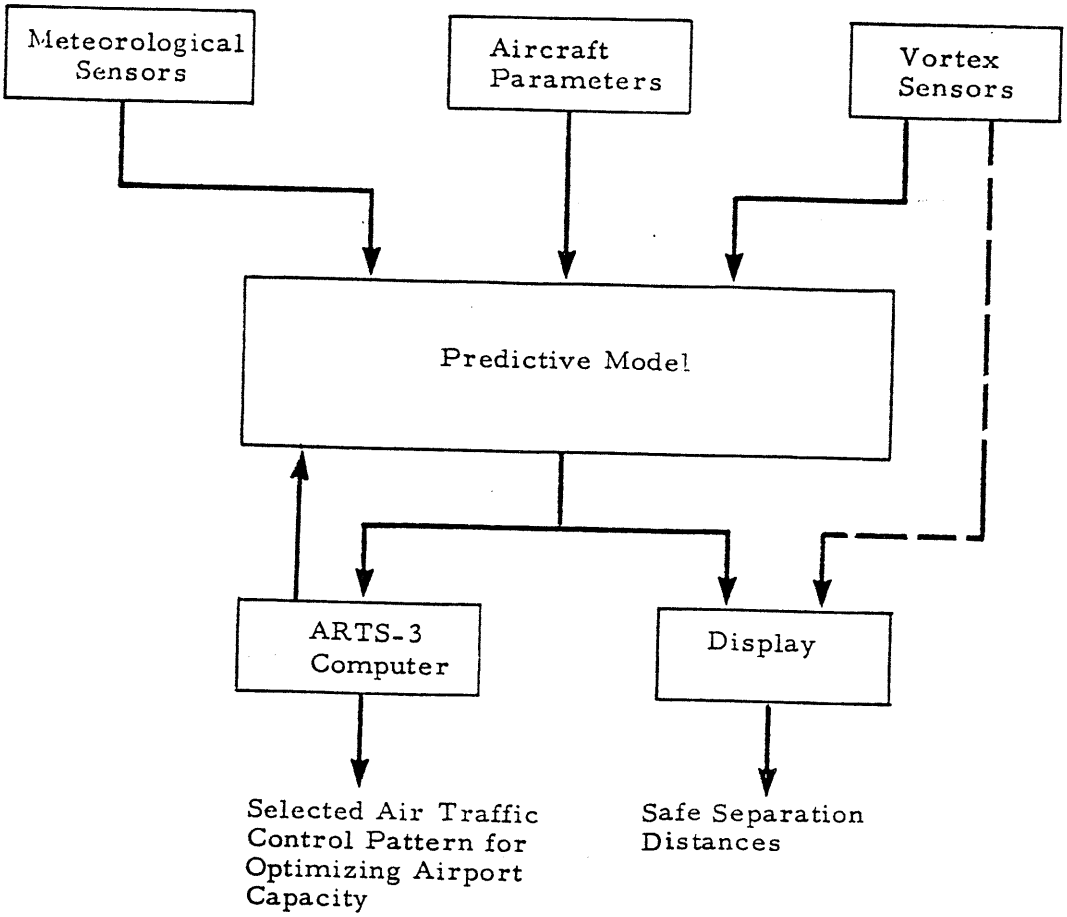

FIGURE 3. THE ROLE OF THE PREDICTIVE MODEL IN THE WAKE VORTEX AVOIDANCE SYSTEM

1.4 WAKE VORTEX AVOIDANCE SYSTEM CONCEPT

1.4.1 Wake Vortex Avoidance System Purpose

The purpose of the WVAS is to select aircraft spacings which ensure safety from wake vortices lingering in the approach corridor and which also minimize aircraft delays. Aircraft delay is the index of performance by which the effectiveness of a WVAS must be judged. It is assumed that the airport will be operated with absolute safety. Therefore, absolute safety is a constraint, and delay is the index of performance. Under the current FAA 3/4/5/6-nautical-mile separation criterion,* it is assumed that the wake vortices persist in the approach corridor until they disintegrate or decay since no reliable method for determining when the wake vortices are transported out of the flight corridor is available. A WVAS will perform two functions. The first is the prediction of vortex residence time based on measured values of meteorological parameters and/or based on recent measured vortex behavior. The second function is the detection and/or tracking of wake vortices.

1.4.2 Characteristics of Aircraft Delay

In order to gain an understanding of the manner in which a WVAS decreases aircraft delay, it is instructive to consider the characteristics of aircraft delay. For the purpose of gaining such an understanding, the equation for delay for a single runway in steady state can serve as an indicator of the characteristics of delay of landing aircraft at airports. Aircraft delay is technically defined as waiting time in the queue, and average

*A 4-nautical-mile separation for a heavy aircraft following another heavy, 5 nautical miles for a large aircraft following a heavy, 4 nautical miles for a light aircraft following a large aircraft, and 6 nautical miles for a light aircraft following a heavy. All other spacings are 3 nautical miles. Heavy aircraft are defined as aircraft with a maximum certificated takeoff weight of at least 300,000 lb. Light aircraft are defined as aircraft with a maximum certificated takeoff weight of less than 12,500 lb. (All models of the Gates Learjet are considered to be light.) All other aircraft are classified as large.

delay is given by (Ref. 28)

$$W_q = \frac{\lambda[E^2[\Delta t] + Var[\Delta t]]}{2(1 - \lambda E[\Delta t])} \tag{3}$$

where

λ = average arrival rate (aircraft per unit time)

$E[\Delta t]$ = expected value (mean) of interarrival time over the runway threshold: the inverse of $E[\Delta t]$ is theoretical runway capacity, and

$Var[\Delta t]$ = variance in interarrival time over the runway threshold.

It is noted that Δt is the interarrival time at the runway threshold when aircraft are continuously available for landing. Let Δt_3, Δt_4, and Δt_5 be the interarrival times for 3-, 4-, and 5-nautical-mile separations. (For 135-knot approach ground speeds, Δt_3 = 80 sec, Δt_4 = 107 sec, and Δt_5 = 128 sec). If the number of light aircraft is negligible, and h is the fraction of aircraft which are heavy,

$$E[\Delta t] = h^2 \Delta t_4 + h(1 - h) \Delta t_5 + (1 - h) \Delta t_3. \tag{4}$$

Figure 4 shows Eq. (3) for the interarrival times indicated above for a 135-knot approach speed. Delay for a uniform 2-nautical-mile separation is shown for comparison. Delays can become very significant when airports exceed 50% of their theoretical capacity. The annual delay cost is based upon an average direct operating cost of $1200 per block hour (Ref. 29) and 200,000 landings per year at the airport. For small delay, all of the elements of direct operating cost do not increase with delay time (e.g., crew salaries and maintenance burden do not increase as a result of small delays). Fuel cost may be considered as the minimum cost of delay, since fuel is always consumed during any delay. If fuel costs alone are considered, the delay cost is approximately 40% of the cost shown in Fig. 4 since fuel cost is approximately 40% of total direct operating cost (Ref. 29). Figure 4 shows that moderate decreases in delay can cause significant savings. Figure 4 does not include the cost of delay to takeoff aircraft as a result of landing delay, nor does it include the value of time of the passengers.

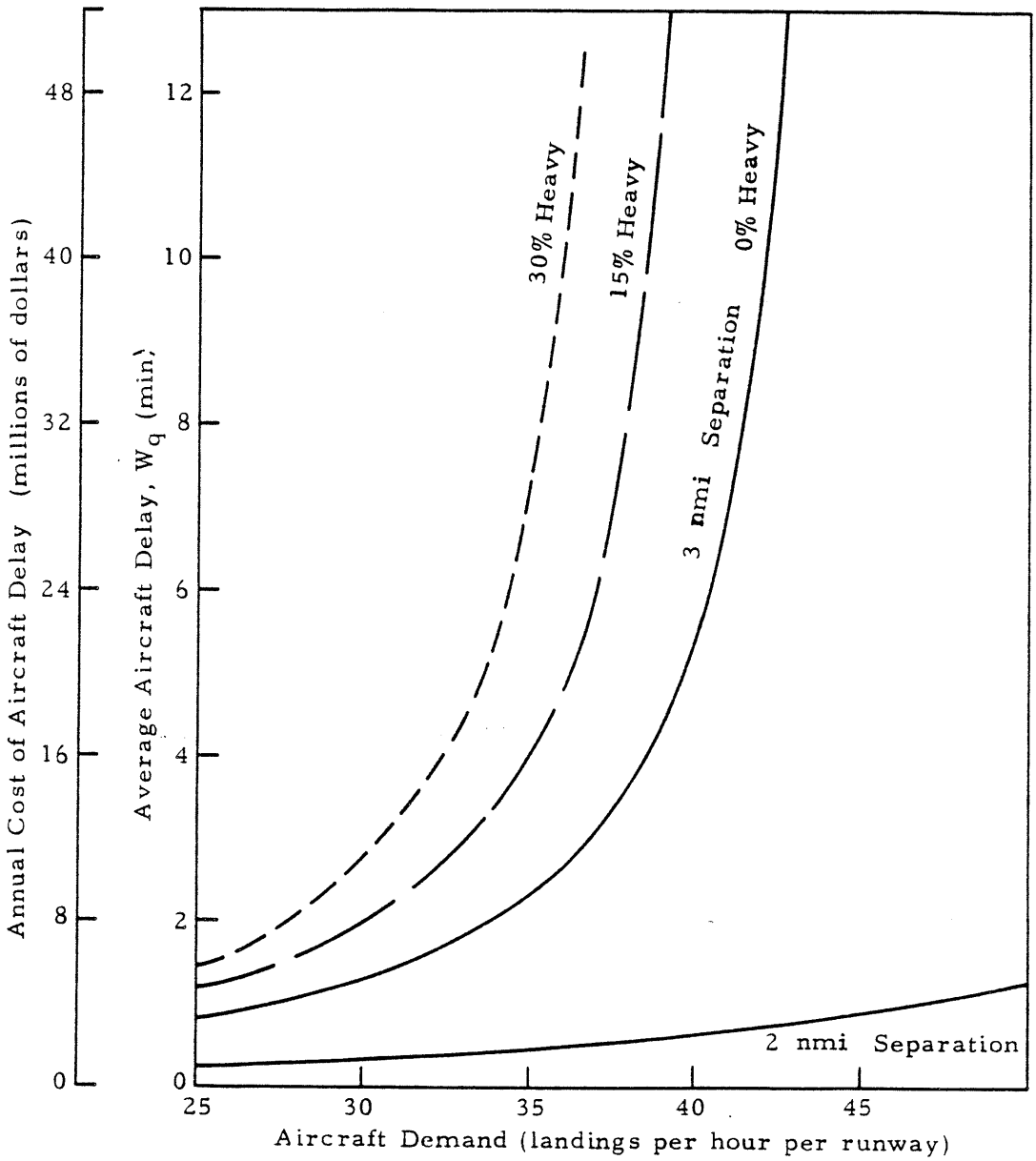

FIGURE 4. EFFECT OF AIRCRAFT DEMAND ON AIRCRAFT DELAY WITH VORTEX-IMPOSED SPACING CRITERIA (Cost based on 200,000 landings per year and direct operating cost of $1200 per hour)

The nonlinearity of the curves in Fig. 4 indicates that for airports operating near theoretical capacity, delay costs will grow much faster than traffic growth. For example, from the derivative of Eq. 3 with respect to λ, for an airport operating at 75% of theoretical capacity (i.e., $\lambda E[\Delta t] = .75$), a 2% traffic growth (average annual growth rate, Ref. 1) causes an 8% increase in delay. Therefore, delays due to vortex-imposed constraints can be expected to increase significantly as moderate aircraft traffic growth continues. Similarly, small increases in airport capacity can cause significant decreases in delay.

Figure 4 shows the delay for uniform 2-nautical-mile separations. It is seen that there are significant delay improvements which can be realized from 2-nautical mile separations. The uniform 2-nautical-mile separation is the ultimate goal of the Wake Vortex Avoidance System.

1.4.3 Comparison of the Wake Vortex Avoidance System with the Vortex Advisory System

Currently, the WVAS is still in the concept stage. However, a field validation of a modest cost Vortex Advisory System (VAS) is being performed at Chicago's O'Hare International Airport. The VAS is described in Refs. 3 and 27. The modest-cost system consists of a set of seven meteorological towers (each tower being near the approach end of one or two runways) with triple sets of wind sensors on each tower. The aircraft spacing (uniform 3 nautical mile or 3/4/5/6 nautical miles) is determined by a microprocessor on the basis of measured wind.* A small display shows one-minute averages of wind speed and direction, gusts, and recommended aircraft separations (i.e., uniform 3-nautical-mile or 3/4/5/6-nautical-mile separations).

*The wind criterion is an ellipse with a major axis of 12.5 knots aligned in the runway direction and a minor axis of 5.5 knots normal to the runway direction. If the wind is outside of the ellipse, vortex residence time is sufficiently short so that a 3-nautical-mile separation is always safe. If the wind is inside the ellipse, the 3-nautical-mile separation cannot be certified, and the 3/4/5/6-nautical-mile separation is used.

The WVAS is intended to have a higher level of sophistication than that for the VAS. In addition, the WVAS will use vortex detection. The increased sophistication of the WVAS will yield decreased delay by two mechanisms: decreased separation for a wider set of meteorological conditions than those allowed by the VAS and use of spacing standards which are between the 3/4/5/6-nautical-mile and uniform 3-nautical-mile separations used in the VAS. These mechanisms are discussed below.

A spacing standard cannot be used unless it can be certified as being safe. There are many meteorological conditions for which the 3-nautical-mile separation is safe, but cannot be certified by the relatively simple criteria used by the Vortex Advisory System. Therefore, the complete WVAS will use a more sophisticated meteorological measurement and calculation system than that used by the VAS. The WVAS will thus allow certification of the 3-nautical-mile separation for a greater fraction of airport operation time and for a wider range of meteorological conditions than is possible with the VAS.

The concept of the VAS could, in principle, be extended to allow 2-nautical-mile separations. However, the wind criteria for 2-nautical-mile separations would be too large to allow frequent use of the 2-nautical-mile separation. Only the WVAS can certify 2-nautical-mile separations for a significant portion of airport operating time.

The VAS can specify one of two distinct spacing standards (3/4/5/6 nautical miles or uniform 3 nautical miles), whereas the WVAS will be able to specify intermediate spacing criteria. The WVAS will be able to give reduced separations on days when the 3-nautical-mile separation cannot be certified, whereas the VAS cannot certify any reduction in separation unless the 3-nautical-mile separation can be certified.

For the reasons described above, it is expected that there will be many days for which the WVAS can certify reduced spacings, but for which the VAS cannot certify reduced spacings. Since the wind speed criterion of the VAS

is a function of the angle between the wind direction and the runway direction, particular problems are incurred by airports which have only one runway direction (e.g., Los Angeles International Airport and the Hartsfield Atlanta International Airport) since the choice of runway direction is limited. It is noted that small reductions in separations can cause significant reductions in delay.

The vortex detection capability of the WVAS can have significant impact on delay. This impact is shown graphically in Fig. 5. For a given wind condition (i.e., mean wind parameters measured over a time span on the order of 10 min), there is a probability distribution function that the vortex residence time is greater than time, t. A sample of the distribution function is shown in Fig. 5. The distribution has a long "tail"; the derivative of the distribution function with respect to vortex residence time is very small for small probabilities. For the VAS, the separation distance must be chosen so that the probability that vortex residence time will exceed the separation time is essentially zero. This must be done because there is no backup system to warn of a long vortex residence time. However, for the WVAS, the separation distance may be chosen so that the probability that vortex residence time is greater than separation time is some small value (e.g., 0.2%). This is possible because there is a backup system (vortex detection) to warn for that small fraction of the time when vortex residence time exceeds separation time. A missed approach can be executed in such cases. Because of the long "tail" of the probability distribution function, the acceptance of a small probability that vortex residence time will exceed separation time allows significant reductions in separation times. This can allow a very significant reduction in delay.

1.5 OBJECTIVE OF THE PRESENT INVESTIGATION

The primary objective of the study described herein was to use a set of specific data collected at John F. Kennedy International Airport in 1975 to gain as much understanding about the behavior of aircraft wake vortices and the operation of Wake Vortex Avoidance Systems as was possible with the

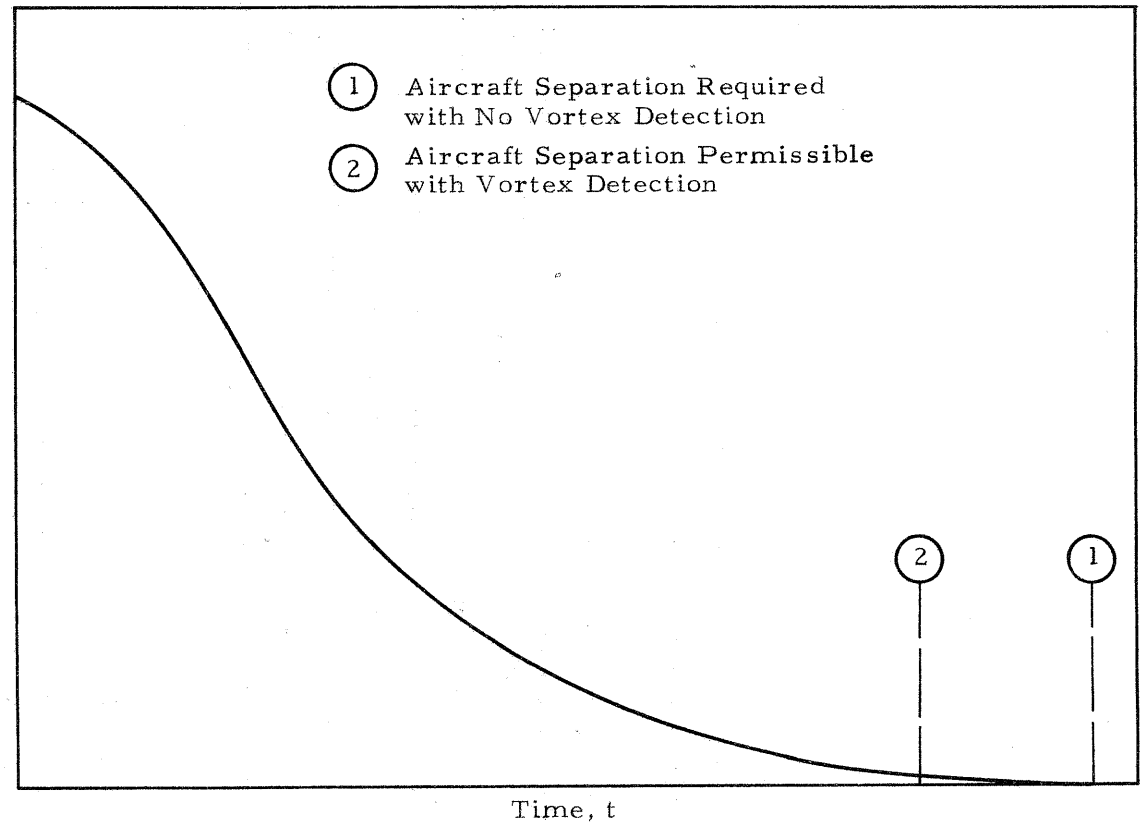

FIGURE 5. CHARACTERISTICS OF VORTEX RESIDENCE TIME PROBABILITY FUNCTION

available data. As mentioned earlier, the intent of the study was the effecting of a transition between earlier vortex research conducted in a research environment and implementation of a pre-prototype wake vortex avoidance system in an operational environment. The study started with a set of tasks by which the primary objective would be accomplished. The set of tasks contained some inherent assumptions about the characteristics of vortex behavior, the characteristics of the meteorological data being measured, and the quantity of data to be obtained. In performing the work, it became obvious that some of the inherent assumptions used in defining the original tasks were questionable. This does not imply that the original set of tasks was defined carelessly or erroneously. It does imply that many characteristics of vortices and wake vortex avoidance systems were learned while performing the tasks, and that some changing of the original tasks by which the primary objective would be achieved was appropriate.

Section 1.5 discusses the initial objectives (i.e., the tasks by which the primary objective was to be accomplished as defined at the initiation of the work described in this report), some of the reasons for modifying the objectives, and the final objectives. The reasons for modifying the objectives are discussed in detail in the analysis sections which constitute the main body of this report. The primary tool by which the initial and final objectives of this study were to be accomplished was a computerized data management system for the vortex data recorded. Much of the effort for the contract under which this report is written was used to construct the data management system.

1.5.1 Initial Objectives

The initial set of objectives by which the primary objective was to be accomplished centered around three subjects: (1) verification and improvement of an existing vortex transport analytic model; (2) determination of characteristic values for meteorological parameters, and (3) examination of data from various vortex sensors and comparison of vortex parameters

as measured by the various sensors. The original intent was the comparison of calculated vortex trajectories with measured vortex trajectories on a flyby-by-flyby basis. This would establish the reliability of the analytic model. Alternative models for different aspects of the analytic model (e.g., a power-law form or a logarithmic form for describing the wind profile with altitude) would be compared with measured vortex trajectories to determine which models best described actual vortex behavior. In addition, characteristic values of specific parameters (e.g., power-law exponent) could be determined.

1.5.2 Modification of Objectives

As the data were analyzed, the objectives were changed for several reasons. First, calculated and measured vortex trajectories could not be compared on a flyby-by-flyby basis since the primary meteorological tower was located 3300 ft from the vortex corridor, and the wind in the vortex corridor often differed significantly from that measured at the tower; the wind near the vortex corridor was measured, but a profile could not be obtained because the maximum altitude of measurement was 40 ft. Second, there was an inherent uncertainty in aircraft weight, spanwise loading factor, and airspeed. In previous tests conducted in a research environment, values for these parameters were known, but they were unknown in the operational environment. Aircraft weight has a very significant effect on transport time. Since it was impossible to know values for some very important parameters, the comparison of calculated and vortex tracks to determine optimal forms for the analytic model would be meaningless since any variations in the results calculated from alternative forms of the analytic model would be overshadowed by the uncertainty in the values of parameters to be used in the analytic model with which the measured results were to be compared.

Third, the characteristic values of meteorological parameters did not emerge. While values of atmospheric parameters such as roughness length and power-law exponent can be defined for wind averaging times on the order of 15 minutes, such characteristic values do not exist for averaging times

of one to two minutes. The shorter averaging time is necessary because it is the approximate life time of the vortex. Fourth, the quantity of vortex sensor data was much less than that originally anticipated. The acoustic systems (Doppler acoustic and monostatic acoustic systems) did not function concurrently with the laser Doppler velocimeter and the ground wind vortex sensing system. The laser Doppler velocimeter was not on site for the entire test. Therefore, the only sensor comparison which could be performed was that between the laser Doppler velocimeter and the ground wind vortex sensing system.

The data and analyses of data which led to the above conclusions are contained in the following sections of this report.

1.5.3 Final Objectives

In the analysis of the data which led to the conclusions discussed above in Section 1.5.2, it became obvious that the uncertainties which prevented the analysis of the data on a flyby-by-flyby basis were identical with the uncertainties which would exist in an operational WVAS. Therefore, the available data were indicative of most of the data which would be available in an operational WVAS. Therefore, the objectives were changed to answer the following questions: If the analytic model is used with appropriate upper and lower limits on values of independent parameters for which values could not be measured in the test, do the results bound the scatter observed in measured values of dependent parameters? What meteorological parameters have definable values for short averaging times and what meteorological parameters do not have definable values for short averaging times? What meteorological parameters should be used in a WVAS? In what form should meteorological parameters be presented and used? What is the role of vortex sensing in a WVAS? What useful information can be derived from vortex sensors?

1.6 REPORT OUTLINE

Most of the effort during the performance of the contract under which this report is written was expended in processing data from the Kennedy International Airport test site and in creating a data management system for analyzing the data. However, the main body of the report is the results of analysis based on selective data retrievals using the data management system. The data management system is described in Appendix A.

Section 2 contains a discussion of vortex characteristics from analytical considerations. The section is presented for three reasons. First, a simple analytical model which has not previously been presented has been formulated. Second, the section serves as a background for understanding the measurements to be discussed in later sections. Third, vortex characteristics from analytical considerations are discussed as they relate to an operational WVAS in a manner in which they have not previously been presented.

Section 3 is a discussion of the Kennedy International Airport test site, the data measured, and the data processing. Section 4 is a discussion of conclusions which are related to meteorological and vortex parameters and which were reached by selective retrievals of data from the data management system. Section 5 discusses the capability of vortex sensing and the role of vortex sensing in an operational WVAS. The techniques by which the measurements made by vortex sensors may be used to effect vortex prediction are formulated and discussed. Section 6 broaches a set of operational wake vortex avoidance systems based on conclusions reached in previous sections. Section 7 presents conclusions and recommendations.

2. VORTEX CHARACTERISTICS FROM ANALYTIC CONSIDERATIONS

This section contains a discussion of wake vortex characteristics from analytical considerations. The discussion presented in this section will aid in the interpretation of results from the JFK tests to be presented in later sections. The discussion will show the trends which should be expected, define the magnitude of expected data scatter, and indicate how scatter in the data could be reduced if the test were to be repeated or in an operational environment.

The first part of this section presents a new model for calculating vortex transport time in a uniform crosswind. The model does not use numerical integration of the vortex transport equations as previous models have done (Refs. 10 and 11). The model presented in this section will be used extensively in the comparison with measured values of transport time in future sections. The dominant mechanisms of vortex transport are presented, and the expected variations in vortex transport time due to uncertainties in values of the independent parameters during the JFK tests are presented. The effect of the baseline (i.e., distance inbound from the middle marker) on vortex transport is presented from theoretical considerations. This will aid in the interpretation of experimental data comparing different baselines. In addition, conclusions of interest are reached; the conclusions could not be reached from the experimental data because of a lack of data at baselines close to the runway threshold. Theoretical considerations of vortex decay and vortex disintegration conclude this section.

2.1 CHARACTERISTICS OF VORTEX TRANSPORT IN UNIFORM CROSSWIND

In order to understand the concepts of vortex transport to be presented in the following sections, it is instructive to examine the characteristics of vortex transport (particularly transport time) in a uniform crosswind.

It is assumed that the strengths of the port and starboard vortices are equal and constant. The altitudes of the two vortices are assumed to be equal. The vortex transport equations are (Ref. 3):

$$\dot{Z} = \frac{-\Gamma}{2\pi(Y_2 - Y_1)} + \frac{\Gamma}{2\pi}\left[\frac{Y_2 - Y_1}{(2Z)^2 + (Y_2 - Y_1)^2}\right] \tag{5}$$

and

$$\dot{Y} = V_\infty \pm \frac{\Gamma}{4\pi Z}\left[\frac{(Y_2 - Y_1)^2}{(2Z)^2 + (Y_2 - Y_1)^2}\right] \tag{6}$$

where Z is the altitude of the vortex pair and Y_1 and Y_2 are the lateral positions of the vortices from the port and starboard wings of the aircraft, respectively, as shown in Fig. 6a. The + and - are applicable to the starboard and port vortices, respectively.

In the absence of a crosswind (i.e., $V_\infty = 0$), the vortex trajectory is a hyperbola. In this condition, the vortex descent is symmetric with respect to a vertical plane:

$$Y_2 = -Y_1 = Y. \tag{7}$$

From the vortex transport equations,

$$\dot{Y}/\dot{Z} = -(2Y)^3/(2Z)^3, \tag{8}$$

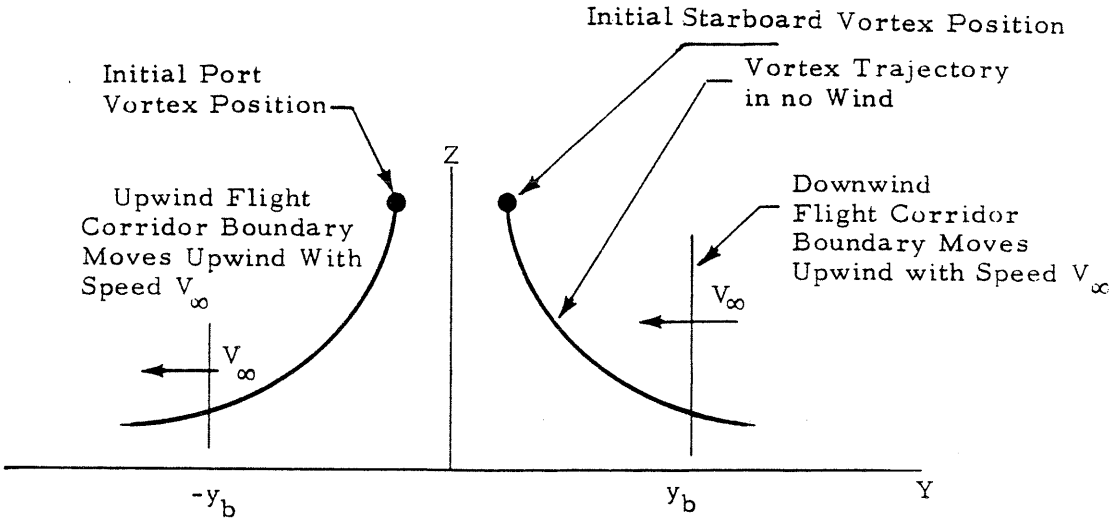

(a) Initial Vortex Geometry

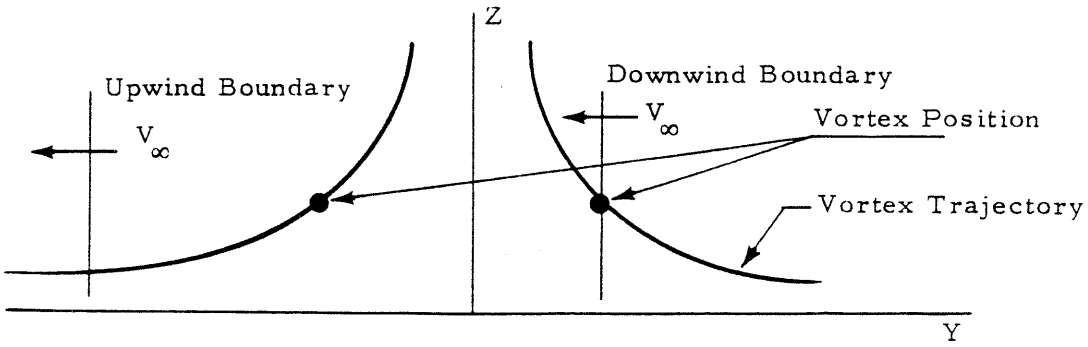

(b) Vortex Geometry at Time Downwind Vortex Leaves Flight Corridor

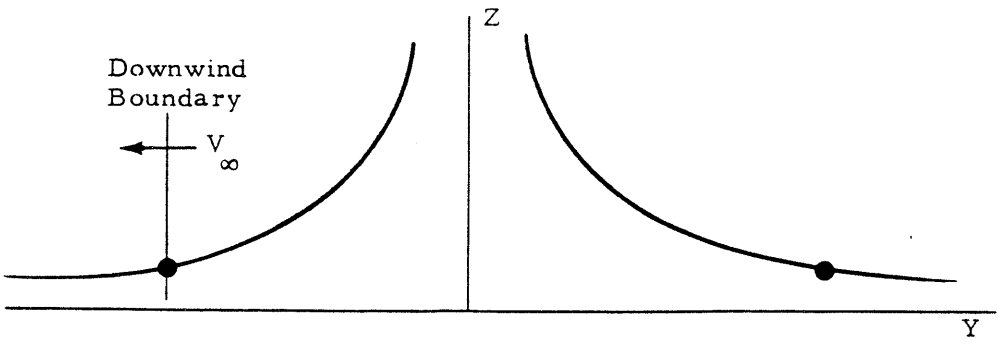

(c) Vortex Geometry at Time Upwind Vortex Leaves Flight Corridor

FIGURE 6. VORTEX GEOMETRY FOR VORTEX TRANSPORT TIME CALCULATION (Coordinate System is Fixed Relative to the Wind)

or

$$-dZ/Z^3 = dY/Y^3 \tag{9}$$

and hence,

$$1/Y^2 + 1/Z^2 = \text{Constant} = C, \tag{10}$$

which is the equation of the hyperbola representing the vortex trajectory in the absence of a crosswind.

This result can be used to calculate the time for which a vortex remains in a vortex corridor of width $2y_b$ for a uniform crosswind. The coordinate system is referenced to the wind with the origin in the y-direction taken as the aircraft axis at the time of aircraft passage, and y_b is the distance of the vortex corridor boundary from that origin. The origin coincides with the extended runway centerline and is transported downwind (relative to the extended runway centerline) at the crosswind velocity. Since the coordinate system is fixed on the wind, the crosswind is zero relative to the coordinate system. From Eqs. (6) and (7),

$$\dot{Y} = \frac{\Gamma}{4\pi Z}\left[\frac{Y^2}{Z^2+Y^2}\right] . \tag{11}$$

Using Eq. (10) for Z,

$$\dot{Y} = \frac{\Gamma}{4\pi C}\left[\frac{CY^2-1}{Y^2}\right]^{3/2} , \tag{12}$$

where the value of C is calculated from Eq. (10) using the initial values of Y and Z (e.g., $Y = b'/2$, b' being the initial vortex separation distance, and Z = initial vortex altitude). Integrating Eq. (12) gives

$$t + D = \frac{4\pi}{\Gamma C}\left[\frac{CY^2-2}{(CY^2-1)^{1/2}}\right] , \tag{13}$$

where D is the constant of integration determined by $Y = b'/2$ at $t = 0$. If the lateral boundaries of the vortex corridor are at $\pm y_b$ at $t = 0$, at later time, t, the boundaries of the vortex corridor (referenced to the wind-based coordinate system) are at

$$Y = -V_\infty t \pm y_b , \tag{14}$$

with a + or - denoting downwind or upwind flight corridor boundaries, respectively.

The geometry is shown in Fig. 6. The time in Eq. (13) is the time required for the vortex to reach position Y. The time in Eq. (14) is the time for the boundary to reach position Y. The transport time is the time at which the vortex and the boundary are at the same position at the same time. For simplicity, time is eliminated between Eqs. (13) and (14), and the result is

$$\frac{(\pm y_b - Y)}{V_\infty} + D = \frac{4\pi}{\Gamma C} \left[\frac{CY^2 - 2}{(CY^2 - 1)^{1/2}} \right] . \tag{15}$$

Let

$$F(Y) = \frac{4\pi}{\Gamma C} \left[\frac{CY^2 - 2}{(CY^2 - 1)^{1/2}} \right] - D + \frac{Y \mp y_b}{V_\infty} , \tag{16}$$

with the top sign on y_b denoting the downwind boundary and the lower sign denoting the upwind boundary. Physically, F(Y) is the difference between the time at which the vortex reaches position Y and the time at which the boundary reaches position Y. The vortex residence time is obtained by solving Eq. (16) for Y when $F(Y) = 0$ (using a Newton-Raphson iteration beginning with $Y = \pm b'/2$) and solving for transport time from Eq. (14).

2.1.1 Vortex Transport Time Characteristics

It is instructive to examine the conditions under which various solutions to Eq. (16) exist. Physically, it is desired to determine the conditions under which each of the vortices will exit from each of the vortex corridor boundaries.

For the downwind vortex ($Y > 0$) and downwind boundary (top sign on y_b), the definition of D in Eq. (13) for the initial condition ($Y = b'/2$ at $t = 0$) gives for $t = 0$

$$F(b'/2) = (b'/2 - y_b)/V_\infty < 0, \tag{17}$$

assuming that the vortex corridor width exceeds the vortex separation distance. As Y becomes large ($CY^2 >> 1$),

$$F(Y) \cong \frac{4\pi}{\Gamma C}\sqrt{CY^2} + Y/V_\infty > 0 . \tag{18}$$

There is, therefore, one solution of the downwind vortex crossing the downwind vortex corridor boundary (i.e., $F(Y) = 0$). The vortex geometry for this solution is shown in Fig. 6b. This solution can be determined from Newton iteration on Eq. (16) with the initial "solution" being $Y = b'/2$. The transport time may be calculated with the solution value of Y by using Eq. (13) or (14). By substituting the lower sign of y_b for the upwind boundary, it may be shown mathematically (as well as from physical reasoning) that the downwind vortex cannot cross the upwind boundary.

For the upwind vortex ($Y < 0$) crossing the upwind boundary, the initial condition gives

$$F(-b'/2) = \frac{-b'/2 + y_b}{V_\infty} > 0 . \tag{19}$$

For large values of Y,

$$F(Y) \cong \frac{4\pi}{\Gamma C}\sqrt{CY^2} + Y/V_\infty = \frac{4\pi}{\Gamma\sqrt{C}}\ Y\ + Y/V_\infty$$

$$= Y\left[1/V_\infty - 4\pi/\Gamma\sqrt{C}\right]. \tag{20}$$

Therefore, since $Y < 0$,

$$F(Y) > 0 \quad \text{if} \quad V_\infty > \Gamma\sqrt{C}/4\pi \tag{21}$$

and

$$F(Y) < 0 \quad \text{if} \quad V_\infty < \Gamma\sqrt{C}/4\pi \tag{22}$$

for large values of Y. Therefore, if

$$V_\infty > \Gamma\sqrt{C}/4\pi\ , \tag{23}$$

a solution to Eq.(16) does not exist, and the upwind vortex does not cross the upwind boundary. If

$$V_\infty < \Gamma\sqrt{C}/4\pi\ , \tag{24}$$

the upwind vortex crosses the upwind boundary (cf. Fig. 6c). The value of Y may be determined by Newton interation on Eq.(16). The initial value of Y should be a negative value of about five wingspans.

For the condition of the upwind vortex crossing the downwind boundary,

$$F(-b'/2) = \frac{-b'/2 - y_b}{V_\infty} < 0\ . \tag{25}$$

Similarly, for large absolute values of Y

$$F(Y) > 0 \text{ if } V_\infty > \Gamma\sqrt{C}/4\pi \,, \tag{26}$$

and

$$F(Y) < 0 \text{ if } V_\infty < \Gamma\sqrt{C}/4\pi \,. \tag{27}$$

If

$$V_\infty > \Gamma\sqrt{C}/4\pi \,, \tag{28}$$

one solution exists and may be found by Newton iteration on Eq. (16) beginning with $Y = -b'/2$. If

$$V_\infty < \Gamma\sqrt{C}/4\pi \,, \tag{29}$$

either no solution or two solutions exist. It is necessary to determine if F(Y) is positive for any values of Y. The maximum value of F(Y) occurs when $F'(Y) = 0$. This occurs when

$$Y^2 = \frac{1}{C - \left[4\pi C V_\infty/\Gamma\right]^{2/3}} \,. \tag{30}$$

Solving for F(Y) with this value of Y (denoted by Y_m) yields the number of times the upwind vortex crosses the downwind boundary. If

$$V_\infty < \Gamma\sqrt{C}/4\pi \tag{31}$$

and

$$F(Y_m) < 0 \,, \tag{32}$$

there is no solution. Physically, the upwind vortex approaches the downwind boundary, but is transported upwind by its image vortex before it crosses the boundary. If

$$V_\infty < \Gamma \sqrt{C}/4\pi \tag{33}$$

and

$$F(Y_m) > 0 , \tag{34}$$

two solutions exist. Physically, the upwind vortex crosses the downwind boundary, but is then transported upwind by its image vortex and reenters the vortex corridor through the downwind boundary. The values of Y for which the boundary crossings occur may be calculated by solving Eq. (16).

It is noted that the upwind vortex always remains in the vortex corridor longer than the downwind vortex. Therefore, the maximum vortex transport time is given by the upwind vortex crossing the downwind boundary if

$$V_\infty > \Gamma \sqrt{C}/4\pi , \tag{35}$$

and by the upwind vortex crossing the upwind boundary if

$$V_\infty < \Gamma \sqrt{C}/4\pi . \tag{36}$$

2.1.2 Universal Nondimensional Parameters of Vortex Transport Time

Equations (14) and (16) suggest that a set of nondimensional parameters of vortex transport time exists. Several different sets of nondimensional parameters may be chosen. The set which is presented herein was chosen because one parameter is a function of the vortex corridor only, and a second parameter is a function of aircraft type only.

Multiplying Eq. (16) by V_∞ / y_b and rearranging gives

$$F(Y) = \frac{4\pi V_\infty y_b}{\Gamma C y_b^2}\left[\frac{C y_b^2 (Y/y_b)^2 - 2}{\left(C y_b^2 (Y/y_b)^2 - 1\right)^{\frac{1}{2}}}\right] - DV_\infty / y_b + Y/y_b \mp 1 = 0. \qquad (37)$$

Similarly, Eq. (14) becomes

$$Y/y_b = - V_\infty t/y_b \mp 1. \qquad (38)$$

These equations are non-dimensional. From them, four non-dimensional parameters which uniquely define vortex behavior may be generated. The first is the vortex transport time parameter,

$$P_t = V_\infty t/y_b . \qquad (39)$$

The second is the vortex strength parameter,

$$P_s = 4\pi V_\infty y_b/\Gamma . \qquad (40)$$

The third nondimensional parameter is the boundary parameter

$$P_b = C y_b^2 = y_b^2 \left(\frac{1}{Y_o^2} + \frac{1}{Z_o^2}\right) , \qquad (41)$$

where Y_o and Z_o are the initial values for Y and Z, respectively. For a given vortex corridor (i.e., initial altitude and vortex corridor width), the boundary parameter is a function of aircraft wing span only. For an elliptically loaded wing,

$$P_b = y_b^2 \left(\frac{64}{\pi^2 b^2} + \frac{1}{Z_o^2}\right). \qquad (42)$$

The variable used in solving Eq. (37) is

$$\eta = Y/y_b. \tag{43}$$

Equation (31) is now

$$F(\eta) = \frac{P_s}{P_b}\left(\frac{P_b\,\eta^2 - 2}{(P_b\,\eta^2 - 1)^{\frac{1}{2}}}\right) - D_1 + \eta \mp 1 = 0. \tag{44}$$

Recalling the method by which D was calculated from Eq. (13), D_1 is calculated from the initial value of the first term on the right side of Eq. (44). Thus,

$$D_1 = \frac{P_s}{P_b}\left[\frac{P_b\,\eta_o^2 - 2}{(P_b\,\eta_o^2 - 1)^{\frac{1}{2}}}\right], \tag{45}$$

where

$$\eta_o = Y_o/y_b = \left[P_b - (y_b/Z_o)^2\right]^{-\frac{1}{2}}. \tag{46}$$

This equation introduces the fourth non-dimensional parameter, the vortex corridor parameter,

$$P_v = y_b/Z_o. \tag{47}$$

Plots of nondimensional vortex transport time may be obtained in the following manner. The vortex corridor parameter, P_v, and boundary parameter, P_b, are selected. They may be selected for a particular corridor size and aircraft type. For each selected value of the vortex strength parameter,

P_s, D_l is calculated from Eq. (45), and Eq. (44) is solved for η by an iterative technique. The transport time parameter is then solved by

$$P_t = \pm 1 - \eta, \tag{48}$$

which is derived from Eq. (38).

From the reasoning related to Eqs. (35) and (36), it may be shown that the upwind vortex exits from the downwind flight corridor boundary if

$$P_s > \sqrt{P_b}, \tag{49}$$

and the top sign is applicable in Eqs. (44) and (48). If

$$P_s < \sqrt{P_b}, \tag{50}$$

the upwind vortex exits from the upwind vortex corridor boundary, and the bottom sign is applicable in Eqs. (44) and (48).

Figure 7 shows a sample plot of nondimensional vortex parameters for selected aircraft.

2.2 DOMINANT MECHANISMS IN VORTEX TRANSPORT MODEL

The general vortex transport model is an analytic tool which determines the lateral and vertical displacement of each vortex of the trailing vortex pair as a function of time for specified values of aircraft parameters and a given crosswind profile. An important output from the vortex transport model is the calculated vortex transport time, which is defined as the time after aircraft passage at which both vortices have been transported outside the corridor defined by boundaries $\pm$150 ft from the runway centerline. Since it has been shown that vortices located outside the $\pm$150 ft corridor do not pose a threat to following aircraft (cf. Section 1.2.1), the calculated vortex transport time is an indication of the safe separation time calculated for the aircraft type and prevailing meteorological parameters. Therefore, for an operational WVAS it is important to determine the sensitivity of the calculated vortex transport time to variations in crosswind characteristics and aircraft parameters.

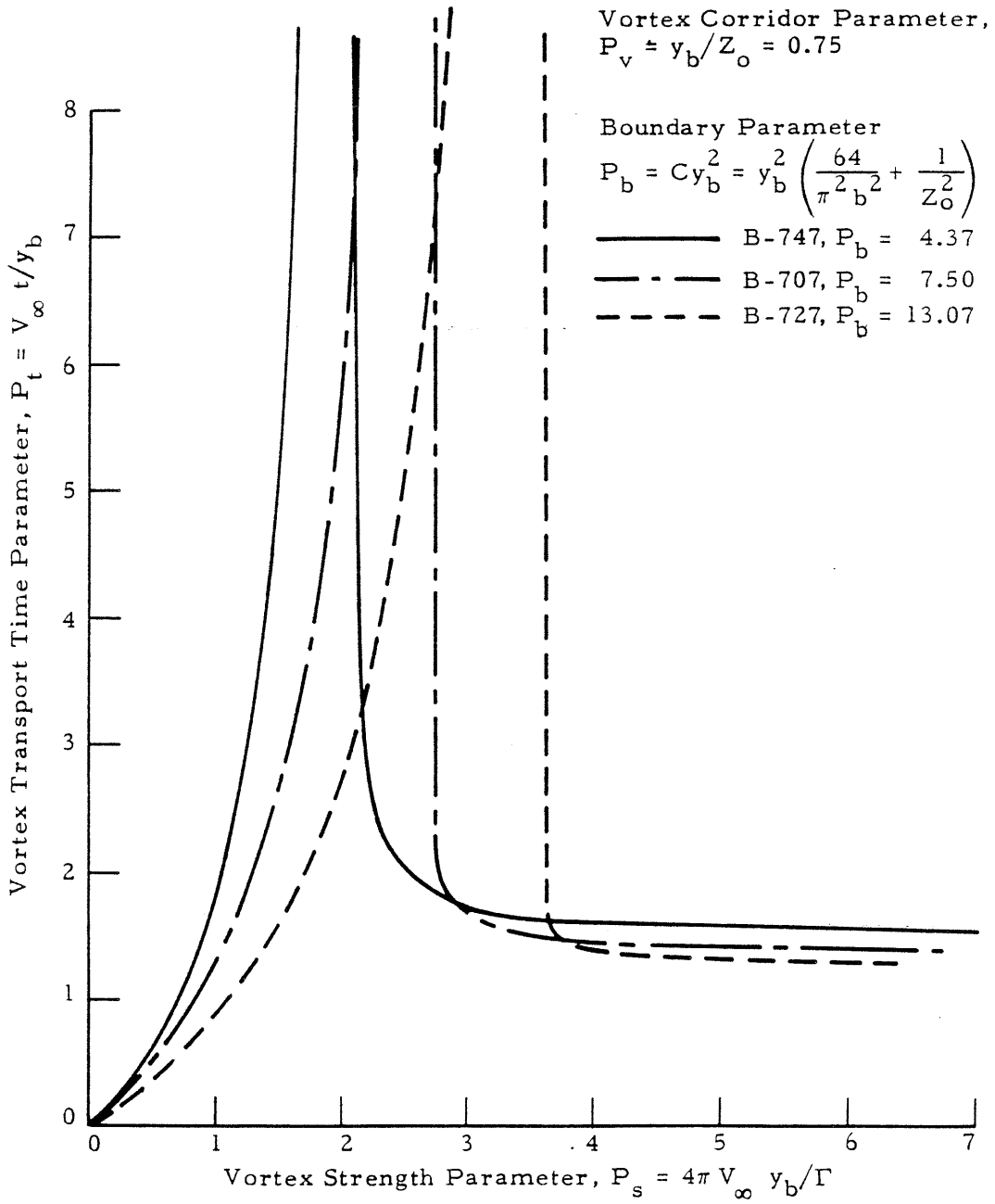

FIGURE 7. NONDIMENSIONAL VORTEX TRANSPORT TIME PARAMETERS

The vortex transport model assumes a constant vortex strength, Γ, and assumes that the altitudes of the port and starboard vortices are equal. The vortex transport equations are (Eqs. (5) and (6))

$$\dot{Z} = \frac{-\Gamma}{2\pi(Y_2 - Y_1)} + \frac{\Gamma}{2\pi}\left[\frac{Y_2 - Y_1}{(2Z)^2 + (Y_2 - Y_1)^2}\right] \tag{51}$$

and

$$\dot{Y} = V_\infty \pm \frac{\Gamma}{4\pi Z}\left[\frac{(Y_2 - Y_1)^2}{(2Z)^2 + (Y_2 - Y_1)^2}\right], \tag{52}$$

where

$$\Gamma = \frac{W_A}{\rho b K U_\infty}, \tag{53}$$

where

Z = vortex altitude
Γ = vortex strength
Y_1 = port vortex lateral position
Y_2 = starboard vortex lateral position
V_∞ = crosswind
W_A = aircraft weight
ρ = air density
b = aircraft wing span
K = aircraft spanwise loading coefficient
and
U_∞ = aircraft airspeed.

Physically, the spanwise loading coefficient is the ratio of lift generated by the wing to the lift which would be generated if the wing loading (lift per unit span of the wing) were uniform at the value of spanwise loading at the

wing root. The wing loading is proportional to the bound circulation, $\Gamma'(y)$, of the wing. The spanwise loading coefficient is

$$K = \frac{2}{b\Gamma'_o} \int_o^{b/2} \Gamma'(y)\, dy \ , \tag{54}$$

where

$\Gamma'(y)$ = bound circulation on the wing, and

Γ'_o = bound circulation at the wing root.

For elliptically loaded wings,

$$K = \pi/4 \ , \tag{55}$$

which is the assumption made for calculated values of vortex parameters in this report.

Detailed derivations of Eqs. (51) through (55) are presented in Ref. 3.

Analysis of the analytic vortex transport model consisted of establishing the sensitivity of the model to the basic input parameters including crosswind characteristics (crosswind as a function of altitude) and aircraft parameters (aircraft type, landing weight, altitude, and aircraft position relative to the ILS). Conclusions related to other effects such as buoyancy, wind shear, and viscous vortex-ground interactions could not be reached from the JFK data. The influence of the above parameters on the wake vortex transport time in the approach corridor is discussed below.

2.2.1 Influence of Crosswind on the Calculated Vortex Transport Time

The calculated vortex transport time as a function of crosswind (defined as the wind vector component which is normal to the runway direction) is shown

in Figs. 8, 9 and 10 for uniform, power law, and logarithmic crosswind profiles. The nominal values of aircraft parameters shown in Table 1 were used for calculation of the transport times. For low values of crosswind (< 4 ft/sec), the upwind and downwind vortices exit from the upwind and downwind vortex corridor boundaries, respectively. For high values of crosswind, both vortices exit from the downwind boundary. It is noted that the upwind vortex always leaves the vortex corridor later than the downwind vortex. Therefore, the vortex transport time can be calculated from the motion of the upwind vortex.

The calculated value of vortex transport time is shown as a function of crosswind at the reference altitude, $V_{z\ ref}$, and exponent, P, for a power-law profile in Fig. 9. The 20-ft altitude is used as the reference since available measurements are generally made at this altitude. The power-law exponents ranging from 0.1 to 0.4 are representative of the wind profiles observed during unstable to moderately stable atmospheric conditions. The power-law profile was chosen as the basic profile for use in this study because a previous study (Ref. 30) showed that vortex trajectories calculated with the power-law wind profile matched measured vortex trajectories better than trajectories calculated with other profiles.

The curves in Fig. 9 appear to indicate a sensitivity of the vortex transport time to the 20-ft crosswind and to the value of the power-law exponent. However, a closer examination of the phenomenon reveals that the transport time is not sensitive to the shape of the wind profile, per se, but is sensitive to the value of the crosswind at an altitude higher than 20 ft.

Because the reference altitude was taken below the minimum altitude to which the vortex descends (i.e., approximately half the initial vortex separation distance), the effect of increasing the power-law exponent, P, is to increase the value of crosswind which the vortex experiences during its entire trajectory. The effect shown in Fig. 9 is essentially that of a difference in

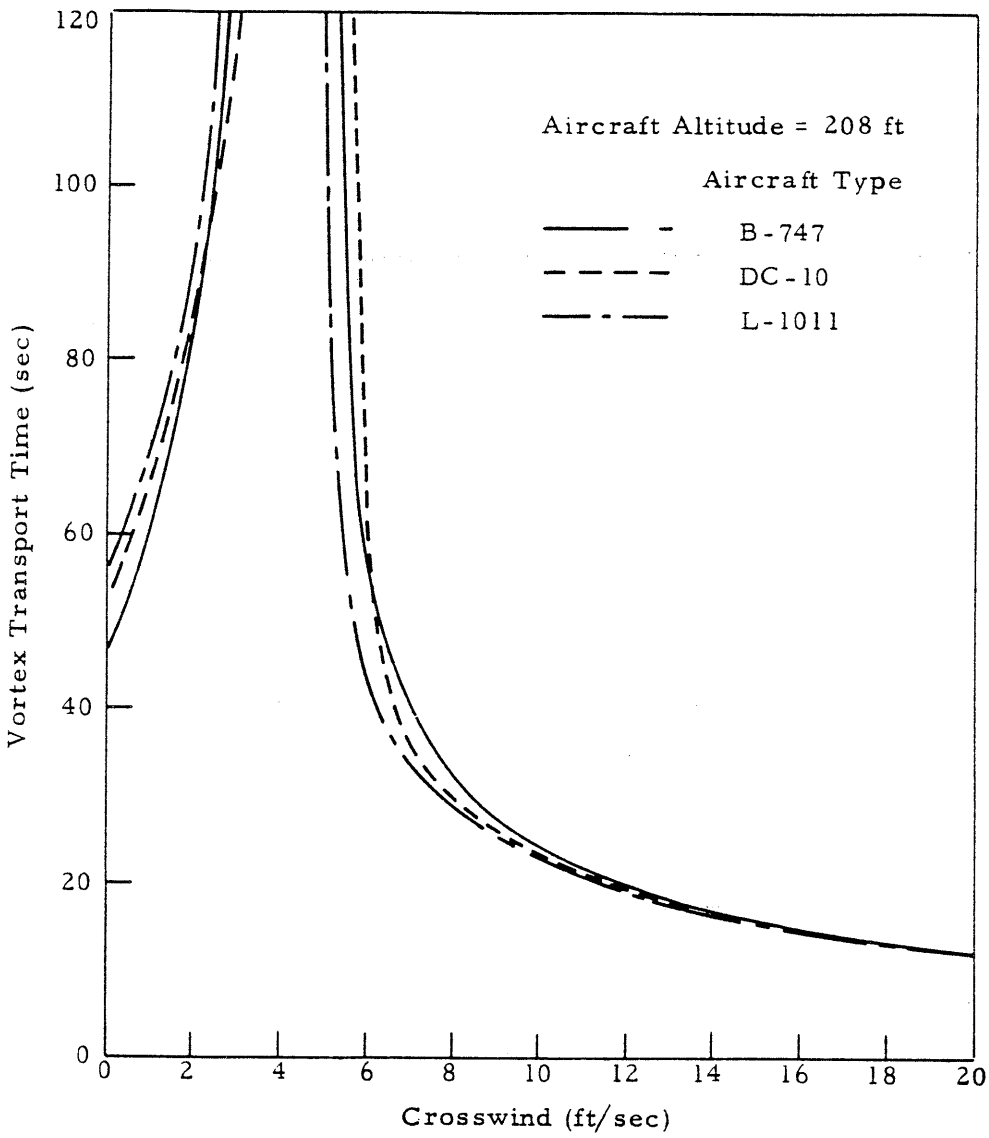

FIGURE 8. CALCULATED VORTEX TRANSPORT TIME FOR UNIFORM CROSSWIND

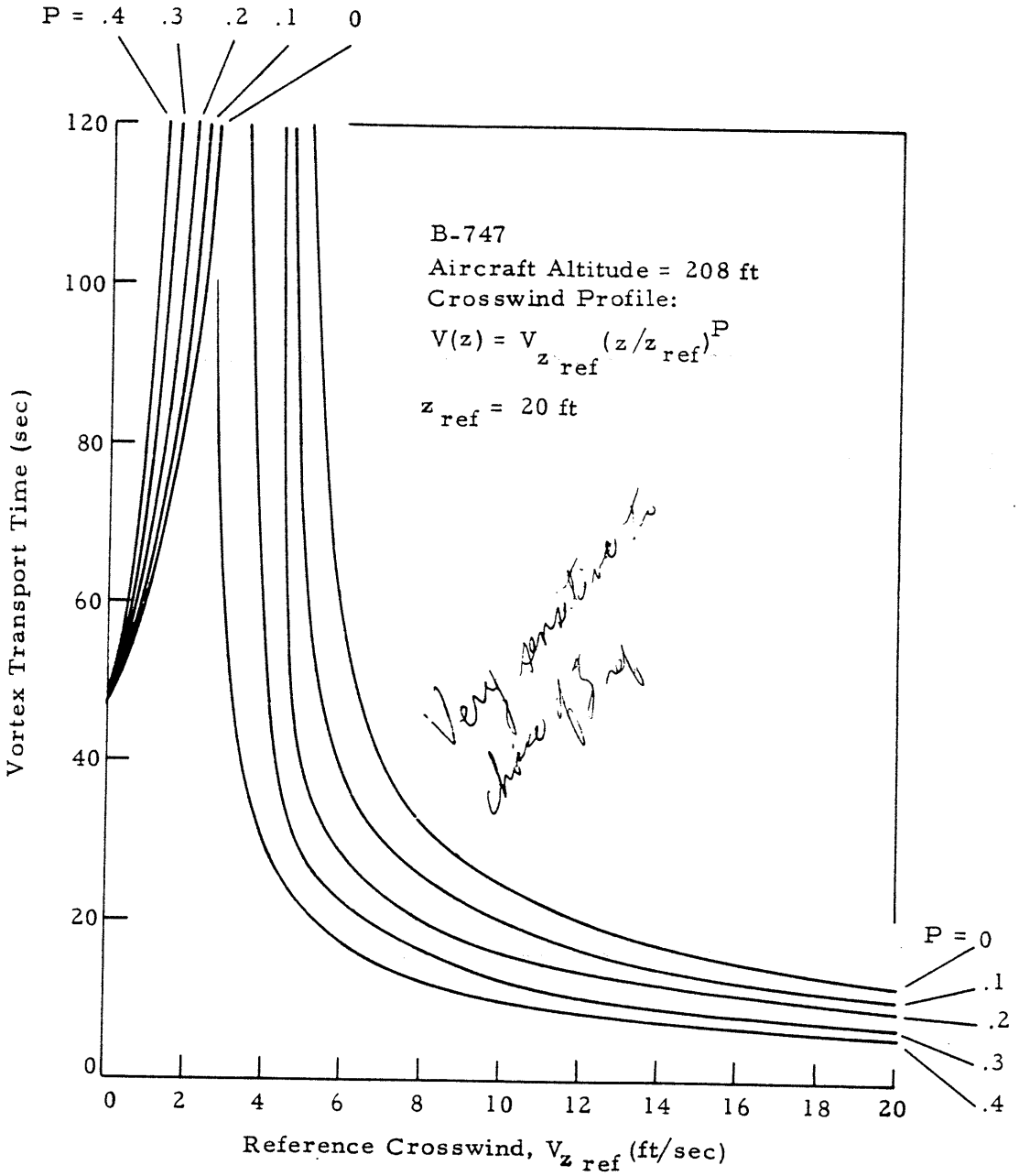

FIGURE 9. CALCULATED VORTEX TRANSPORT TIME FOR CROSSWIND DESCRIBED BY POWER-LAW PROFILE

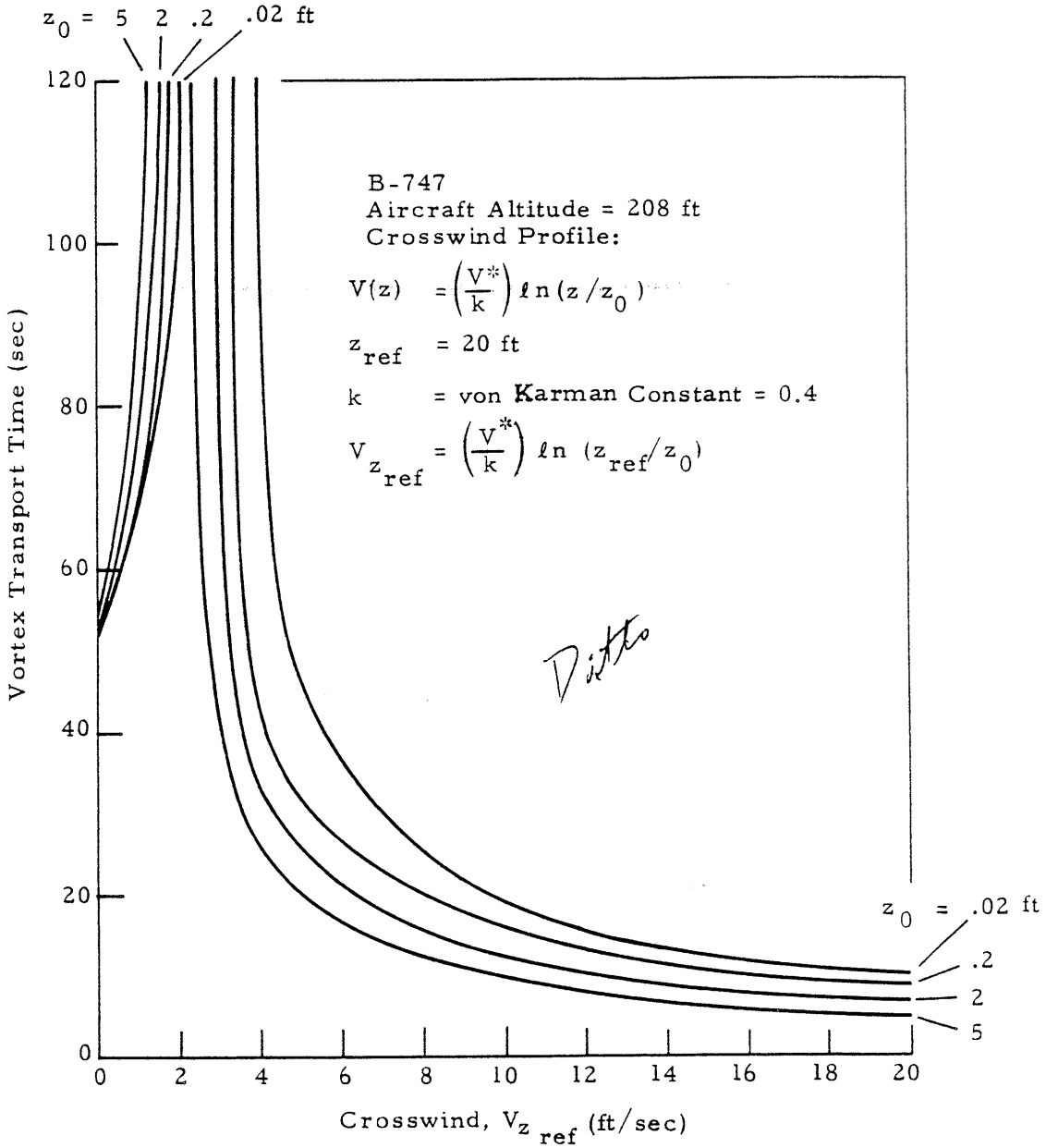

FIGURE 10. CALCULATED TRANSPORT TIME FOR CROSSWIND DESCRIBED BY LOGARITHMIC PROFILE

Add 757, 767, A340 ?

Table 1

AIRCRAFT CHARACTERISTICS FOR CALCULATED VORTEX TRAJECTORIES

Aircraft Type	Wingspan (ft)	Landing Weight (lb)	Airspeed (ft/sec)	Vortex Strength (ft^2/sec)	Initial Vertical Speed (ft/sec)
B-747	195.7	462,878	237.7	5397	-5.59
B-707	145.0	194,400	231.8	3137	-4.38
B-727	108.0	126,750	212.7	2993	-5.61
B-737	93.0	81,500	183.4	2562	-5.58
DC-10	165.3	335,375	234.7	4689	-5.74
DC-9	89.4	63,544	215.6	1788	-4.05
DC-8	148.4	199,375	230.3	3164	-4.32
L-1011	155.3	298,409	234.7	4441	-5.79
VC-10	146.2	200,000	230.0	3193	-4.43
BAC-111	93.5	64,154	237.7	1553	-3.37

wind from the reference altitude to the asymptotic altitude (i.e., minimum altitude to which the vortex descends asymptotically) of the vortex pair. Figure 11 shows curves similar to Fig. 9, but with the reference altitude taken as 77 ft, which is the asymptotic altitude for an elliptically loaded B-747. For this condition the effect of the power-law exponent is almost negligible. Of particular significance is the fact that there is little dependence on the value of the exponent for large values of transport time. The spread in the lines of Figs. 9 and 11 is an indication of uncertainty in vortex transport time based on wind measured at the asymptotic altitude (i.e., Fig. 11) compared with uncertainty based on wind measured at the 20-ft altitude and extrapolated to higher altitudes on the basis of a power-law exponent (i.e., Fig. 9). Figures 9 and 11 clearly show that the uncertainty in residence time decreases as the altitude of the wind measurement approaches the vortex asymptotic altitude.

The conclusion of this analysis is that direct wind measurement at the asymptotic altitude is preferable to wind measurement at another altitude with extrapolation to the asymptotic altitude.

2.2.2 Influence of Aircraft Parameters on the Calculated Vortex Transport Time

Variations in aircraft type, landing weight, altitude, and lateral displacement from the localizer centerline result in changes in the wake vortex transport time in the vortex corridor and are discussed below.

The calculated vortex transport time is shown for heavy and large jet transports in Figs. 8 and 12, respectively. The vortex transport time is relatively insensitive to aircraft type within each of the two broad aircraft groups (heavy and large), based upon the nominal values of aircraft parameters in Table 1. For a given initial altitude, vortex corridor width and crosswind, the vortex transport time is primarily a function of the vertical speed of the vortex pair. Equation (10) shows that the vortex trajectory in

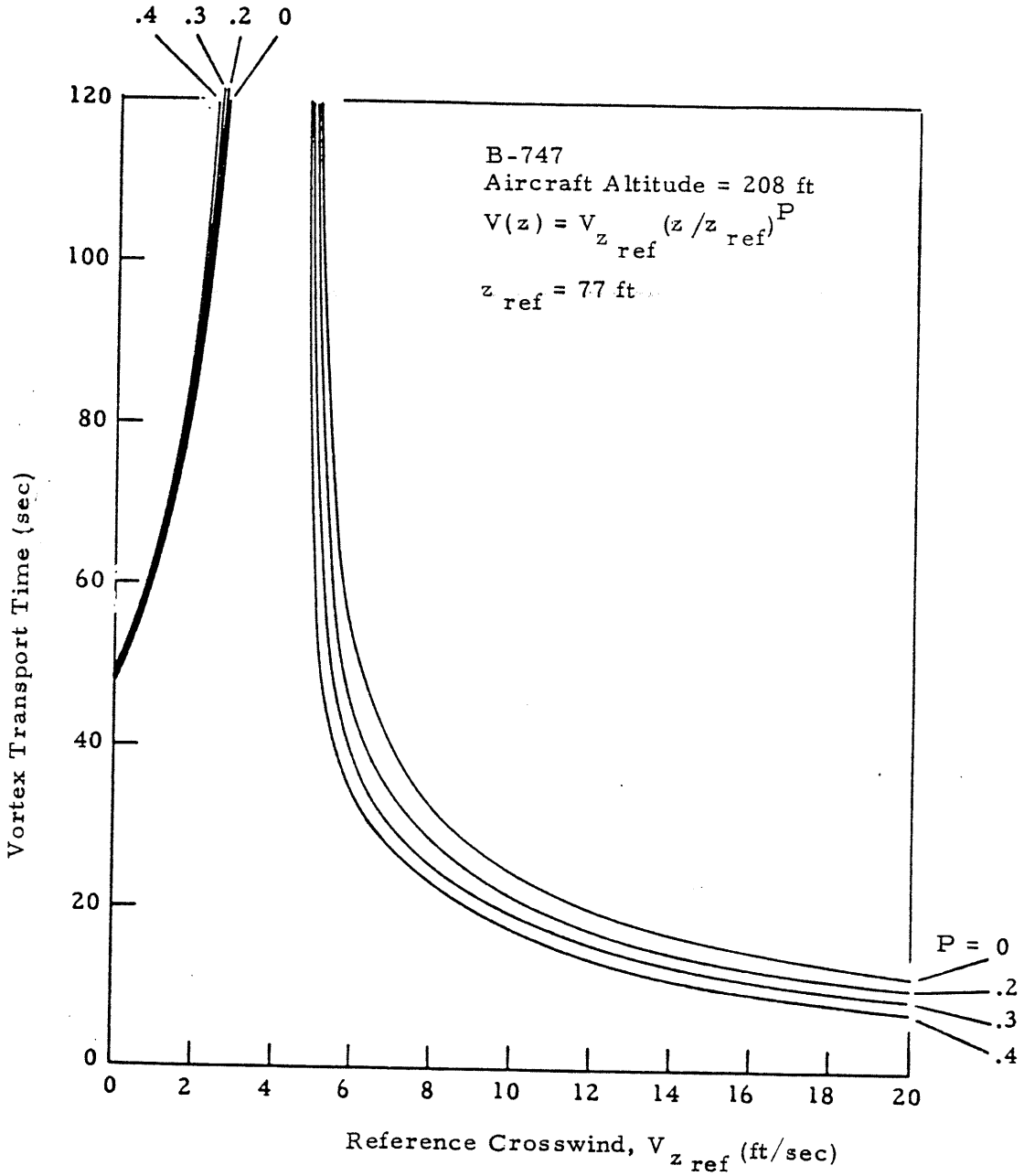

FIGURE 11. CALCULATED TRANSPORT TIME FOR CROSSWIND DESCRIBED BY POWER-LAW PROFILE WITH MODIFIED REFERENCE ALTITUDE

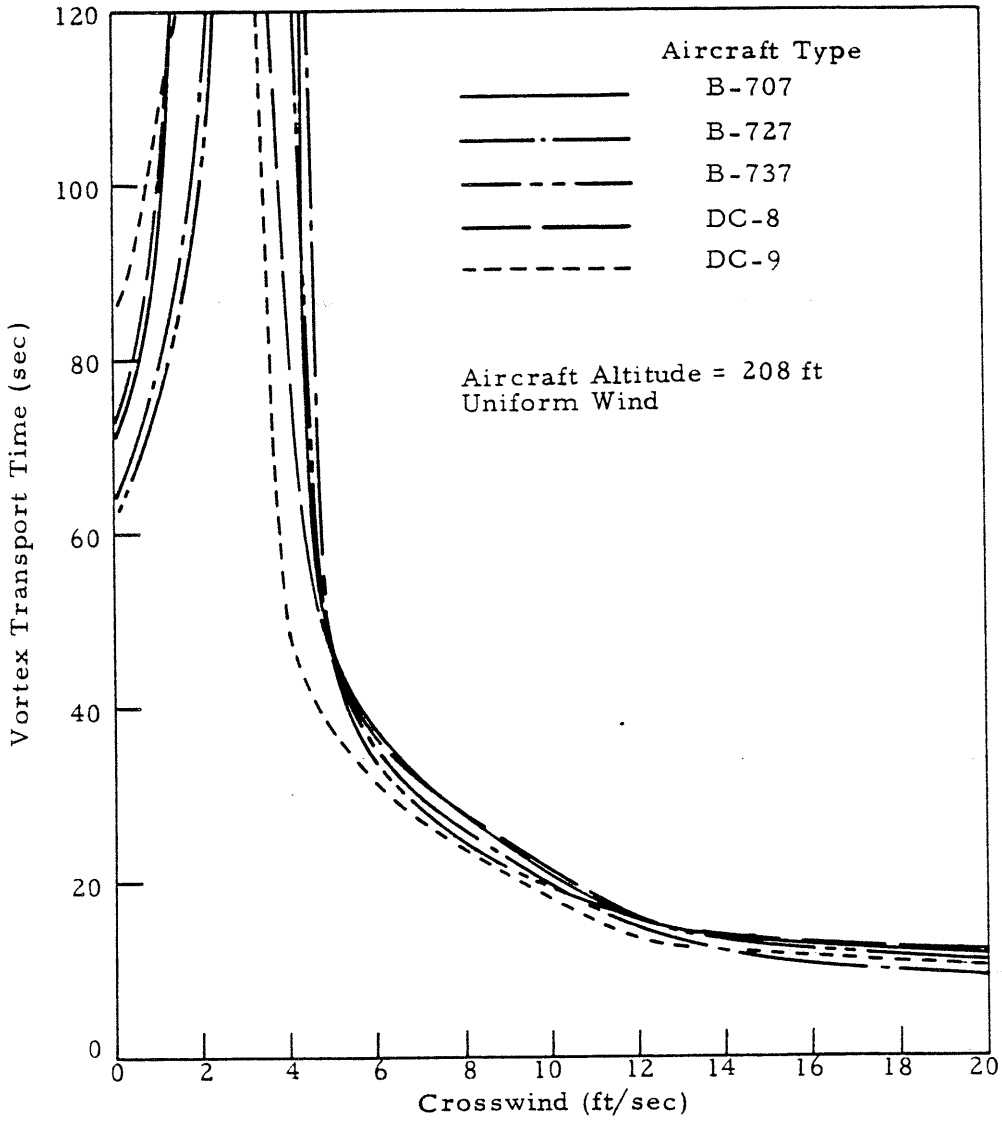

FIGURE 12. CALCULATED VORTEX TRANSPORT TIME FOR LARGE TRANSPORTS IN UNIFORM WIND

the wind-fixed coordinate system is a hyperbola which passes through the initial vortex position of the vortex, regardless of the speed at which the vortex moves along the trajectory. Therefore, for a given initial vortex position, the transport time is a function of the speed with which the vortex moves along the trajectory, which is proportional to the initial vertical speed of the vortex pair. This speed is (Ref. 3)

$$\frac{dZ}{dt} = - \frac{C_L U_\infty}{4 \pi K^2 AR} \tag{56}$$

where

C_L = lift coefficient

and

AR = wing aspect ratio.

The nominal values of each of the parameters affecting vertical speed (i.e., lift coefficient, C_L; approach air speed, U_∞; spanwise loading coefficient, K; and aspect ratio, AR) do not vary significantly between different aircraft types. This is shown in Table 1, which shows that vertical speeds of the vortex pair do not vary greatly between aircraft types. Therefore, it should be expected that transport times which are based upon nominal values of aircraft parameters should not be expected to be significantly different for different aircraft types. Figures 8 and 12 show some difference between wide-body aircraft (as a class) and narrow-body aircraft (as a class).

The influence of aircraft landing weight on the wake vortex transport time in the approach corridor for a given aircraft type is shown in Fig. 13. The results indicate that the vortex transport time is very sensitive to the aircraft landing weight at low crosswind conditions, i.e., < 7 ft/sec. If the crosswind is strong enough so that the vortex leaves the flight corridor before entering ground effect, aircraft weight has no effect on vortex transport time. If ground effect occurs within the vortex corridor, there are two mechanisms by which weight affects transport time. First, both the descent velocity and the

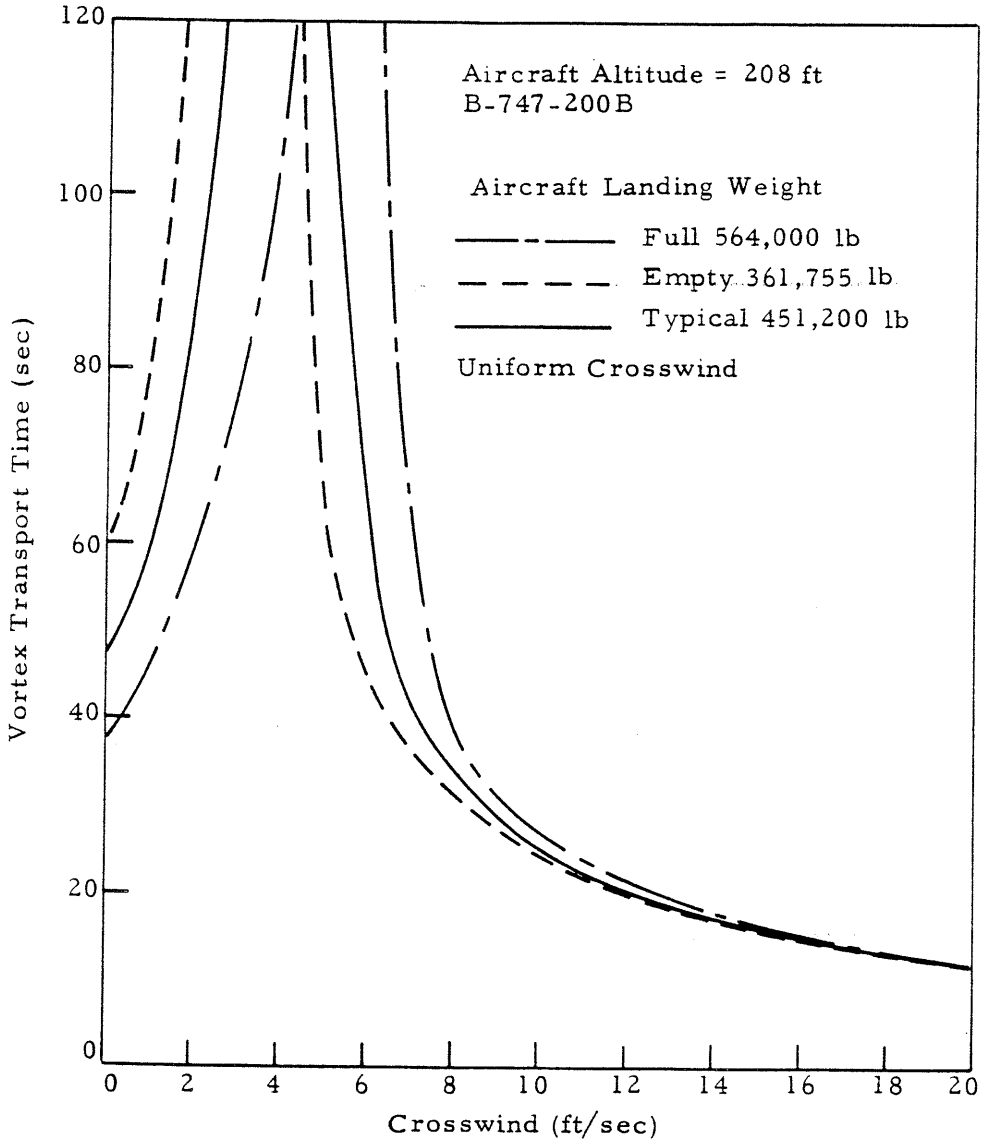

FIGURE 13. EFFECT OF AIRCRAFT LANDING WEIGHT ON CALCULATED TRANSPORT TIME

velocity at which each vortex moves horizontally (relative to the wind) in ground effect are directly proportional to aircraft weight for constant flight speed. The descent velocity (alternative form of the above equation) for an elliptically loaded wing is (Ref. 3)

$$\frac{dZ}{dt} = - \frac{8L}{\pi^3 \rho U_\infty b^2} , \tag{57}$$

where

L = lift,
ρ = atmospheric density,
U_∞ = flight speed,
b = wing span.

Equation (57) is identical with Eq. (56) with

$$K = \pi/4 \tag{58}$$

for an elliptically loaded wing and

$$L = \frac{1}{2} \rho C_L b^2 U_\infty^2 / AR . \tag{59}$$

The asymptotic velocity at which the vortex moves horizontally with respect to the wind in ground effect may be shown to be (i.e., let $Y >> Z$ in Eq. (11), use Eq. (10) for Z, let $Y_o = \pi b/8$ for elliptic wing loading, and let vortex strength, $\Gamma = 4L/\pi \rho U_\infty b$ (Ref. 3))

$$\dot{Y} = \frac{L}{\pi^2 \rho U_\infty b} \sqrt{\frac{64}{\pi^2 b^2} + \frac{1}{Z_o^2}} \tag{60}$$

where Z_o is the initial vortex altitude. This velocity reduces to the magnitude of the initial descent velocity as Z_o becomes large. Because of this effect, an increase in the aircraft landing weight decreases the vortex transport time when the crosswind is below the critical value of crosswind (i.e., the value of crosswind below which the upwind vortex exits from the upwind boundary) because the increased horizontal velocity of the upwind vortex acts with the wind in removing the vortex from the flight corridor. An increase in aircraft weight increases the vortex transport time when the crosswind is above the critical value of crosswind because the increased horizontal velocity acts against the crosswind in removing the vortex from the flight corridor.

Second, an increase in the landing weight increases the critical value of crosswind at which the vortex stalls in the approach corridor, and which also discriminates between upwind and downwind exit of the upwind vortex. In general, the upwind vortex exits the corridor from the upwind boundary if (cf. Section 2.1.1)

$$V_\infty < \Gamma \sqrt{C/4\pi} \tag{61}$$

and from the downwind boundary if

$$V_\infty > \Gamma \sqrt{C/4\pi} \ . \tag{62}$$

Since for a given aircraft configuration the vortex strength is directly proportional to aircraft weight, the critical value of the crosswind which discriminates between upwind and downwind exit of the vortex is directly proportional to aircraft weight.

The above discussion indicates that variations in aircraft weight have a much greater effect on vortex transport time than differences between aircraft types (within a class of wide-body or narrow-body aircraft).

The influence of aircraft altitude at the middle marker position on the wake vortex transport time is shown in Fig. 14. The results show that the

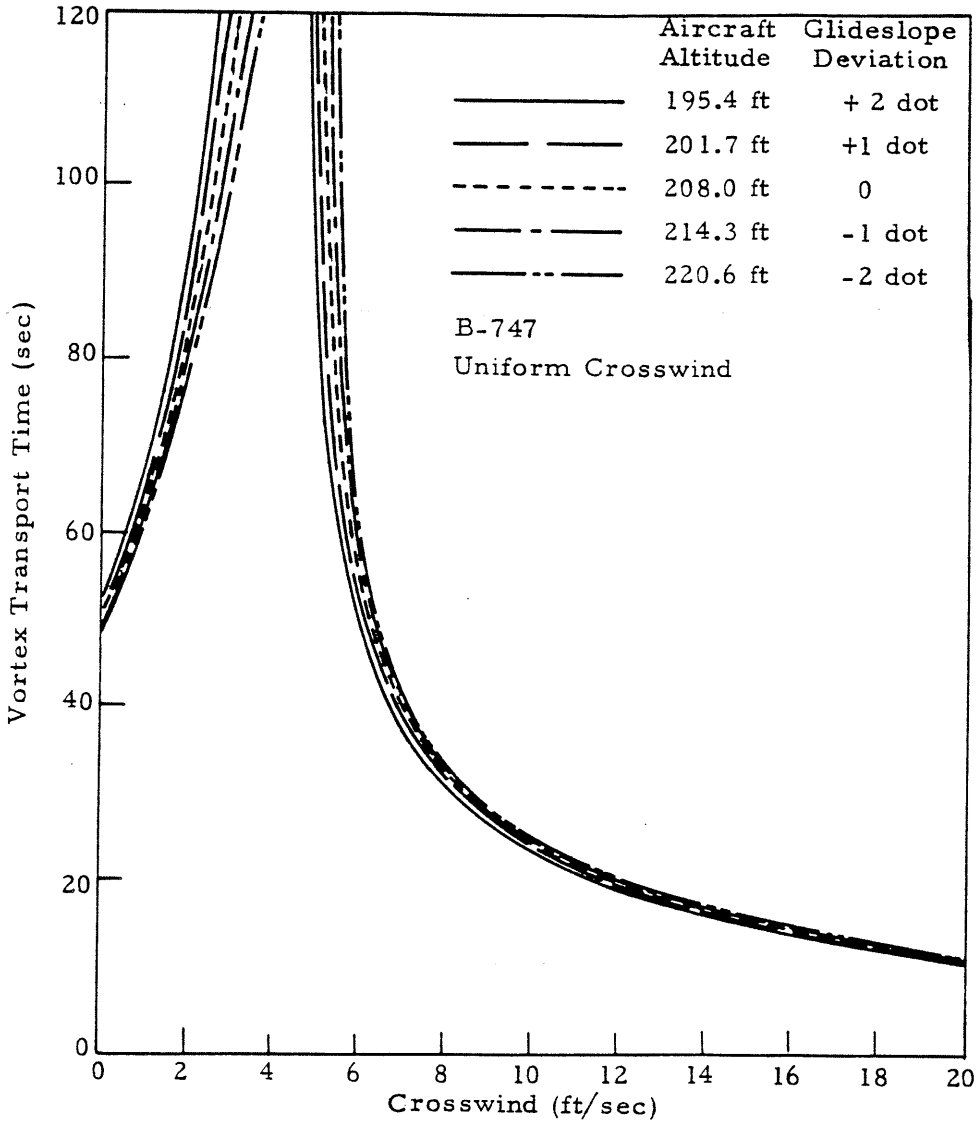

FIGURE 14. INFLUENCE OF AIRCRAFT ALTITUDE AT THE MIDDLE MARKER ON VORTEX TRANSPORT TIME

vortex transport time is relatively insensitive to normal variations in aircraft altitude. (Experienced pilots can generally stay on the glideslope within 1 division or dot on the glideslope indicator.)

The influence of aircraft lateral displacement on the wake vortex transport time in the vortex corridor is shown in Fig. 15. Variations in aircraft lateral displacement about the localizer centerline indicate a noticeable 20- to 80-sec variation in the vortex transport time at low crosswind velocities. For higher crosswind velocities, the effect of aircraft displacement on vortex transport time is small. It is noted that the $\pm$50-ft deviation from the localizer centerline is a $\pm 3\sigma$ variation (Ref. 19).

From the results shown above, variations in aircraft weight and lateral displacement from the localizer centerline can exert a significant influence on the calculated vortex transport time in the vortex corridor. Since the calculated vortex transport time in the WVAS is based on nominal values of aircraft parameters, this can be an important consideration. For example, the vortex of a B707-120 at minimum operating weight, spanwise loading coefficient of 0.8, 5 knots above nominal landing speed, and 10 ft above and 20 ft to the side of the ILS at the middle marker has a vortex strength of 1895 ft^2/sec and a transport time of 113 sec for no crosswind. By contrast, a B-707-320C at maximum landing weight, spanwise loading coefficient of 0.75, 5 knots below nominal landing speed, and centered on the ILS has a vortex strength of 4246 ft^2/sec and a transport time of 47 sec for no crosswind. The corresponding values for the nominal values of aircraft parameters shown in Table 1 is a vortex strength of 3135 ft^2/sec and a transport time of 66 sec.

In addition to the direct effect of unknown values of aircraft parameters by virtue of the effect on vortex descent rate, unknown values of aircraft parameters also affect vortex transport time in the determination of the

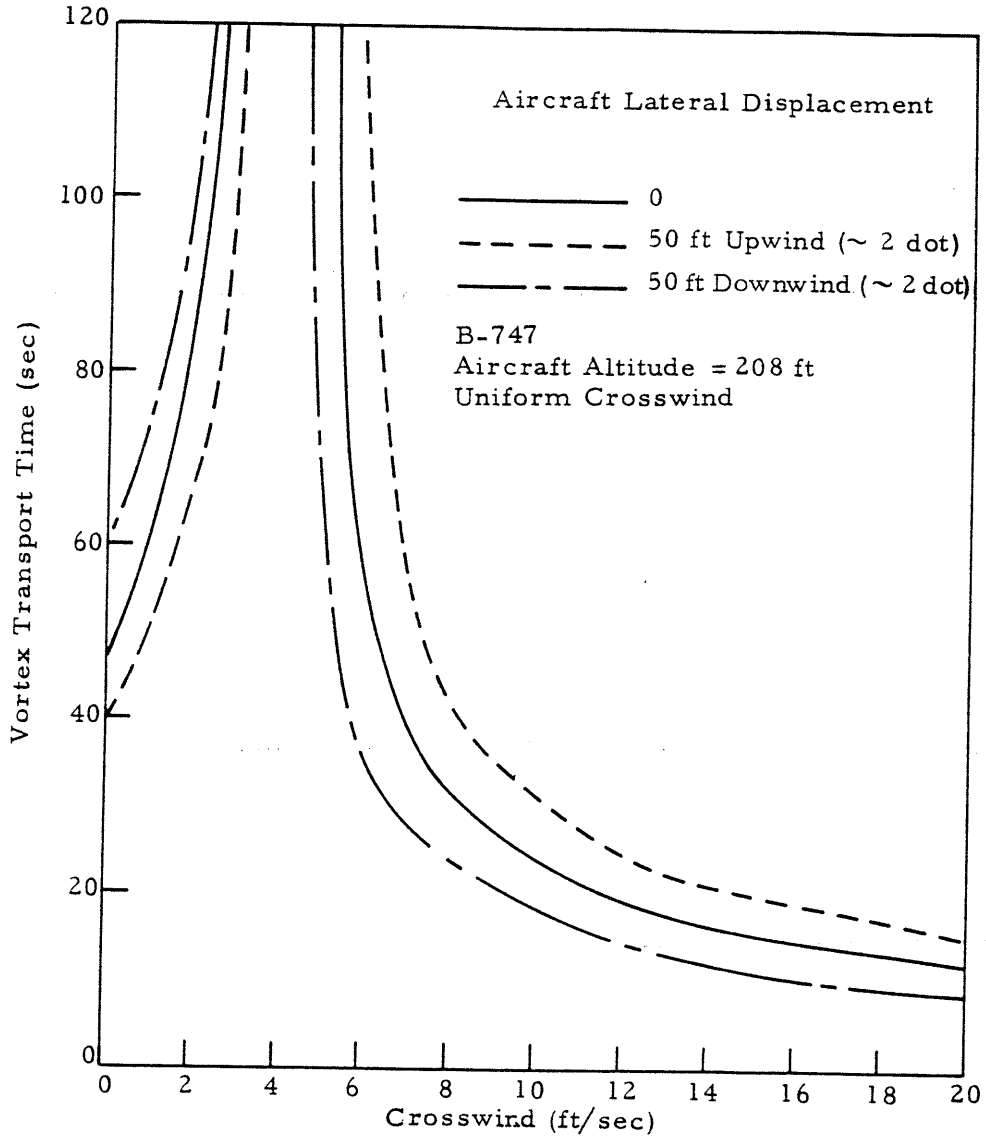

FIGURE 15. INFLUENCE OF AIRCRAFT POSITION FROM LOCALIZER CENTERLINE ON VORTEX TRANSPORT TIME

corridor boundary from which the upwind vortex exits. For constant crosswind, the upwind vortex for the B-707-120 described above will exit the upwind boundary for crosswinds less than 3 ft/sec and will exit the downwind boundary for crosswinds greater than 3 ft/sec. By contrast, for B-707-320C described above, the critical value of crosswind is 6.4 ft/sec. For the nominal condition (Table 1), the critical value of crosswind is 4.5 ft/sec. In a constant crosswind of 5 ft/sec, the B-707-120 would have a calculated transport time of 231 sec (although life time would prevent residence time from being that long).

Since the calculated vortex transport time is sensitive to aircraft weight, the above results suggest that an indirect determination of the aircraft weight through measurement of the vortex descent rate in the early part of the vortex trajectory may be a useful input to the WVAS. Aircraft weight can also be determined by pressure sensors under the flight path (Ref. 12). The pressure sensor senses the downwash of the aircraft as it passes the sensor.

2.2.3 Influence of Initial Altitude on Calculated Vortex Transport Time

One of the most important influences on vortex transport time is the influence of initial aircraft altitude. All aircraft altitudes between 20 ft (the altitude of the wing at touchdown) and 200 ft (the middle marker) are of concern because a following aircraft is sufficiently low that it may encounter a vortex in ground effect. From the results of Section 2.1.1, Eqs. (35) and (36), the upwind vortex exits the flight corridor from the downwind vortex corridor boundary if

$$V_\infty < \Gamma\sqrt{C}/4\pi = \frac{\Gamma}{4\pi Y_o}\sqrt{1+Y_o^2/Z_o^2} \qquad (63)$$

and from the upwind vortex corridor boundary if

$$V_\infty > \frac{\Gamma}{4\pi Y_o}\sqrt{1+Y_o^2/Z_o^2} \qquad (64)$$

The value of the critical crosswind velocity which discriminates between downwind and upwind exit of the upwind vortex is a strong function of Z_o at low altitudes (i.e., $Y_o/Z_o > 1$). Therefore, a crosswind which would cause the upwind vortex to rapidly exit the flight corridor for an aircraft altitude of 200 ft can cause the vortex to stall in the flight corridor for an aircraft altitude of less than 50 ft. Figure 16 shows vortex transport time as a function of crosswind for initial vortex altitudes of 200, 120, 80, and 40 ft.

Figure 16 presents a very important conclusion which is not evident from the data measured at JFK. The lowest altitude for which a significant quantity of JFK data was available was 130 ft, and the phenomenon shown in Fig. 16 would not be evident at that altitude. Figure 16 indicates that a short vortex transport time at one point along the flight path (from the middle marker to the touchdown zone) does not imply a short transport time at all points along the flight path. Figure 16 shows that, since the aircraft must traverse all altitudes between 200 ft and 40 ft, there is always a range of points along the flight path for which the calculated vortex transport time exceeds 120 sec when the crosswind is between 3 ft/sec and 14 ft/sec.

In interpreting Fig. 16, it must be remembered that it is assumed that the vortex roll-up process occurs out of ground effect and that the vortex then descends into ground effect. However, it is expected that when the vortex roll-up occurs in ground effect, the ground has a significant effect on the roll-up process. Little analytical or experimental work on the roll-up process in ground effect or on vortex demise mechanisms which may exist when roll-up occurs in ground effect has been done. Limited measurements (Ref. 19) indicate that vortices generated at altitudes less than a quarter of a wing span dissipate rapidly. It is expected that vortex life time is a monotonic decreasing function of altitude as the altitude at which the vortex was generated decreases from less than half of a wing span. (Unpublished data tends to corroborate this statement.)

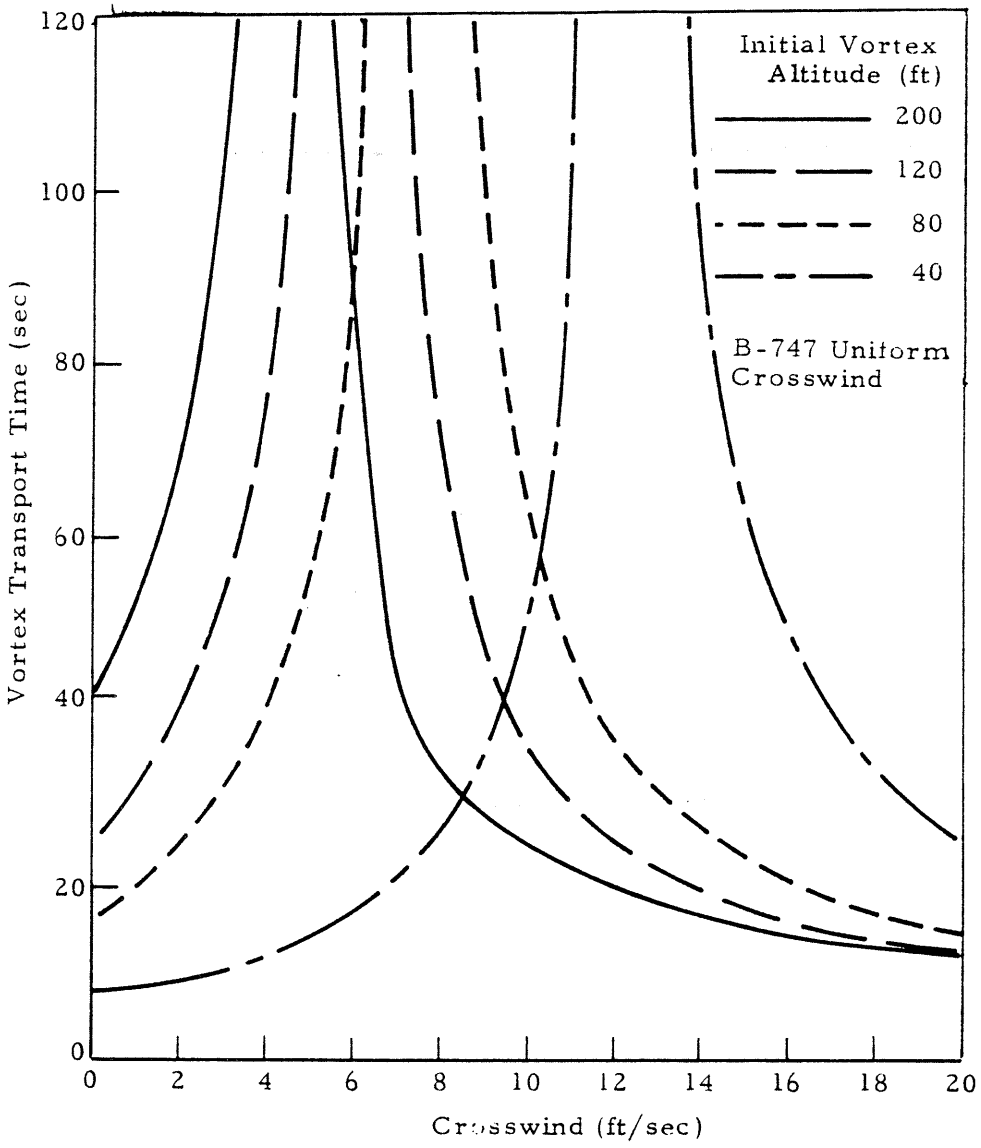

FIGURE 16. INFLUENCE OF INITIAL VORTEX ALTITUDE ON VORTEX TRANSPORT TIME

2.2.4 Influence of Other Vortex Phenomena

Two vortex phenomena have been omitted from consideration in this study because their influences are minor and are not completely understood. These are the influences of wind shear and vortex buoyancy (Ref. 30).

The tilting or banking of the plane containing the vortex pair has been observed experimentally at altitude (Ref. 31) and in ground effect (Ref. 32), as well as in operational situations (Refs. 33 and 24). Occasionally in the light aircraft tests, long segments of the wake were observed to roll past the vertical resulting in bank angles exceeding 90 degrees. It appears that crosswind shear or crosswind shear gradients are responsible for the observed rolling tendency of wakes.

Crosswind shear (change in crosswind with respect to altitude) in the vicinity of the wake implies an ambient, coherent vorticity field aligned parallel with the vorticity associated with the vortex pair. Interactions between the two vortical flows could produce opposite changes in the circulations of the counter-rotating vortices. Thus, the velocities induced by each vortex on the other (the descent speeds) would be unequal and wake roll, manifesting itself as an altitude mismatch between vortices, could occur for the descending pair.

There is, however, a lack of definitive experimental evidence or agreement about which direction the wake will roll under given shear conditions — apparently because of the relatively weak deterministic influences of shear on wake roll. For light shear, it is possible that random vertical atmospheric convection of each of the vortices could overwhelm any shear-induced motions, resulting in atmospherically influenced, random roll directions. For increasing shear however, any deterministic shear effects should produce definite wake-rolling behavior. Full-scale aircraft wake measurements by Tombach et al. (Ref. 32) show a definite negative correlation between the sense of the shear and the sense of the tilting, so that the upwind vortex (the shear being

produced in the sense of that of a boundary layer) descends relative to the downwind vortex a large percentage of the time, especially when the shear strength becomes significant. On the other hand, measurements reported by Brashears et al. (Ref. 24) show tilting in both directions, with a preference for tilting in the opposite sense to that noted by Tombach et al. when the shear was relatively strong. The Brashears et al. data also show, for weak shears, a tendency toward tilting in the same sense as that noted by Tombach. In this case, however, random effects could dominate the weak deterministic influence of the shear. In fact, the Brashears et al. data show the least tendency for tilting at a nonzero value of shear, where the opposite strong shear and weak shear tendencies are balanced out. An explanation for this behavior is not apparent however. Variations in ground effects and differences in aircraft scale between the two sets of data may be a factor.

In addition to the tilting, another dramatic (and operationally more significant) aspect to wake behavior occurs simultaneously. Whenever the wake banks, the upper (generally downwind) vortex appears to break up (decay) well ahead of the other vortex, often leaving one vortex drifting alone for some time before it decays. The single remaining vortex does not attempt to link with its image below the ground as has been observed when both vortices appproach the ground, but rather invariably experiences vortex breakdown.

It appears that the factors causing vortex tilting are neither intuitively obvious nor have they been sufficiently illuminated by full-scale, atmospheric flight tests, or theoretical analysis. The most significant aspect of wake tilting from an operational standpoint is the occurrence of the solitary vortex. It is undoubtedly some manifestation of flow asymmetry associated with wind shears, turning flight, etc., which produces the conditions for the creation of the solitary vortex, which so far has eluded proper understanding. Such long-lived vortices could present operational hazards since they appear to be rare events and, as such, the conditions for their occurrence may not be predictable.

Because the mechanisms of wind shear in influencing wake tilting is incompletely understood and is an anomolous condition, it was decided to omit it from the analytical modeling of vortex behavior in this study.

The upward acceleration, a, of the vortex due to buoyancy is

$$a = \frac{2g}{\rho_\infty r_c^2} \int_o^{r_c} (\rho_\infty - \rho(r))\, r\, dr \tag{65}$$

where

g = acceleration due to gravity = 32.2 ft/sec^2

ρ_∞ = ambient air density

r_c = radius of the outer boundary of the vortex cell

$\rho(r)$ = vortex air density

r = radial coordinate direction of the vortex.

For the static underpressure due to the vortex motion (Ref. 3)

$$\rho(r) = \left[\rho_\infty^{k-1} - \frac{k-1}{k} \frac{\rho_\infty^{k}}{\rho_\infty} \frac{\Gamma^2}{2\pi r^2} \right]^{\frac{1}{k-1}} \tag{66}$$

where

k = ratio of specific heats for air = 1.4

ρ_∞ = atmospheric pressure.

For a B-707 with a vortex strength, Γ, of 3137 ft^2/sec and a vortex cell radius, r_c, of 20 ft, the upward acceleration is 0.65 ft/sec^2 or approximately

0.02 g. For buoyancy caused by engine exhaust entrainment,

$$\rho = \rho_\infty \, T_\infty / T \tag{67}$$

where

T_∞ = ambient air temperature

T = vortex air temperature.

Then

$$a = g(1 - T_\infty / T) \tag{68}$$

An engine exhaust entrainment which causes the vortex to be 10°F warmer than the surrounding atmosphere will induce a 0.017g upward acceleration. The effect of descent through a non-adiabatic atmosphere is described by Eq. (68). (In an adiabatic atmosphere the vortex always has the same temperature as the atmosphere since it is compressed adiabatically as it descends). The standard atmosphere temperature lapse rate at the surface is -1.56°F/1000 ft. Therefore, if the vortex descends 100 ft through an isothermal atmosphere, the temperature difference between the vortex and the atmosphere is 0.156°F, and the corresponding acceleration due to buoyancy is 0.00029 g (assuming $T_\infty = 540^\circ$R).

The effect of vortex buoyancy on vortex transport was not included in the analytical calculation of vortex transport for several reasons. First, the effect of vortex buoyancy due to descent through a non-adiabatic atmosphere is negligible. Second, confirmation of the effects of exhaust entrainment would require measurement of the temperature of the vortices. Such measurements were beyond the intent of the study. Third, the effect of static underpressure requires a good estimate of the vortex cell boundary radius, r_c. This number cannot be easily defined. Fourth, since both buoyancy

and vortex decay cause an upward acceleration of the vortex, it would be difficult to distinguish the effects of buoyancy from the effects of decay from the measured data. Fifth, there is some drag mechanism which prevents the vortex from accelerating without bound and causes the vortex to reach a terminal velocity which is believed to be small because the buoyant forces are of the order of 0.02 g. (The phenomenon is similar to the one in which a helium-filled balloon quickly reaches a terminal velocity relative to its surrounding air.)

The justification for omitting the effect of buoyancy from the analytic model is the measured vortex trajectories from JFK. If buoyancy is present (and the vortices move vertically through the air which surrounds them), they will move together since they are acted upon by the Kutta-Joukowski force. The Kutta-Joukowski force on a body with circulation and velocity through a fluid is

$$F = -\rho_\infty (\dot{\bar{Z}} - \bar{w}) \times \Gamma \tag{69}$$

where w is the velocity of the surrounding air. Since there was no observable tendency for the vortices to move toward each other, it is concluded that buoyancy is not a significant phenomenon affecting vortex transport.

2.3 VORTEX DEMISE

The previous discussion has centered on vortex transport. At the initiation of the study under which this report is written it was believed that vortex transport was a far more dominant mechanism in the determination of vortex residence time than was vortex demise. Therefore, the vortex tracking algorithm used for processing data from the ground wind vortex sensing system at JFK does not accurately determine vortex life time. None of the vortex sensing systems which were included in this analysis measured vortex strength (although the LDV can measure vortex strength when operated in a different scan mode). The monostatic acoustic vortex

sensing system was at the JFK test site and it can measure vortex strength, but it was not included in the DMS because of lack of concurrent meteorological data.

There are three mechanisms by which vortex demise (i. e., the limit to vortex life time) may occur. The first and second are vortex bursting and mutual annihilation by Crow Instability. Both of these are catastrophic mechanisms of vortex demise. The third mechanism is viscous decay by which the strength of the vortex decreases sufficiently so that it will not be hazardous to following aircraft. Usually, one of the catastrophic demise mechanisms is the limiting factor for vortex life time. The mechanisms of vortex demise are summarized in Ref. 3.

Figure 17 shows distribution functions of vortex life time for given values of wind speed as measured at Heathrow International Airport (Ref. 12). The figure clearly shows that life time places an upper bound on residence time, even if transport time is large.

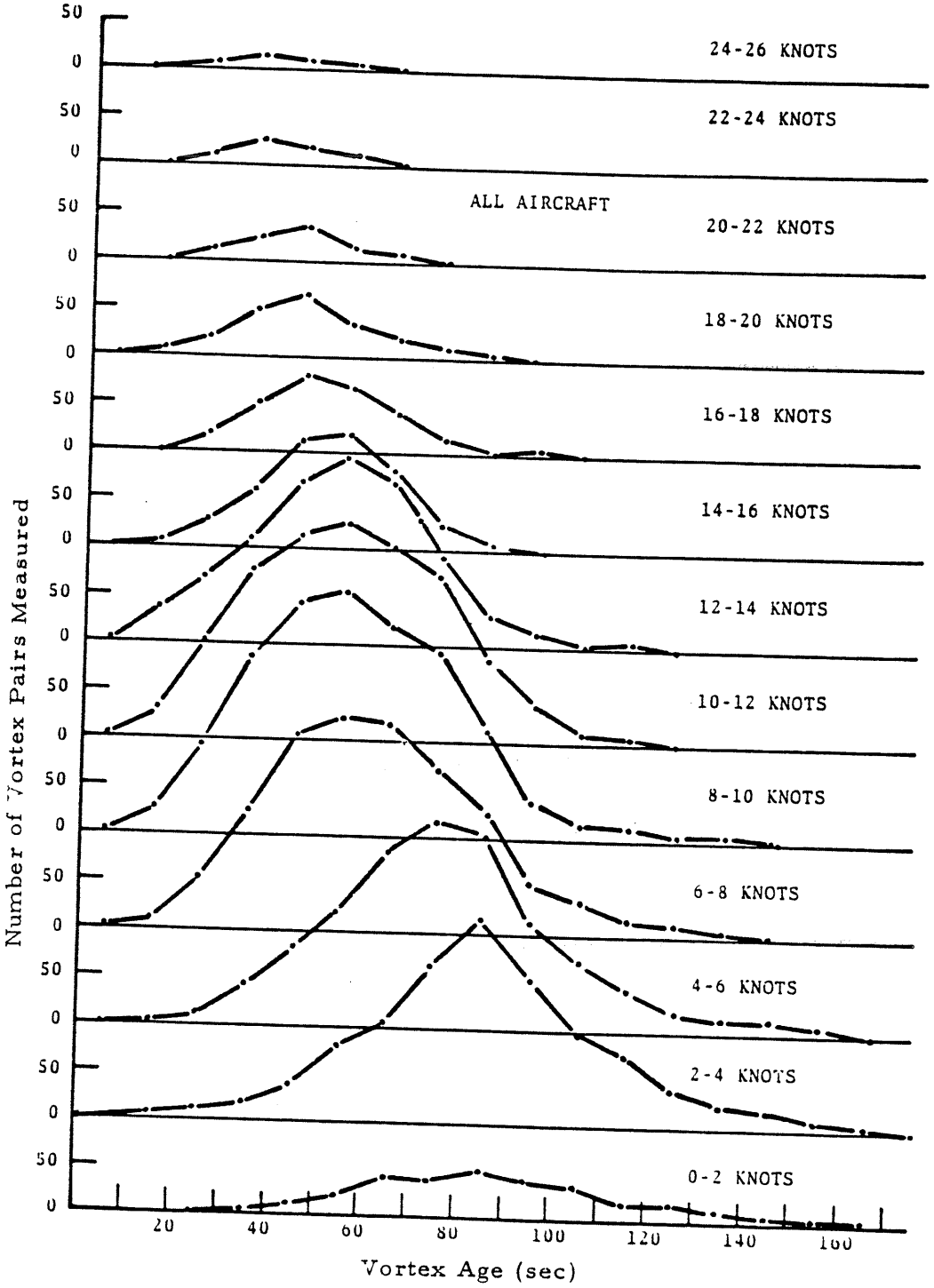

FIGURE 17. DISTRIBUTION OF VORTEX LIFE TIMES

3. DATA BASE OF WAKE VORTEX AND METEOROLOGICAL MEASUREMENTS

The data base for the analysis of wake vortex behavior is wake vortex and meteorological measurements made by the Department of Transportation, Transportation Systems Center (DOT-TSC) at the John F. Kennedy International Airport (JFK) in Jamaica, New York, during 1975. In order to compile a data base of measured wake vortex parameters and measured meteorological parameters, the data have been incorporated into a computerized data management system (DMS). A total of 1320 flybys have been cataloged into the DMS. The cataloged data files contain vortex trajectories (vortex altitude and lateral position as a function of time) for two laser Doppler velocimeter systems, calculated vortex trajectories for each of four baselines, vortex trajectories (vortex lateral position as a function of time) for each of the three ground wind anemometer lines, vortex residence time (time for which the vortex remains in the flight corridor) for calculated and measured vortex trajectories, and selected meteorological parameters. To summarize the relevant characteristics of the wake vortex and meteorological measurements, a description of the test site and a brief discussion of the data acquisition, data processing, and the results from the general data base are given.

3.1 KENNEDY INTERNATIONAL AIRPORT TEST SITE

As a part of a comprehensive program by DOT-TSC to monitor the behavior of wake vortices in the vortex corridor, the meteorological and vortex parameters from aircraft landing on runway 31R at JFK were monitored by an array of ground wind anemometers, two laser Doppler velocimeter (LDV) systems, and four instrumented meteorological towers. Acoustic vortex sensors were also used, but the results were not placed in the data management system because of unavailability of concurrent meteorological data. A plan

view of the test site is given in Fig. 18, and a cross-sectional view of the instrumentation arrangement at baseline 1 is given in Fig. 19.

A log of aircraft flybys was maintained. Each log entry specified the aircraft type and time of passage over baseline 1. Aircraft models were not recorded. For example, a DC-8-50, DC-8-61, DC-8-62, and DC-8-63 would all be recorded as a DC-8.

3.2 METEOROLOGICAL PARAMETERS

A summary of meteorological measurements recorded is presented in Table 2. The table also shows a summary of meteorological parameters which were calculated from the measured parameters and stored in the data management system. Data averages were taken over 128 sec following aircraft passage. (The 128 sec is the time between successive aircraft for the 5-nautical-mile separation of a large aircraft following a heavy aircraft at a 135-knot approach speed.)

Table 3 shows the detailed list of measured and calculated meteorological parameters for which the DMS was designed. The DMS was designed to accommodate a larger set of meteorological parameters than that which was available at JFK. In particular, wind measurements at the 140-ft altitude of Tower 3 were not available at JFK, but are listed in Table 3 because the DMS was designed to accommodate such measurements. Where averages are listed (e.g., USTAR(14)), they are averages of all indicated values for which valid values could be calculated. (All values could not be calculated for all flybys because of missing data.) A description of the meteorological parameters shown and their relevance to vortex behavior is presented in Ref. 34.

The initial intent of the study described in this report included determining which set of meteorological parameters was the most useful for calculating or predicting vortex behavior. This necessitated the calculation of a large set of meteorological parameters to permit comparison of results based on different sets of meteorological parameters. Therefore, Table 3

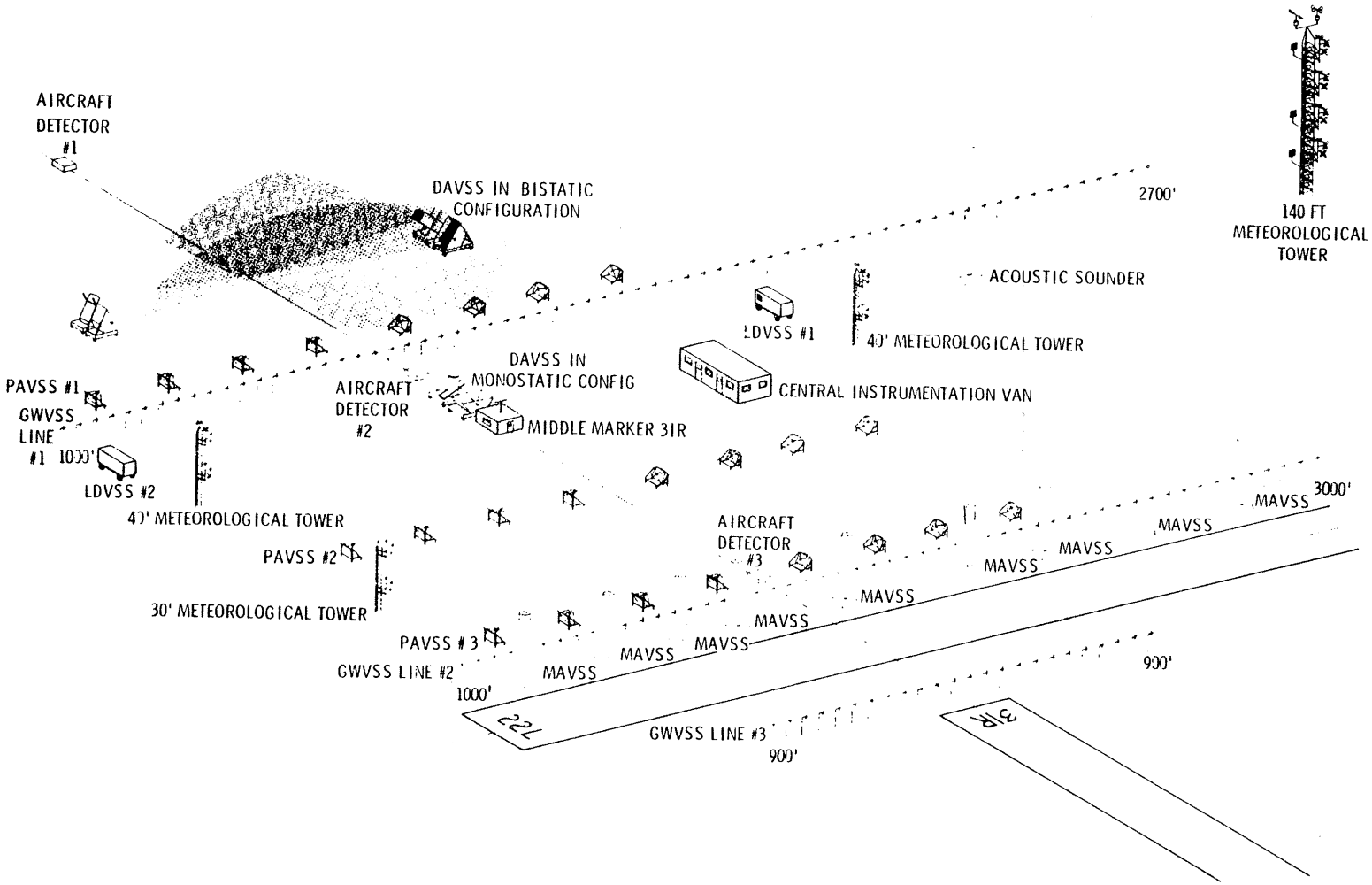

FIGURE 18. KENNEDY INTERNATIONAL AIRPORT TEST SITE

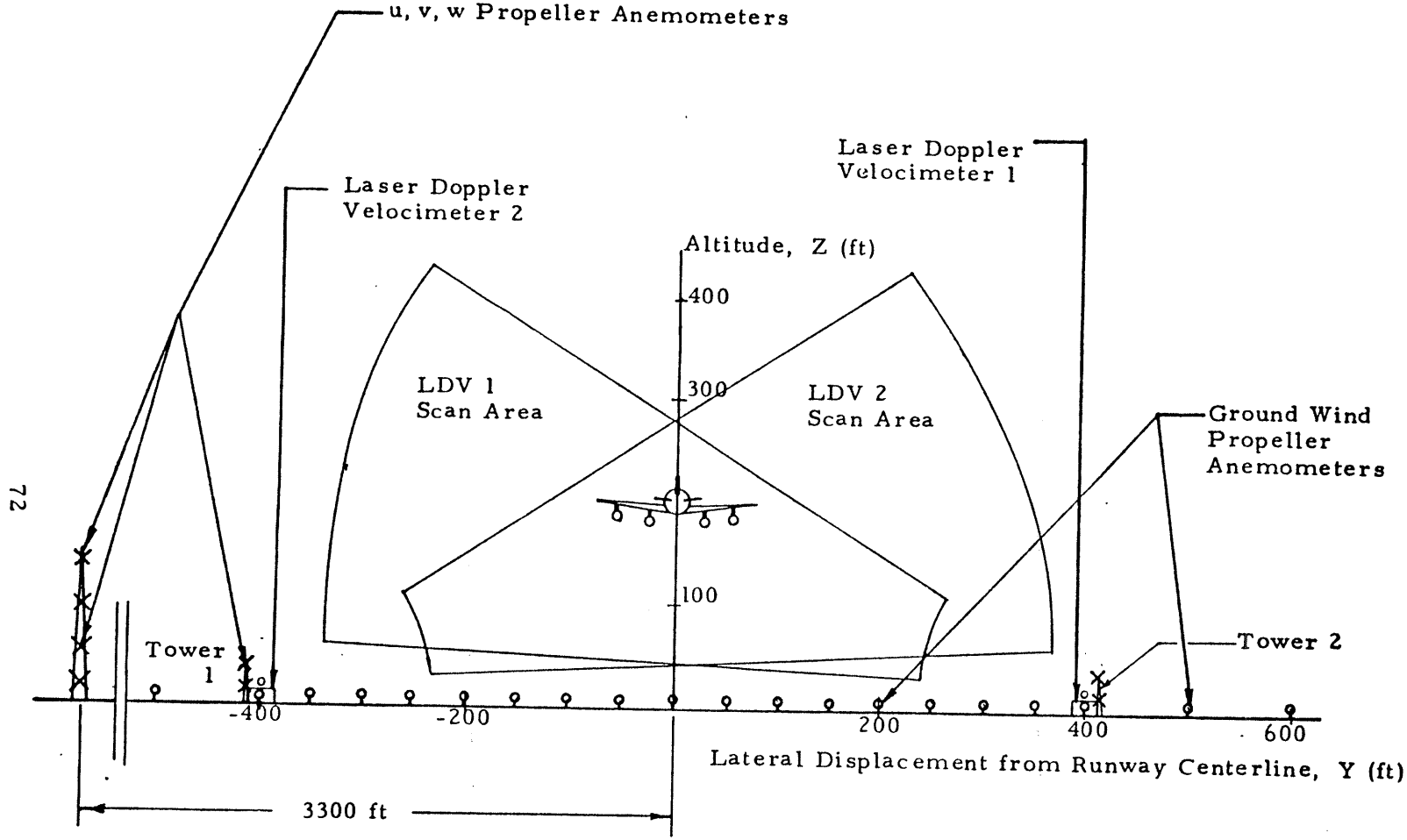

FIGURE 19. INSTRUMENTATION AT BASELINE 1 FOR WAKE VORTEX TESTS

Table 2

MEASURED WINDS AND CALCULATED METEOROLOGICAL PARAMETERS

Measured Winds

u = Headwind

v = Crosswind (positive from port side)

w = Vertical Component of Wind (positive upward)

Tower	Measurement Altitudes(ft)
1	20, 40
2	20, 40
3	25, 50, 100, 135
4	20, 30

Calculated Meteorological Parameters

Average of all winds for 128 sec after aircraft passage

Standard deviation of all winds for 128 sec after aircraft passage

Average wind speed for all winds for 128 sec

Average wind direction for all winds for 128 sec

$V_{z_{ref}}$ and P for least-squares fit for wind speed: $V = V_{z_{ref}} (z/z_{ref})^P$ for tower 3

A and B for least-squares fit for wind direction: $\theta = A + Bz$ for tower 3

Table 3

CALCULATED METHOROLOGICAL PARAMETERS AND SYMBOLS USED IN DATA REPORT*

Profile of Horizontal Component of Wind Velocity in Power-Law Form

PLAW	(1,1)	Tower 1	Reference Height
	(2,1)		Reference Velocity
	(3,1)		Exponent
	(1,2)	Tower 2	
	(2,2)		
	(3,2)		
	(1,3)	Tower 3	
	(2,3)		
	(3,3)		
	(1,4)	Tower 4	
	(2,4)		
	(3,4)		

Power-Law Profile for Horizontal Wind Speed

$$P = \frac{\ell n(u_h(2)/u_h(1))}{\ell n(z(2)/z(1))}$$

Wind Direction Profiles

NPOLY		Order of Polynominal
COEF	(1)	Least-Squares Curve Fit of
COEF	(2)	Coefficients for Polynominal
COEF	(3)	$\theta = COEF(1) + Z*COEF(2) + Z^2*COEF(3)$

Horizontal Wind Direction Profile, Tower 3

Profile of Horizontal Component of Wind Velocity in Logarithmic Form

USTAR1	(1)	20 and 40 ft Tower 1
	(2)	20 and 40 ft Tower 2
	(3)	25 and 50 ft Tower 3
	(4)	25 and 100 ft Tower 3
	(5)	25 and 135 ft Tower 3
	(6)	25 and 140 ft Tower 3
	(7)	50 and 100 ft Tower 3
	(8)	50 and 135 ft Tower 3
	(9)	50 and 140 ft Tower 3
	(10)	100 and 135 ft Tower 3
	(11)	100 and 140 ft Tower 3
	(12)	135 and 140 ft Tower 3
	(13)	20 and 30 ft Tower 4
	(14)	Avg. of 1 → 13 for Type 1 Friction Velocity

Friction Velocity Type 1

$$u_* = \frac{0.4*(u_h(2) - u_h(1))}{\ell n\left(\frac{Z(2)}{Z(1)}\right)}$$

*Notation given at end of Table 3 .

**For tower 3, reference velocity and exponent obtained by least-squares curve fit for all four altitudes.

Table 3 (Continued)

Profile (Continued)

USTAR2	(1)	20 ft Tower 1
	(2)	40 ft Tower 1
	(3)	20 ft Tower 2
	(4)	40 ft Tower 2
	(5)	25 ft Tower 3
	(6)	50 ft Tower 3
	(7)	100 ft Tower 3
	(8)	135 ft Tower 3
	(9)	140 ft Tower 3
	(10)	20 ft Tower 4
	(11)	30 ft Tower 4
	(12)	Avg. of 1 – 11 for Type 2 Fric. Vel.

Friction Velocity Type 2

$$u_* = \frac{\sigma_h}{2.5}$$

USTAR4	(1)	Tower 1
	(2)	Tower 2
	(3)	Tower 3
	(4)	Tower 4

Average Friction Velocity for Tower (Type 1 and 2)

ROUGH1	(1)	20 and 40 ft Tower 1
	(2)	20 and 40 ft Tower 2
	(3)	25 and 50 ft Tower 3
	(4)	25 and 100 ft Tower 3
	(5)	25 and 135 ft Tower 3
	(6)	25 and 140 ft Tower 3
	(7)	50 and 100 ft Tower 3
	(8)	50 and 135 ft Tower 3
	(9)	50 and 140 ft Tower 3
	(10)	100 and 135 ft Tower 3
	(11)	100 and 140 ft Tower 3
	(12)	135 and 140 ft Tower 3
	(13)	20 and 30 ft Tower 4
	(14)	Avg. of 1 – 13 for Type 1 Roughness Length

Roughness Length Type 1

$$z_o = \exp\left[\frac{\frac{u_h(2)}{u_h(1)}\ln(z(1)) - \ln(z(2))}{\frac{u_h(2)}{u_h(1)} - 1}\right]$$

ROUGH2	(1)	20 ft Tower 1
	(2)	40 ft Tower 1
	(3)	20 ft Tower 2
	(4)	40 ft Tower 2
	(5)	25 ft Tower 3
	(6)	50 ft Tower 3
	(7)	100 ft Tower 3
	(8)	135 ft Tower 3
	(9)	140 ft Tower 3
	(10)	20 ft Tower 4
	(11)	30 ft Tower 4
	(12)	Avg. of 1 – 11 for Type 2 Roughness Length

Roughness Length Type 2

$$z_o = \exp\left(\ln(Z) - .5\frac{u_h}{\sigma_w}\right)$$

ROUGH4	(1)	Tower 1
	(2)	Tower 2
	(3)	Tower 3
	(4)	Tower 4

Average Roughness Length For Tower (Type 1 and 2)

Table 3 (Continued)

Wind Shear Parameters

VGRAD(1, 1)	20 and 40 ft Tower 1	u Wind Shear, $\partial u/\partial z$
(1, 2)	20 and 40 ft Tower 2	
(1, 3)	25 and 50 ft Tower 3	
(1, 4)	25 and 100 ft Tower 3	
(1, 5)	25 and 135 ft Tower 3	
(1, 6)	25 and 140 ft Tower 3	
(1,7)	50 and 100 ft Tower 3	
(1, 8)	50 and 135 ft Tower 3	
(1, 9)	50 and 140 ft Tower 3	
(1, 10)	100 and 135 ft Tower 3	
(1, 11)	100 and 140 ft Tower 3	
(1, 12)	135 and 140 ft Tower 3	
(1, 13)	20 and 30 ft Tower 4	
(1, 14)	Avg. of 1 – 13 for u Wind Shear	
VGRAD(2, 1)	20 and 40 ft Tower 1	v Wind Shear, $\partial v/\partial z$
(2, 2)	20 and 40 ft Tower 2	
(2, 3)	25 and 50 ft Tower 3	
(2, 4)	25 and 100 ft Tower 3	
(2, 5)	25 and 135 ft Tower 3	
(2, 6)	25 and 140 ft Tower 3	
(2, 7)	50 and 100 ft Tower 3	
(2, 8)	50 and 135 ft Tower 3	
(2, 9)	50 and 140 ft Tower 3	
(2, 10)	100 and 135 ft Tower 3	
(2, 11)	100 and 140 ft Tower 3	
(2, 12)	135 and 140 ft Tower 3	
(2, 13)	20 and 30 ft Tower 4	
(2, 14)	Avg. of 1 – 13 for v Wind Shear	
VGRAD(3, 1)	20 and 40 ft Tower 1	w Wind Shear, $\partial w/\partial z$
(3, 2)	20 and 40 ft Tower 2	
(3, 3)	25 and 50 ft Tower 3	
(3, 4)	25 and 100 ft Tower 3	
(3, 5)	25 and 135 ft Tower 3	
(3, 6)	25 and 140 ft Tower 3	
(3, 7)	50 and 100 ft Tower 3	
(3, 8)	50 and 135 ft Tower 3	
(3, 9)	50 and 140 ft Tower 3	
(3, 10)	100 and 135 ft Tower 3	
(3, 11)	100 and 140 ft Tower 3	
(3, 12)	135 and 140 ft Tower 3	
(3, 13)	20 and 30 ft Tower 4	
(3, 14)	Avg. of 1 – 13 for w Wind Shear	
VGRAD(4, 1)	20 and 40 ft Tower 1	u_h Wind Shear, $\partial u_h/\partial z$
(4, 2)	20 and 40 ft Tower 2	
(4, 3)	25 and 50 ft Tower 3	
(4, 4)	25 and 100 ft Tower 3	
(4, 5)	25 and 135 ft Tower 3	
(4, 6)	25 and 140 ft Tower 3	
(4, 7)	50 and 100 ft Tower 3	

Table 3 (Continued)

Wind Shear Parameters (Continued)

VGRAD	(4, 8)	50 and 135 ft Tower 3	u_h Wind Shear, $\partial u_h/\partial z$
	(4, 9)	50 and 140 ft Tower 3	
	(4, 10)	100 and 135 ft Tower 3	
	(4, 11)	100 and 140 ft Tower 3	
	(4, 12)	135 and 140 ft Tower 3	
	(4, 13)	20 and 30 ft Tower 4	
	(4, 14)	Avg. of 1 – 13 for u_h Wind Shear	
HORGR4	(1)	Tower 1	Average u Wind Shear for Each Tower
	(2)	Tower 2	
	(3)	Tower 3	
	(4)	Tower 4	

Temperature Parameters

TEMP	(1)	10 ft Tower 2	Temperature
	(2)	40 ft Tower 2	
	(3)	10 ft Tower 3	
	(4)	50 ft Tower 3	
	(5)	140 ft Tower 3	
TEMPA2		Average Temp. for Tower 2	°C
TEMPA3		Average Temp. for Tower 3	
TEMP	(6)	ΔT from (10 to 40 ft) Tower 2	°C/100 ft
	(7)	ΔT from (10 to 50 ft) Tower 3	
	(8)	ΔT from (10 to 140 ft) Tower 3	
ATEMP		Average ΔT from Tower 3	
TEMP	(9)	Potential Temp. from (10 to 40 ft) Tower 2	°C/100 ft
	(10)	Potential Temp. from (10 to 50 ft) Tower 3	
	(11)	Potential Temp. from (10 to 140 ft) Tower 3	
APTEMP		Average Potential Temp. from Tower 3	
PRESH		Pressure Millibars	
HUMED		Humidity Per Cent	

Stability Parameters

IPASQ	(1, 1)	Tower 1	Pasquill Class According to Power of Power-Law Curve
	(1, 2)	Tower 2	
	(1, 3)	Tower 3	
	(1, 4)	Tower 4	
	(2, 1)	Tower 1	Pasquill Class According to Air Speed at 10-ft level
	(2, 2)	Tower 2	
	(2, 3)	Tower 3	
	(2, 4)	Tower 4	
	(3, 2)	Tower 2	Pasquill Class According to dT/dZ
	(3, 3)	Tower 3	
RICH	(1)	Richardson Number, Tower 2	
	(2)	Richardson Number, Tower 3	
	(3)	Average Richardson Number	

Table 3 (Continued)

Stability Parameters (Continued)

DISIP	(1, 1)	20 ft Tower 1
	(2, 1)	40 ft Tower 1
	(3, 1)	20 ft Tower 2
	(4, 1)	40 ft Tower 2
	(5, 1)	25 ft Tower 3
	(6, 1)	50 ft Tower 3
	(7, 1)	100 ft Tower 3
	(8, 1)	135 ft Tower 3
	(9, 1)	140 ft Tower 3
	(10, 1)	20 ft Tower 4
	(11, 1)	30 ft Tower 4
	(12, 1)	Avg. of 1 – 11 for Dissipation Rate of Type 1
DISIP	(1, 2)	20 ft Tower 1
	(2, 2)	40 ft Tower 1
	(3, 2)	20 ft Tower 2
	(4, 2)	40 ft Tower 2
	(5, 2)	25 ft Tower 3
	(6, 2)	50 ft Tower 3
	(7, 2)	100 ft Tower 3
	(8, 2)	135 ft Tower 3
	(9, 2)	140 ft Tower 3
	(10, 2)	20 ft Tower 4
	(11, 2)	30 ft Tower 4
	(12, 2)	Avg. of 1 – 11 for Dissipation Rate of Type 2
DISIP	(1, 3)	20 ft Tower 1
	(2, 3)	40 ft Tower 1
	(3, 3)	20 ft Tower 2
	(4, 3)	40 ft Tower 2
	(5, 3)	25 ft Tower 3
	(6, 3)	50 ft Tower 3
	(7, 3)	100 ft Tower 3
	(8, 3)	135 ft Tower 3
	(9, 3)	140 ft Tower 3
	(10, 3)	20 ft Tower 4
	(11, 3)	30 ft Tower 4
	(12, 3)	Avg. of 1 – 11 for Dissipation Rate of Type 3
DISIP	(1, 4)	20 ft Tower 1
	(2, 4)	40 ft Tower 1
	(3, 4)	20 ft Tower 2
	(4, 4)	40 ft Tower 2
	(5, 4)	25 ft Tower 3
	(6, 4)	50 ft Tower 3
	(7, 4)	100 ft Tower 3
	(8, 4)	135 ft Tower 3
	(9, 4)	140 ft Tower 3
	(10, 4)	20 ft Tower 4
	(11, 4)	30 ft Tower 4
	(12, 4)	Avg. of 1 – 11 for Dissipation Rate of Type 4

Dissipation Rate Type 1

$$\epsilon^{1/3} = \frac{\text{(Friction Velocity)}}{(.4)^{1/3} z}$$

Dissipation Rate Type 2

$$\epsilon^{1/3} = (\text{Type 1}) \frac{\left((1 - \frac{1}{3}(\text{RICH}) * (1 - 18(\text{RICH}))^{1/4}\right)^{1/3}}{(1 - 18(\text{RICH}))^{1/3}}$$

Dissipation Rate Type 3

$$\epsilon^{1/3} = \frac{0.4^{2/3} u_h}{z^{1/3} \ln\left(\frac{z}{\text{(Roughness Length)}}\right)}$$

Dissipation Rate Type 4

$$\epsilon^{1/3} = \frac{0.4^{2/3} n}{z^{1/3}}$$

Table 3 (Continued)

Stability Parameters (Continued)

(13, 1)	Tower 1	Average Dissipation Rate for Each Tower (Types 1, 2, 3, 4)
(13, 2)	Tower 2	
(13, 3)	Tower 3	
(13, 4)	Tower 4	
BRUNT2	Brunt-Vaisala Period for Tower 2	
BRUNT3	Brunt-Vaisala Period for Tower 3	
STAB2	Stability Length for Tower 2	
STAB3	Stability Length for Tower 3	

Mean Wind and Wind Variance Parameters

VBAR(N, M)	N =	1	20 ft	Tower 1
		2	40 ft	Tower 1
		6	20 ft	Tower 2
		7	40 ft	Tower 2
		11	25 ft	Tower 3
		12	50 ft	Tower 3
		13	100 ft	Tower 3
		14	135 ft	Tower 3
		17	20 ft	Tower 4
		18	30 ft	Tower 4
	M =	1	u ft/sec	128-sec Average of Wind Velocity
		2	v ft/sec	
		3	w ft/sec	
		4	u_h ft/sec	
		5	v_h ft/sec	
		6	angle deg	
VVAR(N, M)	Same Nomenclature as Above			Variance of Wind Velocity for 128-sec Record.

Notation

P = power law exponent

u = down runway wind components

u_* = friction velocity for logarithmic profile

u_h = horizontal component of wind velocity

u_{href} = horizontal component of wind velocity at reference altitude

Table 3 (Concluded)

Notation (Continued)

v = cross runway wind component

w = vertical wind component

z = vertical coordinate direction

z_0 = roughness length for logarithmic profile

z_{ref} = reference altitude for power law profile

$\epsilon^{1/3}$ = turbulent dissipation rate

σ_h = standard deviation of horizontal component of wind velocity

is a list of all parameters which were deemed to have some relationship to vortex behavior.

3.3 VORTEX DETECTORS

The presence of wake vortices near the ground was detected by each of three rows of single-axis propeller driven anemometers as shown in Figs. 18 and 19. The propeller anemometers measure crosswind. In the data processing, if the variance of the signal from a single sensor did not exceed 0.02 $(ft/sec)^2$ over the 128-second average following aircraft passage, the lack of variance was interpreted as a sign that the anemometer was not functioning properly, and the sensor was declared to be dead. All active sensor data were filtered with a weighted 17-second averaging filter. The filter was weighted with a half sine wave extending over the averaging period. For the vortex tracking calculation, the position of the starboard vortex was the lateral position of the anemometer exhibiting the maximum crosswind velocity (using the filtered values). Similarly, the position of the port vortex was the lateral position of the anemometer exhibiting the minimum crosswind velocity. A sample vortex track as generated in this manner is shown in Fig. 20. A false indication of the vortex position occurs after the vortex leaves the lateral extent of the anemometer array.

The time of port (or starboard) vortex passage over an anemometer which had been determined to be closest to the vortex was defined as the time at which the wind measured by that sensor was a maximum (or minimum). By plotting the times at which the vortex passed over sensors at the various lateral positions, a plot of vortex lateral position as a function of time was generated. The vortex transport time was generated by smoothing the time-lateral position curve and determining the time at which the last vortex crossed the flight corridor boundary. False signals could easily be distinguished from true vortex tracks in determining residence time.

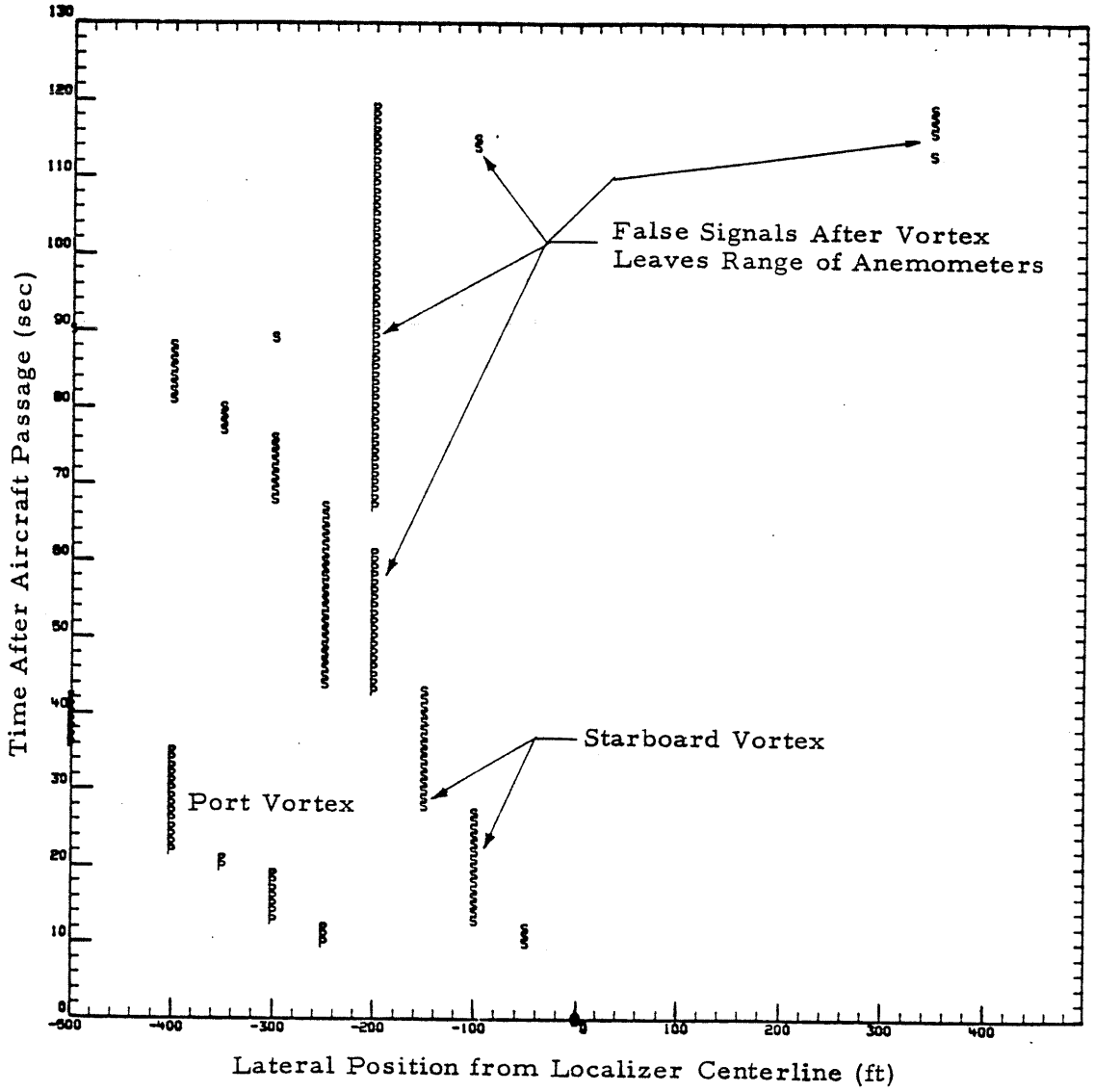

FIGURE 20. SAMPLE VORTEX TRACKS FROM GROUND WIND ANEMOMETER

Two characteristics of the ground wind sensor are important in interpreting data from it. First, reliable data are obtained only when the vortex is close to the ground. This limitation is inherent in the ground wind system. Second, false points could be generated after the vortex left the flight corridor. However, these were eliminated in the determination of transport time as described above.

Wake vortex trajectories were also measured by two laser Doppler velocimeter (LDV) systems deployed at JFK. The scan area used for the test is shown in Fig. 19. For each position of the focal volume in space, the backscattered laser intensity, I, and the aerosol velocity (line-of-sight velocity relative to the LDV system measured by the Doppler shift in the returned signal), V, were recorded. The data processing algorithm used to calculate vortex location is discussed in Ref. 15. It is presented briefly here.

For the first vortex, the algorithm checks the number of data points in a scan frame (i.e., a single complete scan of the scan area shown in Fig. 19) to ensure that a sufficient number of data points exist (> 2) to define a vortex. Then it selects the highest intensity, I, in a scan frame and uses the y, z coordinates of this point as the center of a correlation circle of radius R (Fig. 21), where R is selected by the system operator based on vortex generation, aircraft type, and previous experience. Once the correlation circle has been defined, the algorithm requires that at least B percent of the points which lie within the circle have an I greater than or equal to A percent of the initially selected I. If this criterion is not met, the selected I is discarded as a spurious signal, and the next highest I is selected until the A and B percentage criterion is met. Once this occurs, weighted average Y and Z position coordinates are computed for all points in the circle using intensity, I, and line-of-sight component of velocity, V, as the weighting function:

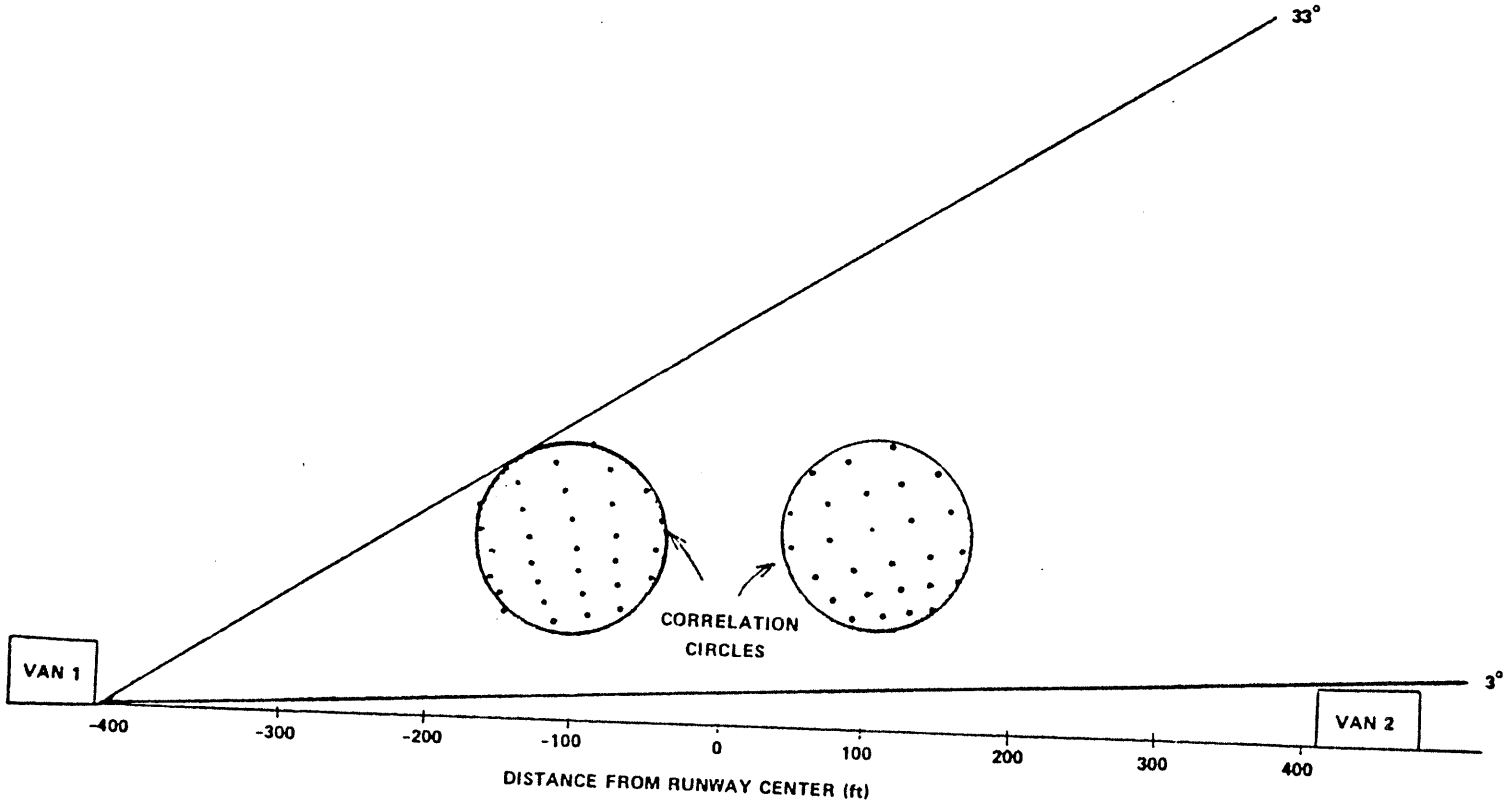

FIGURE 21. VORTEX LOCATION ALGORITHM OUTLINE (Ref. 15)

$$Y = \frac{\sum V_i I_i y_i}{\sum V_i I_i}$$

$$Z = \frac{\sum V_i I_i z_i}{\sum V_i I_i}$$

where Y and Z are the vortex centroid y and z positions, respectively.

Following this calculation, all the data points outside a circle of radius $N_s \cdot R$, centered at the previously calculated vortex center (Y, Z), are examined to determine the highest remaining V. (N_s is an operator-selectable multiplication factor (1,2,etc.).) If this point has C percent of the number of data points in its correlation region that were found in the first vortex's correlation region and if B percent of the point in its correlation region have V greater than A percent of the highest V in vortex one, then a second vortex exists in the scan frame. If this criterion is met, then a weighted average is found for its location as described for the first vortex.

3.4 CALCULATED VORTEX TRAJECTORIES

The calculated wake vortex trajectories were generated from a theoretical model (Ref. 3) using the aircraft location, wing span, weight, and airspeed as inputs. The spanwise wing loading was assumed to be elliptic. The input parameters and resulting vortex strength for each aircraft type are shown in Table 1. The aircraft were assumed to be centered on the runway centerline at altitudes of 200, 172, 135, and 78 ft, respectively, for baselines 1, 2, 3 and 4. Although the complete theoretical vortex transport model contains many transport and decay mechanisms, the calculated trajectories for the data management system considered vortex transport by mutual induction and crosswind only.

The trajectories were calculated by a fourth-order Runge-Kutta integration of the transport equations

$$\dot{Z} = \frac{-\Gamma}{2\pi(Y_2 - Y_1)} + \frac{\Gamma}{2\pi}\left[\frac{Y_2 - Y_1}{(2Z)^2 + (Y_2 - Y_1)^2}\right]$$

and

$$\dot{Y} = V_\infty \pm \frac{\Gamma}{4\pi Z}\left[\frac{(Y_2 - Y_1)^2}{(2Z)^2 + (Y_2 - Y_1)^2}\right]$$

where Z is the altitude of the vortices and Y_1 and Y_2 are the lateral positions of the port and starboard vortices, respectively. The + and - are applicable to the starboard and port vortices, respectively. The crosswind, V_∞, was that of the Tower 3 power-law profile. Therefore, for Tower 3,

$$V_\infty = V_{z\,ref}\,(z/z_{ref})^P \sin\theta$$

where θ is the wind direction profile as shown in Table 3.

3.5 VORTEX DATA REPORTS

The wake vortex and meteorological measurements obtained by the JFK data collection system have been processed with the DMS software, stored on tape and disk, and tabulated into data reports. A sample data report is shown in Tables 4-7 and Figs. 22-30. The definitions of the meteorological parameters are listed in Table 3. The calculated vortex trajectories for Baseline 2 have been omitted for brevity – no vortex measurements were made at Baseline 2. The data access keys (Table 7) are parameters which are used to selectively recall data from the DMS. The symbols used for the data access keys are shown in Table 8.

Table 4

WIND PROFILE PARAMETERS FOR DATA REPORT

MET DATA FOR FLYBY NUMBER 314 DATE 4/17/75 TIME OF DAY 16.35.47 AIRCRAFT TYPE DC8

PLAW(1,1) = 20.0000 PLAW(2,1) = 13.5482 PLAW(3,1) = .0749 PLAW(1,2) = 20.0000 PLAW(2,2) = 18.0988 PLAW(3,2) = -.0203

PLAW(1,3) = 20.0000 PLAW(2,3) = 16.5574 PLAW(3,3) = -.0575 PLAW(1,4) = 20.0000 PLAW(2,4) = 14.6972 PLAW(3,4) = -.1559

COEF(1) = -39.4638 COEF(2) = -.1302 COEF(3) = 13.9304 NPOLY = 1

	USTAR1	USTAR2	USTAR4	ROUGH1	ROUGH2	ROUGH4
1	.9167	.8316	.6291	.0000	.0016	.2658
2	-.1462	.6390	1.0563	.0000	.7957	.0007
3	-.7209	1.5665	.3335	.0000	.0002	.0003
4	*********	1.7485	.4639	*********	.0019	.0267
5	-.3702	1.4532		.0000	.0000	
6	*********	.9865		*********	.0019	
7	*********	*********		*********	*********	
8	-.1254	.7777		.0000	.0000	
9	*********	*********		*********	*********	
10	*********	.7577		*********	.0782	
11	*********	1.5223		*********	.0019	
12	*********	1.1426		*********	.0979	
13	-.8884			.0000		
14	-.3058			.0000		

VGRAD ARRAY

1	2	3	4	5	6	7	8	9	10	11	12	13	14
.0267	-.1451	-.2933	********	-.0490	********	********	.0228	********	********	********	********	.3786	-.0099
-.0267	-.2042	-.2145	********	-.0344	********	********	.0186	********	********	********	********	9665	.0842
.0490	-.2179	-.1582	-.0397	********	********	.0195	********	********	********	********	********	.2074	-.0150
.0361	.0127	-.0500	********	-.0142	********	********	-.0037	********	********	********	********	-.0901	-.0224

HORGR4(1) = .0361 HORGR4(2) = -.0127 HORGR4(3) = -.0226 HORGR4(4) = -.0901

RICH(1) = ********* RICH(2) = ********* RICH(3) = *********

GRUNT2 =**********GRUNT3 =**********STAB2 =**********STAB3 =**********

Table 5

TEMPERATURE, STABILITY, AND TURBULENCE PARAMETERS FOR DATA REPORT

MET DATA FOR FLYBY NUMBER 314 DATE 4/17/75 TIME OF DAY 16.35.47 AIRCRAFT TYPE DC8

			TEMP
TEMPA2 =	*********	1	*********
		2	*********
TEMPA3 =	*********	3	*********
		4	*********
ATEMP =	*********	5	*********
		6	*********
PRESH =	*********	7	*********
		8	*********
APTEMP =	*********	9	*********
		10	*********
HUMED =	*********	11	*********

IPASQ ARRAY

	1	2	3	4
1	1	0	0	0
2	3	3	3	3
3	0	0	C	0

DISIP ARRAY

	1	2	3	4
1	.0427	*********	.6271	.8644
2	.0213	*********	.4518	.4051
3	.0717	*********	.3525	3.0675
4	.0358	*********	.2584	3.0331
5	.0181	*********	.2723	2.4505
6	.0091	*********	.1883	.8963
7	.0045	*********	*********	*********
8	.0034	*********	.1223	.4000
9	.0032	*********	*********	*********
10	.0315	*********	.4440	.7176
11	.0210	*********	.3431	2.5369
12	.0238	*********	.3400	1.5961
13	.4021	1.1365	.3971	.6813

Table 6

MEAN WIND AND WIND VARIANCE PARAMETERS FOR DATA REPORT

MET DATA FOR FLYBY NUMBER 314 DATE 4/17/75 TIME OF DAY 16.35.47 AIRCRAFT TYPE DC8

VBAR ARRAY

	1	2	3	4	5	6
1	12.0480	-6.1966	-1.7792	13.5482	.0000	-27.2180
2	12.5829	-6.7312	.2007	14.2702	.0000	-28.1443
3	**********	**********	**********	**********	**********	**********
4	**********	**********	**********	**********	**********	**********
5	**********	**********	**********	**********	**********	**********
6	16.9669	-7.5105	2.6279	18.0988	.0000	-24.5177
7	13.5655	-11.5946	-1.7310	17.8454	.0000	-40.5210
8	**********	**********	**********	**********	**********	**********
9	**********	**********	**********	**********	**********	**********
10	**********	**********	**********	**********	**********	**********
11	14.3712	-8.2428	1.2430	16.5673	.0000	-29.8368
12	7.0379	-13.6056	-2.7117	15.3181	-.0000	-62.6483
13	5.0972	**********	-1.7342	**********	**********	**********
14	8.9772	-12.0253	**********	15.0066	-.0000	-53.2577
15	**********	**********	**********	**********	**********	**********
16	**********	**********	**********	**********	**********	**********
17	9.9640	-10.8040	-.3069	14.6972	.0000	-47.3162
18	13.7495	-1.1393	1.7666	13.7967	.0000	-4.7368

VVAR ARRAY

	1	2	3	4	5	6
1	3.4449	.9113	.5139	4.3222	17.0592	**********
2	2.0000	.5723	3.3175	7.5522	17.6067	**********
3	**********	**********	**********	**********	**********	**********
4	**********	**********	**********	**********	**********	**********
5	**********	**********	**********	**********	**********	**********
6	12.7962	2.6620	.5990	15.3374	5.6263	**********
7	11.1282	8.1295	.8046	19.1073	4.3593	**********
8	**********	**********	**********	**********	**********	**********
9	**********	**********	**********	**********	**********	**********
10	**********	**********	**********	**********	**********	**********
11	10.0095	3.2928	.3169	13.1984	7.9190	**********
12	1.2941	4.8364	.5635	6.0826	4.9939	.0000
13	2.6949	**********	.4929	**********	**********	**********
14	1.3633	2.4462	**********	3.7797	2.2134	**********
15	**********	**********	**********	**********	**********	**********
16	**********	**********	**********	**********	**********	**********
17	1.6622	1.9543	1.7569	3.5882	2.3580	**********
18	14.4981	.0997	2.065	14.4836	1.1483	**********

Table 7

VALUES OF DATA ACCESS KEYS
FOR DATA REPORT

BMS KEYS FOR FLYBY NUMBER	319	DATE 4/17/75	TIME OF DAY	16.35.47	AIRCRAFT TYPE DC8
SITENO =	1.0000		W-VAR =	3.3175	
RUNNO =	319.0000		UH-40 =	19.2702	
DAY =	107.0000		ANG-40 =	338.1443	
YEAR =	75.0000		PASQ-T =	.0000	
TIMEDA =	59747.0000		VDISP =	.0213	
AIRCFT =	DC8		W5HR1 =	-.2933	
LVAN1 =	0000002766		W5HR2 =	.0228	
LVAN2 =	0000002772		W5HR3 =	-.0490	
DACC1 =	0000000000		W5HR4 =	-.2145	
DACC2 =	0000000000		W5HR5 =	.0186	
PRED =	0000016104		W5HR6 =	-.0344	
GRND =	0000014032		PWRLWE =	-.0575	
PACC =	0000000000		PWRLWN =	20.0000	
MET =	0000011747		PWRLWV =	16.5574	
U-40 =	-12.5829		FRICV1 =	-.1254	
V-40 =	-6.7312		FRICV2 =	.7777	
W-40 =	.2007		LIFE1 =	93.9411	
U-VAR =	2.0000		LIFE2 =	67.9451	
V-VAR =	.5723				

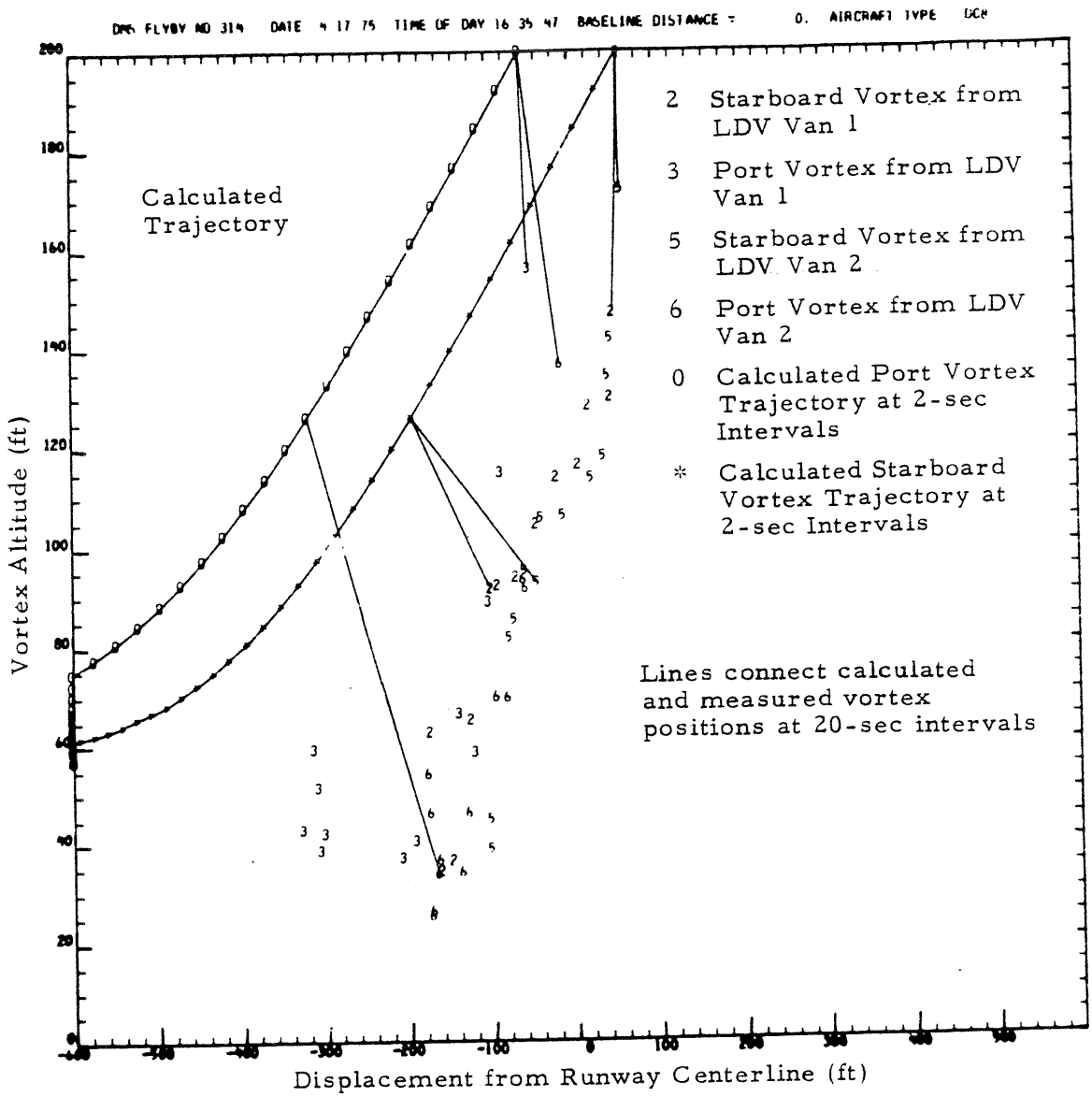

FIGURE 22. CALCULATED AND MEASURED VORTEX TRAJECTORIES FOR BASELINE 1

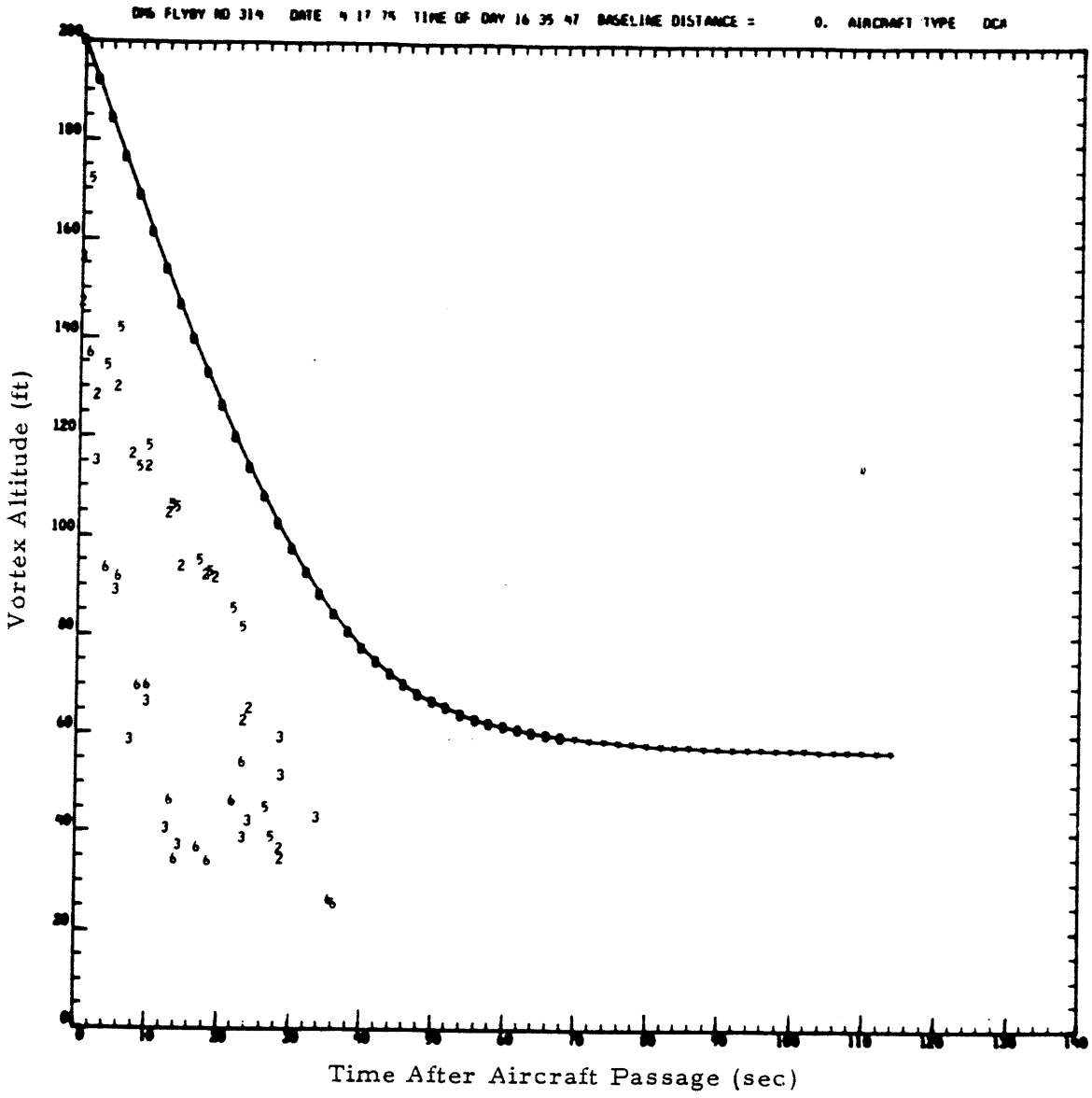

FIGURE 23. CALCULATED AND MEASURED VORTEX ALTITUDE AT BASELINE 1

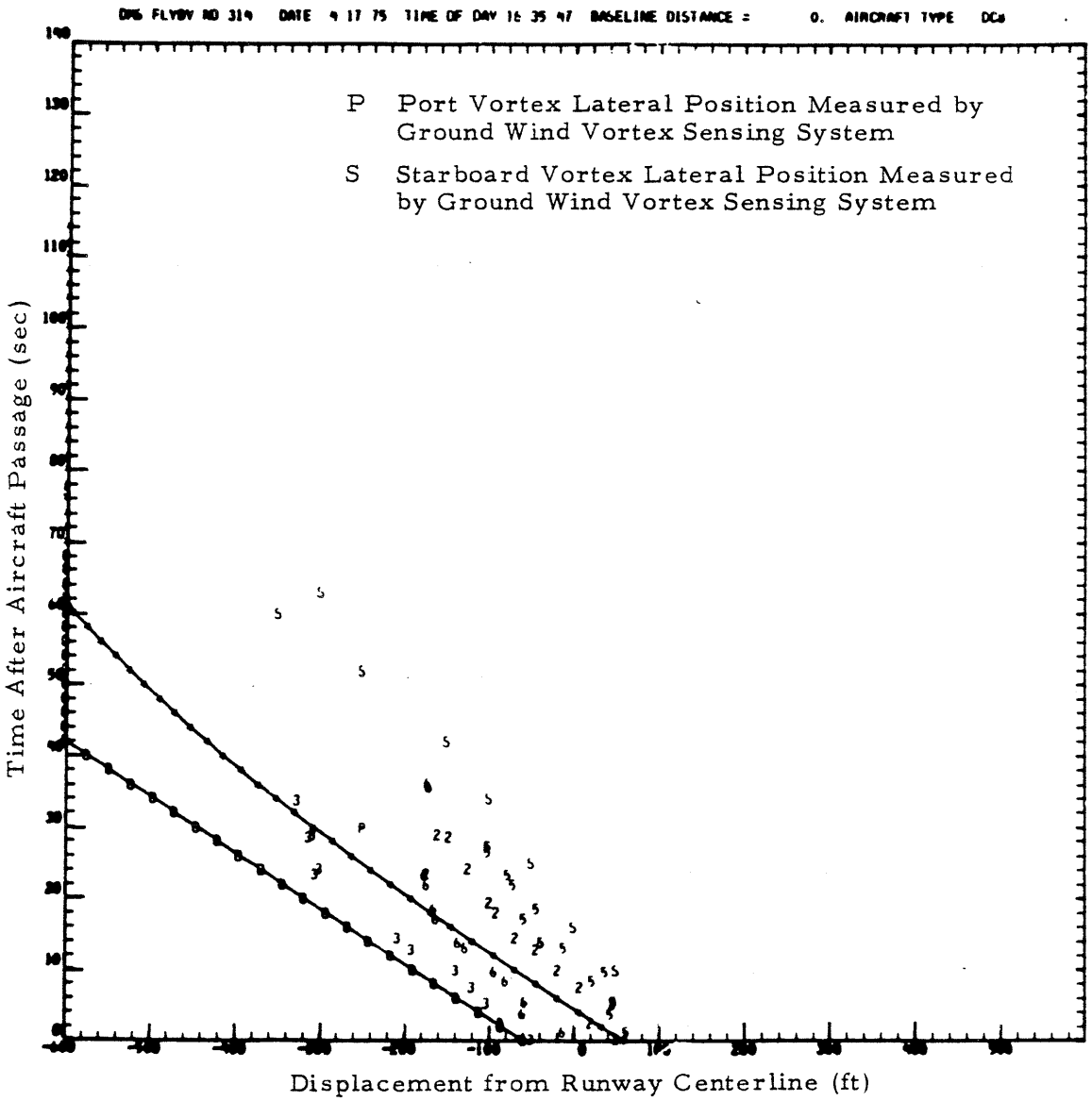

FIGURE 24. CALCULATED AND MEASURED VORTEX LATERAL POSITION FOR BASELINE 1

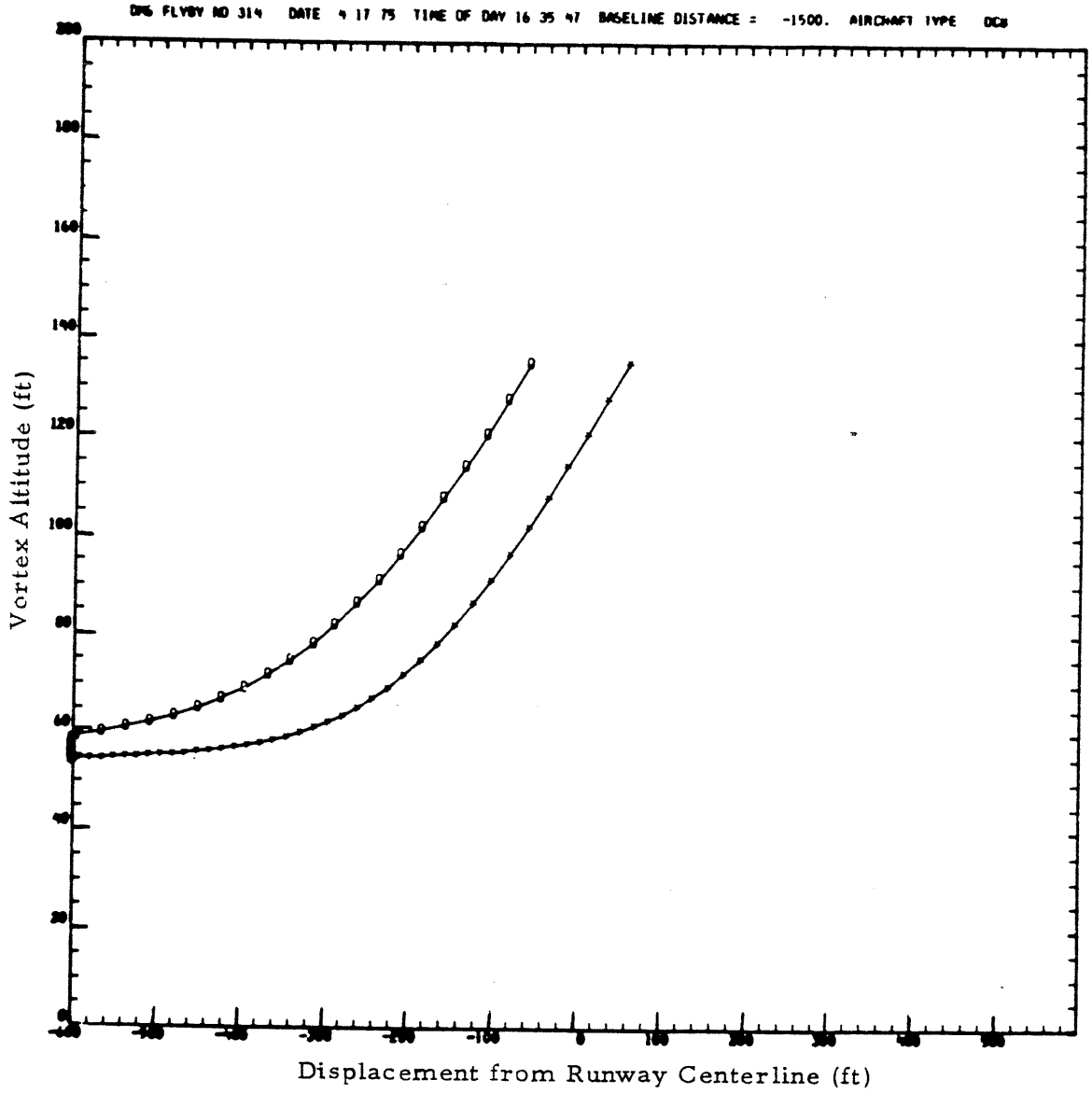

FIGURE 25. CALCULATED VORTEX TRAJECTORY FOR BASELINE 3

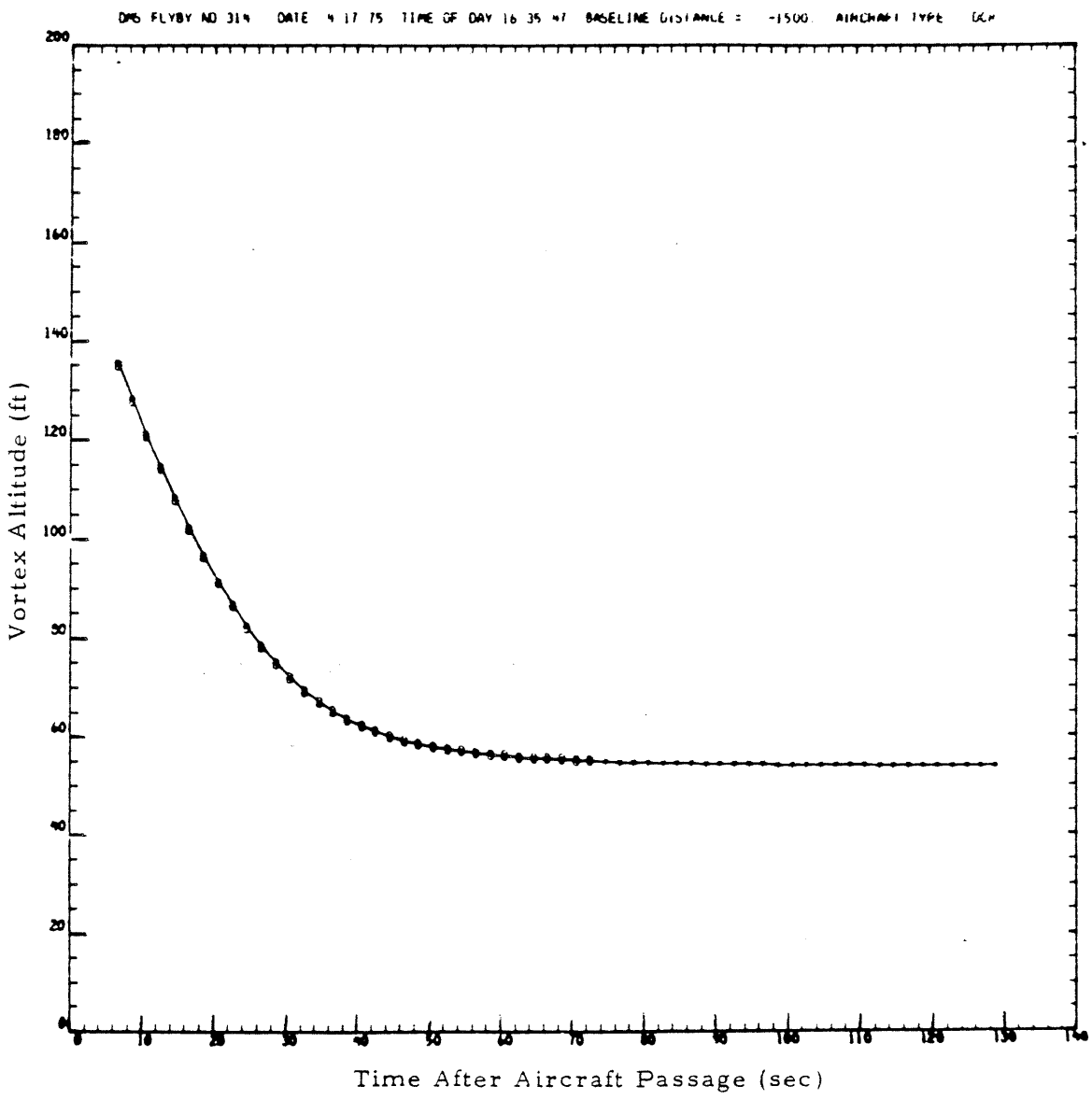

FIGURE 26. CALCULATED VORTEX ALTITUDE FOR BASELINE 3

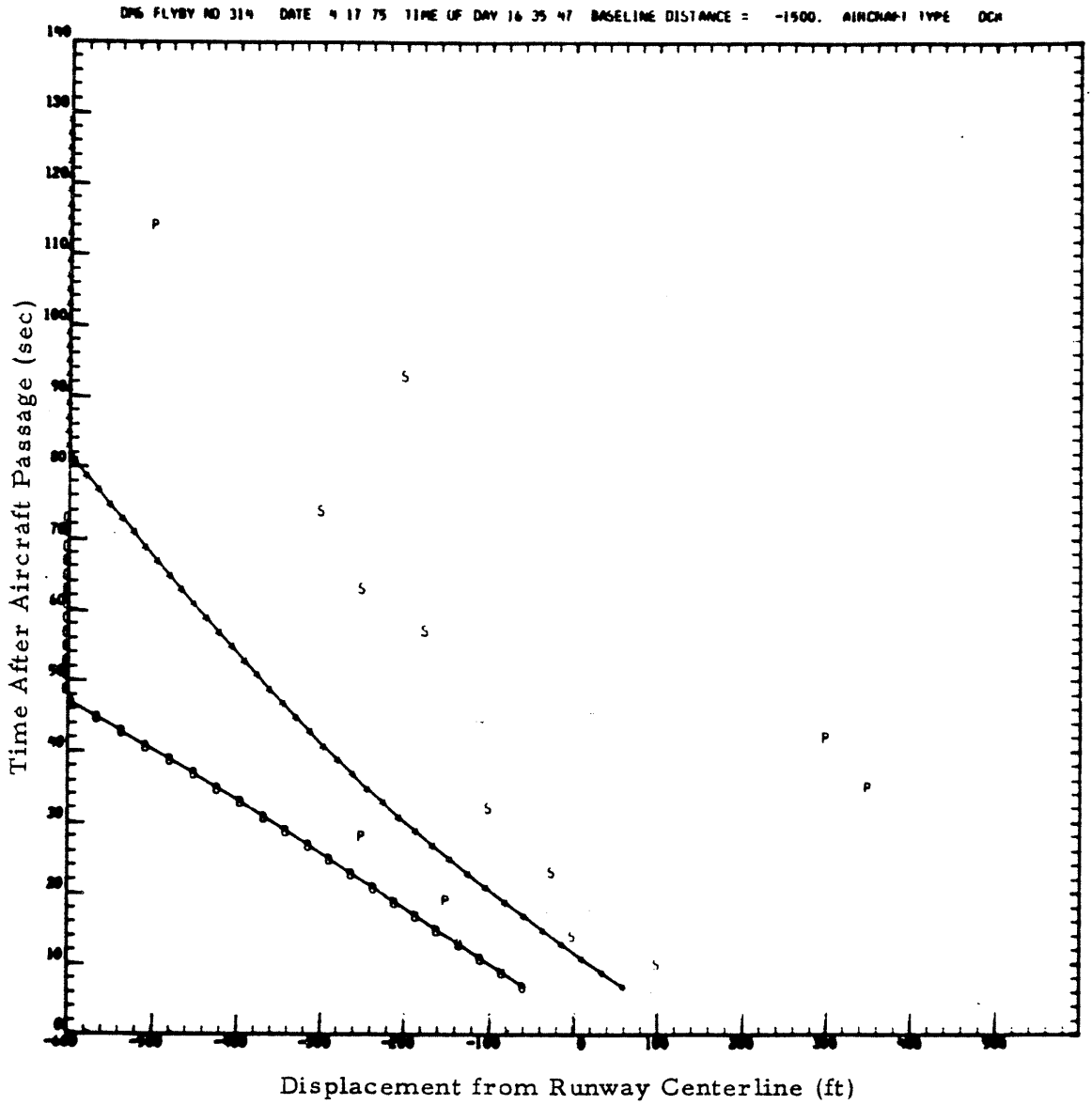

FIGURE 27. CALCULATED AND MEASURED VORTEX LATERAL POSITION FOR BASELINE 3

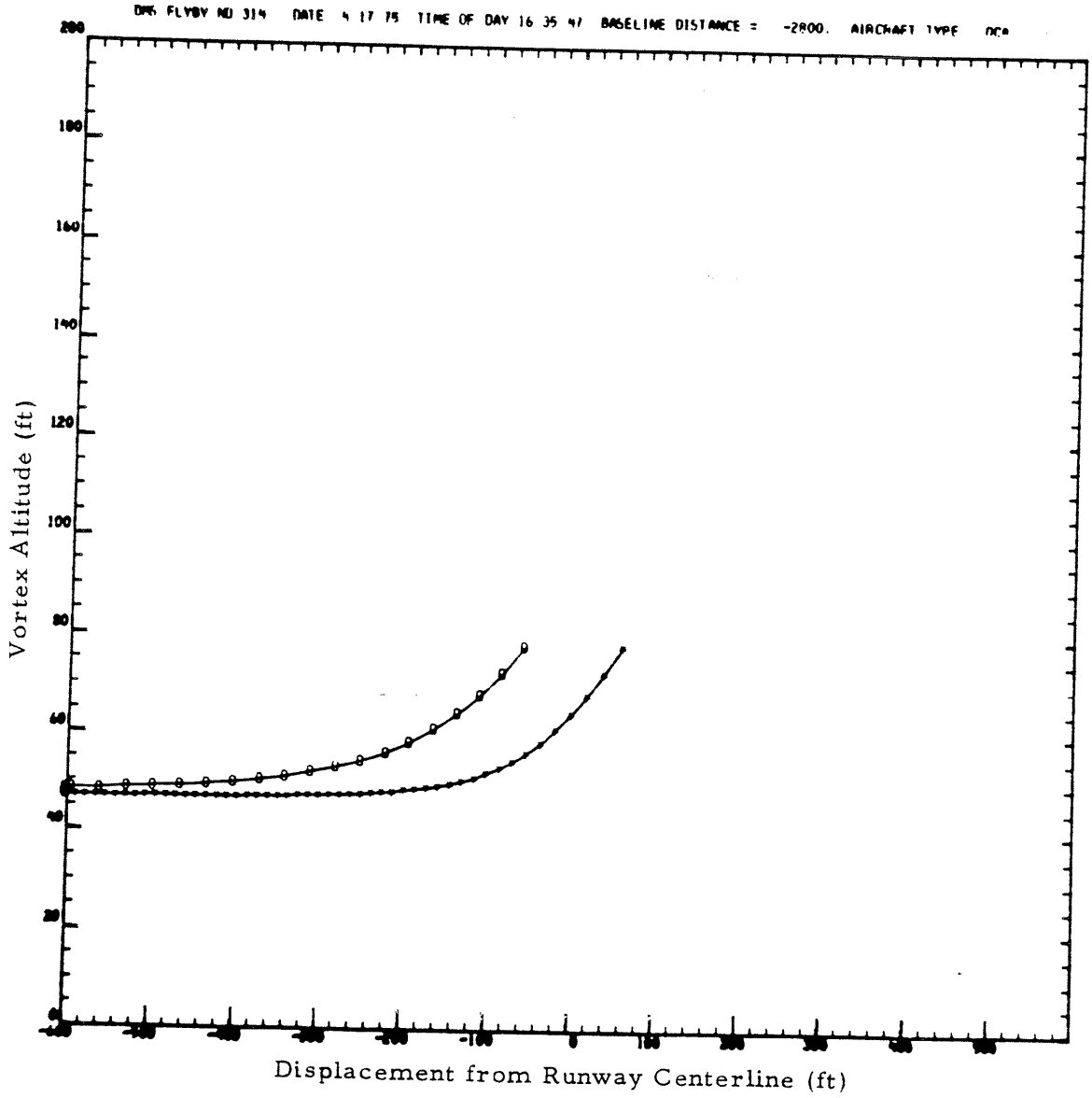

FIGURE 28. CALCULATED VORTEX TRAJECTORY FOR BASELINE 4

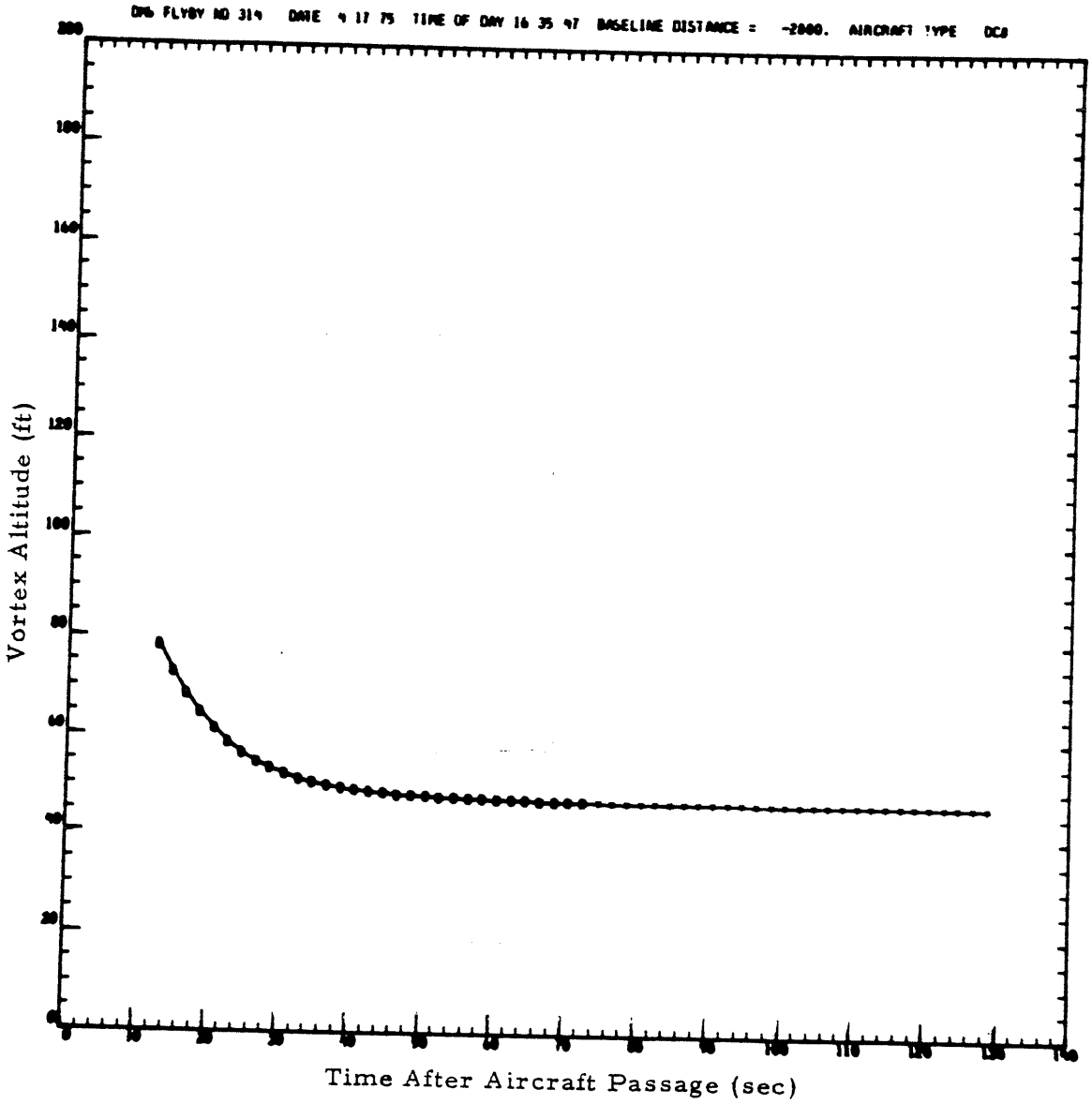

FIGURE 29. CALCULATED VORTEX ALTITUDE FOR BASELINE 4

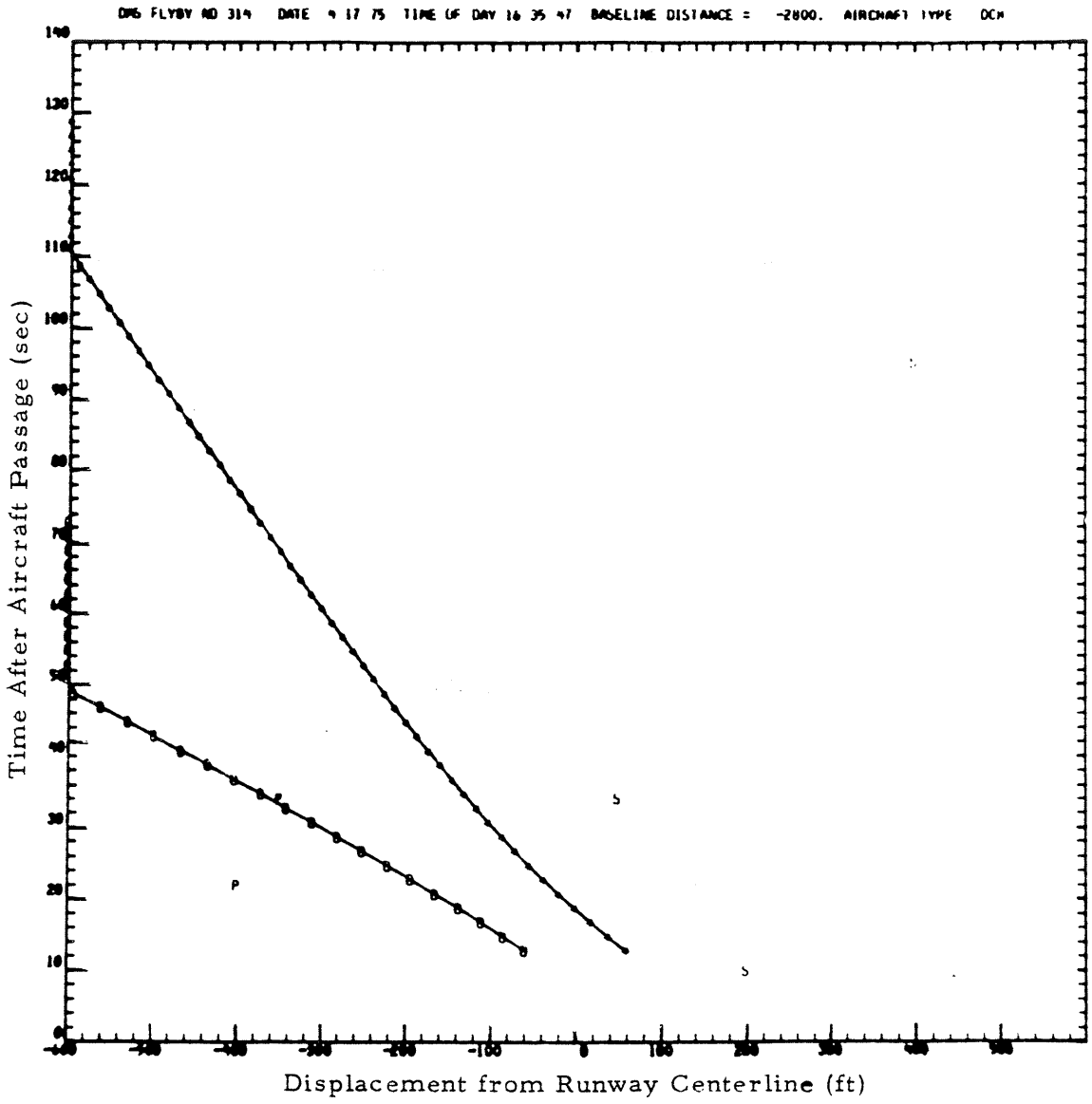

FIGURE 30. CALCULATED AND MEASURED VORTEX LATERAL POSITION AT BASELINE 4

Table 8

DATA ACCESS KEYS FOR VORTEX DATA MANAGEMENT SYSTEM

1. SITENO	Site Number
2. RUNNO	Run Identification Number
3. DAY	Day of Year
4. YEAR	Year
5. TIMEDA	Time of Day in Seconds
6. AIRCFT	Aircraft Type
7. LVAN1	Laser Doppler Velocimeter Van 1, non-zero if data cataloged
8. LVAN2	Laser Doppler Velocimeter Van 2, non-zero if data cataloged
9. DACC1	Doppler Bistatic Acoustic Receiver 1, non-zero if data cataloged
10. DACC2	Doppler Bistatic Acoustic Receiver 2, non-zero if data cataloged
11. PACC	Pulsed Acoustic, non-zero if data cataloged
12. PRED	Calculated track, non-zero if data cataloged
13. GRWD	Ground Wind, non-zero if data cataloged
14. MET	Met Sensor Data, non-zero if data cataloged
15. U-40	Tailwind Down Runway (U at 40 ft) Tower 1
16. V-40	Crosswind (V at 40 ft) Tower 1
17. W-40	Vertical Wind (W at 40 ft) Tower 1
18. UH-40	Horizontal Wind Speed, (U**2 + V**2)**0.5 at 40 ft
19. ANG-40	Direction of Horizontal Wind
20. VDISP	Dissipation Computed from Tower, 140 ft Level
21. WSHR1	Wind Shear, DU/DH, Linear Fit of Large Tower for 25-50 ft
22. WSHR2	Wind Shear, DU/DH, Linear Fit of Large Tower for 50-135 ft

Table 8 (Concluded)

23. WSHR3	Wind Shear, DU/DH, Linear Fit of Large Tower for 25-135 ft
24. WSHR5	Wind Shear, DV/DH, Linear Fit of Large Tower for 50-35 ft
25. U-VAR	Variance of U-Wind Component at 40 ft
26. V-VAR	Variance of V-Wind Component at 40 ft
27. W-VAR	Variance of W-Wind Component at 40 ft
28. UH-VAP	Variance of U-Horizontal Wind Speed at 40 ft
29. PWRLWE	Power-Law Exponent Computed from Large Tower
30. PWRLWH	Power-Law Height Computed from Large Tower
31. PWRLWV	Power-Law Velocity Computed from Large Tower
32. FRICV1	Friction Velocity Computed from Large Tower Wind Speed at 50 and 135 ft
33. FRICV2	Friction Velocity Computed from Variance of Large Tower Wind Speed at 135 ft
34. LIFE1	Vortex Life Time Computed from Universal Life Time Function Using VDISIP
35. LIFE2	Vortex Life Time Computed from McGowan's Life Time Curve Using Power-Law Wind Speed
36. RT-LDV	Maximum Residence Time from Upwind LDV Van
37. LT-LDV	Maximum Life Time from Upwind LDV Van
38. RT-PRED	Maximum Calculated Transport Time Baseline 1
39. RT-GW	Maximum Residence Time from GW Sensor Baseline 1
40. LT-GW	Maximum Life Time from GW Sensor Baseline 1
41. RT-GW2	Maximum Residence Time from GW Sensor Baseline 2
42. LT-GW2	Maximum Life Time from GW Sensor Baseline 2
43. RTPRED2	Maximum Calculated Residence Time Baseline 2
44. TURBUH	Turbulence Level of Wind Speed $\frac{\text{UH-VAR}}{\text{UH-40}}$
45. TURBV	Turbulence Level of Crosswind $\frac{\text{V-VAR}}{\text{V-40}}$
46. VBAR 40	Crosswind at 40 ft Level Tower 2
47. VBAR 50	Crosswind at 50 ft Level Tower 2
48. VBAR 30	Crosswind at 30 ft Level Tower 4

All of the data shown in the sample data report are stored in the DMS. This includes vortex altitude and lateral position as a function of time for both calculated and measured vortex trajectories.

3.6 DATA MANAGEMENT SYSTEM

A computerized vortex data management system (DMS) has been developed for cataloging, indexing, manipulating, and retrieving vortex data as a function of atmospheric, aircraft, and site-dependent parameters. The major capabilities of the DMS include: (1) file maintainence (tape read and write, additions, and corrections of data); (2) arithmetic operations (including statistical manipulation of data); and (3) retrieval of vortex data (plotting and testing). The purpose of the DMS is to catalog the vortex data in such a manner that various correlations and functional relationships can be conveniently determined and efficiently displayed from available vortex track and meteorological data. Thus, it is a useful tool for the refinement of the analytic model and for the formulation of a predictive model.

The DMS operates in two modes. The first mode is the catalog mode in which data are read, calculations necessary to generate values of calculated parameters are performed, and data files of measured and calculated parameters are generated. The second mode is the retrieval mode in which stored data from the data files are retrieved, user-defined calculations are performed on the retrieved data, and printouts and/or plots of the retrieved data (and/or parameters generated from user-defined calculations) are generated. The basis for the retrievals is a set of user-defined values of one or more data access keys. The keys are selected parameters as shown in Table 8. The DMS is described in Appendix A.

The DMS was used extensively in the retrieval mode for the analysis of data to be presented in the next two sections. Virtually all of the computer-generated plots in the next two sections were generated by the DMS operating in the retrieval mode. The DMS was therefore the primary tool by which the analysis of the next two sections was conducted.

4. ANALYSIS OF WAKE VORTEX DATA BASE

This section contains an analysis of particular aspects of wake vortex behavior and associated meteorology. The analysis is based on the analytic transport model and on vortex data and meteorological data measured at JFK. This section begins with presentation of the vortex data. The scatter in the data is observed, and reasons for the scatter in the data are presented. The basis for comparison of calculated results and measured results is presented and justified. It is shown that comparison of calculated trajectories (stored in the DMS) with measured trajectories on a flyby-by-flyby basis is not appropriate. Probability distributions of vortex residence time are presented, and apparent vortex decay is noted.

A discussion of vortex parameters which may be site-dependent is presented. A discussion of meteorological parameters as they relate to time periods of 30 sec to 2 min is presented. The basis for the comparison is the meteorological data measured at JFK.

Section 2 serves as a background for this section since it presents a theoretical basis for analysis of the data presented in this section. This section serves as a background to Sections 5 and 6. The data scatter and meteorological variability presented in this section lead to the conclusion that residence time cannot be calculated and/or predicted on a flyby-by-flyby basis. This conclusion leads to the necessity of the prediction techniques discussed in Section 5. This section concentrates on vortex transport, which is one of the phenomena affecting vortex residence time (the other is vortex life time) The reason for the emphasis on transport in the section is that vortex transport is more amenable to analytic calculation than is vortex life time, and this section concentrates on the ability to use such calculations beneficially in an operational environment. Section 5 presents an approach for prediction of vortex life time.

This section may be considered to be a summary of important vortex-related and meteorological-related observations which are important in the design of an effective WVAS. As such, the conclusions reached in this section serve as the ground rules for the WVAS design considerations presented in Section 6.

4.1 VORTEX TRANSPORT CHARACTERISTICS FROM MEASURED DATA

The objective of the vortex predictive model is to predict the vortex residence time in the approach corridor for some period of time in advance based on current meteorological parameters. Since the predicted vortex residence time is to be used by the WVAS to set safe aircraft separations, the ability of the vortex predictive model to predict the vortex transport time reliably is an important consideration. Predictive reliability consists of two elements; the reliability with which the transport model calculates the actual vortex transport time and the reliability with which the meteorological conditions can be predicted. To assess the reliability of the vortex transport model it is necessary to determine: (1) the ability of the vortex transport model to calculate the vortex transport time accurately based on the current wind profile and assumed aircraft characteristics; (2) the variance between the vortex transport characteristics based on assumed values of aircraft parameters and those of actual values of aircraft parameters; and (3) the ability to extrapolate the current meteorological parameters to future time periods. In the following discussion the reliability of the calculated vortex transport time is investigated. The factors affecting the accuracy of predicted transport time are addressed in Section 4.2.2.

4 1.1 Vortex Characteristics Affecting the Accuracy of Calculated Vortex Transport Time

Ostensibly, the reliability of the transport model should be ascertained by a flyby-by-flyby comparison of the calculated trajectory and transport time with the measured trajectory and transport time. However, when the

vortex transport time is calculated from available tower crosswind measurements and assumed values of aircraft parameters, the sources of uncertainty include: (1) uncertainty in crosswind due to displacement of the tower from the vortex corridor; (2) variations in crosswind with altitude; (3) variations between assumed and actual aircraft parameters; and (4) deviation of aircraft position from the assumed position on the ILS. The sensitivity of the vortex transport model to variations in crosswind and aircraft parameters was illustrated earlier in Section 2.2.

The first two sources of uncertainty are discussed in the following paragraphs. The conclusion of the discussion is that comparison of calculated and measured results on the basis of crosswind measurement at a single altitude from a tower which is close to the vortex corridor is preferable to comparison with calculated results based on a complete velocity profile but with the tower far from the vortex corridor.

A comparison of the wind measured at the 40-ft level of tower 1 (tower closest to the flight path at baseline 1) with that measured at the 50-ft level of tower 3 (tower from which wind data were used for calculated vortex trajectory) is shown in Fig. 31. Winds shown are the 128-sec averages following each flyby. The scatter in the data is significant, suggesting that comparison of calculated and measured trajectories on a flyby-by-flyby basis is not appropriate. (Tower 3 data were used for the calculated trajectory in the DMS because it was the only tower by which a wind profile could be obtained for the altitude range of interest). Therefore, calculation of transport time by the methods of Section 2.1 and using the crosswind measured by tower 1 is used as the basis of comparison of calculated and measured results. It is noted that the 40-ft altitude approximates the asymptotic altitude for the B-727 (cf. Section 2.2.1). As an example of the discrepancy between measured trajectories and trajectories calculated from the wind of tower 3, sample plots of the wake vortex altitude and lateral position as a function of time are given in Figs. 32, 33 and 34. The straight lines in Fig. 32 connect calculated

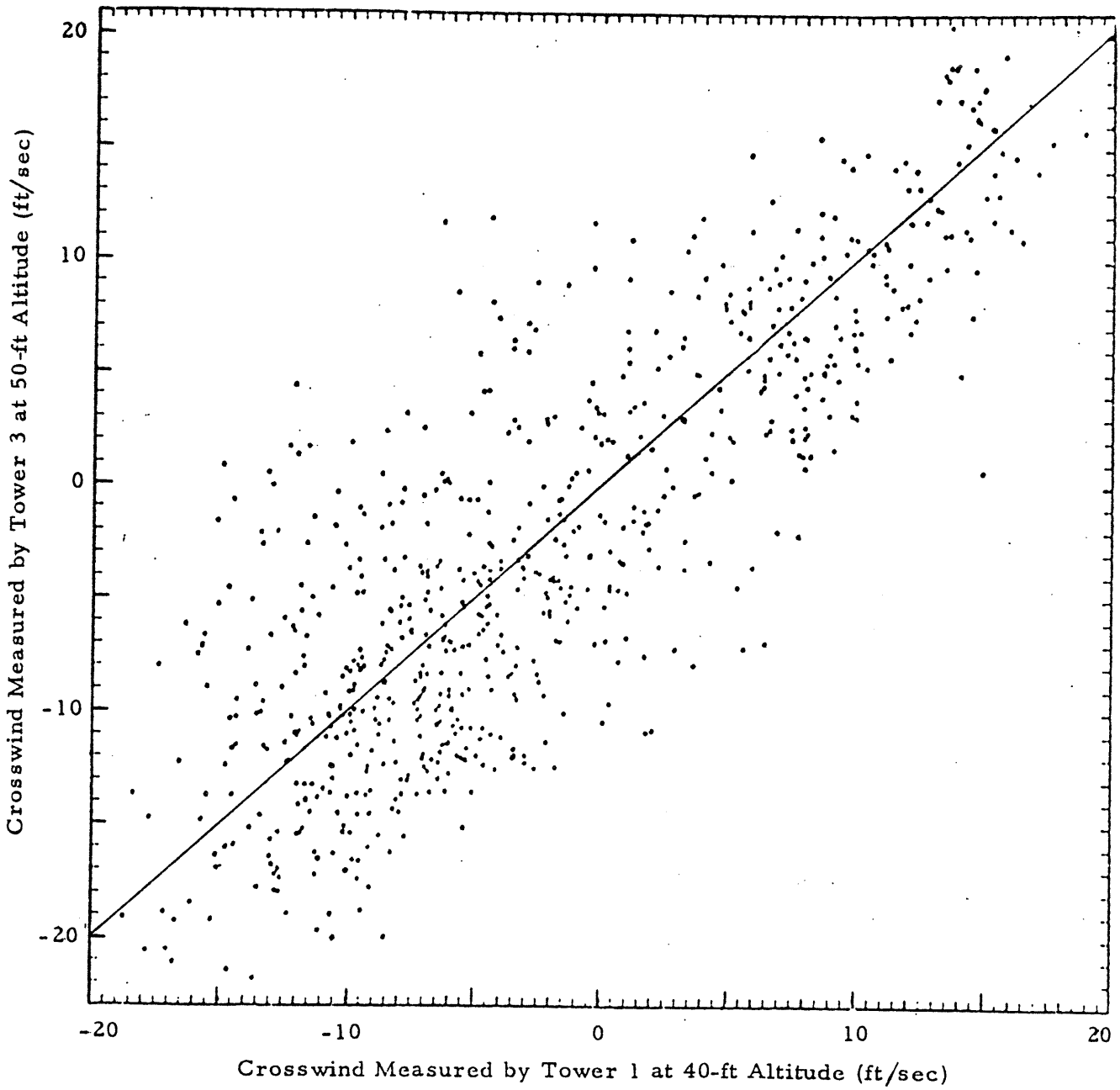

FIGURE 31. COMPARISON OF CROSSWIND MEASURED BY TOWER 1 AND BY TOWER 3

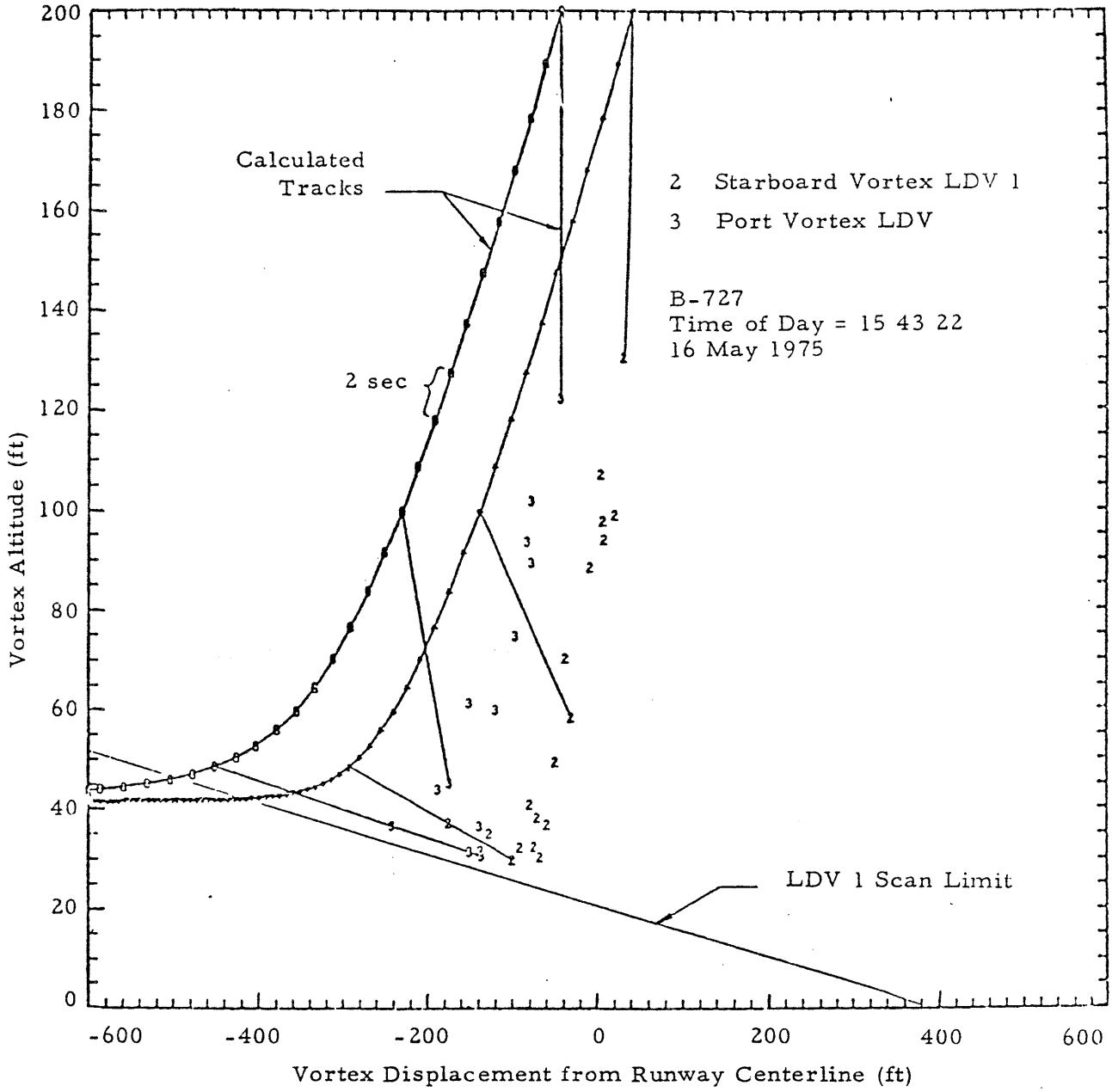

FIGURE 32. EXAMPLE OF CALCULATED AND MEASURED WAKE VORTEX TRAJECTORIES

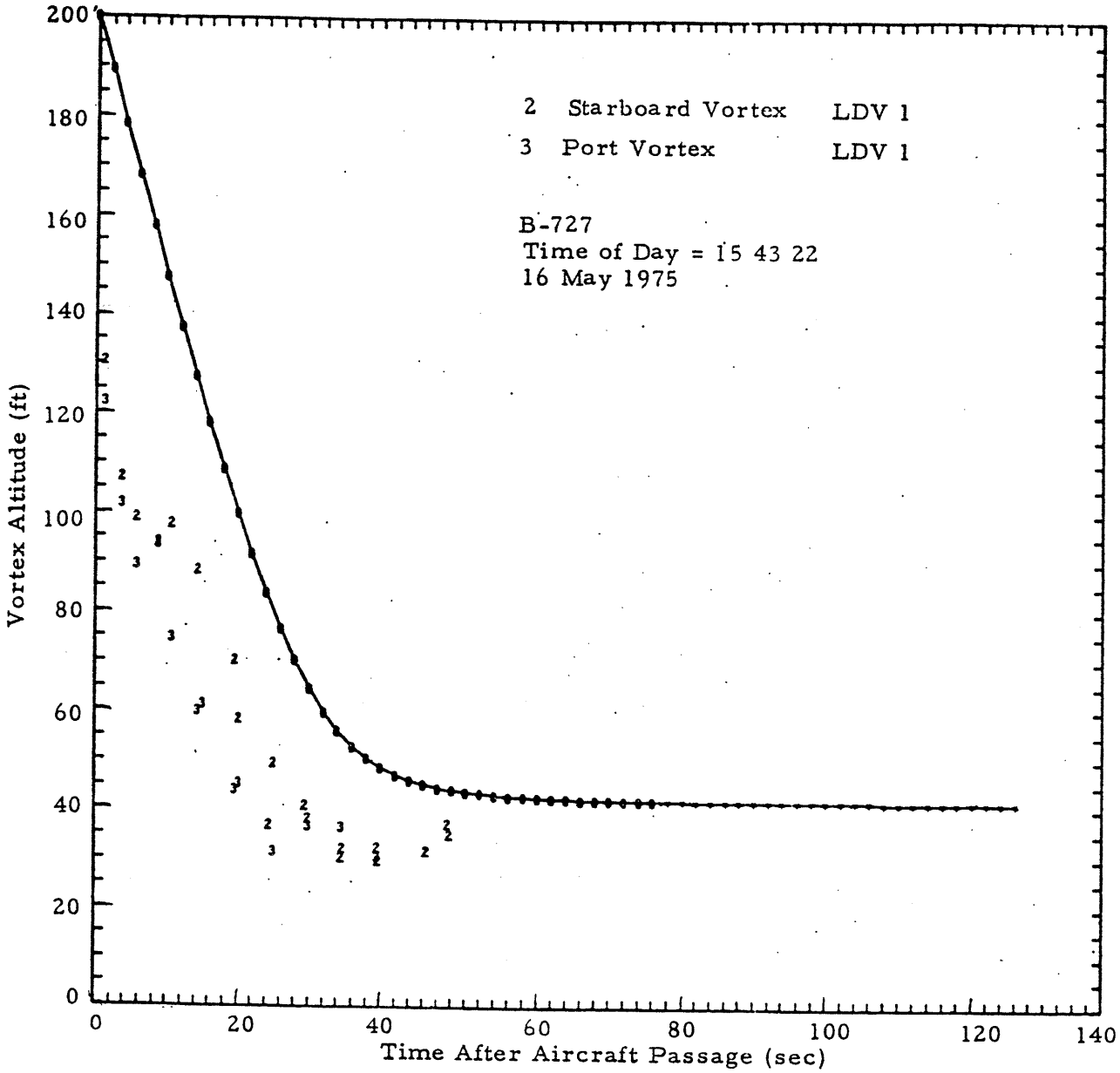

FIGURE 33. EXAMPLE OF CALCULATED AND MEASURED VORTEX ALTITUDE AS A FUNCTION OF TIME

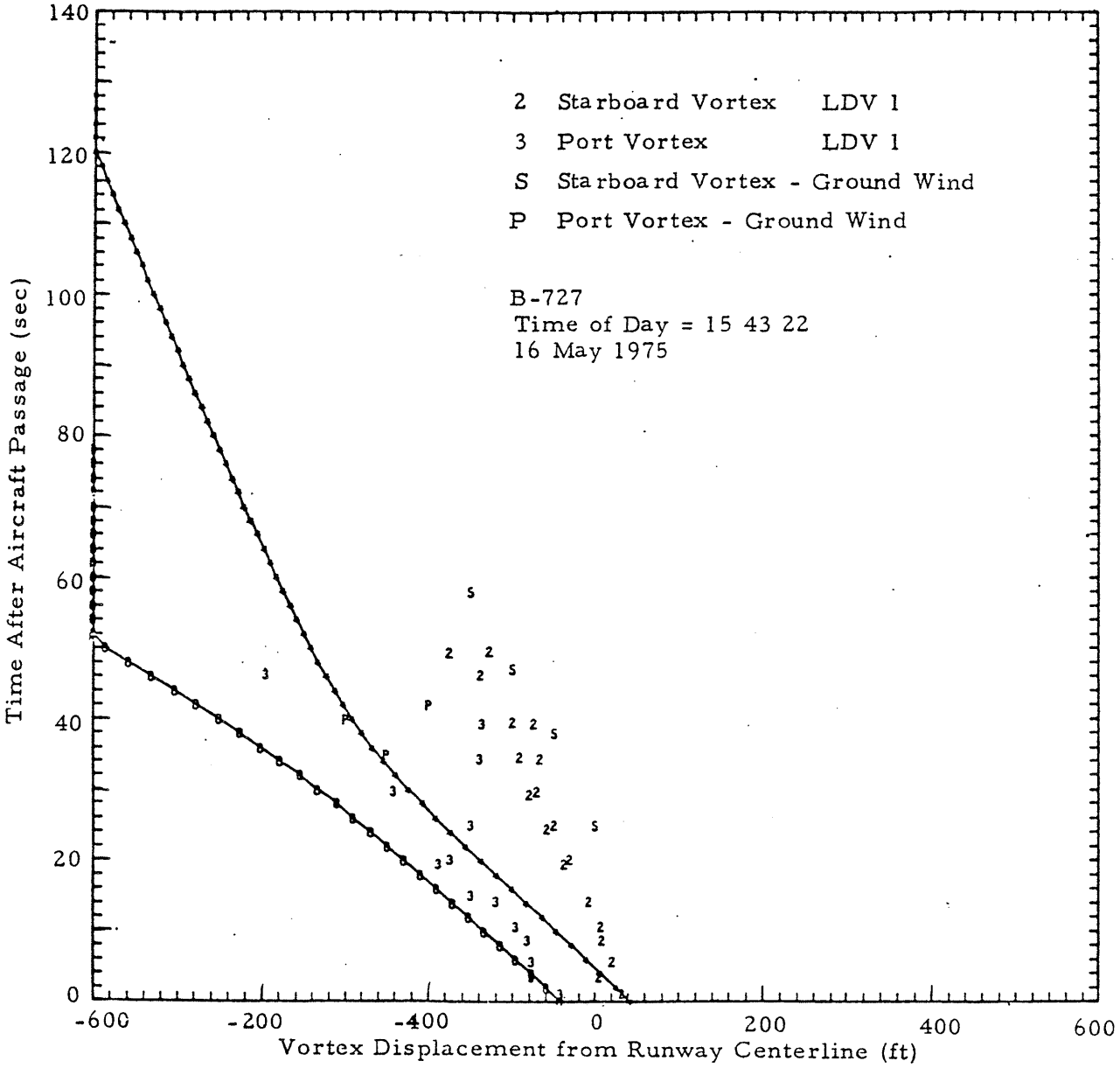

FIGURE 34. EXAMPLE OF CALCULATED AND MEASURED VORTEX LATERAL POSITION AS A FUNCTION OF TIME

vortex positions with LDV-measured vortex position at 20-sec intervals. Although both the calculated and measured vortex trajectories are well defined, they do not agree. In Fig. 34, the lateral positions as measured by the ground wind sensors and by the LDV show good agreement; however, they do not agree with the calculated vortex trajectory. The disagreement is caused by the meteorological tower, upon which the calculated trajectory is based, being located 3300 ft from the runway centerline. For Figs. 32 through 34, the average crosswind for tower 1 (40 ft) was -6.32 ft/sec, whereas that for tower 3 (50 ft) was -9.29 ft/sec. The slopes of the trajectories (i.e., change in vortex lateral position per unit time) shown in Fig. 34 indicate a crosswind of -9.3 ft/sec for the calculated trajectory, -6.7 ft/sec for the measured port vortex, and -4.3 ft/sec for the measured starboard vortex.

In addition to variations in the crosswinds due to tower location, the variations in the crosswinds with altitude also affect the reliability of the calculated vortex transport time.

For the calculated residence time based on a complete wind profile, the wind data measured at 25, 50 and 135 ft were curve fitted to an analytic form in a least-squares sense. Reference 30 had shown that the power-law form was the best wind profile form for vortex calculations. The wind speed was fitted to a power-law curve, and the wind direction was fitted to a linear profile. The form of the crosswind was

$$V = V_{z_o} (z/z_o)^P \sin(A + Bz)$$

An example of the fitted crosswind profile is shown in Fig. 35 with the data measured by the anemometers on the towers. A plot of the individual calculated transport times based on the curve-fitted wind profile is shown as a function of crosswind measured at the 50-ft level in Fig. 36. The uniform

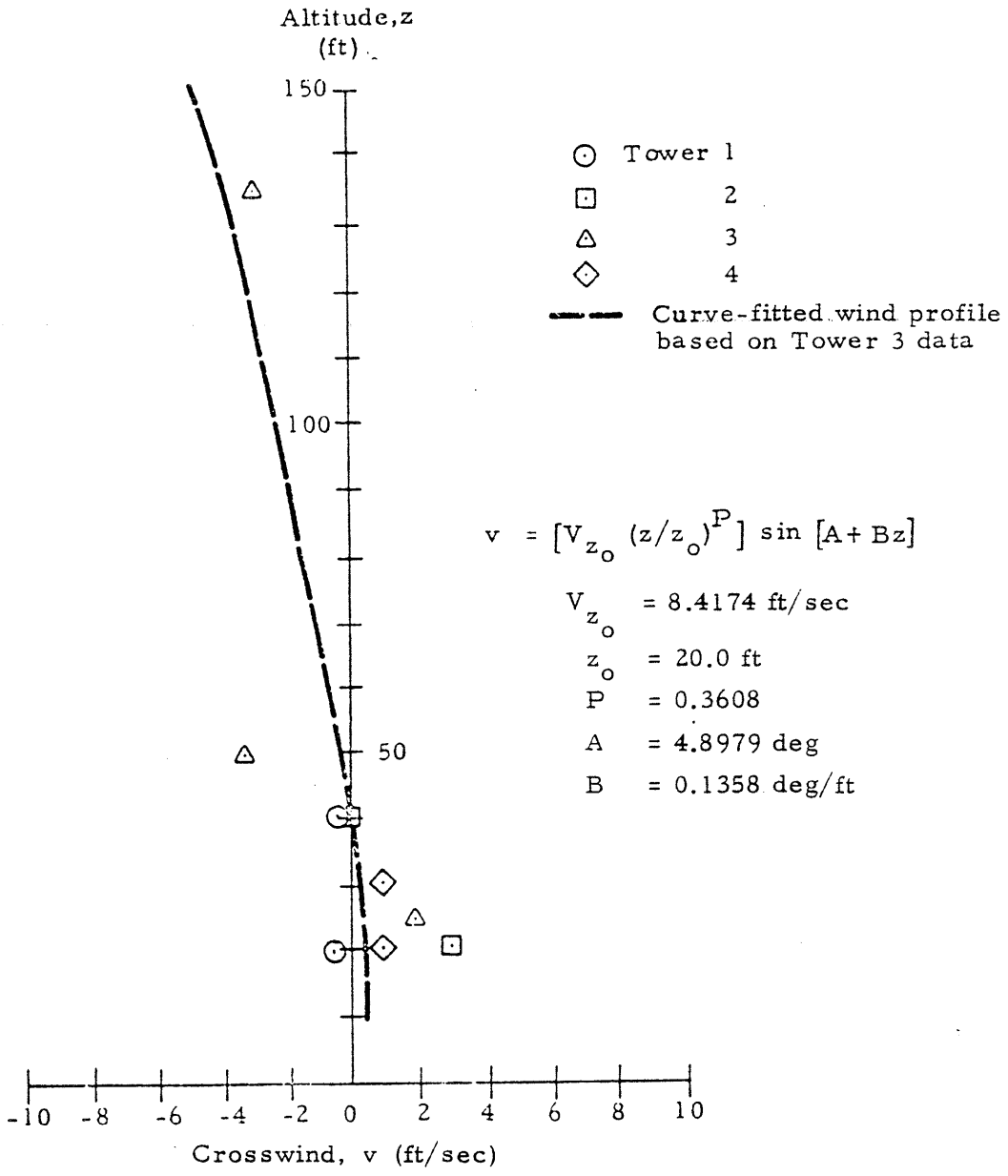

FIGURE 35. COMPARISON OF MEASURED AND CURVE-FITTED WIND DATA

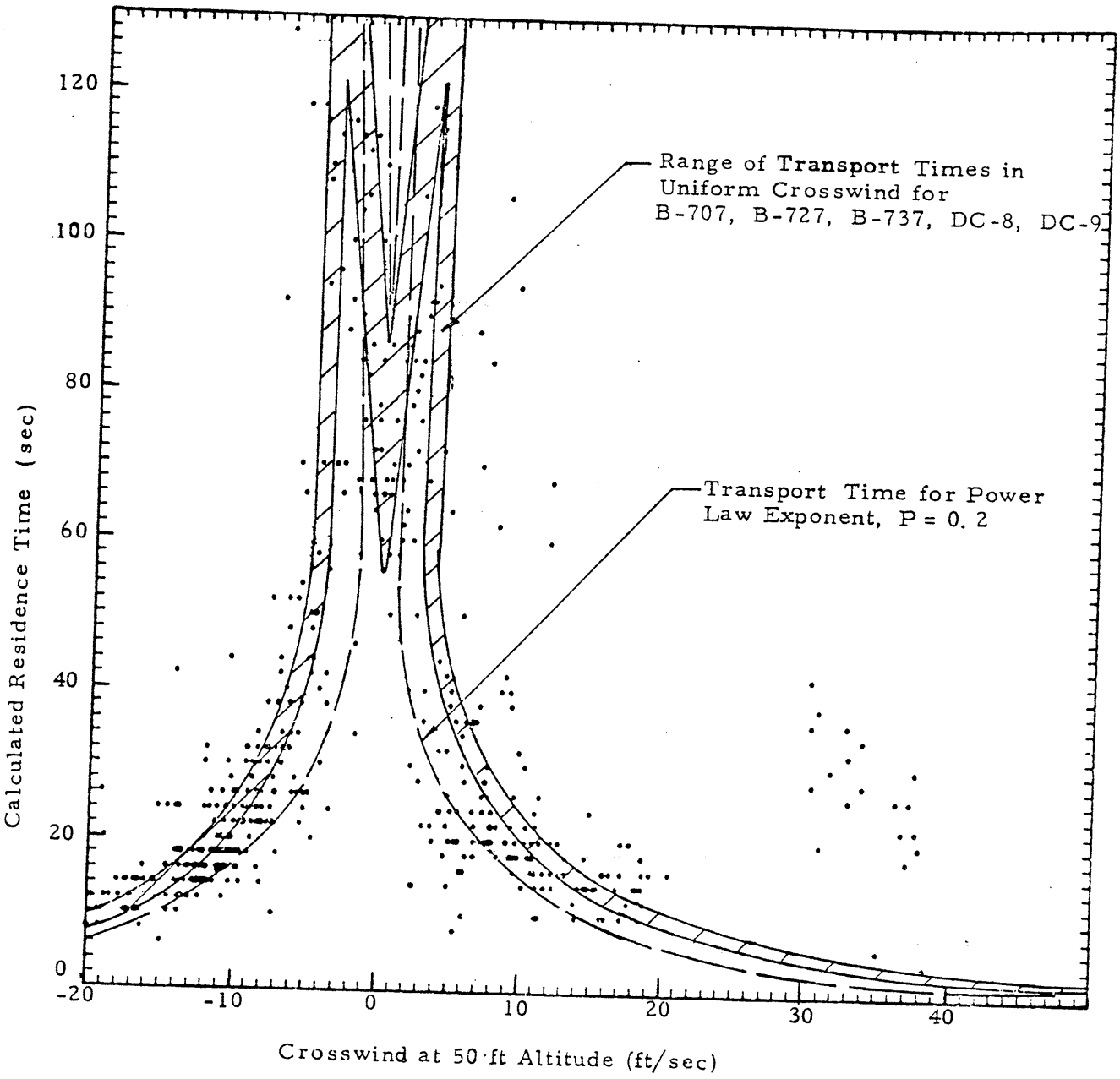

FIGURE 36. CALCULATED TRANSPORT TIME AS A FUNCTION OF CROSSWIND FOR LARGE TRANSPORTS

crosswind transport time and the transport time for a power-law exponent of 0.2 are shown for reference. While much of the scatter may be attributed to a non-zero power-law exponent, some of the scatter results from the condition that the curve fitting implies that the value of wind of the fitted data at 50-ft altitude is not necessarily equal to the measured data at the same altitude. It is noted that it is the measured value which is used as a reference – not the curve-fitted value of wind at 50 ft. For example, for the flyby illustrated in Fig. 35, the value of calculated transport time (shown in Fig. 36) is based upon the dashed line, which gives a crosswind of approximately -0.5 ft/sec at 50-ft altitude. However, the value of crosswind used in Fig. 36 would be the measured value at 50 ft (i.e., -4 ft/sec).

For comparison, Fig. 37 shows the same information as Fig. 36, but with the reference crosswind being the value derived from the curve fit (i.e., the value on the dashed line at 50-ft altitude in Fig. 35). The scatter in Fig. 37 is due to variations in power-law exponent and aircraft type (cf., Fig. 16), whereas that in Fig. 36 is due to these two factors plus the difference between the measured value of wind at 50-ft altitude and the value of wind at 50 ft from the curve fit

While variations in the calculated vortex residence time were noted as a result of variations in the input crosswind, similar variations can result from variations in the input aircraft parameters. The calculated transport time is based on nominal values of aircraft parameters. However, there are unknown variations in aircraft weight (up to $\pm$ 35% of nominal values), variations in wing span (due to different models of a given type), variations in spanwise loading factor (due to different flap settings), variations in airspeed, variations in altitude about glideslope, and variations in lateral position about the runway centerline. The comparison of the vortex residence time measured with ground wind anemometers with expected variation due to variation in aircraft parameters is illustrated in Fig. 38 for wide-body transports and in Fig. 39 for narrow-body transports. The calculated data are transport times, and the measured data are residence times. Residence time may be

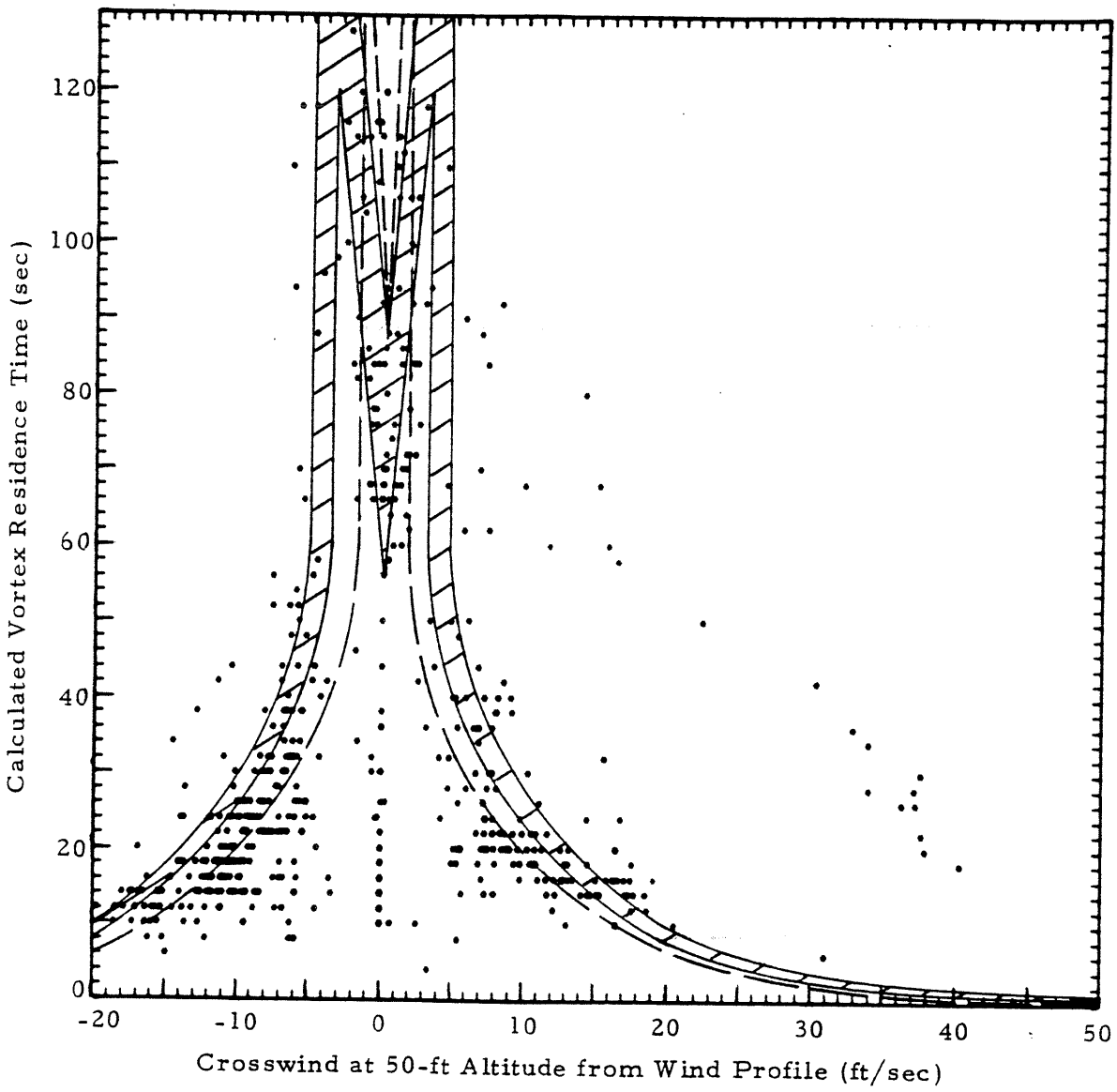

FIGURE 37. CALCULATED RESIDENCE TIME WITH REFERENCE CROSSWIND TAKEN FROM CURVE-FITTED CROSSWIND PROFILE

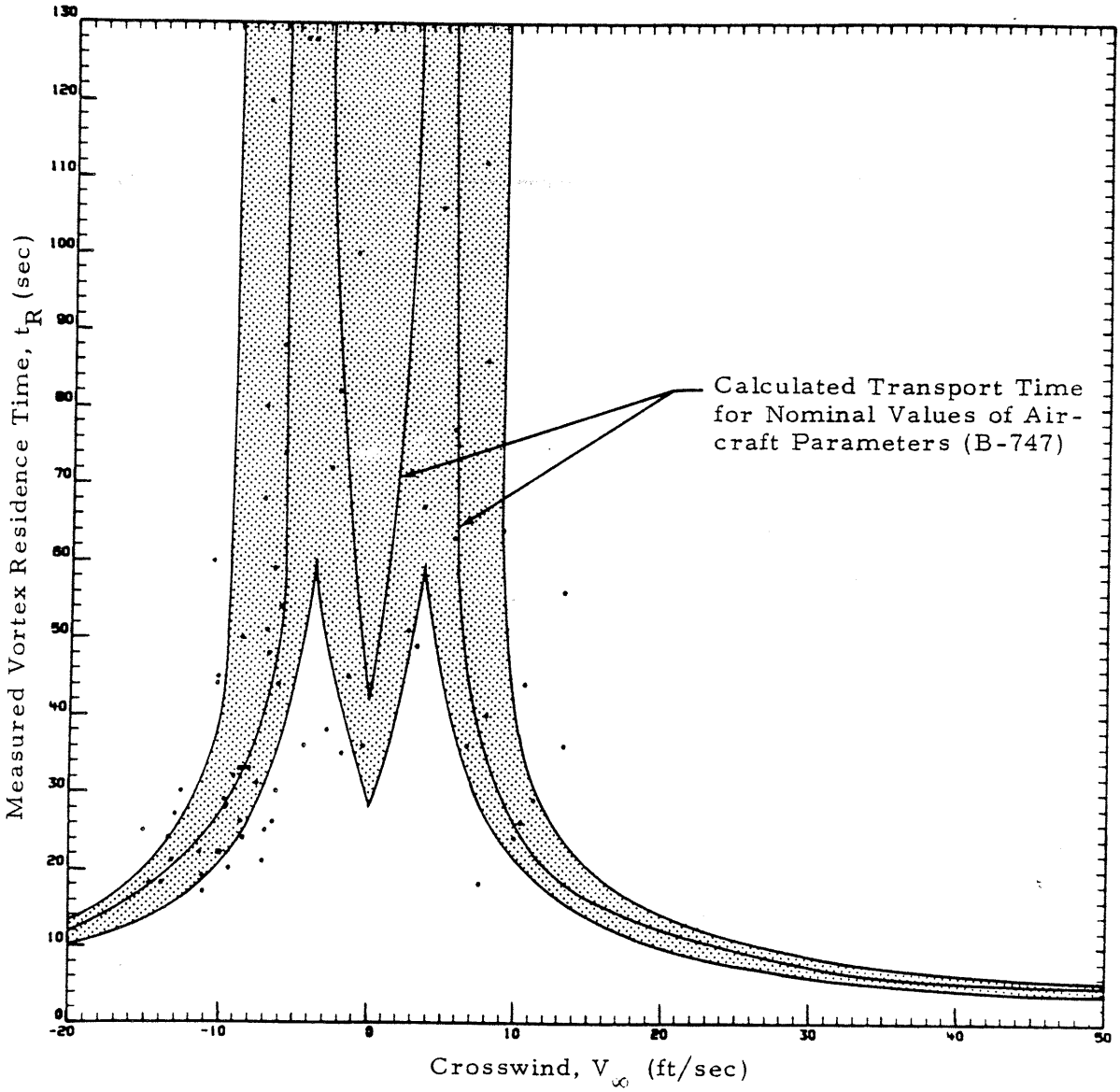

FIGURE 38. VORTEX RESIDENCE TIME FOR WIDE-BODY AIRCRAFT AS MEASURED BY GROUND WIND VORTEX SENSING SYSTEM Shaded area represents expected variations in calculated transport time from expected variations in aircraft parameters

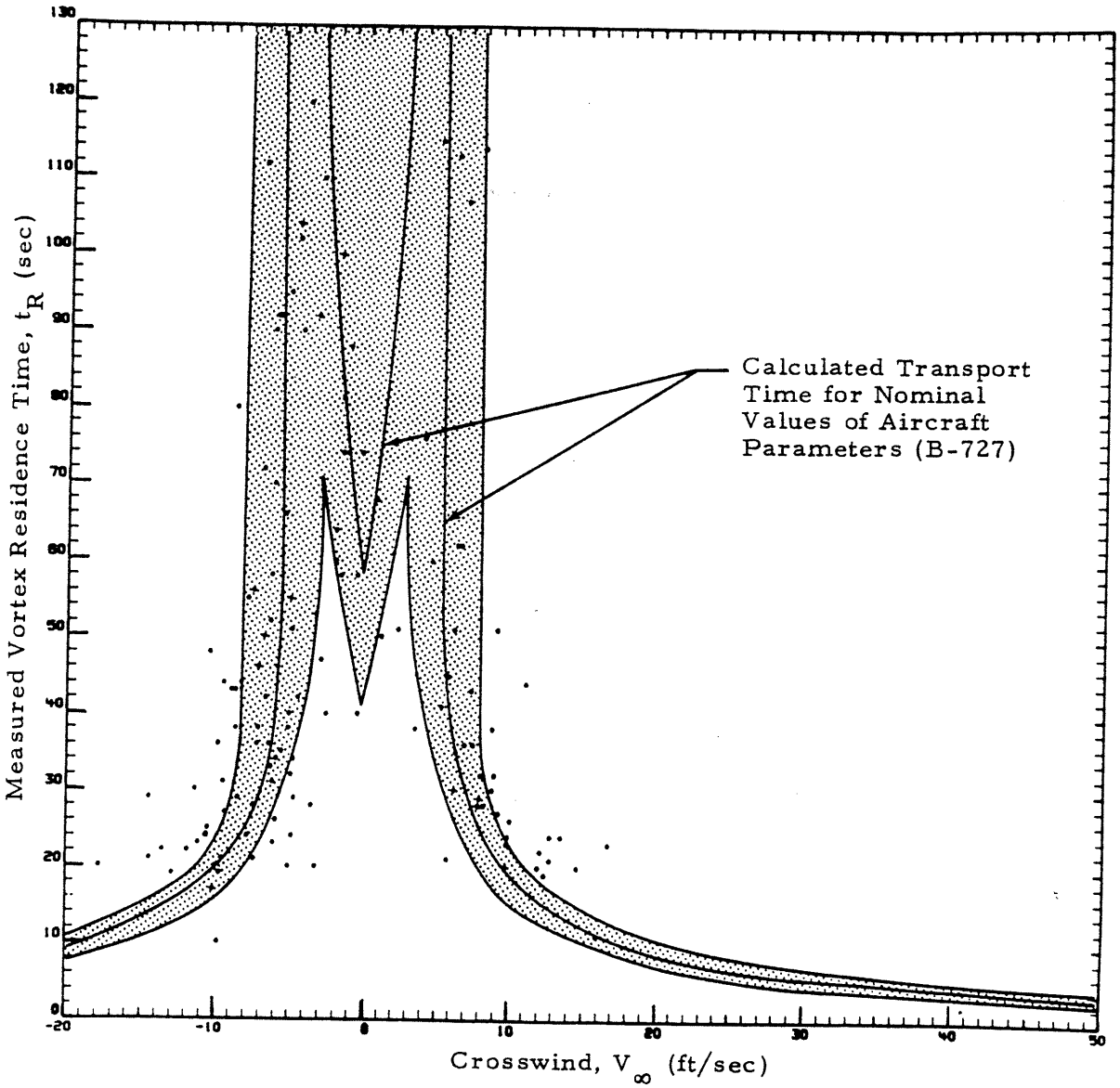

FIGURE 39. VORTEX RESIDENCE TIME FOR NARROW-BODY AIRCRAFT AS MEASURED BY GROUND WIND VORTEX SENSING SYSTEM Shaded area represents expected variations in calculated transport time from expected variations in aircraft parameters

less than (but never greater than) transport time. The expected variation in transport time is based upon minimum and maximum aircraft weights as shown in Table 9, airspeed deviations of 5 knots about the nominal values shown in Table 1, a 20-ft deviation from the glideslope, and a 30-ft deviation from the localizer. Figure 40 shows vortex residence time as measured by the LDV for narrow-body aircraft.

The results indicate that unknown aircraft parameters can account for a noticeable variation in the measured residence time, primarily at low crosswind velocities in the range 0 to 6 ft/sec. The primary effect of variation in aircraft parameters is through the effect on vortex strength and the resultant lateral velocity (relative to the wind) of the vortex in ground effect. Therefore if the crosswind is strong enough so that the vortex exits the flight corridor before entering ground effect, variation in aircraft parameters has no effect on residence time, except for lateral displacement from the localizer. However, if the vortex exits the flight corridor in ground effect, aircraft parameters have a very significant effect on vortex residence time.

In addition to the variations in aircraft parameters, the scatter in the data may also be due to non-uniform wind or averaging problems in time-varying wind. The effect of non-uniform wind is greater for wide-body aircraft than for narrow-body aircraft because the asymptotic altitude of the vortex pair is further from the measurement altitude of 40 ft for wide-body aircraft. Therefore, the difference between the wind at the asymptotic altitude and that at the reference altitude may be greater for the wide-body aircraft. Since the reference crosswind is a 128-sec average, the average wind over the vortex residence time may be different than the 128-sec average used as a reference. This problem is discussed further in Section 4.3.

Table 9

MINIMUM AND MAXIMUM AIRCRAFT WEIGHTS FOR CALCULATING EXTREMES OF VORTEX TRANSPORT TIME

Aircraft Type	Minimum Weight* (lb)	Maximum Weight** (lb)	Fuel Consumption (gal/hr)
B-747	331,412	630,000	3367
B-707	127,942	247,000	1657
B-727	88,893	154,500	1277
B-737	65,056	105,000	901
DC-10	249,760	403,000	2210
DC-9	55,528	110,000	892
DC-8	145,576	240,000	1787
L-1011	254,440	368,000	2340

*Minimum weight is the empty weight plus one hour of fuel for the smallest model of the type.

**Maximum weight is the maximum certificated landing weight for the type.

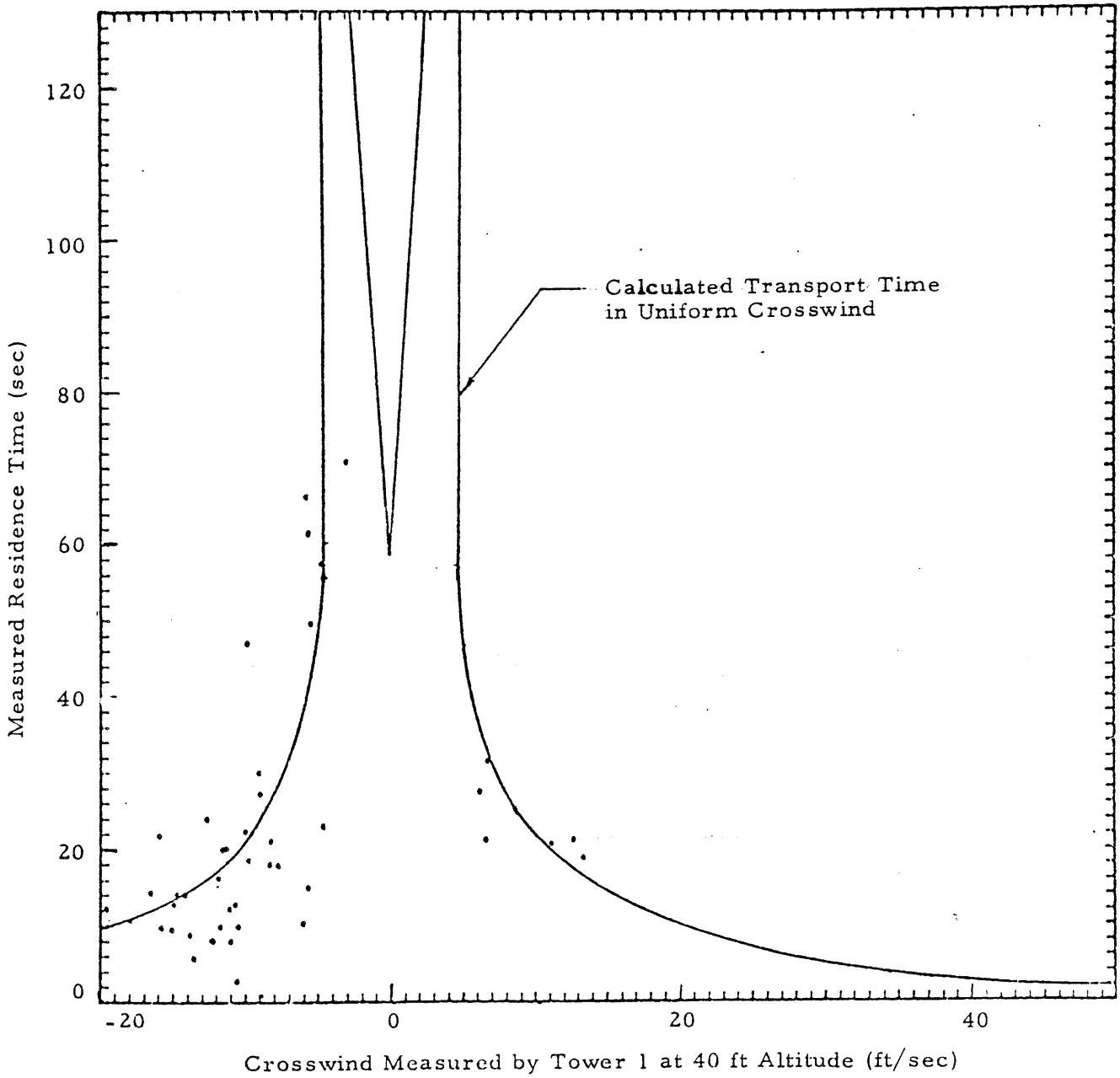

FIGURE 40. VORTEX RESIDENCE TIME MEASURED WITH LASER DOPPLER VELOCIMETER

In summary, the reliability of the calculated vortex residence time has been shown to depend to a large extent on the reliability of the input crosswind at the vortex asymptotic altitude and the accuracy of aircraft parameters. The variations in the input crosswind parameters may be reduced to some extent by using the closest available tower to the runway and by using a uniform profile. Under the restrictions of Federal Aviation Regulations (FAR) Part 77 (Obstructions to Navigable Airspace), the trade-off between a tall tower ($\sim$ 150 ft) far from the flight path and a shorter tower ($\sim$ 60 ft) near the flight path favors the shorter tower. (The glideslope antenna may be an excellent location for wind measurement for vortex calculations.)

Although there is significant scatter in the data, the expected variations bound the measured data. Hence, even though variations in aircraft parameters and meteorological parameters prohibit calculation of transport time on a flyby-by-flyby basis, the bounds are certainly useful for defining limits on aircraft separations.

The results shown in Figs. 38 and 39 suggest that additional accuracy in the input crosswind and aircraft parameters could yield further improvements in the reliability of the calculated vortex residence time. Possible techniques for achieving this additional reliability may include: (1) use of initial vortex descent velocity to infer initial vortex strength parameters; (2) use of initial vortex lateral velocity to infer the proper crosswind velocity; and (3) use of a remote sensor to measure the crosswind at the vortex asymptotic altitude as opposed to a low meteorological tower which (because of clear airspace restriction) can only measure winds at a low altitude. Sections 5.4 and 5.5 discuss methods for achieving a greater reliability by using vortex sensing as a feedback loop.

4.1.2 Vortex Characteristics Affecting the Accuracy of Predicted Vortex Residence Time

Because aircraft spacings must be established up to ten minutes before landing, an effective wake vortex avoidance system must be able to predict

vortex behavior. Therefore, variation of vortex parameters with time of day is very important. Figures 41 and 42 show the variation in crosswind and measured residence time (ground wind anemometer) with time of day for April 17, 1975. It is observed that both of these parameters may vary significantly over a short period of time. The data are given for late afternoon hours. Figure 41 shows a condition which is expected to be common. The wind shows significant variance until sundown, after which the variability of the wind from flyby to flyby is significantly reduced. The late afternoon time period is a period of particular concern because airport demand peaks in the late afternoon for most major airports. Of particular concern is the fact that the wind varies from values for which the vortex is of no concern (>9 ft/sec) to the region where the vortex may be of some concern over a short time period. Sections 5.2 and 5.3 discuss a method of predicting future behavior with time-varying behavior as shown in Figs. 41 and 42.

4.1.3 Apparent Vortex Decay

The apparent vortex decay can be inferred from the measured vortex transport characteristics. The term "apparent vortex decay" is used because the relative vortex strength is inferred from the transport velocity components, rather than from direct strength measurements. From Eq. (6), as Y becomes large (vortices separating in ground effect),

$$\dot{Y} = V_\infty \pm \frac{\Gamma C}{4\pi} = V_\infty \pm \frac{\Gamma}{4\pi} \left[\frac{1}{Y_o^2} + \frac{1}{Z_o^2} \right]^{1/2} . \tag{70}$$

Since the initial vortex descent rate is

$$\dot{Z}_o = - \frac{\Gamma}{4\pi Y_o} , \tag{71}$$

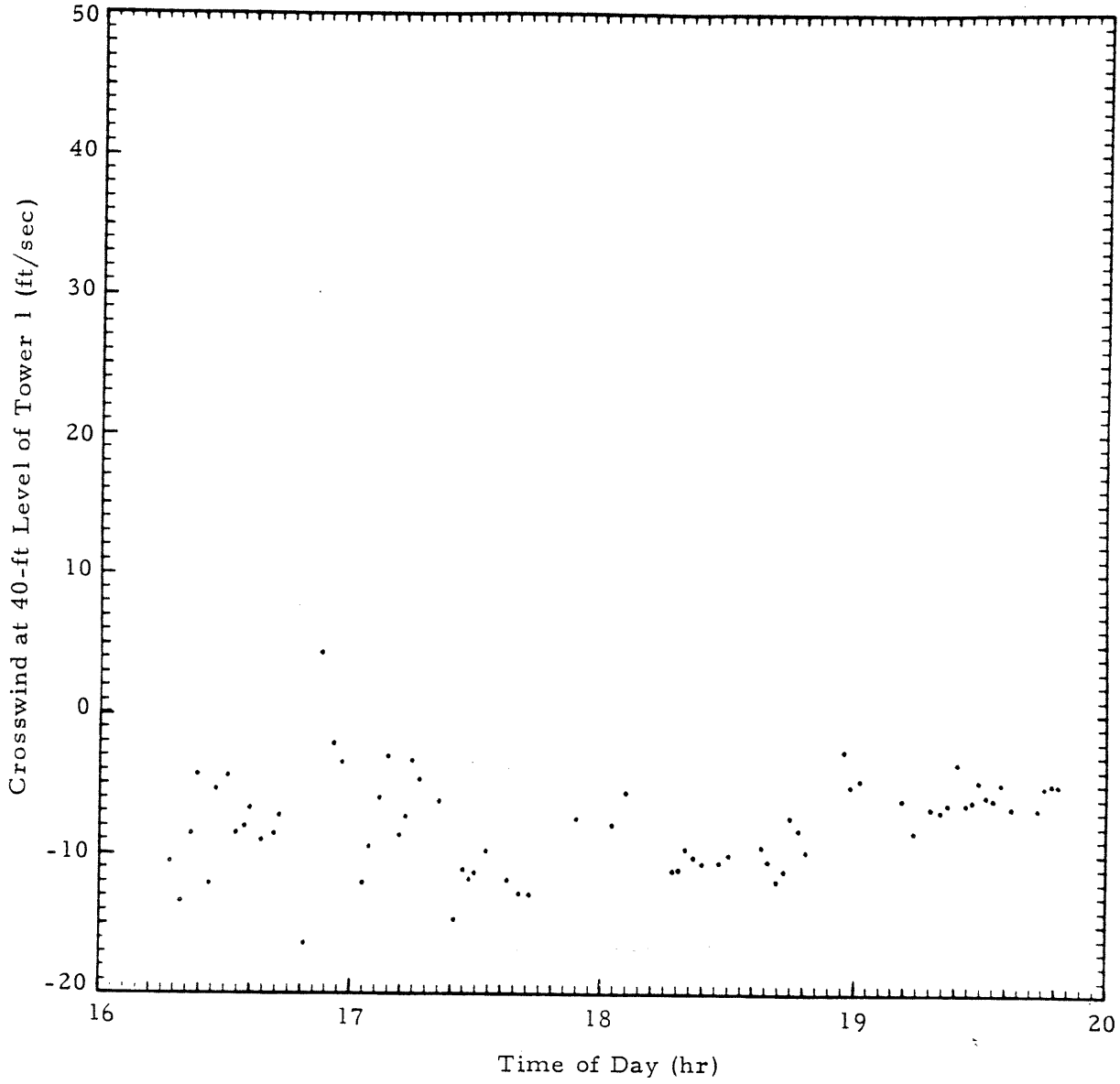

FIGURE 41. VARIATION OF CROSSWIND MEASURED AT 40-FT LEVEL OF TOWER 1 WITH TIME OF DAY FOR APRIL 17, 1975

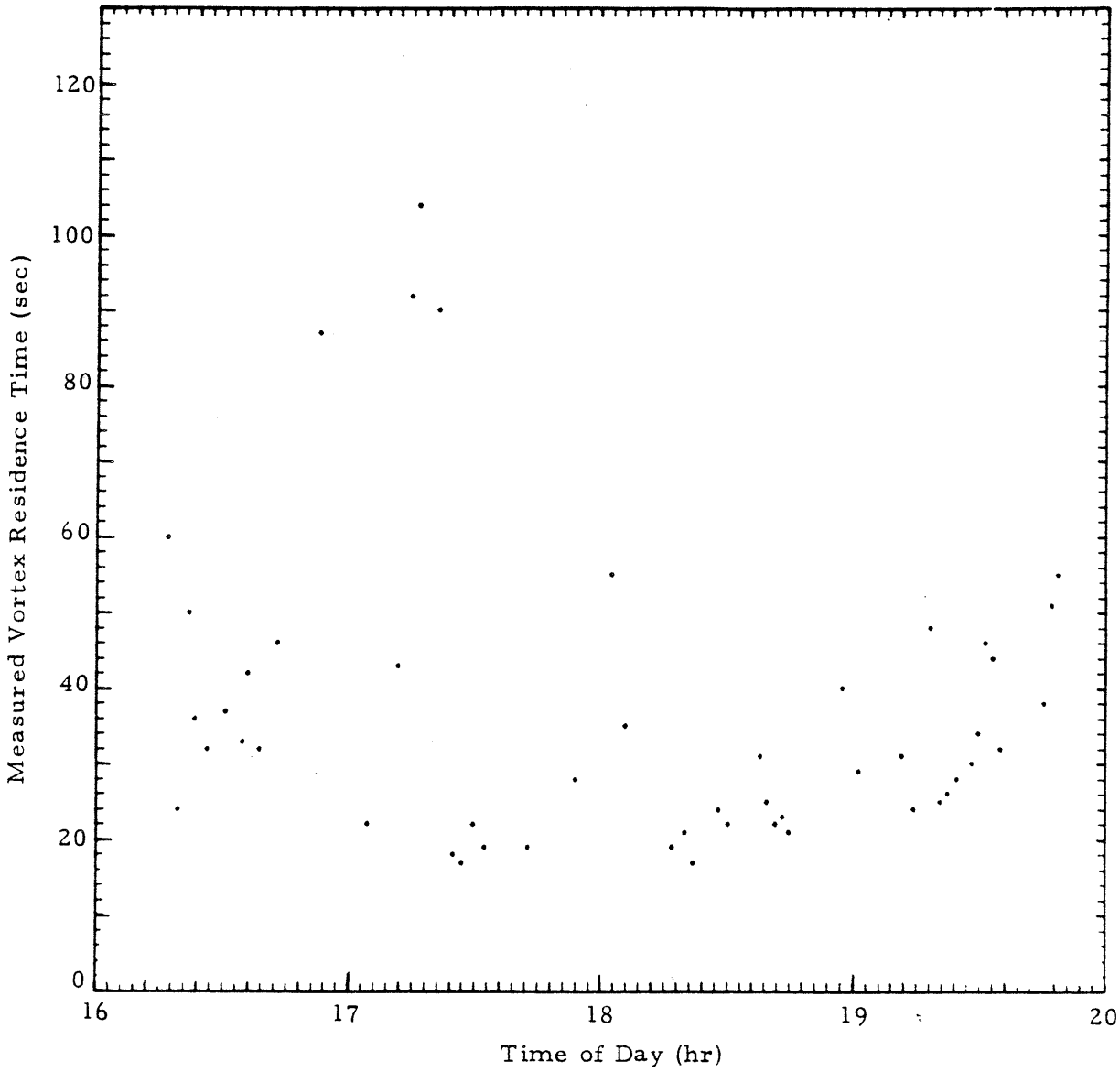

FIGURE 42. VARIATION OF VORTEX RESIDENCE TIME (AS MEASURED BY GROUND WIND ANEMOMETERS) WITH TIME OF DAY FOR APRIL 27, 1975

the asymptotic value of $\dot{Y}$ in ground effect is

$$\dot{Y} = V_\infty \pm \dot{Z}_o \sqrt{1 + Y_o^2/Z_o^2}. \tag{72}$$

For baseline 1 (Z_o = 208 ft), the asymptotic value of $\dot{Y}$ (relative to the wind) in ground effect is approximately the magnitude of the initial descent velocity for a constant vortex strength. Therefore, a comparison of the asymptotic value of $\dot{Y}$ with the magnitude of the initial descent velocity is a measure of the decay of the vortex pair.

For the comparison, the LDV data were used to calculate initial descent rate (from slope of altitude vs. time plot, cf. Fig. 23) and initial crosswind (from slope of lateral position vs. time plot, cf. Fig. 24). Numbers for port and starboard vortices were averaged. The asymptotic values of $\dot{Y}$ were taken from the slope of the ground wind anemometer data of the lateral position vs. time plot, (cf. Fig. 24). Good vortex tracks from the LDV and the ground wind anemometer were necessary to generate a comparison point. For the ground wind anemometer data, if $\dot{Y}_1$ and $\dot{Y}_2$ are the port and starboard transport velocities taken from the plot (recalling that they may be either positive or negative), then

$$\dot{Y} = (\dot{Y}_1 - \dot{Y}_2)/2 \tag{73}$$

is the asymptotic value of $\dot{Y}$ relative to the wind, and the crosswind is

$$V_\infty = (\dot{Y}_1 + \dot{Y}_2)/2. \tag{74}$$

For a constant vortex strength, the value of $\dot{Y}$ given by Eq. (73) should be approximately equal to the initial vortex descent rate (cf. Eq. (72)). Figure 43 shows the asymptotic lateral velocity from Eq. (73) as a function of the average (port and starboard) initial vortex descent rate. Some decay is noted,

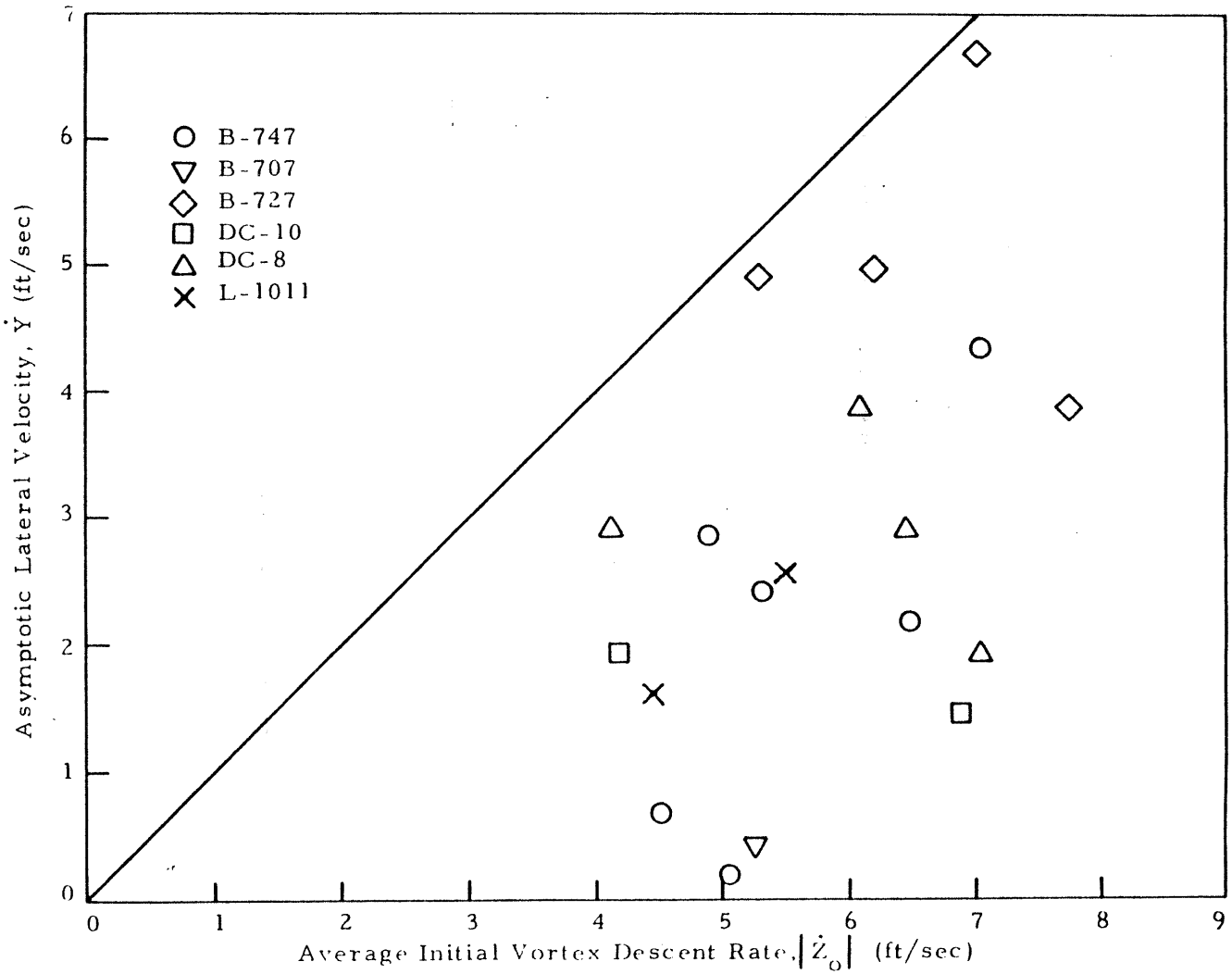

FIGURE 43. APPARENT VORTEX DECAY INFERRED FROM VORTEX TRANSPORT

except for the B-727. The B-727 decay is clearly less than that for other types. It is noted that all other types shown have wing-mounted engines, although this fact cannot be positively identified as the source of the difference. From Eq. (72), it should be expected that the ratio, $\dot{Y}/\dot{Z}_o$, should be less for the B-747 than for other aircraft. However, this does not occur.

The low decay rate of the B-727 has previously been documented. Reference 6 compares the decay rate of the B-747 with the B-727 based on peak recorded tangential velocity (not necessarily an indication of vortex strength) measured by tower-mounted anemometers. The empirically derived peak recorded tangential velocity was

$$V_{\theta_{max}} = (336.4 \text{ ft/sec}) e^{(-.0173/\text{sec})t} \tag{75}$$

for the B-747 and

$$V_{\theta_{max}} = (341.5 \text{ ft/sec}) e^{(-.0126/\text{sec})t} \tag{76}$$

for the B-727.

Except for the B-727, the asymptotic lateral veloctiy is less than 80% of the initial vortex descent rate. This has important implications in determining the value of crosswind above which transport time is less than a stated value. For example, for a B-747 at maximum certificated landing weight, the transport time is less than 60 sec if the crosswind is less than 7.2 ft/sec (Fig. 17). However, because of the effect shown in Fig. 43, the transport time will be less than 60 sec if the crosswind is less than 5.8 ft/sec (80% of 7.2 ft/sec).

A second implication of decay is that for light crosswind (i.e., the upwind vortex exits from the upwind flight corridor boundary), it is not possible to assert that the vortex residence time is less than a stated value

based on vortex transport. For example, from Fig. 13, the transport time for a B-747 at maximum landing weight is less than 60 sec for a crosswind of less than 2 ft/sec. However, if the vortex decays, the transport time may be much greater than 60 sec for a crosswind of 2 ft/sec. Therefore, for a fixed aircraft type and initial vortex altitude, it is always possible to find a magnitude of crosswind above which the transport time is less than some specified value, but (because of decay) it is never possible to find a magnitude of crosswind below which the transport time is less than some specified value.

Figure 44 shows a comparison of the crosswind measured at the asymptotic altitude with that measured at the initial altitude. It should be remembered that the asymptotic altitude measurements are recorded 30-60 sec after the initial altitude measurements. From velocity profile considerations, the crosswind at final altitude should be less than that at the initial altitude. For example, for the DC-8 and B-707, the crosswind at the final altitude should be 0.78 of the crosswind at the initial altitude for a power-law exponent of 0.2 The scatter of the data illustrates that the calculation of vortex transport time on the basis of an assumed velocity profile is not appropriate. Variations in wind due to unsteadiness during the vortex trajectory are much greater than variations in wind due to a velocity profile.

The data shown for Figs. 43 and 44 also illustrate that it is difficult to calculate the entire vortex trajectory from the initial velocity components of the vortex trajectory. In theory, if the vortex remains at a constant strength (or decay occurs at a predictable rate) and the wind is steady, the entire vortex trajectory can be calculated from the initial descent rate and the crosswind at the initial altitude. However, the unsteadiness shown in Figs. 43 and 44 preclude accurate calculation of the vortex trajectories in this manner. Section 5.4 discusses trajectory prediction from initial vortex conditions and presents sample plots of such predictions.

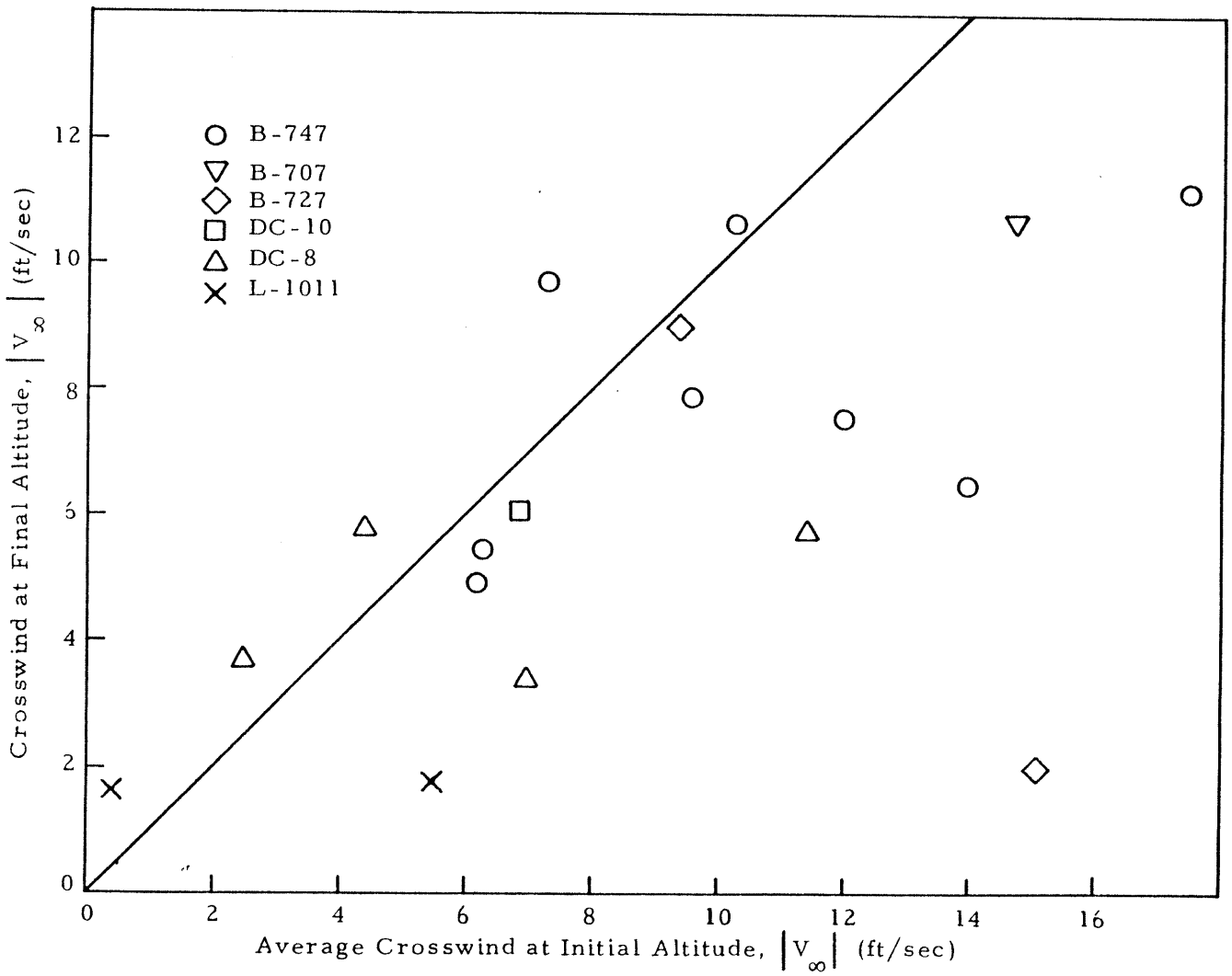

FIGURE 44 INITIAL AND FINAL CROSSWIND INFERRED FROM VORTEX TRANSPORT

4.1.4 Probability Distribution of Residence Time

Figure 5 shows the concept of the probability distribution of residence time. Obviously, the distribution function of residence time is a strong function of crosswind. Figure 5 is a strong function of crosswind. Figure 45 shows the probability distribution of residence times for selected ranges of crosswind. The individual points are the probabilities as calculated and plotted by the DMS. The solid lines are visually fitted smooth curves through the data points plotted by the DMS.

Section 1.4.3 discussed the importance of the "tail" of the distribution function. Figure 45 shows that such a tail exists, but the small quantity of data available for Fig. 45 precludes accurate quantitative definition of the tails. Several thousand flybys would be necessary for such definition.

4.1.5 Multiple Baseline Considerations

One of the important considerations in measurement of vortex residence time is the residence time at several baselines for the same flyby. Figure 46 shows a plot of measured residence time at baseline 2 as a function of residence time at baseline 1. Each point represents one flyby. Baseline 2 is 1500 ft closer to the runway than baseline 1. Figure 46 shows data for wide-body aircraft. The data for narrow-body aircraft show similar scatter.

The scatter in the data is not surprising. Figure 16 shows that significant differences in vortex transport time can occur between baseline 1 (initial vortex altitude of 200 ft) and baseline 2 (initial vortex altitude of 120 ft), even for identical crosswinds at the two baselines. In addition, the crosswind may be different at the two baselines (the distance between the two baselines is approximately half the distance between the two towers in Fig. 31).

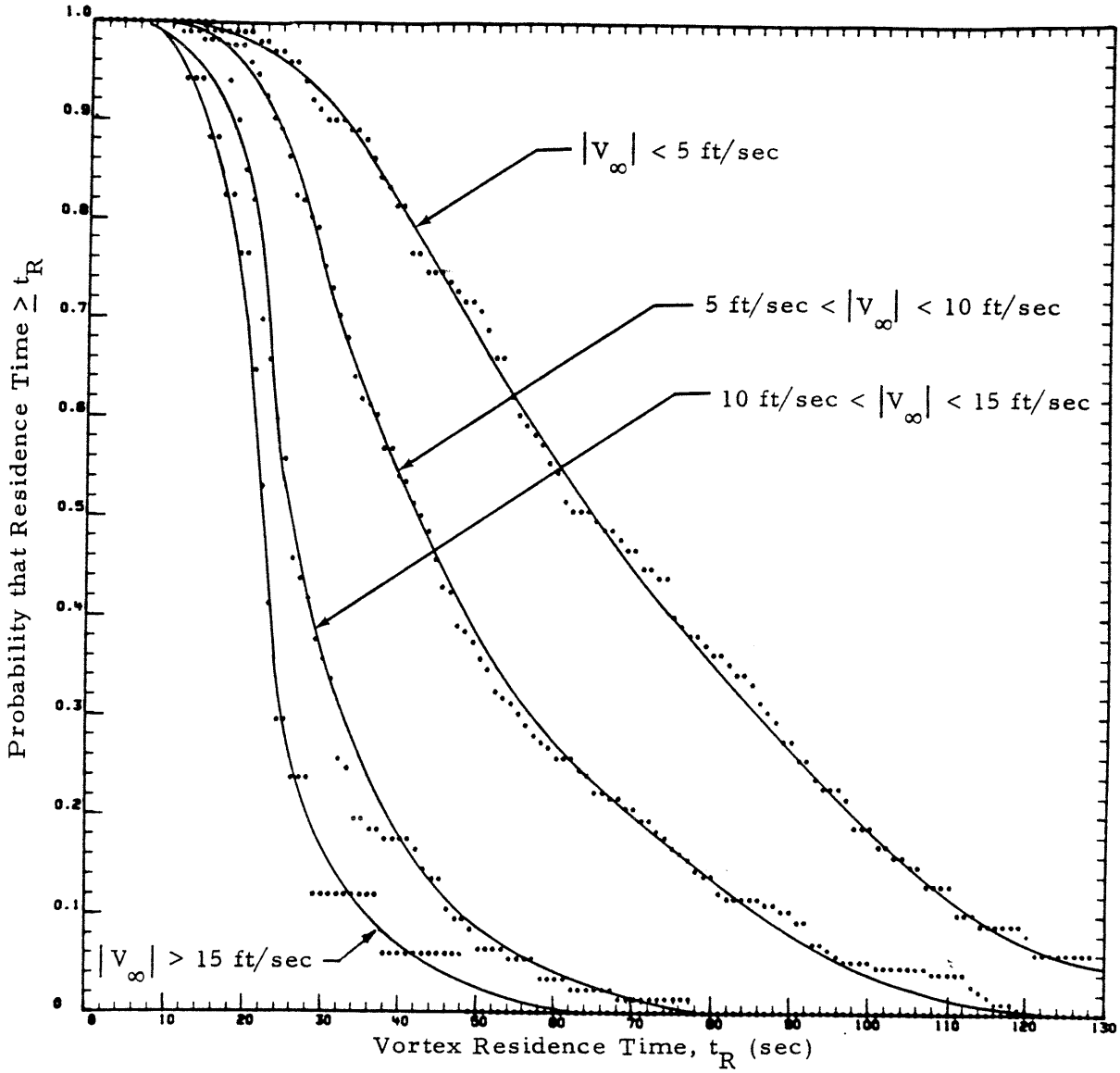

FIGURE 45. PROBABILITY DISTRIBUTION FUNCTION FOR MEASURED VORTEX RESIDENCE TIME AT BASELINE 1

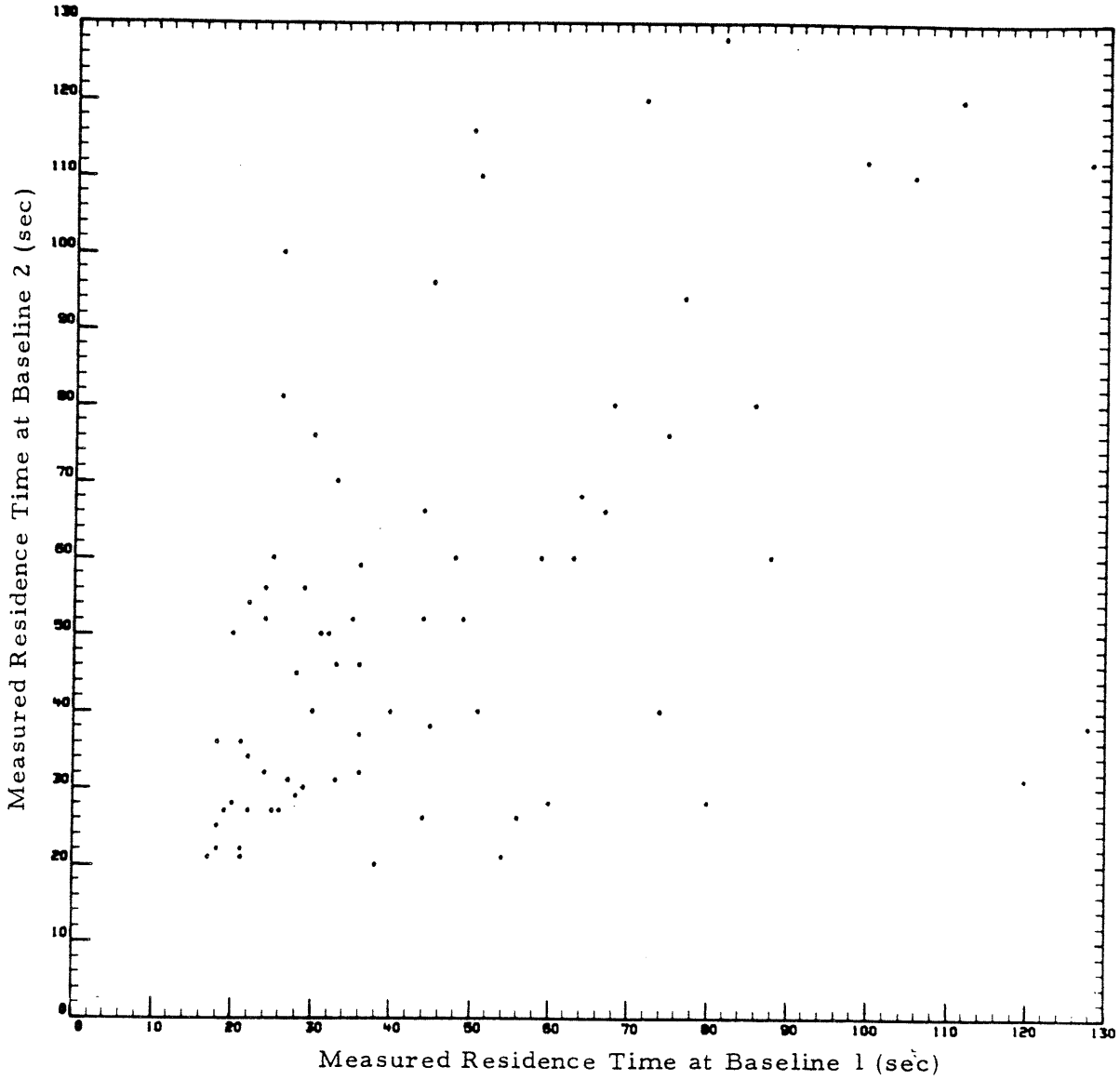

FIGURE 46. COMPARISON OF VORTEX RESIDENCE TIME MEASURED AT BASELINE 2 WITH VORTEX RESIDENCE TIME MEASURED AT BASELINE 1

The measured vortex trajectories for one of the points of Fig. 46 are shown in Figs. 47 and 48. The residence time for baseline 1 is approximately 120 sec, and that for baseline 2 is 31 sec. Figures 46-48 show that a short residence time at one baseline does not imply a short residence time at all baselines.

4.2 SITE DEPENDENCY

When the research program under which this report is written was conceived, it was believed that the wind profile was a very important parameter in vortex transport. This belief was support by calculations performed with the vortex transport model which showed significant variations in the vortex trajectory with variations in the wind profile parameters. The reference altitude was always 20 ft. Because of the apparent dependency of transport time on wind profile parameters, one of the original objectives of the program was to determine if there were characteristic values of wind profile parameters. Because of this original objective, most of the calculated meteorological parameters listed in Table 3 are related to the wind profile or to atmospheric stability, which is an indication of the bluntness of the wind profile. It was believed that the characteristic values of such parameters would be characteristic for a given site, but would vary from site to site.

Section 2.2.2 showed that wind profile parameters do not have a significant effect on vortex transport time if the reference altitude is chosen as the asymptotic altitude of the vortex pair. In this section, it is shown that characteristic values of wind profile parameters do not exist for averaging periods relevant to vortex behavior. Thus, this section shows that characteristic values of wind profile parameters do not exist, and Section 2.2.2 shows that such characteristic values are not necessary. However, the search for characteristic values of wind profile parameters led to a discussion of short-term meteorology as discussed in Section 4.3.

The original objective of obtaining values of site-dependent parameters was to obtain characteristic values which could be used in the vortex transport model. No such parameters were found. The distribution of landing

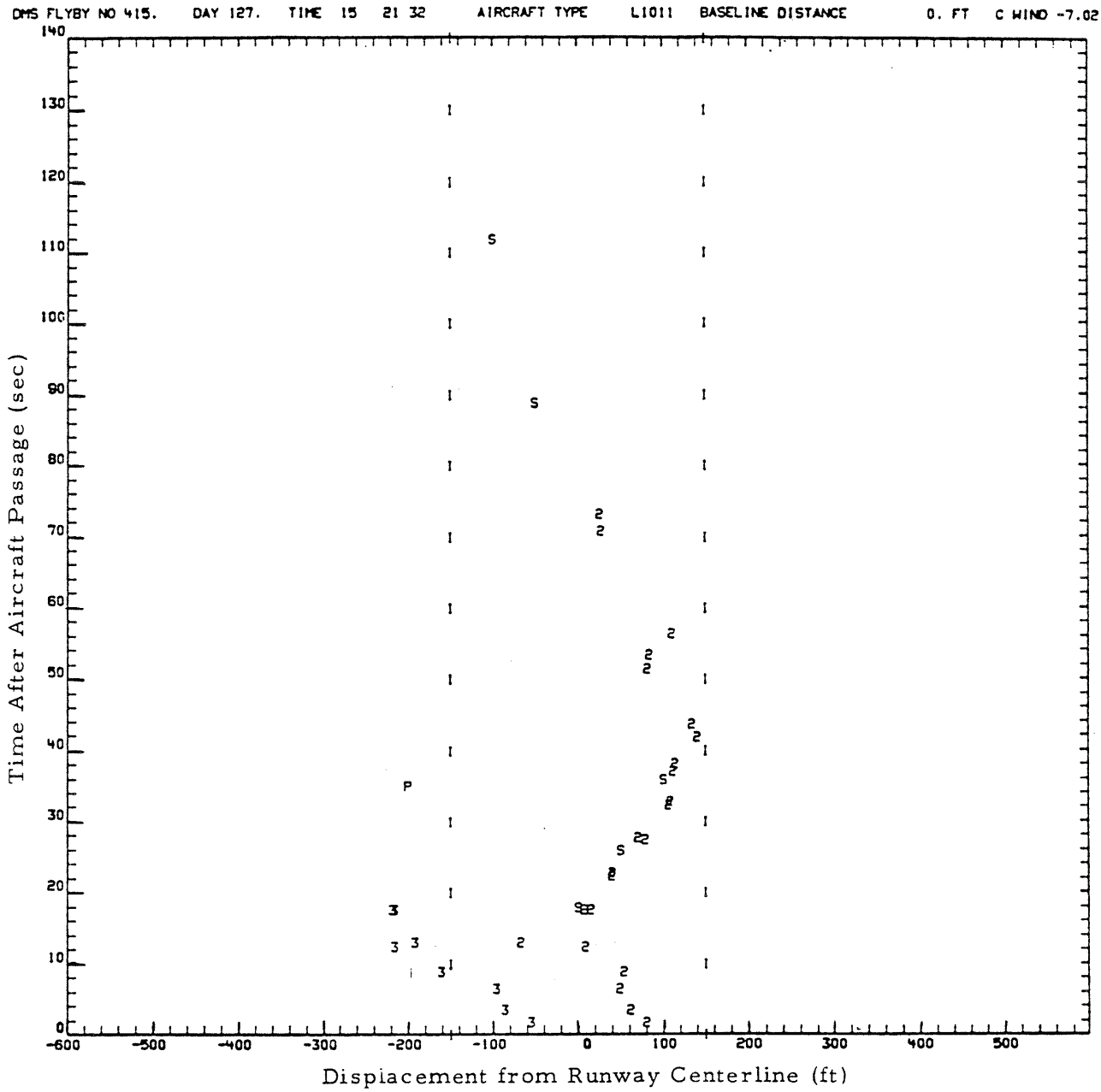

FIGURE 47. VORTEX TRAJECTORY FOR BASELINE 1

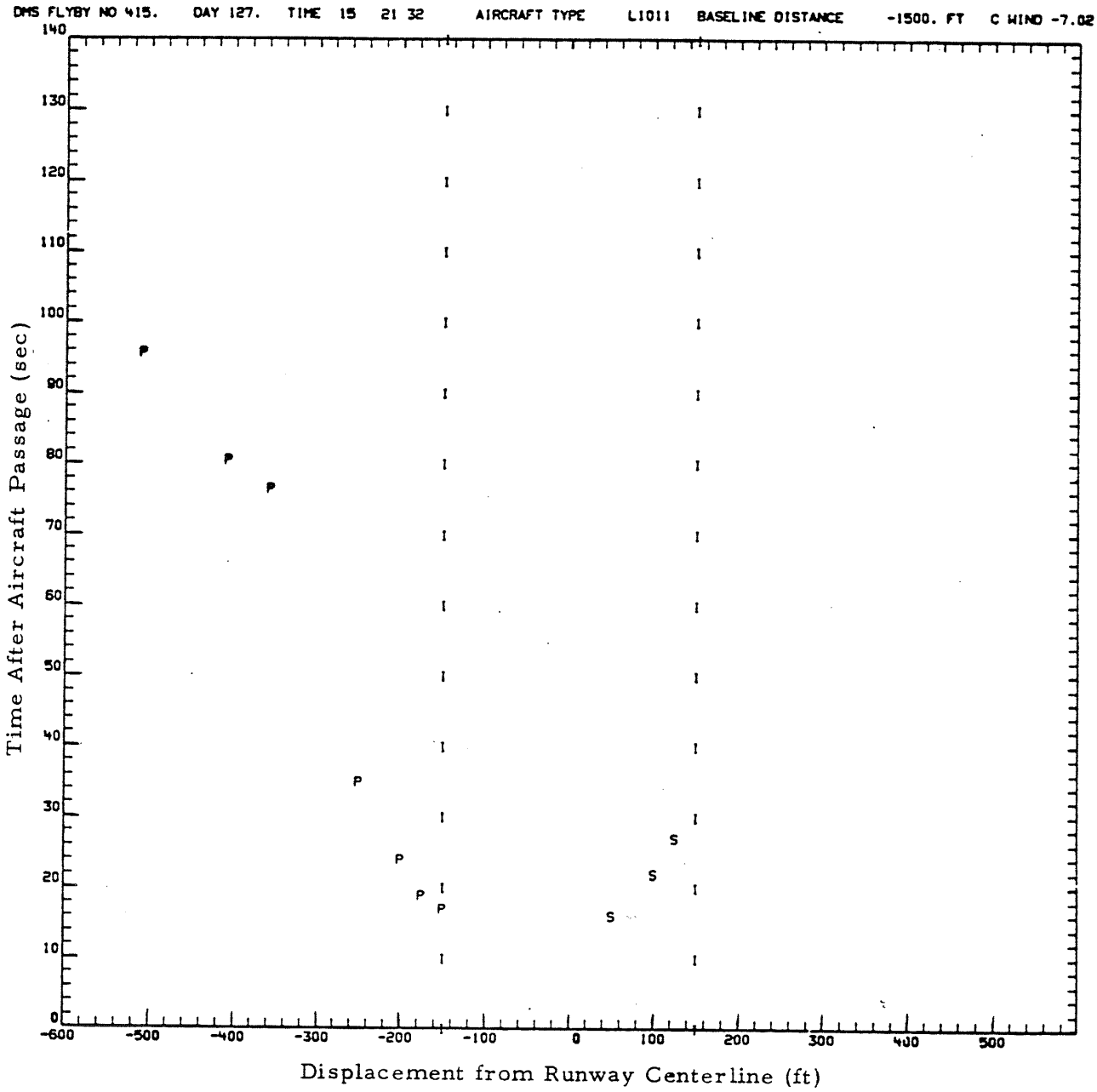

FIGURE 48. VORTEX TRAJECTORY FOR BASELINE 2

weight for each aircraft type may be an airport-dependent parameter, but aircraft weight data were not obtained at JFK. There are, however, two very important site-dependent parameters which affect the usefulness of a WVAS. These are the frequency distributions of wind and runway orientation. These parameters are discussed in Sections 4.2.2 and 4.2.3.

4.2.1 Wind Profile Considerations

Geographical considerations can affect the wind profile for a given site. Geographical considerations include nearby mountain ranges and bodies of water which may influence prevailing winds, turbulence structure, temperature, humidity, cloud cover and seasonal or diurnal variations in these factors. The latitude of the airport affects the strength of the Coriolis forces which, in turn, influence the Ekman spiral in the planetary boundary layer. The latitude also affects the insolation intensity which affects the temperature gradient and, hence, atmospheric stability.

Local terrain features include topography, vegetation and buildings and other structures. These local features affect the shape of the wind profile and conditions of turbulence, and introduce directional variations in these parameters. Since the data used in this study were taken from one site only, conclusions about variations in wind profile parameters from site to site was not feasible.

The meteorological parameters which define the wind profile are power-law exponent and logarithmic profile roughness length (for a logarithmic profile). The distribution of power exponent and logarithmic profile roughness length as a function of mean wind speed is shown in Figs. 49 and 50 for tower 3. The roughness length in Fig. 50 is ROUGH 1 in Table 3. A significant variation in the wind profile characteristics is observed. The large variation in values indicates that characteristic values do not exist.

The lack of a characteristic value is due to the short averaging times. In meteorological measurement, averaging periods of 15 min and longer are

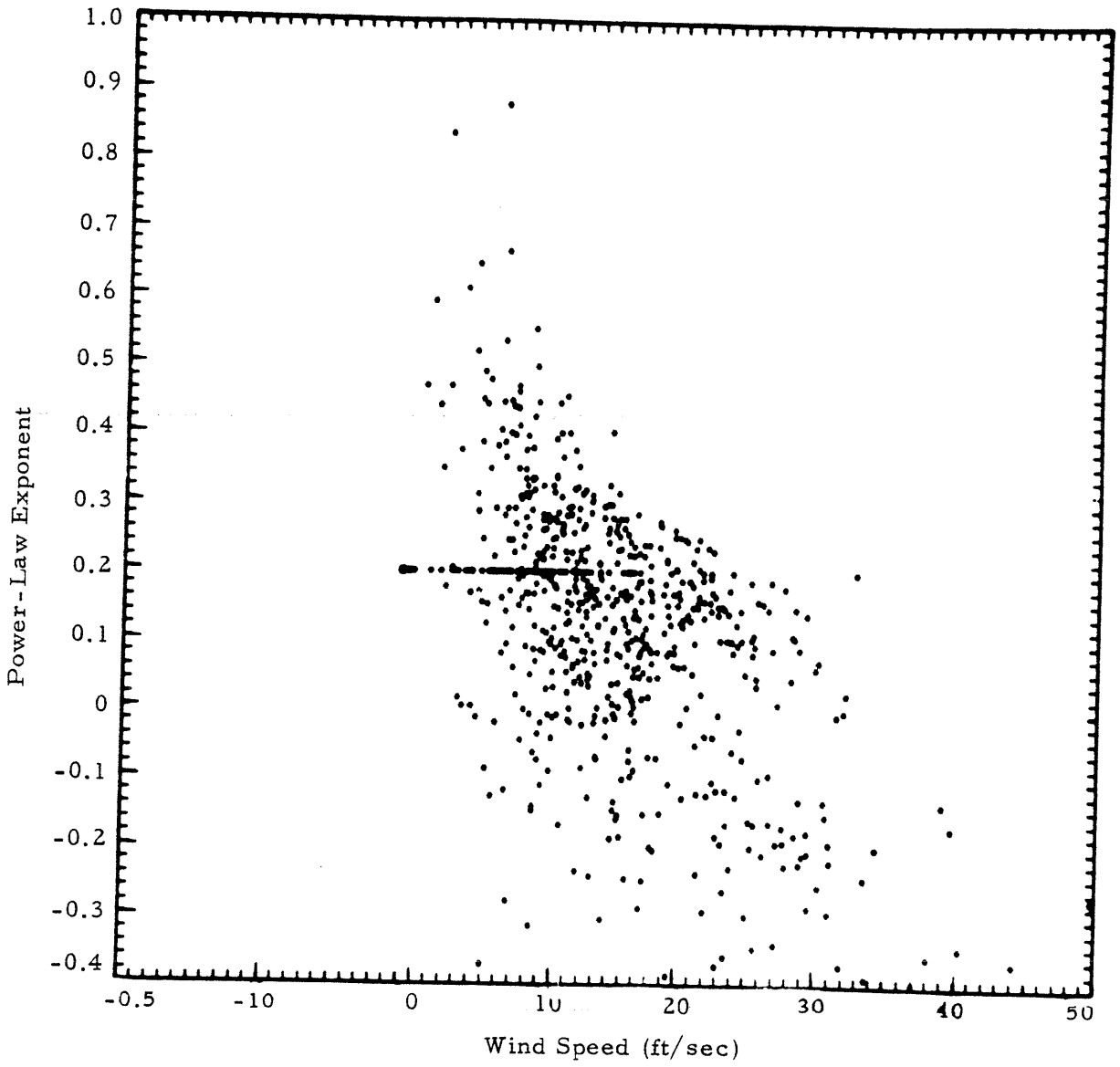

FIGURE 49. VARIATIONS IN POWER-LAW EXPONENT WITH WIND SPEED

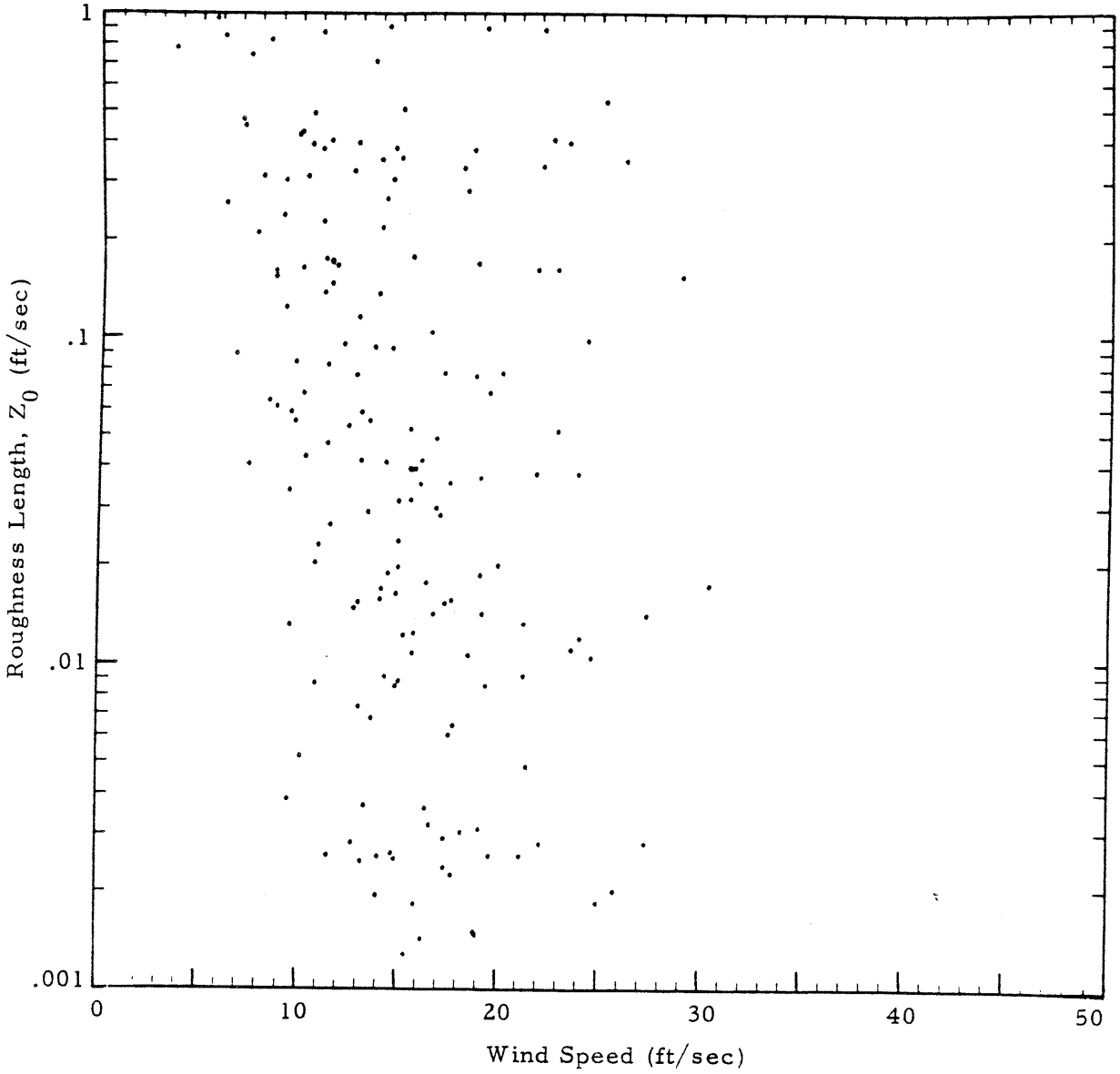

FIGURE 50. ROUGHNESS LENGTH FOR LOGARITHMIC WIND PROFILE AS A FUNCTION OF WIND SPEED

used. These time periods are much too long to have any relevance to vortex behavior. Thus, for the time periods of relevance to vortex behavior, characteristic values of wind profile parameters do not exist.

4.2.2 Wind Considerations

The frequency distribution of the crosswind for a given airport over an extended period is a characteristic site-dependent function. The crosswind distribution obtained for runway 31R at JFK during 1975 is shown in Fig. 51. The crosswind measurements were made over a 128-sec averaging period subsequent to each flyby, the flybys occurring intermittently throughout the year. The mean and the standard deviation of the crosswind velocity observed for the approximately 800 flybys for which crosswind measurements were available were -0.91 ft/sec and 10.9 ft/sec, respectively. It is noted that a negative crosswind velocity and a drift of the wake vortex in the port direction is prevelant. It is noted, however, that the data contained in Fig. 51 are limited to times for which data were taken (usually 0800 to 1700) when runway 31R was active. It does not imply an overall frequency distribution of crosswind. Also, vortex considerations were not a factor in runway selection as they might be with an operational WVAS. The variance in crosswind for all time would be expected to be greater than that shown in Fig. 48 because one of the factors in runway selection is avoidance of large crosswind.

The complete frequency distribution of prevailing wind is a very important site-dependent parameter. Of particular importance is the frequency distribution of wind for times of day when traffic is large enough to require maximum airport capacity and when turbulence is low enough to permit long vortex life. The frequency distribution of turbulence in peak traffic periods is also an important consideration.

Of equal or greater importance is the probability of wind change over a short period of time (1 to 10 min). The conditional probability distribution function at some time, $t_o + \Delta t$, given that the wind at time, t_o, is known is

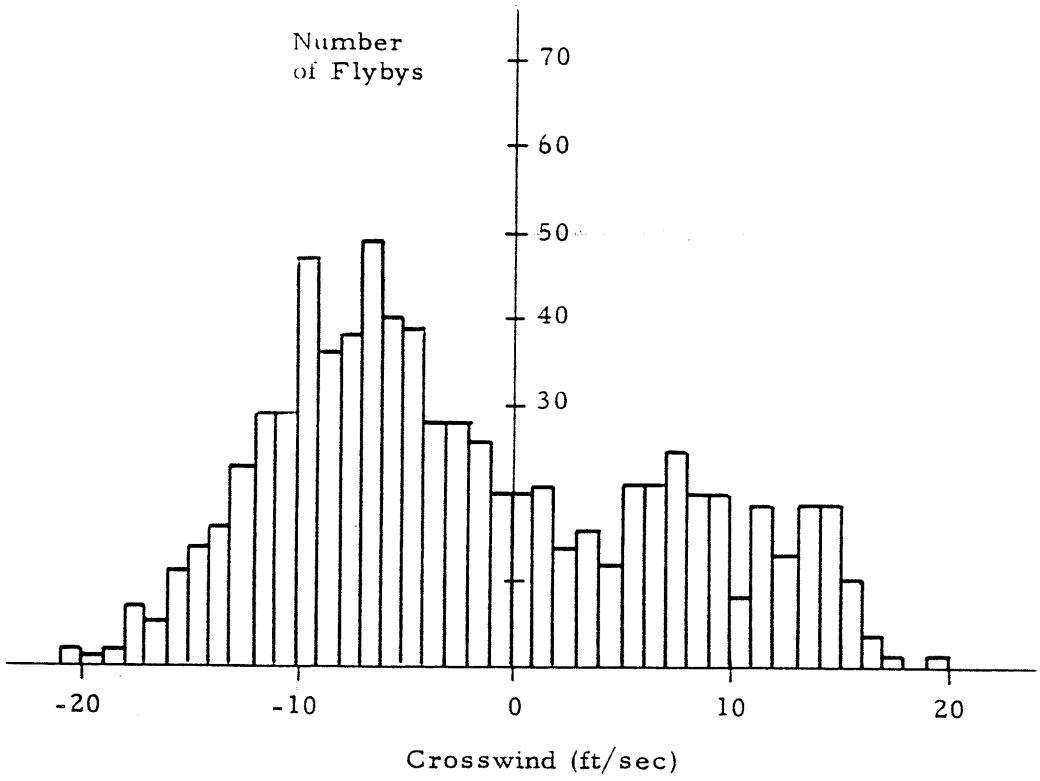

FIGURE 51. DISTRIBUTION OF NUMBER OF FLYBYS AS A FUNCTION OF CROSSWIND VELOCITY MEASURED AT THE 40-FT LEVEL FOR TOWER 1 FOR RUNWAY 31R AT KENNEDY INTERNATIONAL AIRPORT

particularly important. Unfortunately, continuous wind measurements were not made during the data collection phase of the work reported herein, and the calculation of such conditional probabilities is not feasible. The concept of conditional probabilities of wind is deserving of further investigation. The subject of wind prediction is discussed further in Section 5.2.

4.2.3 Runway Orientation

One of the most important site-dependent parameters is the number and orientation of available runways. Since crosswind is an important parameter in the determination of vortex residence time, the runway orientation chosen for a particular wind is an important controllable parameter. The concept of runway selection for vortex considerations is shown in Fig. 52. Kennedy International Airport has two runway orientations: Runways 13-31 and Runways 4-22. Using the criterion of the vortex advisory system (Ref. 3) that vortex residence time always permits 3 n mi aircraft separations if the crosswind exceeds 5.5 knots (9.3 ft/sec), Fig. 52 shows the magnitudes of crosswind for Runways 4-22 and Runway 13-31. For May 27, 1975, Runway 13-31 is the better choice (because of a lower probability of crosswind less than 9.3 ft/sec) until 11:30. After 11:30, Runway 4-22 has no crosswind less than 9.3 ft/sec and is therefore the better runway from consideration of vortex-imposed constraints on aircraft separations. For May 28, 1975, neither runway would permit 3-nautical-mile separations. Figure 53 shows similar information for June 2 and 3, 1975. For June 2, Runway 4-22 is the preferred runway until 12:00, after which neither runway can be approved for 3-nautical-mile separations. On June 3, Runway 4-22 is clearly the preferred runway from consideration of vortex-imposed constraints on aircraft separations.

From the examples shown in Figs. 52 and 53, it is clear that the number of runway orientations available at a specific airport and their orientation relative to prevailing winds are very important site-dependent parameters. A large number of available runway orientations implies a larger probability that a runway with wind favorable to short residence time can be found.

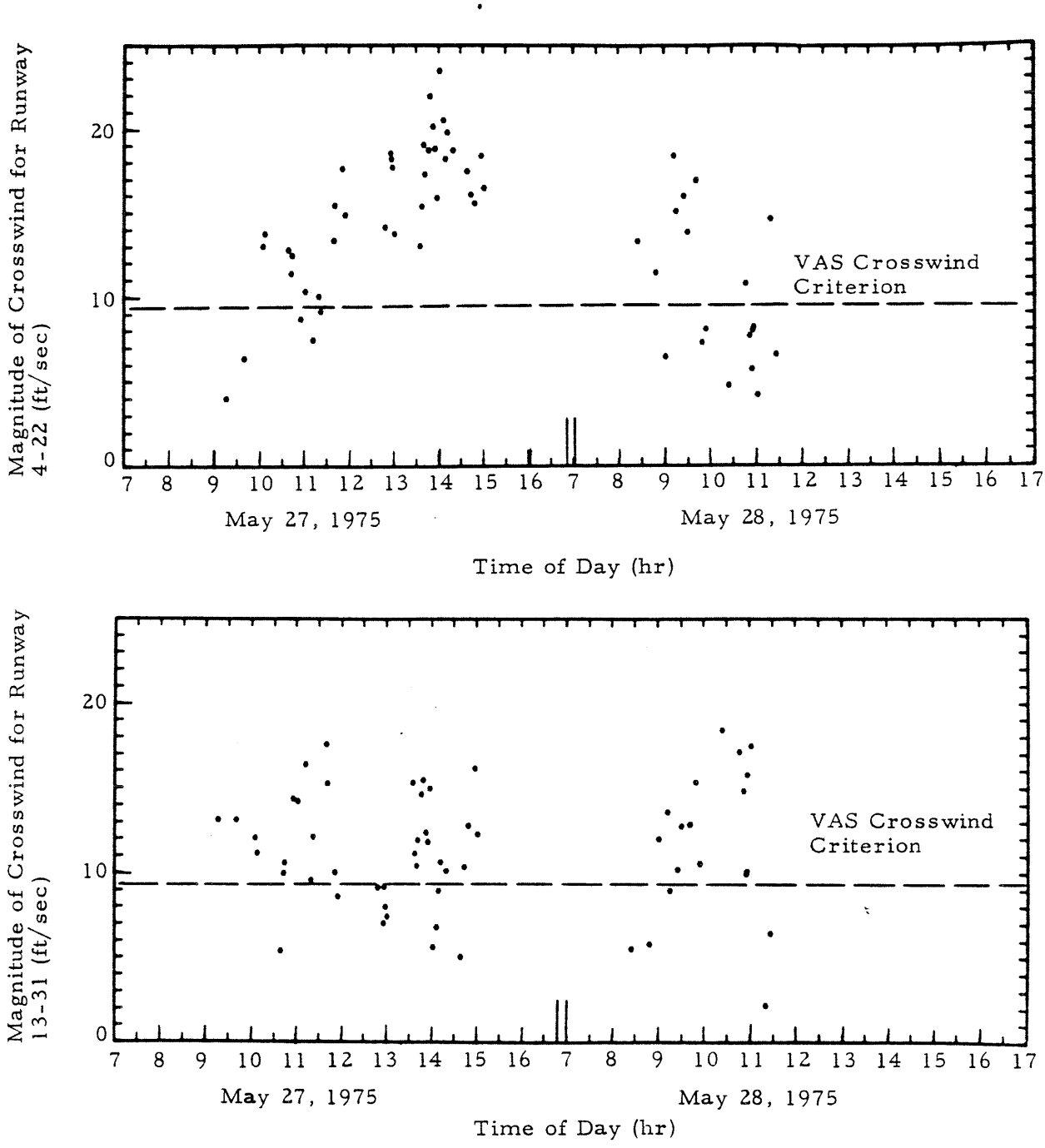

FIGURE 52. EXAMPLE OF CHOICE OF RUNWAY FOR MINIMIZATION OF VORTEX-IMPOSED SEPARATION CRITERIA – MAY 27-28, 1975

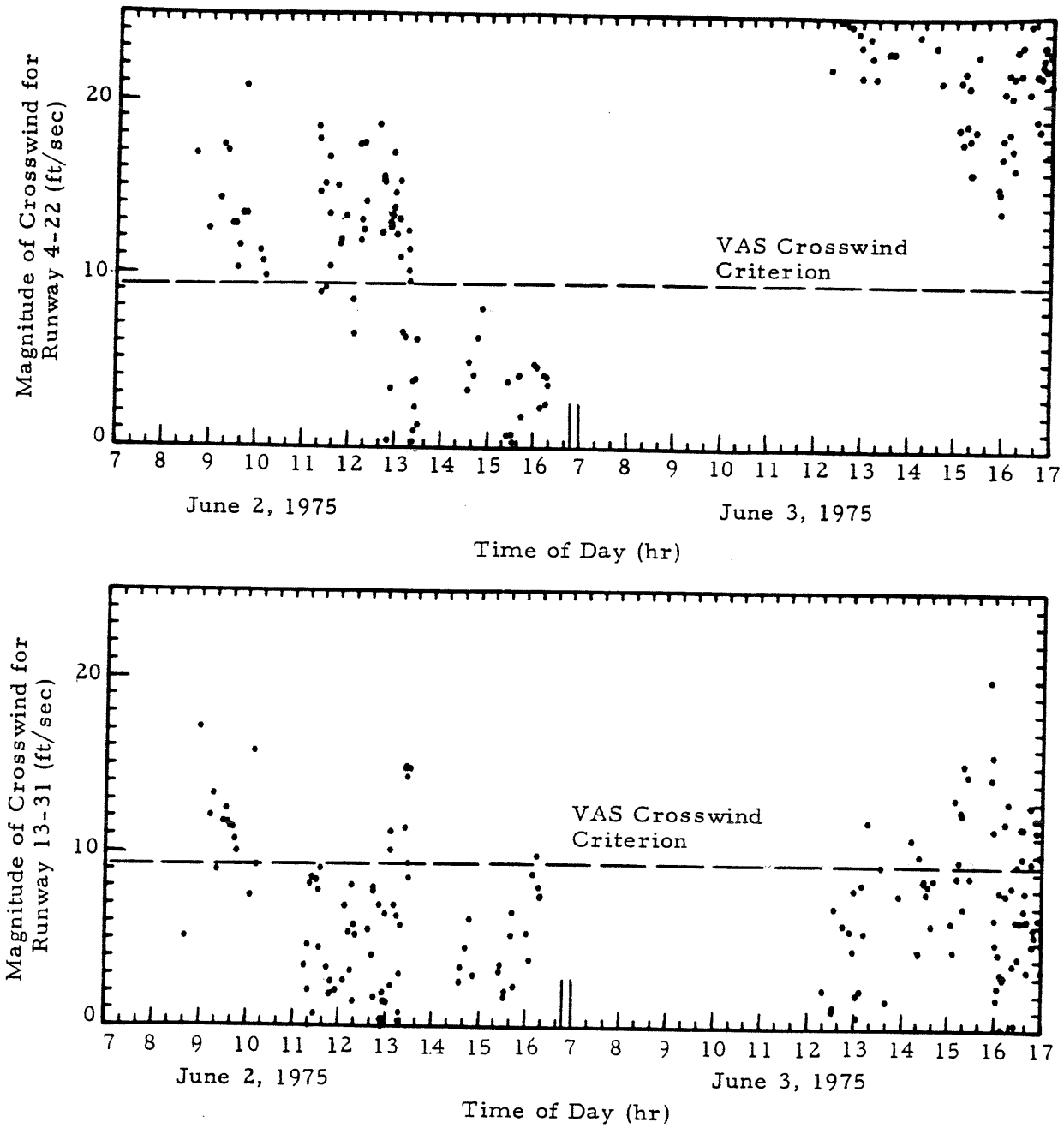

FIGURE 53. EXAMPLE OF CHOICE OF RUNWAY FOR MINIMIZATION OF VORTEX-IMPOSED SEPARATION CRITERIA – JUNE 2-3, 1975

4.3 SHORT-TERM METEOROLOGY

Sections 4.1 and 4.2 show two important observations related to wind: (1) there can be significant differences in crosswind over distances of approximately 3000 ft; and (2) an analysis of the parameters which define the wind speed profile failed to indicate any value which could be considered to be characteristic of the location at which the data were taken. It is noted that the atmosphere has mean characteristics with random perturbations imposed upon it and that the mean characteristics (i.e., characteristic values of power-law exponent and logarithmic roughness length) are obtained by averaging over some time period. From the observed data it is hypothesized that the 128-sec averaging time is too short for the generation of characteristic values of power-law exponent and roughness length and that characteristic values would emerge from longer averaging time (e.g., 15 minutes).

To verify that the variances in the meteorological measurements were real, comparisons of the wind speed and direction recorded by the meteorological towers with those made by the National Weather Service tower and those reported by the control tower were made. A sample of the data, shown in Fig. 54, indicates that the TSC meteorological towers were in general agreement with other available sensors. These results demonstrated that the large variances in the meteorological measurements were a real phenomenon. Possibly they may be attributed to the relatively short sampling period (128 sec) and to the irregular manner in which the measurements were made. The measurements were not made continuously or at fixed time intervals. Instead, they were made subsequent to airplane flybys. It is believed that longer averaging periods and continuous sampling of the meteorological measurements would reduce the variances in the meteorological parameters. For example, the normal variation in crosswind and downwind with time is illustrated in Fig. 55. It can be observed that averaging periods longer than 128 seconds would tend to smooth out the low frequency component present in the signal.

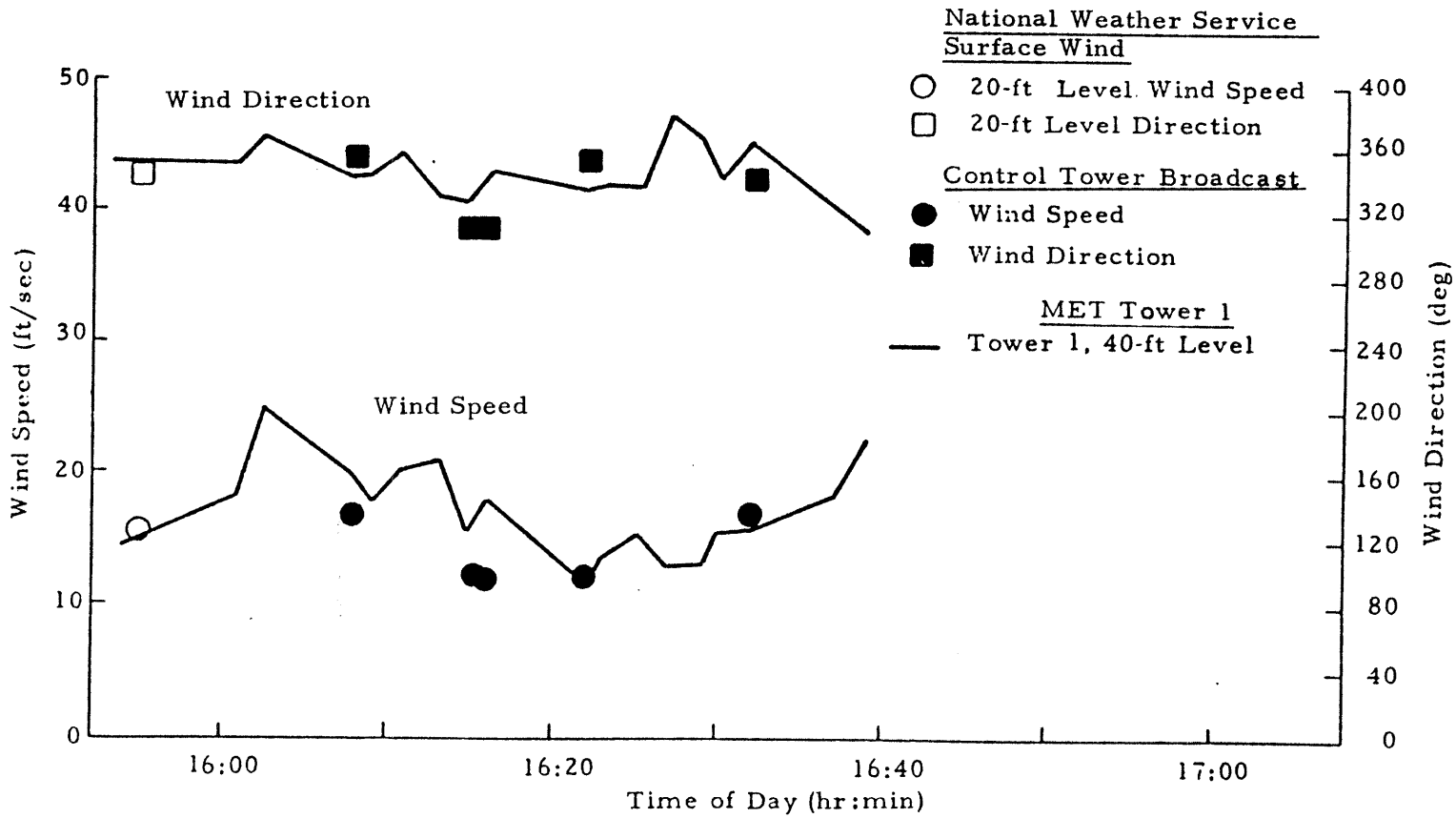

FIGURE 54. COMPARISON OF WIND SPEED AND DIRECTION MEASUREMENTS AT JFK AIRPORT FOR MAY 7, 1975, AS MEASURED BY THE NATIONAL WEATHER SERVICE ANEMOMETER AND BY TOWER 1

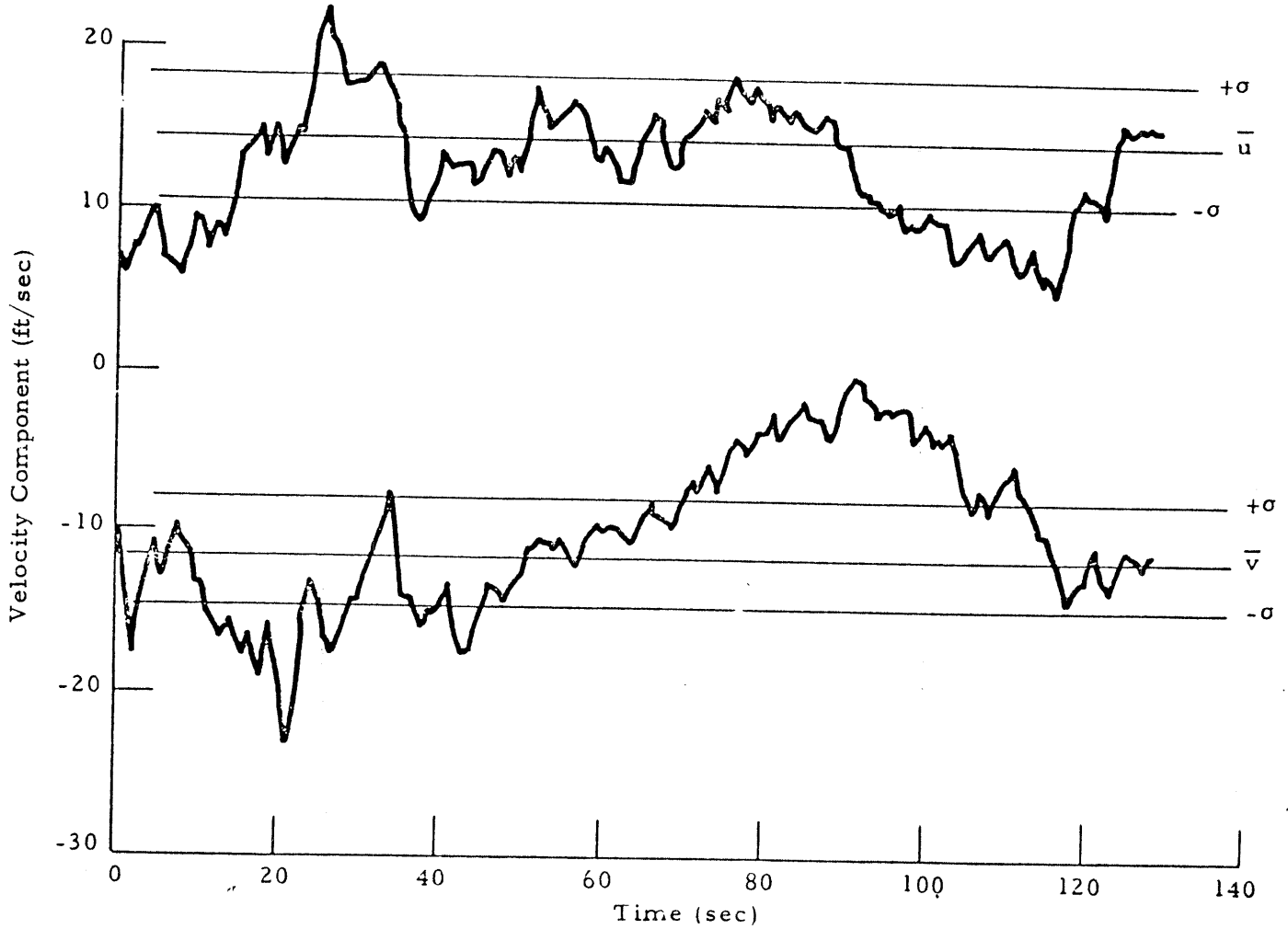

FIGURE 55. TOWER 1, 40-FT LEVEL WIND MEASUREMENTS AT JFK ON MAY 7, 1975, 16:1:16 FOR DC-9 FLYBY CATALOG NO. 426

If longer averaging times are required to produce a characteristic value of terrain-related parameters, such characteristic values would have little meaning in the vortex context. In order for a meteorological parameter to have meaning in the vortex context, it must have a definite value over a period of time approximating the life time of the vortex. Therefore, it is hypothesized that the concepts of a mathematically definable wind profile may have little meaning for the short time periods relevant to vortex lifetime.

The conditions which cause the difference in the crosswinds measured by two towers were investigated. As expected, the difference increases as the distance between the towers increases. Figure 56 shows a comparison in wind measured by tower 2 (located approximately 800 ft from tower 1) with those measured by tower 1. The scatter was significantly less than the comparison between tower 3 and tower 1 shown in Fig. 31.

It was hypothesized that the difference in measured wind between towers might be related to the standard deviation of wind. However, no such relationship was found. Figure 57 shows the difference in winds measured by the towers as a function of the standard deviation of wind measured by tower 1. No discernible functional relationship exists. Apparently the standard deviation of wind at a single sensor is caused by a perturbation of shorter frequency than that which causes the difference between towers. Figure 55 shows both low-frequency and high-frequency perturbations.

Another significant topic related to short-term meteorology is the effect of averaging time on the calculated values of average wind. Figure 55 suggests that average winds resulting from an averaging period of 30 sec or 60 sec could be significantly different from the 128-sec average. Figures 58 and 59 show sample comparisons of short period averages with 128-sec averages. It is probable that some of the scatter in Fig. 39 is due to the fact that the crosswind is a 128-sec average, whereas the vortex phenomenon has an active life of less than 60 sec.

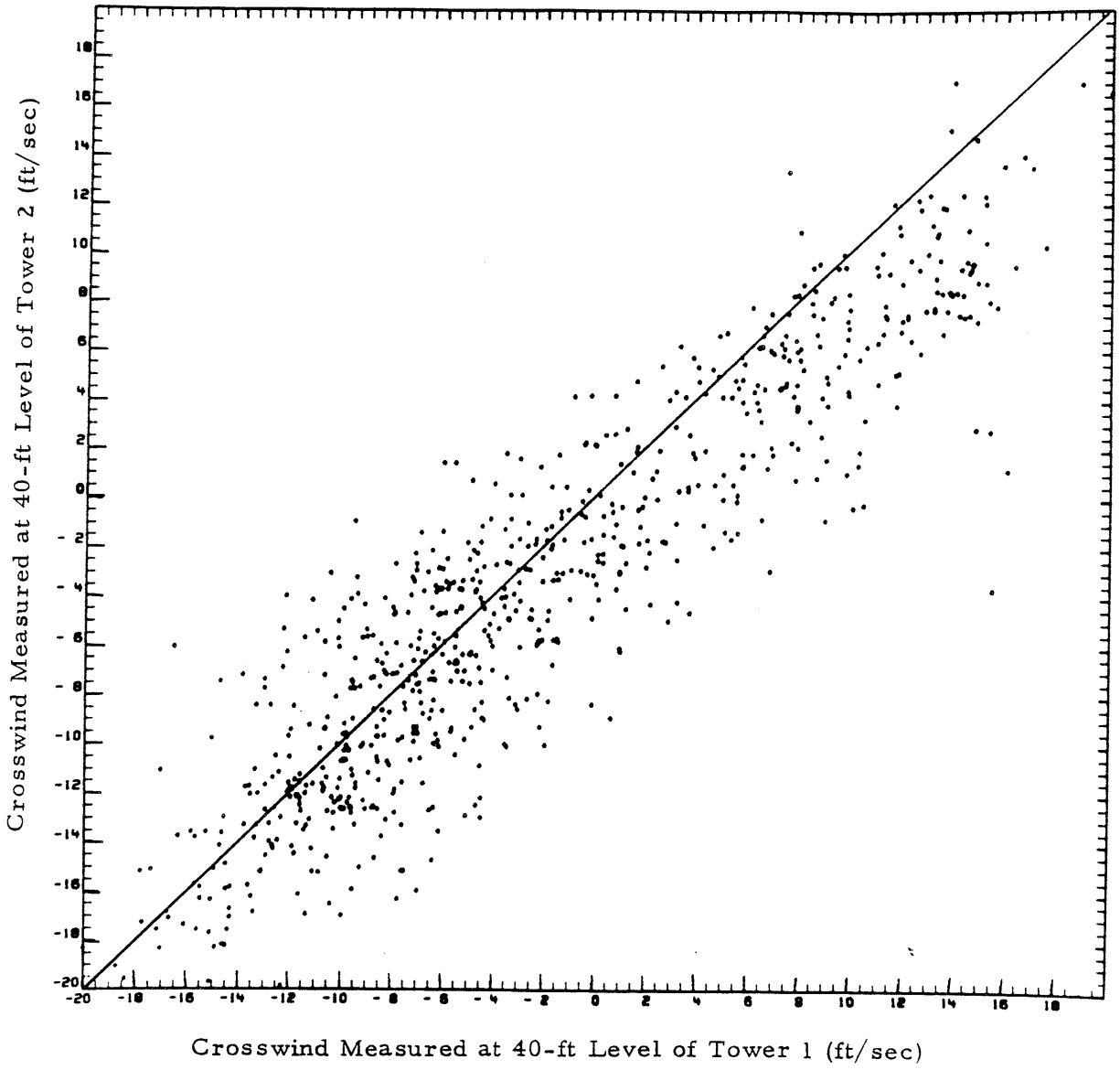

FIGURE 56. COMPARISON OF CROSSWIND MEASURED BY TOWER 2 WITH CROSSWIND MEASURED BY TOWER 1

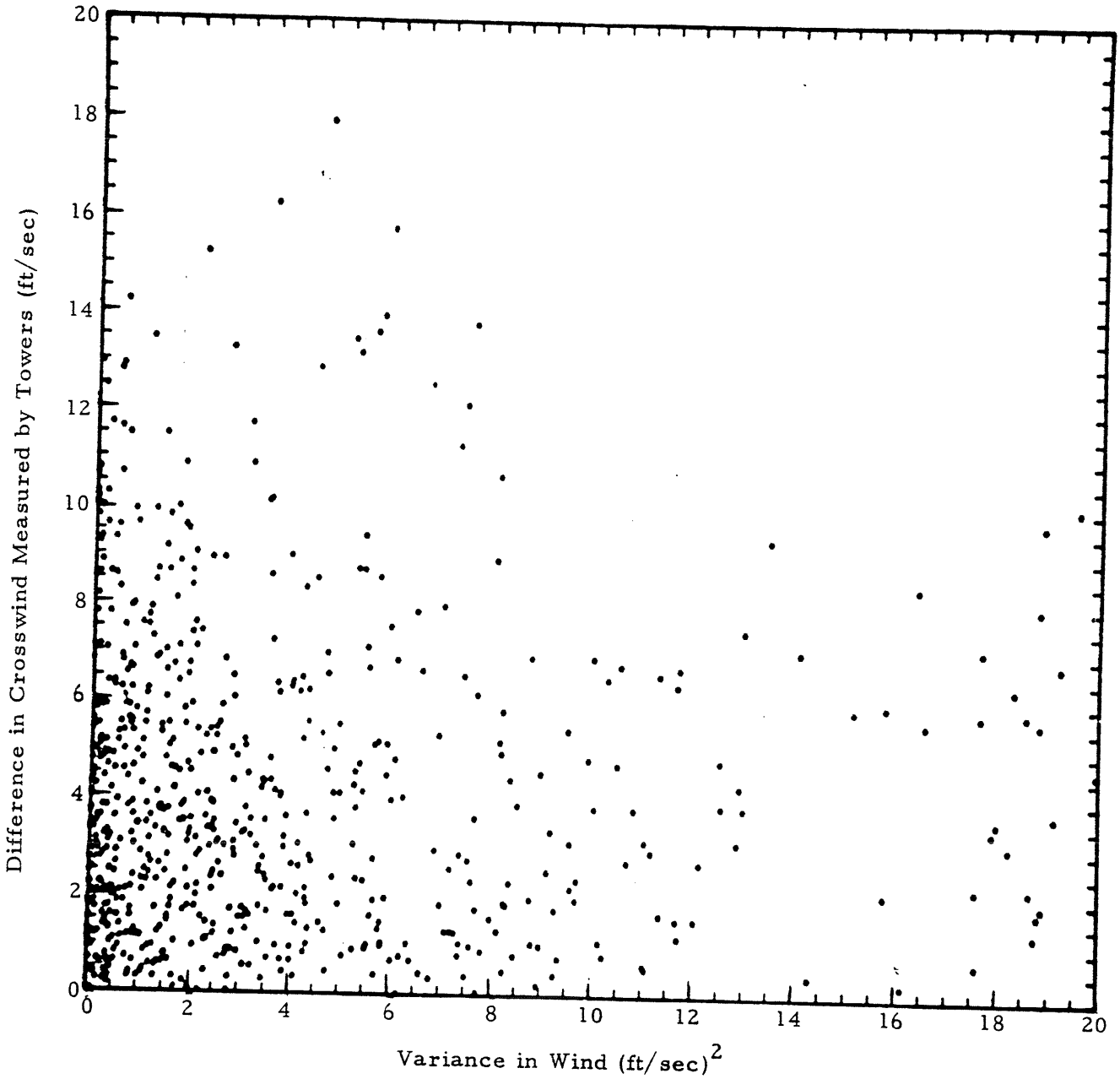

FIGURE 57. DIFFERENCE IN CROSSWIND MEASURED AT TOWER 3 AND CROSSWIND MEASURED AT TOWER 1 AS A FUNCTION OF VARIANCE IN CROSSWIND AT TOWER 1

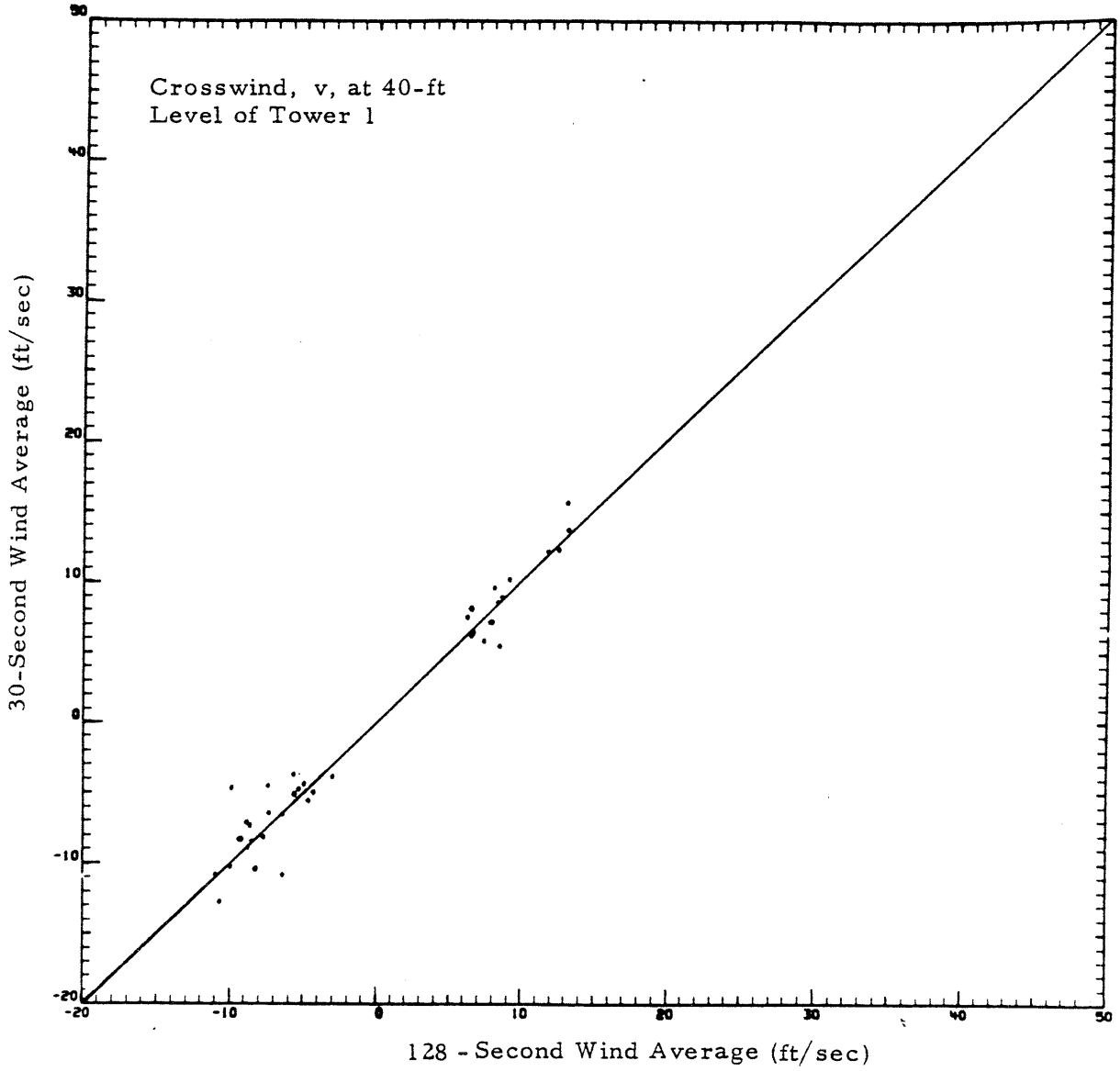

FIGURE 58. COMPARISON OF 30-SECOND WIND AVERAGE WITH 128-SECOND WIND AVERAGE FOR MAY 16, 1975

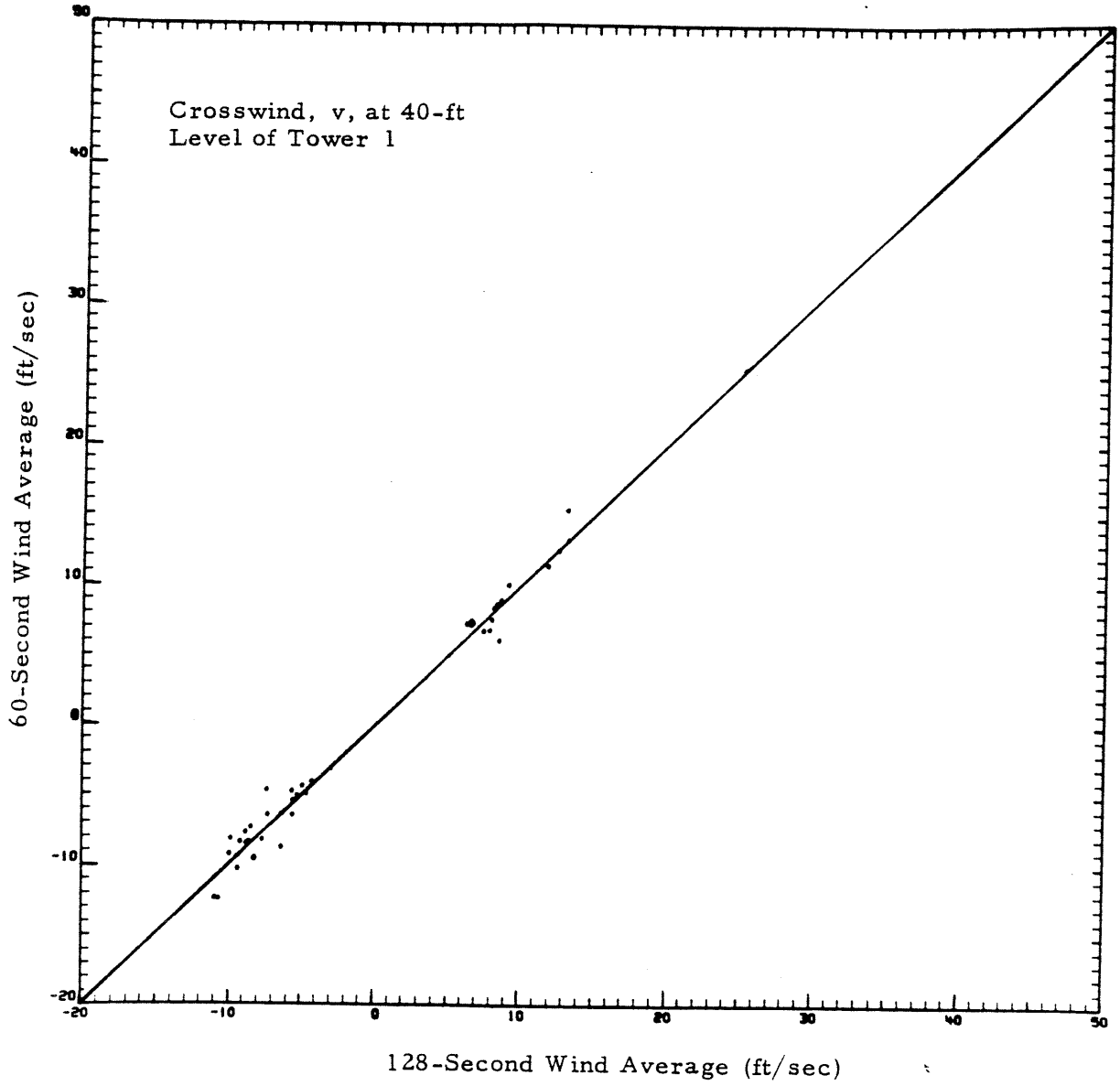

FIGURE 59. COMPARISON OF 60-SECOND WIND AVERAGE WITH 128-SECOND WIND AVERAGE FOR MAY 16, 1975

It is noted that there is no "a priori" best averaging time for wind. The best averaging time is the vortex life time. Therefore, the use of a 60-sec averaging period would give no better results than those given in Fig. 39 because the 60-sec averaging time would not be appropriate for vortices having life times of ~ 30 sec or ~ 120 sec. For the purposes of this report, the long averaging time is more appropriate than a short averaging time because the primary concern is vortices with long life time.

5. VORTEX PREDICTION FROM VORTEX SENSING

From the beginning of the formulation of the concept of wake vortex avoidance systems, it has been assumed that some type of vortex sensor would provide a feedback loop which would be used to predict future vortex behavior. However, prior to this report, no definitive concept of how such feedback should be formulated has been established. The previous sections of this report provide a background against which a feedback formulation must be established. In particular, the uncertainties associated with vortex behavior have been established. The uncertainties are the "noise" of the feedback loop and are extremely important in the formulation of a feedback loop. This section defines several methods for vortex prediction using vortex measurement as feedback information.

The section discusses both short-term residence time prediction and trajectory prediction. Short-term residence time prediction is used to predict vortex residence time for 5 to 30 minutes in advance. The purpose of such prediction is the establishment of appropriate aircraft longitudinal separations at the time at which such separations are normally established. Trajectory prediction is the prediction of the entire vortex trajectory, based upon measurements made during the early part of the trajectory. Its purpose is the use of the "tail" of the probability distribution function shown in Fig. 5. As discussed in Section 1.4, a significant reduction in delay can be achieved by accepting a very small probability that a vortex will not clear the vortex corridor during the time interval between successive aircraft. A missed approach or other evasive maneuver can be performed in the very few cases in which such a condition occurs. However, such a procedure requires an ability to predict vortex residence time soon after generating aircraft passage so that a following aircraft may be given adequate warning if a missed approach or other evasive maneuver will be required. Trajectory prediction provides that capability.

The primary tool of short-term prediction and trajectory prediction is Kalman filtering. Kalman filtering is described in Refs. 35 and 36. One of the advantages of Kalman filtering is that it defines the variance of the values of predicted parameters as well as expected values of such parameters. The first part of this section is an introduction to Kalman filtering. Section 5.2 contains a formulation for the application of Kalman filtering to short-term prediction of winds. Vortex transport time can be predicted from the wind prediction. Such wind prediction is also applicable to the Vortex Advisory System (VAS) as discussed in Section 1.4.3; Section 5.3 contains a formulation for the application of Kalman filtering to short-term prediction of residence time using direct measurement of transport time and life time. Section 5.4 presents trajectory prediction using initial measured vortex trajectory parameters. Section 5.5 presents trajectory prediction using Kalman filtering.

5.1 INTRODUCTION TO KALMAN FILTERING

The basic formulation of Kalman filtering is presented in this section. The formulation presented in Ref. 35 is used. Derivations are not presented, and the reader is referred to Ref. 35 for such derivations.

Kalman filtering for a linear multistage process consists of two elements. The first is an analytic expression which relates the state of the system at the (i+1) stage to the state of the system at the (i) stage with random noise being introduced into the system. A set of measurements (the second element) is then made (with noise in the measurement), and corrections are made to the estimate which had been made by the analytic expression.

In state vector nomenclature, let x_i be the vector of the state variables in stage i. The parameters of the state vector are described probabilistically by the mean

$$E(x_i) = \hat{x}_i \tag{77}$$

and the covariance matrix

$$E\left[(x_i - \hat{x}_i)\,(x_i - \hat{x}_i)^T\right] = P_i \tag{78}$$

where the superscript T denotes the transpose of the vector. The analytic transition equation which relates state (i + 1) to state (i) is

$$x_{i+1} = \Phi\, x_i + \Omega\omega_i \tag{79}$$

where Φ is the state transition matrix and Ω is the matrix which relates the forcing vector to changes in the state vector. The random forcing vector, ω, is described by its mean

$$E(\omega_i) = \bar{\omega}_i \tag{80}$$

and covariance matrix

$$E\left[(\omega_i - \bar{\omega}_i)\,(\omega_i - \bar{\omega}_i)^T\right] = Q_i. \tag{81}$$

The forcing vector, ω, is uncorrelated with the state vector, x. For the (i + 1) stage, the mean value of the state vector is

$$\bar{x}_{i+1} = \Phi\, \hat{x}_i + \Omega\bar{\omega}_i \tag{82}$$

and the covariance matrix of the state vector is

$$M_{i+1} = \Phi\, P_i \Phi^T + \Omega Q_i\, \Omega^T. \tag{83}$$

Because uncertainty is introduced in the transition from state (i) to state (i + 1), the effect of the uncertainty in ω_i in a transition of the type of Eq. (79) is to increase the uncertainty in the knowledge of the stage x_{i+1}. Thus,

$$M_{i+1} \geq P_i\,. \tag{84}$$

Uncertainty of the state (i+1) can be reduced by taking measurements of the state (i+1). Let z be the vector of measurements to be made and let the measurement vector be related to the state vector by

$$z = Hx + \nu \tag{85}$$

where ν is a vector of noise in the measurements with mean

$$E(\nu) = 0 \tag{86}$$

and covariance matrix

$$E(\nu \nu^T) = R. \tag{87}$$

After measurement, the best estimate of the state vector of state (i+1) is

$$\hat{x}_{i+1} = \bar{x}_{i+1} + K(z_{i+1} - H\bar{x}_{i+1}), \tag{88}$$

where

$$K = P_{i+1} H^T R^{-1}, \tag{89}$$

where P_{i+1} is the covariance matrix of the state vector after measurement and is given by

$$P_{i+1} = (M^{-1} + H^T R^{-1} H)^{-1} = M - MH^T (HMH^T + R)^{-1} HM , \tag{90}$$

where the subscript on M has been dropped for convenience. Since measurement always decreases uncertainty,

$$P_{i+1} \leq M_{i+1} . \tag{91}$$

State (i+2) is similarly calculated from state (i+1). The process may be continued beyond the stages for which measurements are available by use of Eqs. (82) and (83). Alternatively, the entire set of equations may be used with $R \rightarrow \infty$, which implies that no useful information may be obtained from measurements. The process is termed "filtering" when measurements are available and is termed "prediction" when the state vector is calculated beyond the highest stage at which measurements are available. The covariance matrix of the state vectors increases monotonically during prediction because no mechanism for decreasing uncertainty exists.

The square root of the eigenvalues and eigenvectors of P define the axes of the 39% likelihood ellipsoid with the center at $\hat{x}$. The 99% likelihood ellipsoid is three times the size of the 39% ellipsoid in linear dimension. The 99% likelihood ellipsoid is an ellipsoid over the components of the state vector, and it is 99% probable that the state vector is contained within the 99% ellipsoid.

5.2 APPLICATION OF KALMAN FILTERING TO WIND PREDICTION

The application of Kalman filtering to wind prediction is now presented. The intent is the use of measured wind to forecast the probability of wind in the near future. By forecasting the probability function of wind, the probability function of vortex transport time can be predicted, and the upper and lower limits on vortex transport time can be forecast. The formulation for wind prediction is presented first, and an example follows.

Let the state variables be the characteristic mean values of headwind and crosswind, u and v, as defined in Section 2. For the measurement of Eq. (85), the 1-min* mean wind is taken as the measurement. The variation in the 15-min* mean wind is used as the forcing function, ω. This choice is

*The selection of certain time intervals in this discussion does not imply that such time intervals are the most appropriate for an operational WVAS. They are used to establish the concept of Kalman filtering of wind.

made because variations in the 15-min mean wind are indicative of atmospheric changes which are occurring and may continue into the future, thus affecting the predicted wind. The variations in the 1-min means are interpreted as being random fluctuations which are not indicative of future trends in the mean wind. Let U and V be the characteristic mean winds, and let u and v be the 1-min mean winds. The state transition equation is

$$\begin{bmatrix} U \\ V \end{bmatrix}_{i+1} = \begin{bmatrix} 1 & 0 \\ 0 & 1 \end{bmatrix} \begin{bmatrix} U \\ V \end{bmatrix}_i + \begin{bmatrix} 1 & 0 \\ 0 & 1 \end{bmatrix} \begin{bmatrix} \bar{\omega}_u \\ \bar{\omega}_v \end{bmatrix}. \tag{92}$$

For stage i, 15-min averages have been calculated at 1-min intervals for the previous 15 min. Then, ω is the difference in 15-min averages between successive 1-min time intervals. Thus, $\bar{\omega}_u$ and $\bar{\omega}_v$ are the means of the difference in 15-min averages between successive 1-min time intervals with the mean (which yields $\bar{\omega}_u$ and $\bar{\omega}_v$) being taken over the previous 15 time intervals. Similarly, Q is the covariance matrix of the difference in 15-min averages between successive 1-min time intervals with the covariance being taken over the previous 15 time intervals. The measurement equation is

$$\begin{bmatrix} u \\ v \end{bmatrix} = \begin{bmatrix} 1 & 0 \\ 0 & 1 \end{bmatrix} \begin{bmatrix} U \\ V \end{bmatrix} + \begin{bmatrix} \nu_u \\ \nu_v \end{bmatrix} \tag{93}$$

where

$$E\left[\nu\nu^T\right] = R \tag{94}$$

is the covariance matrix and is the covariance of the 1-min means measured over the previous 15 min.

The basic data for an example are shown in Table 10. Since continuous wind data were not available for the JFK tests, the wind in the example is taken from wind measured at the Wave Propagation Laboratory's facility at Table Mountain, Colorado, on March 12, 1976, as part of the work described in Ref. 37. Orthogonal wind components, u and v, are used. The last two

Table 10

WIND DATA FOR EXAMPLE OF KALMAN FILTERING OF WIND

Time, t (min)	1-min Mean		15-min Mean Ending at t		Change in 15-min Mean	
	u (ft/sec)	v (ft/sec)	u (ft/sec)	v (ft/sec)	ω_u (ft/sec)	ω_v (ft/sec)
0	16.5	11.1	16.417	12.540	.040	-.240
1	16.3	10.6	16.433	12.280	.026	-.260
2	17.5	12.8	16.533	12.180	.100	-.100
3	16.1	12.8	16.547	12.093	.014	-.087
4	14.9	11.2	16.500	11.920	-.047	-.173
5	15.8	12.4	16.520	11.840	.020	-.080
6	16.6	12.9	16.593	11.807	.073	-.033
7	15.3	12.3	16.573	11.733	-.020	-.074
8	15.5	12.3	16.560	11.680	-.013	-.053
9	15.6	12.6	16.553	11.613	-.007	-.067
10	14.9	12.1	16.393	11.640	-.160	.027
11	13.4	12.4	16.187	11.793	-.206	.153
12	11.3	11.7	15.747	11.907	-.440	.114
13	13.6	12.8	15.460	12.067	-.287	.160
14	14.1	11.6	15.160	12.107	-.300	.040
15	13.5	12.7	14.960	12.213	-.200	.106
16	13.5	11.5	14.773	12.273	-.187	.060
17	13.6	11.0	14.513	12.153	-.260	-.120
18	12.3	10.8	14.260	12.020	-.253	-.133
19	15.0	12.4	14.267	12.100	.006	.080
20	14.1	13.9	14.153	12.200	-.114	.100
21	14.5	11.5	14.013	12.107	-.140	-.093
22	14.7	12.2	13.973	12.100	-.040	-.007
23	14.6	11.3	13.913	12.013	-.060	-.087

columns are the differences in 15-min means. For the example, an estimate of the mean characteristic wind at t = 21 min is made. From Eqs. (79) and (85), Φ, Ω, and H are identity matrices. For the initiation of the Kalman filtering process, the characteristic means are taken as the 15-min mean, and the covariance matrix is the covariance of the 15-min means from t = 6 to t = 20. Therefore, at t = 20 min,

$$\begin{bmatrix} U \\ V \end{bmatrix} = \begin{bmatrix} 14.15 \\ 12.20 \end{bmatrix} \text{ ft/sec} \tag{95}$$

and

$$P = \begin{bmatrix} 0.845 & -0.178 \\ -0.178 & 0.048 \end{bmatrix} (\text{ft/sec})^2. \tag{96}$$

This method of calculation is used only for the initiation of the filtering. In general, the measurement noise (i.e., random perturbations added to the mean characteristic values) is the covariance of the 1-min means taken over 15 min. Thus,

$$R = \begin{bmatrix} 1.740 & 0.461 \\ 0.461 & 0.584 \end{bmatrix} (\text{ft/sec})^2. \tag{97}$$

The expected value and covariance of the forcing vector, ω, is taken from the change in the 15-min means, averaged over a 15-min period. Thus, using the changes in the 15-min mean from t = 6 min to t = 20 min,

$$E(\omega) = \begin{bmatrix} -0.158 \\ 0.024 \end{bmatrix} \text{ ft/sec} \tag{98}$$

and

$$Q = \begin{bmatrix} 0.0191 & -0.0043 \\ -0.0043 & 0.0088 \end{bmatrix} (\text{ft/sec})^2. \tag{99}$$

The expected value and covariance of the characteristic mean winds for t = 21 min are calculated from Eqs. (82) and (83).

$$\begin{bmatrix} U \\ V \end{bmatrix} = \begin{bmatrix} 14.15 \\ 12.20 \end{bmatrix} + \begin{bmatrix} -0.158 \\ 0.024 \end{bmatrix} = \begin{bmatrix} 13.99 \\ 12.22 \end{bmatrix} \text{ ft/sec} \tag{100}$$

and

$$M = P + Q = \begin{bmatrix} 0.864 & -0.182 \\ -0.182 & 0.057 \end{bmatrix} (\text{ft/sec})^2 . \tag{101}$$

This estimate is before measurement is used. The estimate can be improved by use of the measurements at t = 21 min. From Eq. (90),

$$P = \begin{bmatrix} 0.842 & -0.173 \\ -0.173 & 0.053 \end{bmatrix} (\text{ft/sec})^2 \tag{102}$$

and

$$K = PH^T R^{-1} = \begin{bmatrix} 0.711 & -0.858 \\ -0.156 & 0.215 \end{bmatrix} . \tag{103}$$

From Eq. (88), the estimated value of the state vector after measurement is

$$\begin{bmatrix} U \\ V \end{bmatrix} = \begin{bmatrix} 13.99 \\ 12.22 \end{bmatrix} + \begin{bmatrix} 0.711 & -0.858 \\ -0.156 & 0.215 \end{bmatrix} \begin{bmatrix} 0.51 \\ -0.72 \end{bmatrix} = \begin{bmatrix} 14.97 \\ 11.98 \end{bmatrix} \text{ ft/sec.} \tag{104}$$

For the estimated value of the state vector at t = 22, the covariance of the measured values from t = 7 min to t = 21 min is determined to be

$$R = \begin{bmatrix} 1.329 & 0.317 \\ 0.317 & 0.575 \end{bmatrix} (\text{ft/sec})^2 \tag{105}$$

and from the changes in the 15-min mean from t = 7 min to t= 21 min is determined to be

$$E[\omega] = \begin{bmatrix} -0.1338 \\ 0.0211 \end{bmatrix} \text{ (ft/sec)} , \tag{106}$$

and

$$Q = \begin{bmatrix} 0.2700 & 0.0017 \\ 0.0017 & 0.0095 \end{bmatrix} \text{ (ft/sec)}^2. \tag{107}$$

The estimated value and covariance of the state vector at t = 22 min after measurement are

$$\begin{bmatrix} U \\ V \end{bmatrix} = \begin{bmatrix} 14.70 \\ 12.04 \end{bmatrix} \text{ ft/sec} \tag{108}$$

and

$$P = \begin{bmatrix} 0.442 & -0.076 \\ -0.076 & 0.041 \end{bmatrix} \text{ (ft/sec)}^2 . \tag{109}$$

Similarly, at t= 23 min after measurement,

$$\begin{bmatrix} U \\ V \end{bmatrix} = \begin{bmatrix} 14.53 \\ 12.06 \end{bmatrix} \text{ ft/sec} \tag{110}$$

and

$$P = \begin{bmatrix} 0.302 & -0.044 \\ -0.044 & 0.040 \end{bmatrix} \text{ (ft/sec)}^2. \tag{111}$$

To illustrate prediction, it is assumed that no measurement past t= 23 min is available. The estimated value and covariance before measurement for t= 24 min is given by Eqs. (82) and (83)

$$\begin{bmatrix} U \\ V \end{bmatrix} = \begin{bmatrix} 14.55 \\ 12.00 \end{bmatrix} \text{ ft/sec} \tag{112}$$

and

$$M = \begin{bmatrix} 0.316 & -0.047 \\ -0.047 & 0.049 \end{bmatrix} (\text{ft/sec})^2. \tag{113}$$

For the measurement, $R \rightarrow \infty$, which implies an infinite noise in the measurement. Therefore, the estimated value and covariance after measurement are identical to those given above before measurement, and P = M. The square root of the eigenvalues of P and the corresponding eigenvectors are

$$\sqrt{\lambda} = 0.569 \text{ ft/sec}, \quad \begin{bmatrix} u \\ v \end{bmatrix} = \begin{bmatrix} 1 \\ -0.170 \end{bmatrix} \text{ ft/sec} \tag{114}$$

$$\sqrt{\lambda} = 0.203 \text{ ft/sec}, \quad \begin{bmatrix} u \\ v \end{bmatrix} = \begin{bmatrix} 1 \\ 5.899 \end{bmatrix} \text{ ft/sec} \tag{115}$$

The square root of the eigenvalues and eigenvectors define the 39% likelihood ellipse. The 99% likelihood ellipse (i.e., the state vector is known to lie within the 99% likelihood ellipse with 99% certainty) is three times the size of the 39% ellipse in linear dimension. The 99% likelihood ellipse for the 1-min prediction is shown in Fig. 60. The VAS ellipse (i.e., if the wind is outside the ellipse, vortex residence time is less than 80 sec) is shown for reference.

To get the 99% ellipse of the 1-min mean, the R matrix (covariance matrix which relates uncertainty of the 1-min mean to the mean characteristic value) is added to the P matrix (which represents uncertainty in the mean characteristic values). For t = 9 to 23 min,

$$R = \begin{bmatrix} 1.116 & 0.247 \\ 0.247 & 0.609 \end{bmatrix} (\text{ft/sec})^2, \tag{116}$$

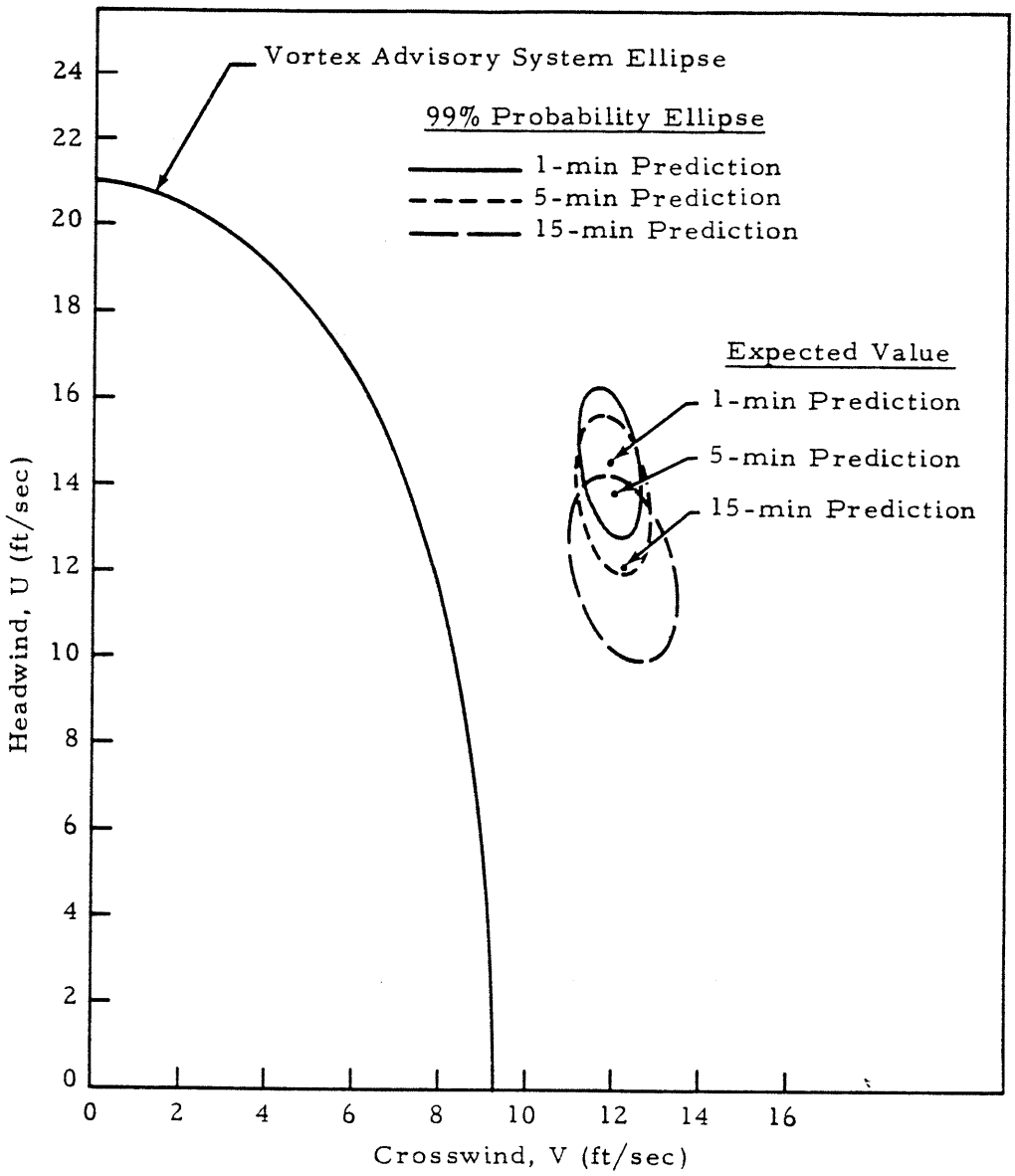

FIGURE 60. EXAMPLE OF PREDICTION OF MEAN WIND BASED ON KALMAN FILTERING

and since P = M,

$$P + R = \begin{bmatrix} 1.432 & 0.200 \\ 0.200 & 0.658 \end{bmatrix} \text{ (ft/sec)}^2. \tag{117}$$

The eigenvalues and corresponding eigenvectors of P + R are

$$\sqrt{\lambda} = 1.217 \text{ ft/sec}, \quad \begin{bmatrix} u \\ v \end{bmatrix} = \begin{bmatrix} 1 \\ .243 \end{bmatrix} \text{ ft/sec} \tag{118}$$

$$\sqrt{\lambda} = .781 \text{ ft/sec}, \quad \begin{bmatrix} u \\ v \end{bmatrix} = \begin{bmatrix} 1 \\ -4.11 \end{bmatrix} \text{ ft/sec} \tag{119}$$

The 99% likelihood ellipse for the 1-min prediction of the 1-min mean wind is shown in Fig. 61.

Repetitive use of Eqs. (82) and (83) gives further predictions. At t = 28 min, the estimated value and covariance matrix are

$$\begin{bmatrix} U \\ V \end{bmatrix} = \begin{bmatrix} 13.85 \\ 12.09 \end{bmatrix} \text{ ft/sec} \tag{120}$$

and

$$P = \begin{bmatrix} 0.372 & -0.059 \\ -0.059 & 0.087 \end{bmatrix} \text{ (ft/sec)}^2. \tag{121}$$

The value of the R matrix in Eq. (116) is retained since no newer data are available. The 99% likelihood ellipse for the mean characteristic values, U and V, is shown in Fig. 60, and the 99% likelihood ellipse for the 1-min means, u and v, is shown in Fig. 61.

For t = 38 min (15-min prediction),

$$\begin{bmatrix} U \\ V \end{bmatrix} = \begin{bmatrix} 12.08 \\ 12.31 \end{bmatrix} \text{ ft/sec} \tag{122}$$

and

$$P = \begin{bmatrix} 0.513 & -0.074 \\ -0.074 & 0.181 \end{bmatrix} \text{ (ft/sec)}^2. \tag{123}$$

The 99% likelihood ellipse is shown in Figs. 60 and 61.

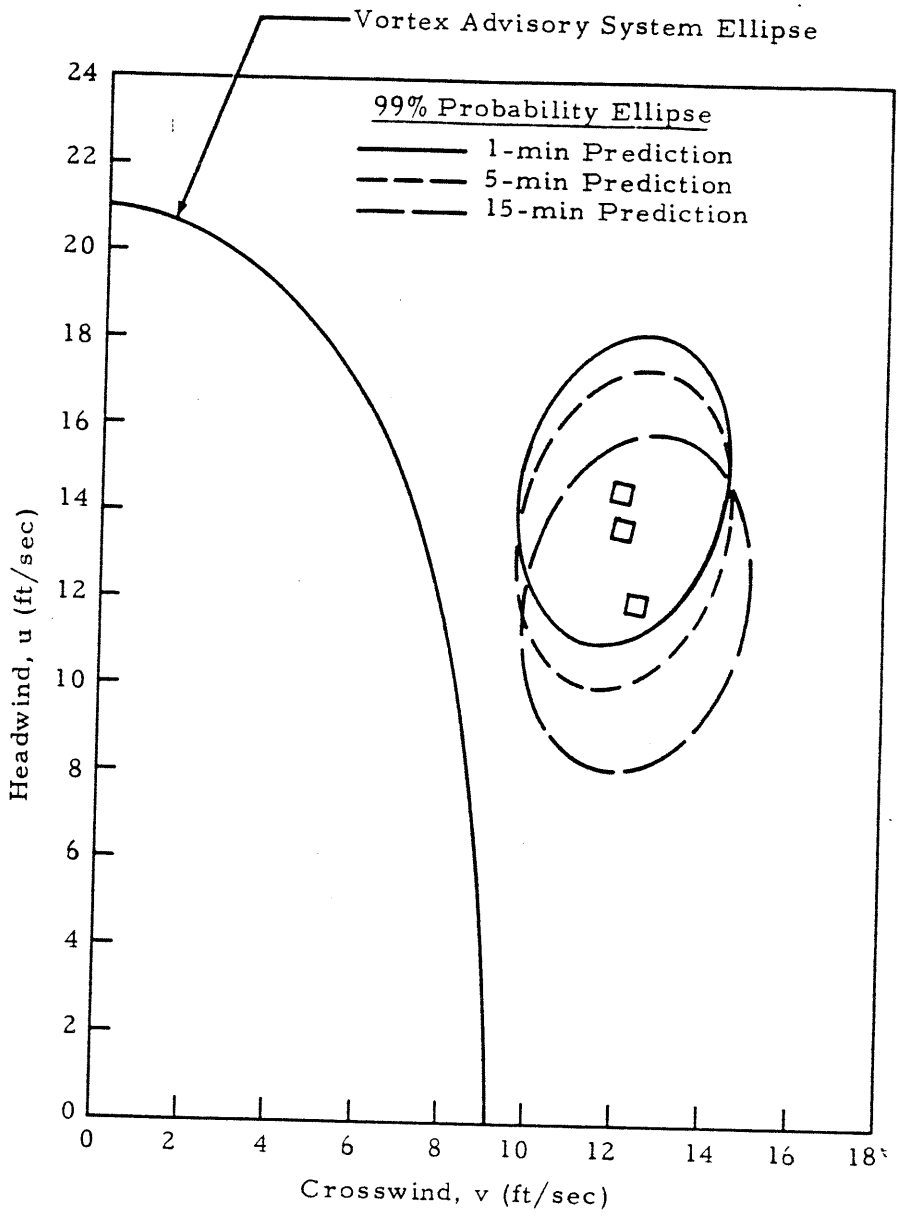

FIGURE 61. EXAMPLE OF PREDICTION OF 1-MIN MEAN WIND BASED ON KALMAN FILTERING

For comparison, the actual values taken from the data from which the example was taken are shown in Table 11. The predicted results agree well with the actual measurements.

Table 11

MEASURED MEAN WINDS FOR WIND PREDICTION EXAMPLE

Time	15-min Mean		1-min Mean	
	u	v	u	v
(min)	(ft/sec)	(ft/sec)	(ft/sec)	(ft/sec)
24	13.86	12.07	14.8	13.5
28	14.42	11.91	15.7	11.1
38	14.10	10.88	13.1	12.1

5.3 PREDICTION OF VORTEX PARAMETERS FROM VORTEX MEASUREMENT

While the prediction of the expected value and covariance of wind can be valuable for vortex transport time, it is not as valuable as the use of direct vortex measurements. Section 4 has shown that many factors in addition to wind affect vortex transport time. The concept developed above can be directly applied to measured vortex parameters.

The state variables are taken as the characteristic mean values of vortex life time, T_L, and vortex residence time, T_R. The measured parameters are vortex life time, t_L, and vortex residence time t_R. The state variable transition equation is

$$\begin{bmatrix} T_R \\ T_L \end{bmatrix}_{i+1} = \begin{bmatrix} 1 & 0 \\ 0 & 1 \end{bmatrix} \begin{bmatrix} T_R \\ T_L \end{bmatrix}_i + \begin{bmatrix} \Delta t & 0 \\ 0 & \Delta t \end{bmatrix} \begin{bmatrix} \omega_R \\ \omega_L \end{bmatrix}. \tag{124}$$

The factor, Δt, which is the time interval between successive updatings of the transition equation and/or making of measurements, is used in the ω

matrix because it is assumed that the magnitude of any atmospheric variation which affects the characteristic mean values is proportional to elapsed time and updating of the transition equation and/or measurements do not occur at regular intervals. At each measurement, the average of the residence time and life time over the previous 30-min time interval is calculated. The difference between the current average and the previous average is then calculated and retained. ω is the difference between the current average and the previous average divided by the elapsed time between the calculation of the two averages. $E(\omega)$ and Q are calculated from the values of ω calculated over the previous 30 minutes.

The measurement equation is

$$\begin{bmatrix} t_R \\ t_L \end{bmatrix} = \begin{bmatrix} 1 & 0 \\ 0 & 1 \end{bmatrix} \begin{bmatrix} T_R \\ T_L \end{bmatrix} + \begin{bmatrix} \nu_R \\ \nu_L \end{bmatrix} \tag{125}$$

and $R = E\left[\nu \nu^T\right]$ is the covariance of the measurements made over the previous 30 min.

The filtering and prediction are conducted in a manner similar to that shown for wind. The result of the prediction is an expected value and a likelihood ellipse for the predicted time. If the 99% likelihood ellipse lies entirely within a region in which either residence time or life time is less than the separation time of aircraft, there is no vortex hazard. If a part of the 99% likelihood ellipse lies within a region for which residence time is greater than the separation time of aircraft, a potential hazard exists.

The data for the example are shown in Table 12 and are taken from a record of residence time and life time as measured by the LDV at JFK on March 21, 1975. If the upwind vortex dies in the vortex corridor, the residence time is set equal to the life time. The example begins at 14:59:00 with an estimate to be made for 15:04:20. To initiate the example, the 30-min

Table 12

VORTEX RESIDENCE TIME AND LIFE TIME DATA FOR EXAMPLE OF VORTEX PREDICTION

Time (Hr: Min: Sec)	Aircraft Type	Measured Value		Average Over Previous 30 min		Random Forcing Function	
		Residence Time, t_R (sec)	Life Time, t_L (sec)	Residence Time, T_R (sec)	Life Time, T_L (sec)	ω_R (sec/min)	ω_L (sec/min)
14 05 04	DC-8	59	64	–	–	–	–
14 08 18	DC-10	65	65	–	–	–	–
14 15 05	B-727	45	56	–	–	–	–
14 16 58	B-727	23	23	–	–	–	–
14 22 07	B-747	86	86	–	–	–	–
14 25 54	DC-8	60	60	–	–	–	–
14 27 48	DC-8	49	49	52.1	57.6		
14 29 12	DC-8	36	36	50.1	54.9	-1.429	-1.929
14 31 18	B-727	44	44	49.4	53.7	-0.333	- .571
14 33 14	Lear	33	33	50.0	51.6	0.310	-1.086
14 35 08	B-727	30	45	47.1	47.7	-1.526	-1.000
14 36 06	B-707	28	35	45.4	48.4	-1.759	-1.345
14 40 50	DC-8	40	40	43.1	46.1	-0.486	-0.486
14 41 59	DC-10	82	82	46.3	49.1	2.783	0.609
14 44 06	DC-8	82	82	46.8	49.3	0.236	0.094
14 49 07	B-747	86	86	52.2	54.0	1.076	0.937
14 51 43	B-747	60	69	52.8	55.2	0.231	0.462
14 57 07	B-747	40	64	48.3	52.9	-0.833	-0.426
14 59 00	B-747	21	38	46.0	52.1	-1.221	-0.425
15 04 20	B-707	50	50	48.9	56.1	0.544	0.750

averages calculated over the 30-min period ending at 14:59:00 are used. Thus, initially

$$\begin{bmatrix} T_R \\ T_L \end{bmatrix} = \begin{bmatrix} 46.0 \\ 52.1 \end{bmatrix} \text{ sec} \tag{126}$$

and

$$P = \begin{bmatrix} 7.572 & 6.740 \\ 6.740 & 7.600 \end{bmatrix} \text{ sec}^2 . \tag{127}$$

From the values of ω_L and ω_R from 14:29:12 through 14:59:00,

$$E(\omega) = \begin{bmatrix} -.246 \\ -.264 \end{bmatrix} \text{ sec/min} \tag{128}$$

and

$$Q = \begin{bmatrix} 1.532 & 1.269 \\ 1.269 & 1.309 \end{bmatrix} (\text{sec/min})^2 . \tag{129}$$

From the measurements from 14:29:12 through 14:59:00,

$$R = \begin{bmatrix} 389.8 & 322.4 \\ 322.4 & 320.7 \end{bmatrix} \text{ sec}^2 . \tag{130}$$

Using Eqs. (82) and (83) for $\Delta t = 5.33$ min, the estimated residence time and life time at 15:04:20 before measurement are

$$\begin{bmatrix} T_R \\ T_L \end{bmatrix} = \begin{bmatrix} 44.69 \\ 50.69 \end{bmatrix} \text{ sec} \tag{131}$$

with covariance matrix

$$M = \begin{bmatrix} 51.15 & 42.84 \\ 42.84 & 44.83 \end{bmatrix} \text{ sec}^2 . \tag{132}$$

Using Eqs. (88) through (90), after measurement

$$P = \begin{bmatrix} 45.42 & 37.99 \\ 37.99 & 39.45 \end{bmatrix} \text{ sec}^2 \tag{133}$$

and

$$\begin{bmatrix} T_R \\ T_L \end{bmatrix} = \begin{bmatrix} 45.26 \\ 50.45 \end{bmatrix} \text{ sec.} \tag{134}$$

Vortex residence time and life time may also be predicted. From the measurements from 14:35:08 through 15:04:20,

$$R = \begin{bmatrix} 433.7 & 331.9 \\ 331.9 & 300.3 \end{bmatrix}. \tag{135}$$

From the values of ω from 14:35:08 through 15:04:20,

$$E(\omega) = \begin{bmatrix} -.096 \\ .117 \end{bmatrix} \text{ sec/min} \tag{136}$$

and

$$Q = \begin{bmatrix} 1.706 & 1.392 \\ 1.392 & 1.174 \end{bmatrix} \text{ sec}^2. \tag{137}$$

For the 5-min prediction, $\Delta t = 5$ min. From Eq. (82)

$$\begin{bmatrix} T_R \\ T_L \end{bmatrix} = \begin{bmatrix} 44.78 \\ 51.04 \end{bmatrix} \text{ sec} \tag{138}$$

and from Eq. (83)

$$P = \begin{bmatrix} 88.07 & 72.79 \\ 72.79 & 68.80 \end{bmatrix} \text{ sec}^2. \tag{139}$$

As shown for wind prediction, the 99% ellipse for residence time and life time is given from the eigenvectors and square root of the eigenvalues for R + P. The eigenvalues and eigenvectors of R + P are for (for the 5 min prediction)

$$\sqrt{\lambda} = 29.28 \text{ sec}, \begin{bmatrix} T_R \\ T_L \end{bmatrix} = \begin{bmatrix} 1 \\ 0.829 \end{bmatrix} \text{ sec}, \tag{140}$$

and

$$\sqrt{\lambda} = 5.80 \text{ sec}, \begin{bmatrix} T_R \\ T_L \end{bmatrix} = \begin{bmatrix} 1 \\ -1.206 \end{bmatrix} \text{ sec}. \tag{141}$$

The 99% ellipse is shown in Fig. 62.

For the 15-min prediction, $\Delta t = 15$ min. Then

$$\begin{bmatrix} T_R \\ T_L \end{bmatrix} = \begin{bmatrix} 43.82 \\ 52.20 \end{bmatrix} \text{ sec} \tag{142}$$

and the eigenvalues and eigenvectors of R + P are

$$\sqrt{\lambda} = 37.80 \text{ sec}, \begin{bmatrix} T_T \\ T_L \end{bmatrix} = \begin{bmatrix} 1 \\ 0.828 \end{bmatrix} \text{ sec}, \tag{143}$$

$$\sqrt{\lambda} = 6.18 \text{ sec}, \begin{bmatrix} T_T \\ T_L \end{bmatrix} = \begin{bmatrix} 1 \\ -1.207 \end{bmatrix} \text{ sec}. \tag{144}$$

The 99% ellipses are relatively large because of the large variance in measured residence time and measured life time as shown in Table 11. The example was deliberately chosen to illustrate vortex prediction with significant variance in measured values of vortex parameters. Most of the uncertainty represented by the ellipses is due to the variance in measured vortex parameters. The 99% ellipses would be much smaller if the variance in the measured values of residence time and life time were smaller (as would be expected on many days).

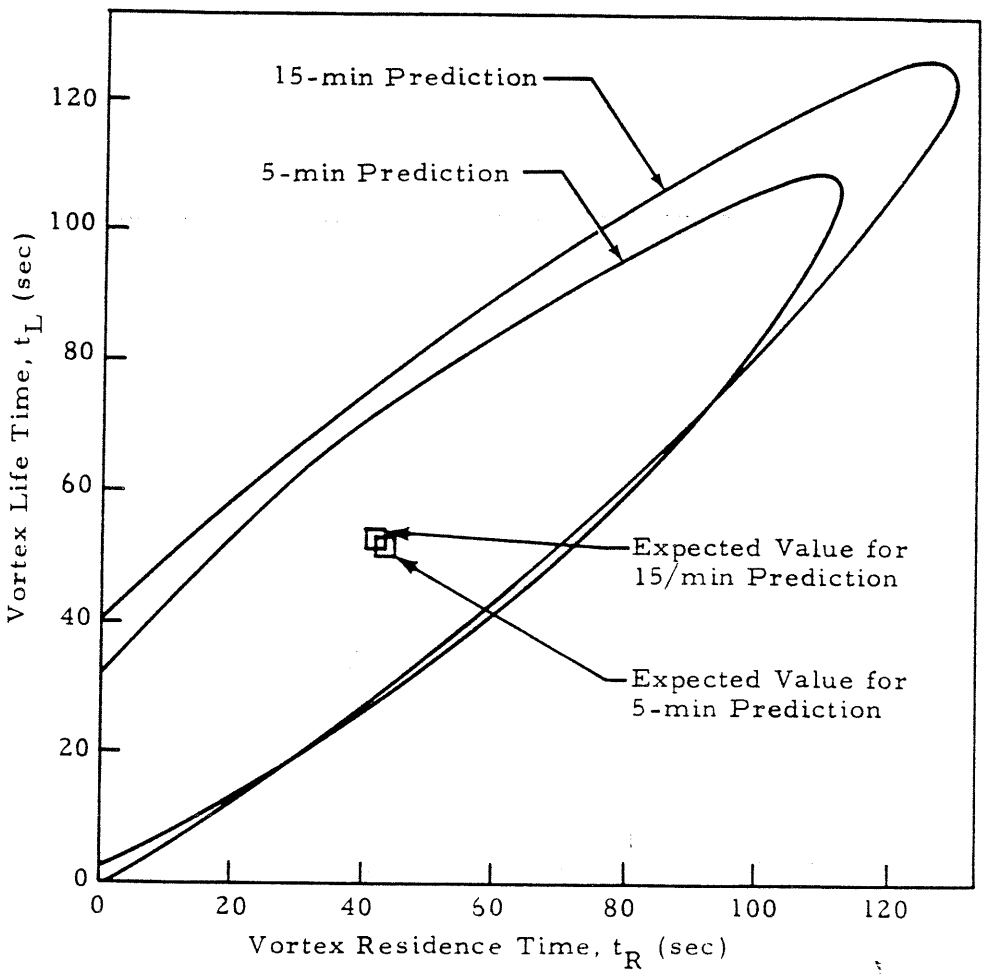

FIGURE 62. PREDICTED VORTEX PARAMETERS FROM MEASURED PARAMETERS

The purpose of the example is the illustration of the concept of vortex prediction by Kalman filtering. It should be construed as a promising technique for vortex prediction in an operational WVAS, but also as a technique which will require further study and refinement.

For example, measurement of residence time alone may give information as useful as measurement of residence time and life time. The ellipses in Fig. 60 show the possibility of conditions which are obviously impossible. For example, the ellipses extend into the region where residence time and life time are negative. Also, the ellipses show that residence time may be greater than life time, which is impossible. The technique of vortex prediction by Kalman filtering is very promising, but will require further study and refinement.

The vortex measurement instruments appropriate for this type of prediction are instruments which can measure both residence time and life time. Life time must be measured, even if the vortex is transported far from the vortex corridor. For this reason, the ground wind anemometer system is probably the most appropriate measurement system. It is possible that residence time could not be measured accurately because the vortex is transported out of the vortex corridor before it descends to the ground. This causes no problem since the conservative approach would be to label the first time that the vortex is detected as the residence time. If no vortex is detected after aircraft passage, the system defaults to an appropriate short life time.

The purpose of this prediction technique is to provide short-term residence time prediction for the purpose of specifying appropriate aircraft spacings. This technique does not provide trajectory prediction which is the prediction of the entire vortex trajectory, based upon measurements made in the early part of the trajectory. Trajectory prediction is discussed next.

5.4 TRAJECTORY PREDICTION FROM VORTEX INITIAL CONDITIONS

The simplest method of vortex prediction is calculation of the vortex trajectory based on measured values of the initial vortex position and initial

velocities. Examples of vortex trajectories (calculated from Eqs. (5) and (6)) are shown in Figs. 63, 64 and 65.* The initial altitude and descent rate were obtained from the measured altitude versus time plot (cf. Fig. 23). The initial lateral position was assumed to be the theoretical vortex separation (for elliptic loading) for the aircraft type, and the initial value of the slope of the lateral position-versus-time curve was assumed to be the wind.

The agreement between calculated and measured vortex tracks was much better when the initial values of the parameters were taken from the measured trajectories than when assumed initial conditions were used (cf. Fig. 24). One reason for this was the fact that the vortex sheet from the wing descends in the downwash as it rolls up into the vortex. Thus, the initial altitude of the rolled-up vortex pair is less than the aircraft altitude. Although good agreement between calculated and measured trajectories was observed in general, Figs. 63, 64, and 65 show that the calculated trajectory can differ significantly from the measured trajectory. The reasons for this are vortex decay, wind change, or both vortex decay and wind change. Figure 63 shows the effect of decay. Decay is indicated because both of the measured trajectories move inboard of the calculated trajectories. Figure 64 shows the effect of a change in crosswind. Such a change is indicated by the fact that both vortices move to the left of the calculated trajectories, indicating an increase in the magnitude of crosswind. In this case, the measured vortex transport time is less than that indicated by the calculated trajectory, but the vortex exits from the opposite flight corridor boundary than that indicated by the calculated trajectory. Some decay is also present in Fig. 64.

Figure 65 shows a combination of decay and crosswind change. The figure shows that the actual residence time can be significantly greater than that calculated from the calculated trajectory initialized by measured values of the parameters. For comparison, Figs. 66 and 67 show the same data as

*The creation of these plots is a good example of the use of the DMS. The creation of these plots is described in Appendix E.

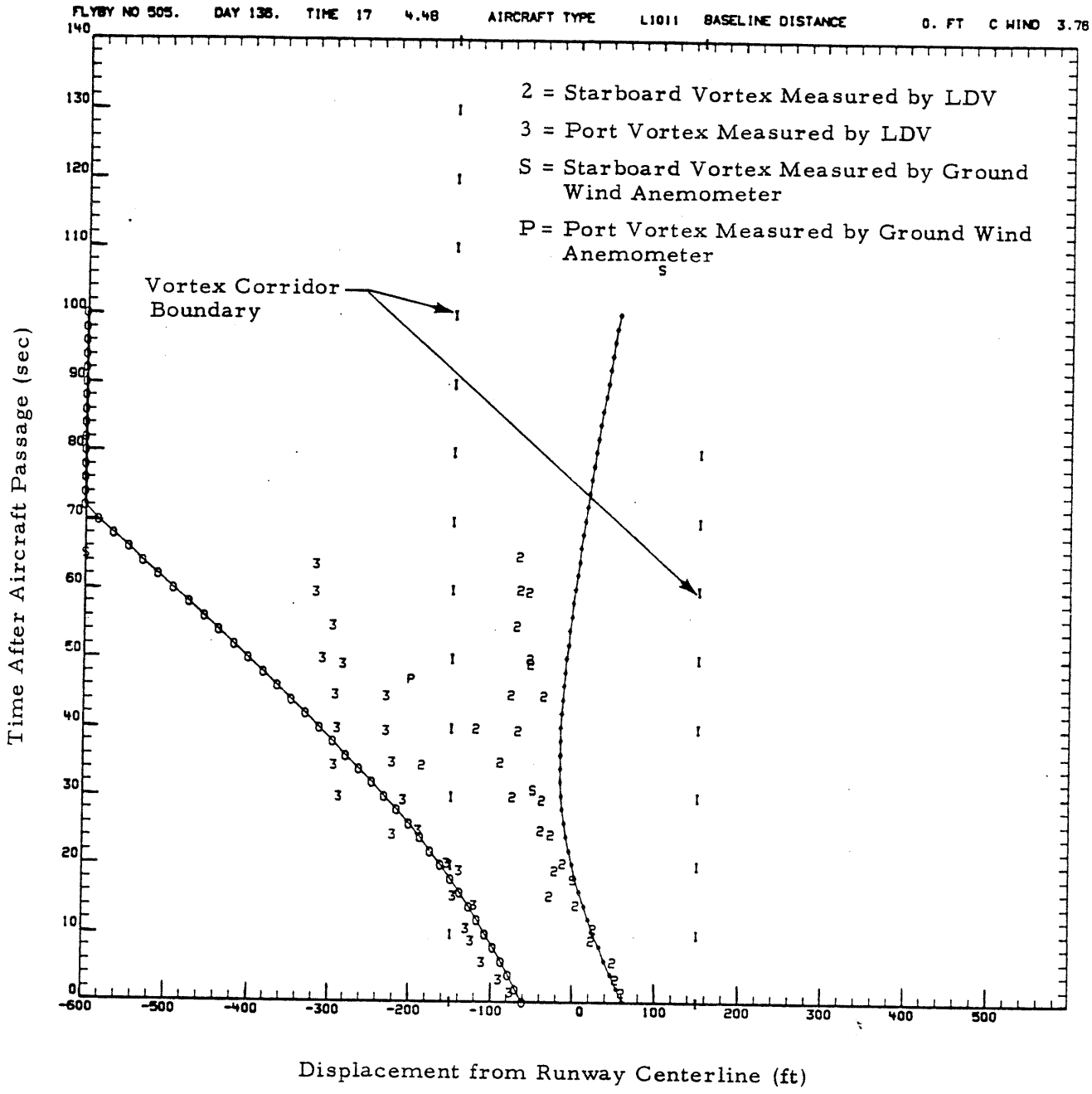

FIGURE 63. EXAMPLE OF VORTEX TRAJECTORY CALCULATED FROM MEASURED INITIAL VALUES OF VORTEX PARAMETERS – FLYBY 505

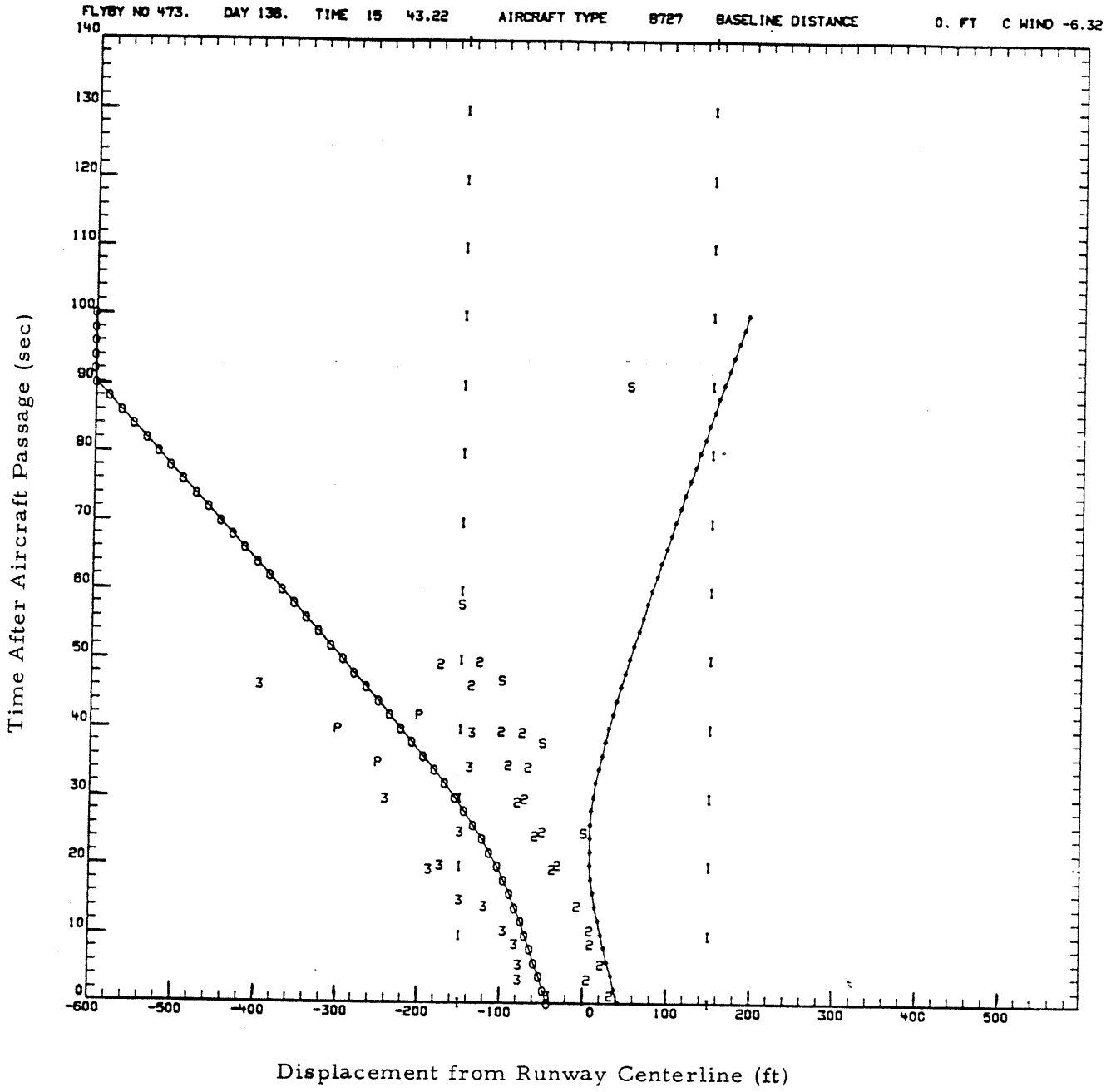

FIGURE 64. EXAMPLE OF VORTEX TRAJECTORY CALCULATED FROM MEASURED INITIAL VALUES OF VORTEX PARAMETERS – FLYBY 473

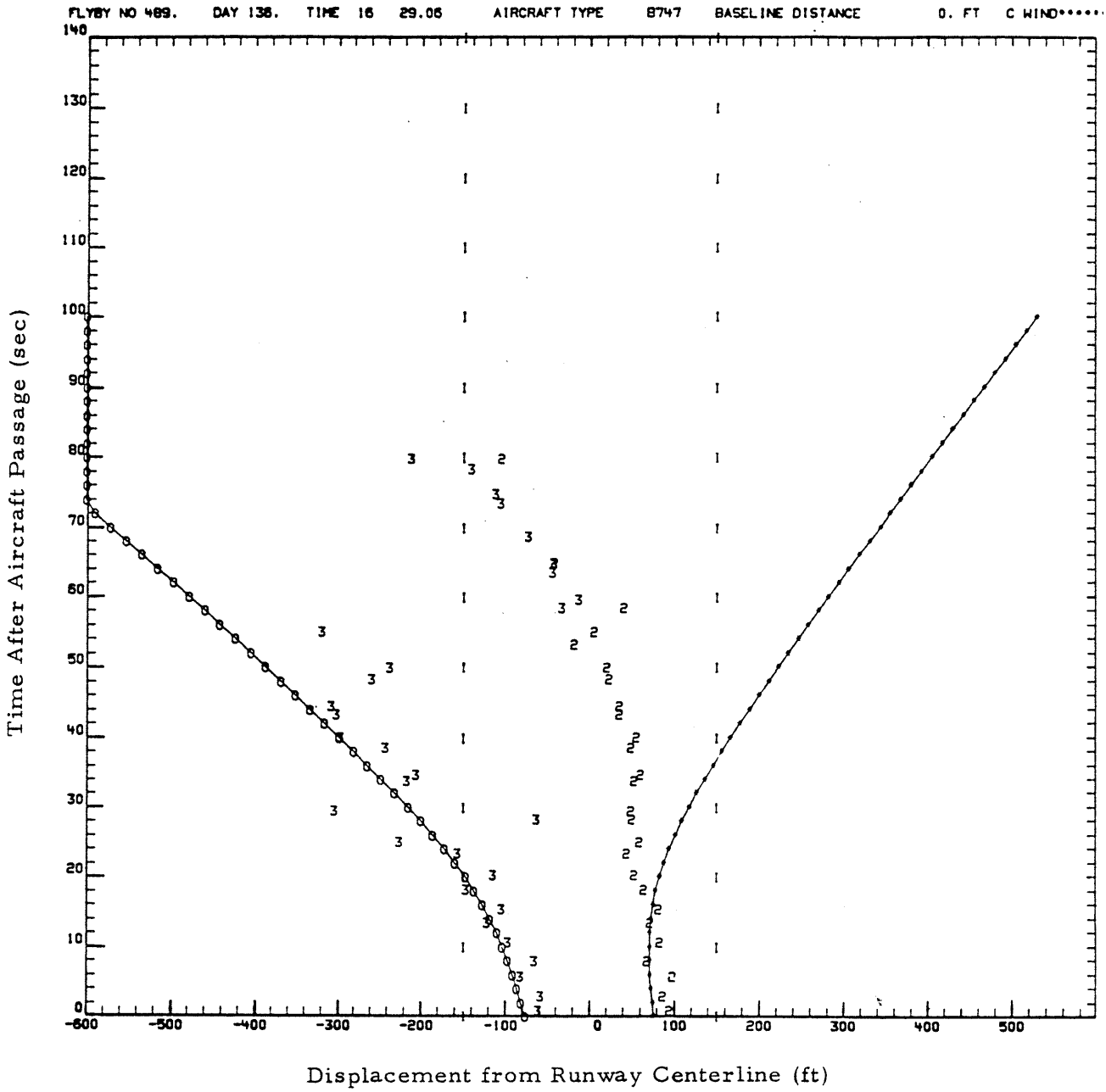

FIGURE 65. EXAMPLE OF VORTEX TRAJECTORY CALCULATED FROM MEASURED INITIAL VALUES OF VORTEX PARAMETERS – FLYBY 489

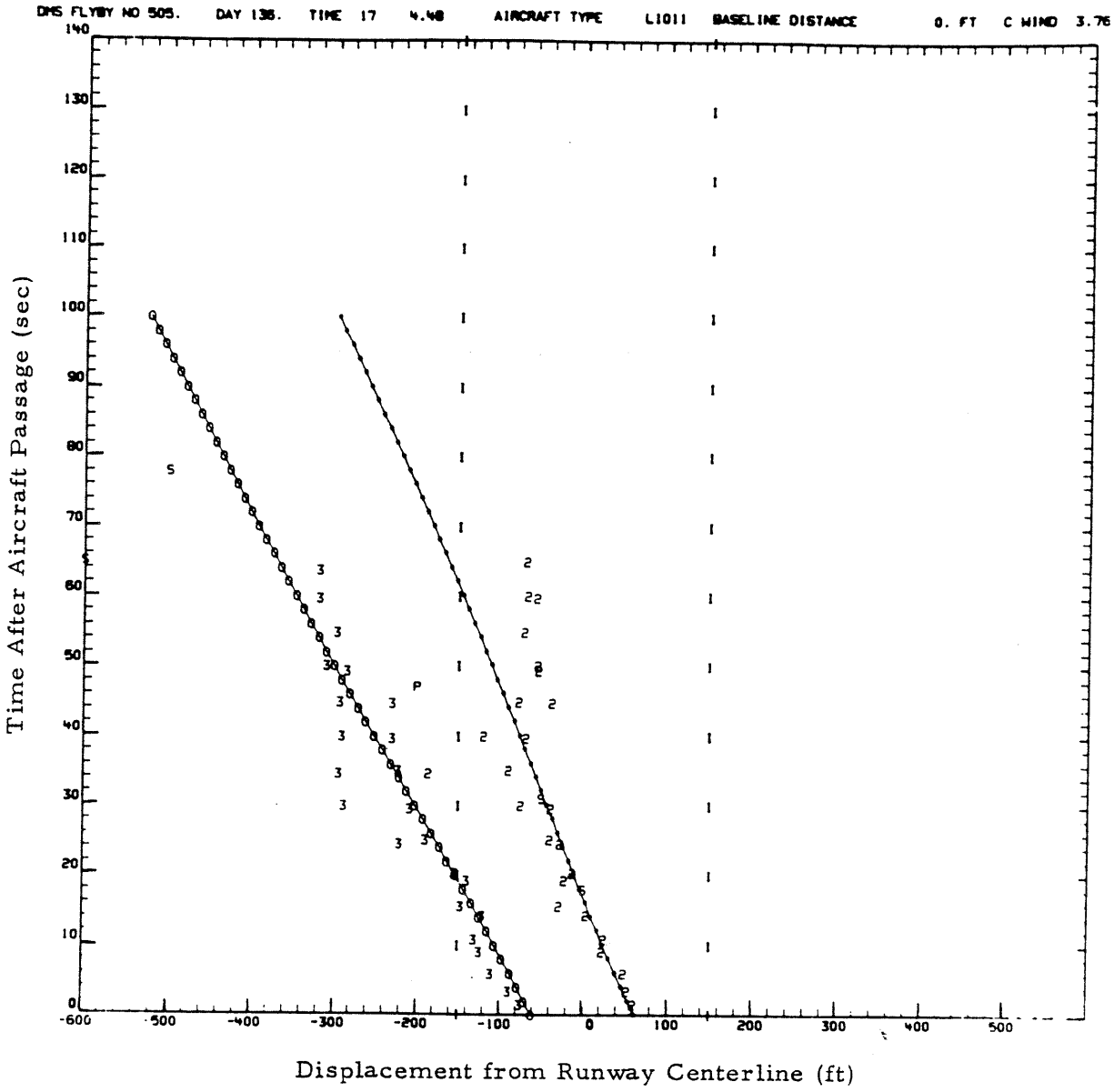

FIGURE 66. EXAMPLE OF VORTEX TRAJECTORY CALCULATED FROM MEASURED INITIAL VALUES OF VORTEX PARAMETERS WITH ASSUMED VORTEX DECAY – FLYBY 505

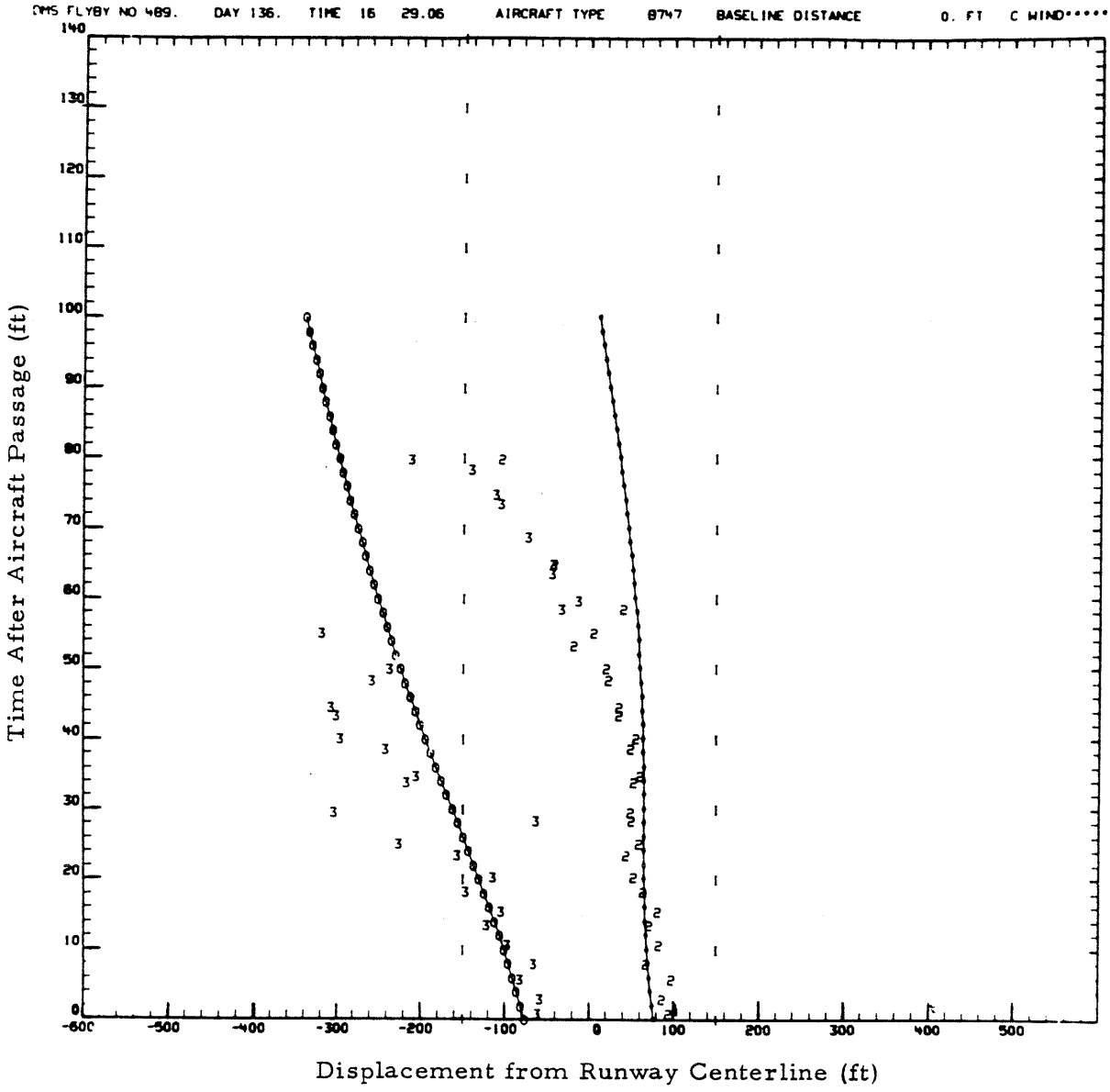

FIGURE 67. EXAMPLE OF VORTEX TRAJECTORY CALCULATED FROM MEASURED INITIAL VALUES OF VORTEX PARAMETERS WITH ASSUMED VORTEX DECAY – FLYBY 489

Figs. 63 and 65, but with a constant vortex decay rate of 1% of current vortex strength per second. This gives an exponential decay.

While agreement between calculated and measured vortex trajectories is good when an assumed decay rate is used, it is recognized that decay rates and wind changes are random. Kalman filtering would allow continuous updating of the calculated trajectory to modify the calculated trajectory according to changing crosswind and decay rates as well as providing likelihood ellipsoids of the calculated results. Vortex prediction by Kalman filtering is discussed next.

5.5 TRAJECTORY PREDICTION AND TRANSPORT TIME PREDICTION WITH KALMAN FILTERING

In this section, two formulations of trajectory prediction with Kalman filtering are presented. The first is the prediction of the remaining part of the vortex trajectory based upon measurements made in the early part of the trajectory. The second formulation is the prediction of vortex transport time based upon measurements made in the early part of the trajectory.

For a nonlinear system, the formulation of the Kalman filtering problem is altered slightly. The nonlinear functions are assumed to occur in the transition equation (Ref. 35)

$$x_{i+1} = f(x_i) + \Omega \omega_i \tag{145}$$

and in the measurement equation

$$z_{i+1} = h(x_{i+1}) + \nu, \tag{146}$$

where $f(x_i)$ and $h(x_{i+1})$ are nonlinear functions. For the state transition, the expected value of the state vector is

$$\bar{x}_{i+1} = f(\hat{x}_i) + \Omega \bar{\omega}_i, \tag{147}$$

and the covariance matrix is

$$M_{i+1} = \frac{\partial f}{\partial x_i} P_i \left(\frac{\partial f}{\partial x_i}\right)^T + \Omega Q_i \Omega^T . \tag{148}$$

After measurement, the estimated value of the state vector is

$$\hat{x}_{i+1} = \bar{x}_{i+1} + K(z_i - h(x_i)), \tag{149}$$

where

$$K = P_{i+1} \left(\frac{\partial h}{\partial x}\right)^T R^{-1} . \tag{150}$$

The covariance matrix is

$$P_{i+1} = M_{i+1} - M_{i+1} \left(\frac{\partial h}{\partial x}\right)^T \left[\frac{\partial h}{\partial x} M_{i+1} \left(\frac{\partial h}{\partial x}\right)^T + R\right]^{-1} \frac{\partial h}{\partial x} M_{i+1} . \tag{151}$$

5.5.1 Trajectory Prediction

For trajectory prediction, the five state variables are:

Z = Vortex altitude,
Y_1 = Port vortex lateral position,
Y_2 = Starboard vortex lateral position,
Γ = Vortex strength, and
V_∞ = Crosswind.

For convenience, let

$$B(Y_1, Y_2, Z) = \frac{1}{2\pi} \left[\frac{Y_2 - Y_1}{(2Z)^2 + (Y_2 - Y_1)^2} - \frac{1}{Y_2 - Y_1}\right] \tag{152}$$

and

$$G(Y_1, Y_2, Z) = \frac{1}{4\pi Z}\left[\frac{(Y_2 - Y_1)^2}{(2Z)^2 + (Y_2 - Y_1)^2}\right]. \tag{153}$$

The state transition equations (omitting the i and i+1 subscripts) are

$$Z = Z + \Gamma B(Y_1, Y_2, Z)\Delta t \tag{154}$$

$$Y_1 = Y_1 + \left[V_\infty - \Gamma G(Y_1, Y_2, Z)\right]\Delta t \tag{155}$$

$$Y_2 = Y_2 + \left[V_\infty + \Gamma G(Y_1, Y_2, Z)\right]\Delta t \tag{156}$$

$$\Gamma = \Gamma + \omega_\Gamma \Delta t \tag{157}$$

$$V_\infty = V_\infty + \omega_v \Delta t \tag{158}$$

where ω_Γ and ω_v are random variables which represent random changes per unit time in Γ and V_∞. The measured parameters were chosen to correspond to those available for the JFK tests. One LDV system and one ground wind anemometer system are assumed. The measurement equations are

$$Z_{1L} = Z + \nu_1 \tag{159}$$

$$Z_{2L} = Z + \nu_2 \tag{160}$$

$$Y_{1L} = Y_1 + \nu_3 \tag{161}$$

$$Y_{2L} = Y_2 + \nu_4 \tag{162}$$

$$Y_{1G} = Y_1 + \nu_5 \tag{163}$$

$$Y_{2G} = Y_2 + \nu_6 \tag{164}$$

$$\dot{Z}_{1L} = \Gamma B(Y_1, Y_2, Z) + \nu_7 \tag{165}$$

$$\dot{Z}_{2L} = \Gamma B(Y_1, Y_2, Z) + \nu_8 \tag{166}$$

$$\dot{Y}_{1L} = V_\infty - \Gamma G(Y_1, Y_2, Z) + \nu_9 \tag{167}$$

$$\dot{Y}_{2L} = V_\infty + \Gamma G(Y_1, Y_2, Z) + \nu_{10} \tag{168}$$

$$\dot{Y}_{1G} = V_\infty - \Gamma G(Y_1, Y_2, Z) + \nu_{11} \tag{169}$$

$$\dot{Y}_{2G} = V_\infty + \Gamma G(Y_1, Y_2, Z) + \nu_{12}. \tag{170}$$

Z is vortex attitude, and Y is vortex lateral position. A 1 subscript refers to the port vortex, and a 2 subscript refers to the starboard vortex. The L subscript refers to a measurement made by the LDV, and a G subscript refers to a measurement made by the ground wind anemometer system. The ν values refer to the measurement noise. The elements of the noise vector are assumed to be uncorrelated, so the R matrix is a diagonal matrix. In particular,

$$\nu_7 \propto \frac{1}{|\dot{Z}_1|} \tag{171}$$

and

$$\nu_8 \propto \frac{1}{|\dot{Z}_2|} \cdot \tag{172}$$

This assures that Z measurements are not used to determine vortex strength when the vortices are widely separated. The measured values of $\dot{Y}$ and $\dot{Z}$ are taken as differences in measured values of Y and Z divided by the elapsed time between the measurements. The technique requires some knowledge of vortex behavior and vortex measurement in order to place realistic values on the expected values of ω_Γ and ω_v and on the covariances of ω_Γ, ω_v, and the elements of the ν matrix.

This technique has an inherent disadvantage. Although expected values and likelihood ellipsoids can be drawn for vortex position, conversion of the likelihood ellipsoids for transport time is not easy. Hence, the development of this technique is not pursued further, and a more appropriate technique is introduced.

5.5.2 Transport Time Prediction

For this formulation, it is desired to predict transport time, rather than predict the vortex trajectory. The formulation for the transport time calculation presented in Section 2.1 is used. The transport time is calculated for the value of Y for which

$$F(Y) = \frac{4\pi}{\Gamma C}\left[\frac{CY^2 - 2}{(CY^2 - 1)^{1/2}}\right] - D + \frac{Y \mp y_b}{V_\infty} = 0. \qquad (173)$$

Let Y_s be the solution of the above equation. Assume that the solution, Y_s, is known from the initial parameters of the vortex trajectory. If C, Γ, and V_∞ vary during the trajectory, the corresponding change in Y_s is known by

$$\Delta F(Y) = \frac{\partial F}{\partial Y_s}\Delta Y_s + \frac{\partial F}{\partial C}\Delta C + \frac{\partial F}{\partial \Gamma}\Delta\Gamma + \frac{\partial F}{\partial V_\infty}\Delta V_\infty + \frac{\partial F}{\partial D}\Delta D = 0 \qquad (174)$$

since F(Y) is a constant. From Eq. (13),

$$D = \frac{4\pi}{\Gamma C}\left[\frac{CY^2 - 2}{(CY^2 - 1)^{1/2}}\right] - t \qquad (175)$$

The state variables for the Kalman filtering are Y_s, C, D, Γ, V_∞ and Y_D. The parameter, Y_D, is the distance of the origin of the wind-fixed coordinate system (cf. Section 2.1) from the origin of the ground-fixed coordinate system:

$$Y_D = \int V_\infty \, dt \qquad (176)$$

or

$$Y_{D,i+1} = Y_{D,i} + V_\infty \Delta t. \qquad (177)$$

There are six linear transition equations. The first is a result of Eq. (174). All of the state variables, except Y_D, are nominally constant and are changed by the random forcing vector only. The transition equations are

$$Y_{s,i+1} = Y_{s,i} - \frac{1}{\partial F/\partial Y}\left[\frac{\partial F}{\partial C}\omega_C + \frac{\partial F}{\partial D}\omega_D + \frac{\partial F}{\partial \Gamma}\omega_\Gamma + \frac{\partial F}{\partial V_\infty}\omega_v\right] \qquad (178)$$

$$C_{i+1} = C_i + \omega_C \qquad (179)$$

$$D_{i+1} = D_i + \omega_D \qquad (180)$$

$$\Gamma_{i+1} = \Gamma_i + \omega_\Gamma \tag{181}$$

$$V_{\infty,\, i+1} = V_{\infty,\, i} + \omega_v \tag{182}$$

$$Y_{D,\, i+1} = Y_{D,\, i} + V_{\infty,\, i} \cdot \tag{183}$$

For measurement, it is desirable to be able to gain useful information even if only one vortex can be detected. Therefore, let

$$Y_2 - Y_1 = 2(Y_2 - Y_D) = -2(Y_1 - Y_D) \cdot \tag{184}$$

Then Eqs. (152) and (153) are redefined as

$$B(Y_2, Y_D, Z) = \frac{1}{4\pi}\left[\frac{Y_2 - Y_D}{Z^2 + (Y_2 - Y_D)^2} - \frac{1}{Y_2 - Y_D}\right] \tag{185}$$

$$B(Y_1, Y_D, Z) = -\frac{1}{4\pi}\left[\frac{Y_1 - Y_D}{Z^2 + (Y_1 - Y_D)^2} - \frac{1}{Y_1 - Y_D}\right] \tag{186}$$

$$G(Y_2, Y_D, Z) = \frac{1}{4\pi Z}\left[\frac{(Y_2 - Y_D)^2}{Z^2 + (Y_2 - Y_D)^2}\right] \tag{187}$$

$$G(Y_1, Y_D, Z) = -\frac{1}{4\pi Z}\left[\frac{(Y_1 - Y_D)^2}{Z^2 + (Y_1 - Y_D)^2}\right] \cdot \tag{188}$$

The measurements made are the same as those described for trajectory prediction. The form in which the measured parameters are used is slightly different. The measurement equations are

$$\frac{1}{(Y_{1L} - Y_D)^2} + \frac{1}{Z_{1L}^2} = C + \nu_1 \tag{189}$$

$$\frac{1}{(Y_{2L} - Y_D)^2} + \frac{1}{Z_{2L}^2} = C + \nu_2 \tag{190}$$

$$\frac{C(Y_{1L} - Y_D)^2 - 2}{(C(Y_{1L} - Y_D)^2 - 1)^{1/2}} = \frac{\Gamma C}{4\pi}(t + D) + \nu_3 \tag{191}$$

$$\frac{C(Y_{2L} - Y_D)^2 - 2}{(C(Y_{2L} - Y_D)^2 - 1)^{1/2}} = \frac{\Gamma C}{4\pi}(t + D) + \nu_4 \tag{192}$$

$$\frac{C(Y_{1G} - Y_D)^2 - 2}{(C(Y_{1G} - Y_D)^2 - 1)^{1/2}} = \frac{\Gamma C}{4\pi}(t + D) + \nu_5 \tag{193}$$

$$\frac{C(Y_{2G} - Y_D)^2 - 2}{(C(Y_{2G} - Y_D)^2 - 1)^{1/2}} = \frac{\Gamma C}{4\pi}(t + D) + \nu_6 \tag{194}$$

$$\dot{Z}_{1L} = \Gamma B(Y_1, Y_D, Z) + \nu_7 \tag{195}$$

$$\dot{Z}_{2L} = \Gamma B(Y_2, Y_D, Z) + \nu_8 \tag{196}$$

$$\dot{Y}_{1L} = V_\infty - \Gamma G(Y_1, Y_D, Z) + \nu_9 \tag{197}$$

$$\dot{Y}_{2L} = V_\infty + \Gamma G(Y_2, Y_D, Z) + \nu_{10} \tag{198}$$

$$\dot{Y}_{1G} = V_\infty - \Gamma G(Y_1, Y_D, Z) + \nu_{11} \tag{199}$$

$$\dot{Y}_{2G} = V_{\infty} + \Gamma G\,(Y_1, Y_D, Z) + \nu_{12} \tag{200}$$

$$\dot{Y}_{1L} + Y_{2L} = 2_{YD} + \nu_{13} \tag{201}$$

$$\dot{Y}_{1G} + Y_{2G} = 2_{YD} + \nu_{14}. \tag{202}$$

As described previously for trajectory prediction,

$$\nu_7 \propto \frac{1}{|\dot{Z}_1|} \tag{203}$$

and

$$\nu_8 \propto \frac{1}{|\dot{Z}_2|} \tag{204}$$

The elements of the ν matrix are uncorrelated, so R is a diagonal matrix. If, at a given time of measurement, certain measurements are unavailable, the variance of ν for that element of ν is made infinite in the R matrix.

The use of the above formulation with Kalman filtering will provide continuous updates of predicted vortex transport time and likelihood ellipsoids of vortex transport time during the life of the vortex. The purpose of the prediction is to allow early detection of vortices which may not clear the vortex corridor during the separation time between successive aircraft. It is assumed that the airport is operated in such a manner that a very small probability that the vortex will not clear the vortex corridor during the separation time is acceptable.

5.5.3 Vortex Sensing for Trajectory Prediction and Transport Time Prediction

The vortex sensing requirements for trajectory prediction and transport time prediction differ significantly from those discussed earlier for short-term prediction of life time and residence time. For trajectory prediction and transport prediction, a sensor which can sense both vortex altitude and

lateral position as a function of time is required. The LDV and some acoustic sensors are appropriate for this role. The ground wind anemometer has three very serious limitations in this role. First, it cannot be used to improve the estimate of vortex strength based on measurements until the vortices are close to the ground. Second, since vortices cannot be easily detected by the ground wind anemometers when the vortices are far from the ground, the estimate of crosswind cannot be improved by measurement until the vortices are close to the ground. Third, the resolution of the ground wind anemometer system (particularly, for the horizontal velocity of the vortex) may not be adequate. Early estimates of vortex strength and crosswind are imperative for accurate prediction.

Some of the ambiguity of vortex strength could be resolved by use of a device which measures vortex strength (e.g., the monostatic acoustic vortex sensor) or by inferring vortex strength from pressure sensors (which sense the strength of the aircraft downwash) on the ground. However, these measurements would not be as accurate as sensors of vortex position as a function of time and would not provide information to permit improvement of the estimate of crosswind based upon measurement.

6. WAKE VORTEX AVOIDANCE SYSTEM DESIGN CONSIDERATIONS

The data contained in the Data Management System and the analysis contained in Sections 4 and 5 have important implications for the design of an effective Wake Vortex Avoidance System. These design implications are discussed in this section.

6.1 DESCRIPTIVE CHARACTERISTICS OF WAKE VORTEX AVOIDANCE SYSTEMS

The purpose of the Wake Vortex Avoidance System (WVAS) is to allow selection of optimal spacing criteria on final approach. Variable spacing is implied. That is, the spacing between any two particular aircraft may be a function (either continuous or having several selectable discrete values) of the type (or weight class) of the lead aircraft, the type (or weight class) of the following aircraft, and the prevailing meteorological conditions. The performance index of the WVAS (i.e., the criterion by which "optimal" is judged) is the minimization of aircraft delay in the terminal area. Delay is defined as the difference between the time when an aircraft lands and the time when it could have landed if no other aircraft had been in the terminal area. Minimization of delay may include a decrease of minimum separations from the current 3-nautical-mile Instrument Flight Rules (IFR) standard.

The delay process is very complicated, and delay is usually calculated by Monte-Carlo simulation techniques. At most major airports, the delay mechanism for landing aircraft can be described as a multiple server (i.e., multiple runway) non-steady queue. The non-steadiness arises from the variations in aircraft demand (i.e., number of aircraft arrivals per hour) through the day. With an active WVAS, non-steadiness also results from aircraft spacings which are adjusted according to changing meteorological

conditions. For the purposes of this report, the equation for delay for a single runway in steady state can serve as an indicator of the characteristics of delay of landing aircraft at airports. Aircraft delay is discussed in Section 1.4.2. Aircraft delay is technically defined as waiting time in the queue and is given by (Ref. 28)

$$W_q = \frac{\lambda [E^2 [\Delta t] + Var[\Delta t]]}{2 (1 - \lambda E [\Delta t])}$$

where

λ = average arrival rate (aircraft per unit time).

$E[\Delta t]$ = expected value (mean) of interarrival time over the runway threshold. The inverse of $E [\Delta t]$ is theoretical runway capacity.

$Var[\Delta t]$ = variance of interarrival time over the runway threshold.

The value of the Wake Vortex Avoidance System is in increasing runway capacity, or stated alternatively, to decrease $E[\Delta t]$. The effectiveness of decreasing $E [\Delta t]$ to effect a decrease in aircraft delay is a strong function of aircraft demand, λ. It is therefore expected that the manner in which a WVAS is operated during a particular time period of the day will depend on aircraft demand during that time period. For a given airport, several sophistication levels of WVAS may be used, depending on aircraft demand. In the following discussion, several levels of WVAS are described. In the most sophisticated levels when spacings are minimal, the execution of missed approaches may become necessary.

In the following discussion, several principles derived from Section 4 are used. Specifically:

> All wind measurements are to be made at or near the asymptotic altitude for heavy aircraft. Extrapolation of wind to other altitudes on the basis of assumed profiles will not be done.

There is sufficient variance of wind over space so that the wind measured at the meteorological tower over a short averaging period cannot be assumed to be equal to the wind in the approach region for the same time period.

There is sufficient variance of wind over time so that wind may vary between the time when traffic separations are established and the landing of the aircraft.

The detection of turbulence over a known threshold level is a sufficient condition for short vortex life (cf. Fig. 18).

The actual weight of a landing aircraft is a very important parameter in the determination of vortex residence time. The measured residence time for an aircraft cannot be applied to a following aircraft of a similar type (even if wind is constant) unless it is known that the aircraft weights, approach speeds, and aircraft configurations are equal.

The curves shown in Fig. 8 indicate a very steep slope of vortex transport time with respect to crosswind for vortex transport times greater than 60 sec. The use of variable spacing based on crosswind is therefore very doubtful. For example, the difference in crosswind for a spacing based upon a 120-sec transport time and a spacing based upon a 60-sec time is 1 ft/sec. The accuracy with which wind can be measured would not permit the selection of spacings based upon residence times between 60 sec and 120 sec. Sixty seconds is considered to be a minimum separation time in VFR conditions from runway occupancy constraints. Sixty seconds is a 2.25-n.mi. separation at a 135-knot approach speed. It appears that the purpose of transport time in a WVAS may be interpreted as: "From wind conditions measured, it is certain that a separation distance based upon a transport time of 60 sec is safe" or "From wind conditions measured, it cannot be stated with certainty that a separation distance based upon a time of 60 sec is safe, and therefore, separation distance must be based upon life time instead of transport time."

There is no distinction between VFR and IFR for vortex-related constraints. Other considerations may cause differences in separations for VFR and IFR with an operational WVAS in place. However, the physics of the vortex problem are identical for VFR and IFR and therefore the separations imposed by vortex-related constraints are identical for VFR and IFR.

6.2 CONCEPTUAL DESIGN OF A WAKE VORTEX AVOIDANCE SYSTEM

In this section, designs of Wake Vortex Avoidance Systems are discussed at several levels of sophistication. The required level of sophistication may be related to very light, light, moderate, and heavy traffic demand. For the purposes of this discussion, very light traffic demand is defined as $\lambda E[\Delta t] < 0.4$, light is defined as $0.4 < \lambda E[\Delta t] < 0.75$, moderate is defined as $0.75 < \lambda E[\Delta t] < 1.0$, and heavy is defined as $1 < \lambda E[\Delta t]$ where $E[\Delta t]$ is based upon 3/4/5/6-n.mi. separations.

6.2.1 Zeroth-Order System

The most fundamental WVAS is no system. It is optimal for very light traffic demand since reduction of spacing from the 3/4/5/6-n.mi. standard will not reduce aircraft delay, which is very small (average of less than 20 sec per aircraft) for very light traffic demand.

6.2.2 First-Order System

The first-order system is similar to the Vortex Advisory System (VAS). In addition to the measurement of wind, as in the VAS, turbulence measurements are also made. The first-order system assumes the existence of a data base by which life time can be known to be less than certain specified values if turbulence exceeds corresponding threshold values.

The logic diagram for the first-order system is shown in Fig. 68. The prediction method for predicting wind and turbulence is described in Section 5.2. Figure 68 uses an 80-sec separation as an example. Obviously, other separation times could be used. The logic shown in Fig. 68 may be stated as follows: if the 5-min prediction shows that either life time or residence time will be less than 80 sec, the 80-sec separation is used. If the 5-min prediction shows that both life time and residence time may be greater than 80-sec, the current 3/4/5/6-nautical-mile separation standard is used. The 15-min prediction is used to give the controllers warning of future trends.

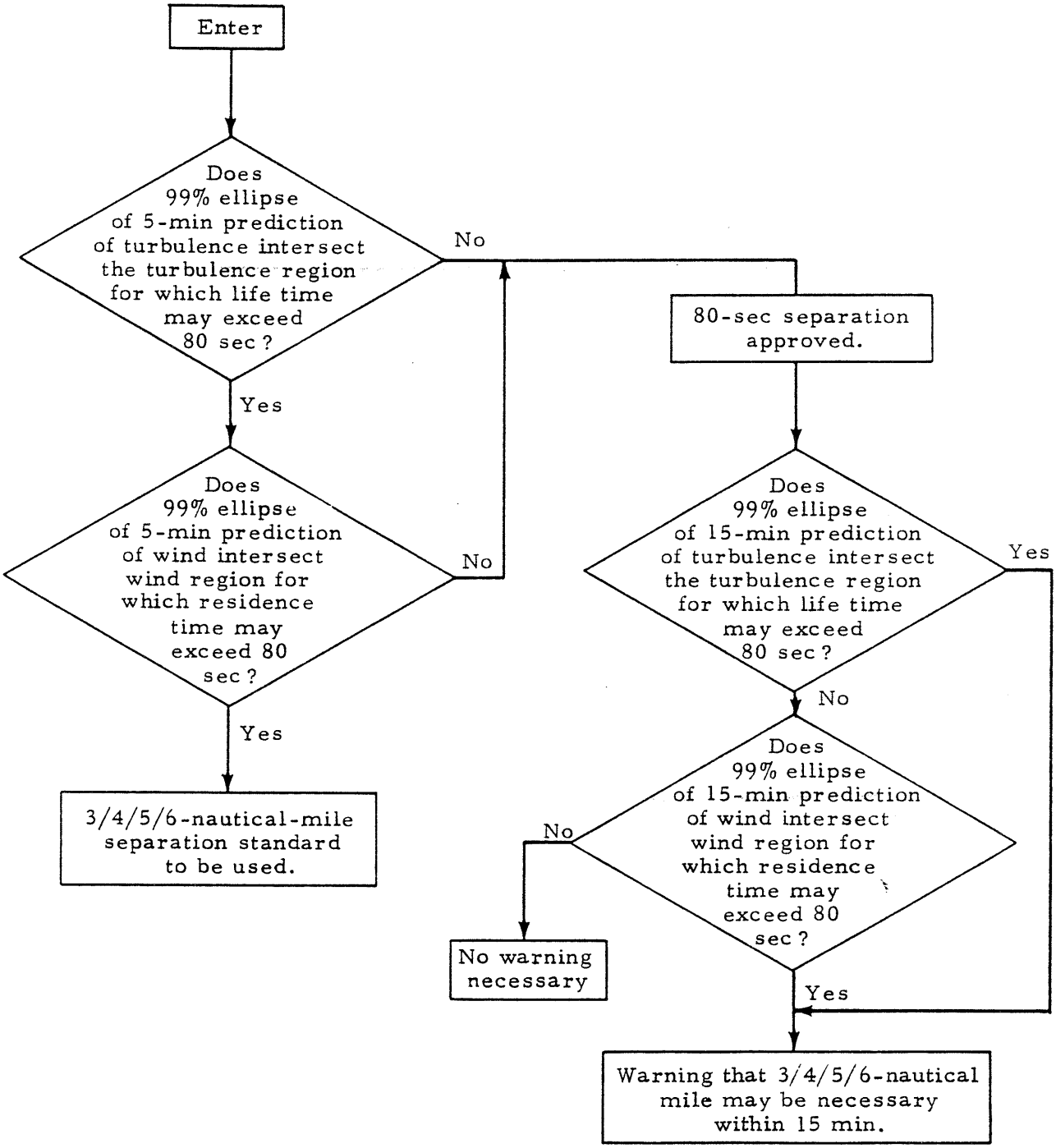

FIGURE 68. FLOW DIAGRAM FOR FIRST-ORDER WAKE VORTEX AVOIDANCE SYSTEM

It is recognized that both predictions include life time. (Life time is inherently included in the VAS ellipses.) However, the separate measurement of turbulence provides an additional criterion for the exclusion of long vortex residence times. This additional criterion (turbulence) will preclude long vortex residence times during periods when the wind criterion alone would not preclude long vortex residence times.

The first-order system has the same limitations as the VAS. Unless the 80-sec separation can be approved, the first-order system cannot allow any reduction in delay.

6.2.3 Second-Order System

The second-order system is based upon vortex prediction as described in Section 5.3. The aircraft separation time is the maximum residence time contained within the 99% ellipse of the 5-min prediction. In addition, the maximum residence time within the 99% ellipse of the 15-min prediction is displayed as an indication of the magnitude of possible change. It may be be appropriate to maintain separate predictions for wide-body aircraft and for narrow-body aircraft. It is anticipated that the ground wind vortex sensing system will be adequate for providing the necessary predictions.

In practice, sensors should be placed at several baselines to allow prediction of the time required for the vortex pair to clear the vortex corridor at all points between the middle marker and the touchdown zone. Figure 16 and Figs. 46-48 showed that a significant difference in residence time can occur for two different baselines. If three baselines were chosen for implementation, a 6-dimensional ellipsoid (i.e., life time and residence time for each of the three baselines) would be used. The values of ν_L and ν_T in the formulation of Section 5.3 are functions of the number of baselines. If few baselines (e.g., 1) are used, the values of ν_L and ν_T must be large to account for uncertainties at locations other than the ones at which measurements are

made. However, if the number of baselines is large (e.g., 5), ν_L and ν_T may be smaller because there is less uncertainty in the region between sensing lines. The optimum number of instrumented baselines is certainly a question requiring further study.

The above technique is valid for the active runway. It is desirable to calculate the 99% probability ellipse for each of the inactive runways to determine if an alternative runway would be preferable. For the inactive runways, the wind measurements of the first-order system are made. The transport time characteristics (mean and variance) are calculated from the wind and expected variations in aircraft parameters. The life time characteristics are taken from the life time behavior at the active runway. The residence time characteristics are calculated, and the 99% probability ellipses are generated for each of the inactive runways.

6.2.4 Third-Order System

The third order system is built upon the second-order system. The aircraft separation time is the maximum residence time contained within some probability ellipse (e.g., 90% ellipse) of the 5-min prediction. It is recalled that the 90% ellipse does not imply that there is a 10% probability that the residence time will be greater than the maximum residence time contained in the 90% ellipse. It merely implies that there is a 10% chance that the residence time lies outside the 90% ellipse. For each landing aircraft, transport time prediction is performed as described in Section 5.5.2. If it is possible that the vortex will not clear the vortex corridor during the aircraft separation time, the pilot of the following aircraft is warned. The pilot continues the approach while continuous updates of estimated residence time are made, based on continuous vortex measurements. If the estimation of long vortex residence time persists, the pilot must execute a missed approach or land further down the runway than normal. The vortex sensors for the third-order system (in addition to those required for the second-order system) are described in Section 5.5.3.

The transport time prediction of the third-order system is similar to the residence time prediction in that the appropriate values for ν are strong functions of the number of instrumented baselines. The appropriate number of instrumented baselines is a subject for further study.

7. CONCLUSIONS AND RECOMMENDATIONS

The preceding sections have discussed vortex behavior based on analytic considerations and based on measurements made at JFK. The formulations for vortex prediction using vortex sensing as a feedback loop have been established, and conceptual designs of WVAS have been presented.

7.1 CONCLUSIONS

A summary of important conclusions which relate directly to the design of an effective WVAS is as follows:

Meteorological parameters, such as power-law exponent and roughness length, which are easily observable for averaging times of the order of 15 min, have little meaning for averaging times of 1 min, which is the average life time for the vortex.

A transport time calculation procedure which does not require numerical integration of the vortex transport equations has been developed.

Vortex residence time can vary significantly from flyby to flyby, even for the same aircraft type (for both analytical and experimental results).

Although vortex residence time can vary significantly, the bounds of vortex parameters can be calculated by considering the extreme values of independent parameters.

The orientation of runways at an airport is an important site-dependent parameter. Of particular importance is the probability that a runway whose orientation yields short vortex residence time can be found.

Kalman filtering is a promising technique for vortex prediction using vortex measurement as a feedback loop. This includes both prediction of residence time for future flybys and prediction of residence time for a given flyby based on measurements during the early portion of the trajectory.

7.2 RECOMMENDATIONS

The methods presented in Section 5 are the first definitive concepts of how vortex sensing can be used to effect vortex prediction. These methods appear to be very promising, but require further development to establish their feasibility for use in an operational WVAS. It is emphasized that reliable vortex prediction is essential for an effective operational WVAS. The recommendations are therefore oriented toward the validation and development of vortex prediction using vortex measurements as the feedback loop.

It is recommended that:

Wind prediction should be validated and improved using continuous wind measurements. Validation implies determining the percentage of times when measured wind lies outside the ellipse that had been predicted for it at some earlier time. The reliability of prediction should be established for several times of prediction and for several probability ellipses. The calculation of ν and ω should be evaluated. In particular, the averaging periods over which ν and ω are calculated should be examined and the prediction discussed in Section 5.2 should be investigated for use in the VAS. Wind prediction should be implemented in real time with 99% ellipses for a 5-min prediction and a 15-min prediction.

Prediction of vortex transport time and life time as described in Section 5.3 should be developed. The data processing algorithms for the ground wind vortex sensing system should be evaluated and modified, if necessary, to provide the data necessary for prediction of vortex parameters with minimum measurement noise. The methods of calculation of ν and ω should be evaluated. The size of the 99% probability ellipse should be evaluated to determine its size under a variety of meteorological and operating conditions. Vortex prediction should be implemented in real time with 99% ellipses for a 5-min prediction. Design and development of alternative sensing systems which sense ground wind due to vortex motion should be initiated.

Prediction of vortex transport time and life time (Section 5.3) should be developed for sensors at multiple baselines. Appropriate values for ν_L and ν_T as functions of the number of baselines should be derived, and an estimate of the optimum number of baselines should be made.

Transport time prediction by Kalman filtering (Section 5.5.2) should be developed and evaluated. The technique should be formulated for several alternative vortex sensing systems. Alternative systems inlcude: the laser Doppler velocimeter,

the pulsed acoustic vortex sensing system, the monostatic acoustic vortex sensing system, and the ground wind vortex sensing system coupled with a pressure sensor for aircraft weight sensing. Appropriate values for the measurement noise parameters, ν, should be established for each of the vortex sensing systems. Of particular significance is the evaluation of alternative probability ellipses (i.e., the square root of the eigenvalues of the P matrix) as a function of time after generating aircraft passage. Trajectories for different aircraft types should be examined to determine if ω should be a function of aircraft type.

8. REFERENCES

1. Anon., "Aviation Forecasts Fiscal Years 1978-1989," Department of Transportation, Federal Aviation Administration, Sep. 1977.
2. Israel, D.R., "Air Traffic Control: Upgrading the Third Generation," Tech. Rev., Vol. 77, No. 3, Jan. 1975, p.14-24.
3. Hallock, J.N. and Eberle, W.R., (Editors), "Aircraft Wake Vortices: A State-of-the-Art Review of the United States R&D Program," FAA-RD-77-23, Transportation Systems Center, Cambridge, MA, Feb. 1977
4. Donaldson, C. duP., Snedeker, R.S., and Sullivan, R.D., "A Method of Calculating Aircraft Wake Velocity Profiles and Comparison with Full-Scale Experimental Measurements," J. Aircraft, Vol. 11, No. 9, Sep. 1974, p. 547-555.
5. Betz, A., "Behavior of Vortex Systems," Zeit. fur angewandt Math. und Mech., Vol. 12, No. 3, June 1932, p. 164-174.
6. Garodz, L.J., Lawrence, D.M., and Miller, N.J., "The Measurement of the Boeing 747 Trailing Vortex System Using the Tower Fly-By Technique," FAA-RD-73-156, National Aviation Facilities Experimental Center, Atlantic City, NJ, June 1974.
7. Garodz, L.J., Lawrence, D.M., and Miller, N.J., "The Measurement of the Boeing 727 Trailing Vortex System Using the Tower Fly-By Technique," FAA-RD-74-90, National Aviation Facilities Experimental Center, Atlantic City, NJ, Aug. 1974.
8. Garodz, L.J., Lawrence, D.M., and Miller, N.J., "The Measurement of the McDonnell-Douglas DC-9 Trailing Vortex System Using the Tower Fly-By Technique," FAA-RD-74-173, National Aviation Facilities Experimental Center, Atlantic City, NJ, Nov. 1974.
9. Crow, S.C., "Stability Theory for a Pair of Trailing Vortices," AIAA J., Vol. 8, No. 12, Dec. 1970, p. 2172-2179.
10. Brashears, M.R. and Hallock, J.N., "Aircraft Wake Vortex Predictive Model," J. Aircraft, Vol. 11, No. 5, May 1974, p. 265-272.
11. Brashears, M.R., Zalay, A.D., Chou, L.C., and Shrider, K.R., "Development of Predictive Wake Vortex Transport Model for Terminal Area Wake Vortex Avoidance," FAA-RD-76-94, Lockheed Missiles & Space Company, Inc., Huntsville, AL, May 1976.
12. Hallock, J.N., Winston, B.P., Burnham, D.C., Sullivan, T.E., McWilliams, I.G., and Wood, W.D., "Joint US/UK Vortex Tracking Program at Heathrow International Airport," FAA-RD-76-58-II, Vol. 2, Transportation Systems Center, Cambridge, MA, Nov. 1977.

13. Balser, M., McNary, C., and Nagy, A., "Acoustic Analysis of Aircraft Vortex Characteristics," FAA-RD-72-81, Xonics Corp., Van Nuys, CA, July 1972.

14. Burnham, D.C., Sullivan, T.E., and Wilk, L.S., "Measurements of Wake Vortex Strength by Means of Acoustic Back Scattering," J. Aircraft, Vol. 13, No. 11, Nov. 1976, p. 889-894.

15. Huffaker, R.M., Jeffreys, H.B., Weaver, E.A., Bilbro, J.W., Craig, G.D., George, R.W., Gleason, E.H., Marrero, P.J., Reinbolt, E.J., and Shirey, J.E., "Development of a Laser Doppler System for the Detection, Tracking, and Measurement of Aircraft Trailing Vortices," FAA-RD-74-213, NASA Marshall Space Flight Center, Huntsville, AL, Mar. 1975.

16. Bernstein, S. and Iversen, J.D., "Dynamic Simulation of an Aircraft Under the Effect of Vortex Wake Turbulence," In: Proceedings of 2nd Atmospheric Flight Mech. Conf., NASA Ames Research Center, Sep. 1972, p. 29.1-29.9.

17. Nelson, R.C., "The Response of Aircraft Encountering Aircraft Wake Turbulence," AFFDL-TR-74-29, Air Force Flight Dynamics Lab., Wright-Patterson Air Force Base, OH, June 1974.

18. Gessow, A., (Editor), "Wake Vortex Minimization," NASA SP-409, National Aeronautics and Space Administration, Washington, DC, Feb. 1976.

19. Hallock, J.N., "Monitoring the Movement of Wake Vortices at Kennedy and Stapleton Airports," In: Proceedings of 5th Annual Symposium of Society of Flight Test Engineers, 1974, p. 4/7-4/12.

20. McWilliams, I.G., "Hazard Extent About Aircraft Wake Vortices – An Analytic Approach," In: Proceedings of Aircraft Wake Vortices Conference, Transportation Systems Center, FAA-RD-77-68, June 1977, p. 23-30.

21. Lamb, H.C., Hydrodynamics, Dover Publications, New York, NY, 1945.

22. Owen, P.R., "The Decay of a Turbulent Trailing Vortex," Aero. Quarterly, Vol. 21, Feb. 1970, p. 69-78.

23. Brashears, M.R. and Hallock, J.N., "Analysis of Predicted Aircraft Wake Vortex Transport and Comparison with Experiment," J. Aircraft, Vol. 12, No. 7, July 1975, p. 619-620.

24. Brashears, M.R., Logan, N.A., and Hallock, J.N., "The Effect of Wind Shear and Ground Plane on Aircraft Wake Vortices," J. Aircraft, Vol. 12, No. 10, Oct. 1975, p. 830-833.

25. Tombach, I.H., "Transport and Stability of a Vortex Wake," MRI-72 FR-1010, Meteorology Research Inc., Altadena, CA, Apr. 1972.

26. Scorer, R.S. and Davenport, L.J., "Contrails and Aircraft Downwash," J. Fluid Mech., Vol. 43, Part 3, Sep. 1970, p. 451-464.

27. Hallock, J.N., Wood, W.D., and Spitzer, E.A., "Vortex Advisory System," In: Proceedings of 7th Conference on Aerospace and Aeronautical Meteorology," Nov. 1976, p. 162-166.

28. Taha, H. A., Operations Research, MacMillan, New York, N. Y., 1971.

29. Anon., "Aircraft Operating Cost and Performance Report," Civil Aeronautics Board, Washington, DC, Aug. 1977..

30. Brashears, M. R. and Hallock, J. N., "Predicitive Motion of Wake Vorticies," Inst. of Electrical Engineers International Conference on the Future of Aircraft All-Weather Operations, London, England, Nov. 1976.

31. Tombach, I. H., "Observations of Atmospheric Effects of Votex Wake Behavior," J. Aircraft, Vol. 10, No. 11, Nov. 1973, p. 641-647.

32. Tombach, I. H., Bate, E. R., and MacGready, P. B., "Investigation of the Motion and Decay of the Vortex Wake of a Light Twin-Engine Aircraft," AV-FR-439, Oct. 1974, AeroVironment, Pasadena, CA.

33. Burnham, D. C., "Effect of Ground Wind Shear on Aircraft Trailing Vorticies," AIAA J., Vol. 10, No. 8, Aug. 1972, p. 1114-1115.

34. Brashears, M. R., Robertson, S. J., Johnson, B. C., Fan, C., and Shrider, K. R., "Wake Vortex Transport Considerations and Meteorological Data Analysis," FAA-RD-74-66, Lockheed Missiles & Space Company, Huntsville, AL, Nov. 1974.

35. Bryson, A. E. and Ho, Y. -C., Applied Optimal Control, John Wiley & Sons, New York, 1975.

36. Gelb, A., Applied Optimal Estimation, The M. I. T. Press, Cambridge, MA, 1974.

37. Brashears, M. R. and Eberle, W. R., "Verification of Wind Measurement with Mobile Laser Doppler System," FAA-RD-77-117, Lockheed Missiles & Space Company, Inc., Huntsville, AL, Sep. 1977.

Appendix A
DESCRIPTION OF WAKE VORTEX DATA MANAGEMENT SYSTEM

A computerized vortex data management system (DMS) for cataloging, indexing, manipulating, and retrieving vortex data as a function of atmospheric, aircraft, and site-dependent parameters has been developed. The major capabilities of the DMS include: (1) file maintainence (tape read and write, additions, and corrections of data); (2) arithmatic operations (including statistical manipulation of data); and (3) retrieval of vortex data (plotting and analysis). The purpose of the DMS is to catalog the vortex data in such a manner that various correlations and functional relationships can be conveniently determined and efficiently displayed from available vortex trajectory and meteorological data. Thus, it is a useful tool for the refinement of the analytic model and for the formulation of a predictive model.

The DMS operates in two modes. The first mode is the catalog mode in which data are read, calculations necessary to generate values of calculated parameters are performed, and data files of measured and calculated parameters are generated. The second mode is the retrieval mode in which stored data from the data files are retrieved, user-defined calculations are performed on the retrived data, and printouts and/or plots of the retrieved data (and/or parameters generated from user-defined calculations) are generated. The basis for the retrievals is a set of user-defined values of one or more data access keys. The keys are selected parameters and are discussed more fully in Section A.2.2.

The DMS uses random access for both storage of new data and retrieval of data prior to processing and presentation in the desired format. This enables the user to retrieve information from drums or disk packs without resorting to extensive time-consuming record-by-record searching.

A.1 DATA MANAGEMENT SYSTEM SOFTWARE ARCHITECTURE

The essential elements of the vortex data management system showing the major computational segments and modules and inputs and outputs are given in Fig. A-1. As shown in Fig. A-1, the DMS program consists of five functional segments labeled MAIN, COMPUTATIONAL, ORDER, PLOTTING, and END. Each segment contains one or more computational modules, and each computational module contains one or more subroutines to perform specific tasks within the program. By virtue of its modular construction, the DMS can be overlayed in core (on the Univac 1108 it was overlayed into less than 65 K of core), and modifications and extensions to the program are readily accommodated. The control input to the DMS consists of control commands to the various computational modules and input data tapes and is determined by the particular type of run desired. The different types of runs available are described in Section A.2. The output of the DMS varies with the type of run requested and is specified for the different types of runs in Section A.2. The MAIN segment of the DMS monitors the entire program. The COMPUTATIONAL segment performs the tape decode and performs the calculations necessary for the generation of calculated parameters. The ORDER segment arranges the input data and values of calculated parameters into the cataloged data files. The PLOTTING segment generates plots and printouts of retrieval parameters and contains the logic for initiating searches from the data base. The END segment closes the permanent data files after updates.

The MAIN segment has access to the Keys file and the Data file. The Keys file consists of values of selected parameters upon which selective retrievals may be based. The Data files contain values of all stored parameters for each flyby, including vortex trajectory data. Values of parameters from the data files may be retrieved; however, the selection of flybys to be retrieved cannot be based on the values of parameters in the Data files.

A more detailed description of each of the DMS segments is presented in the organizational charts shown in Figs. A-2 through A-5. The MAIN segment (Fig. A-2) controls the overall operation of the program and I/O functions and

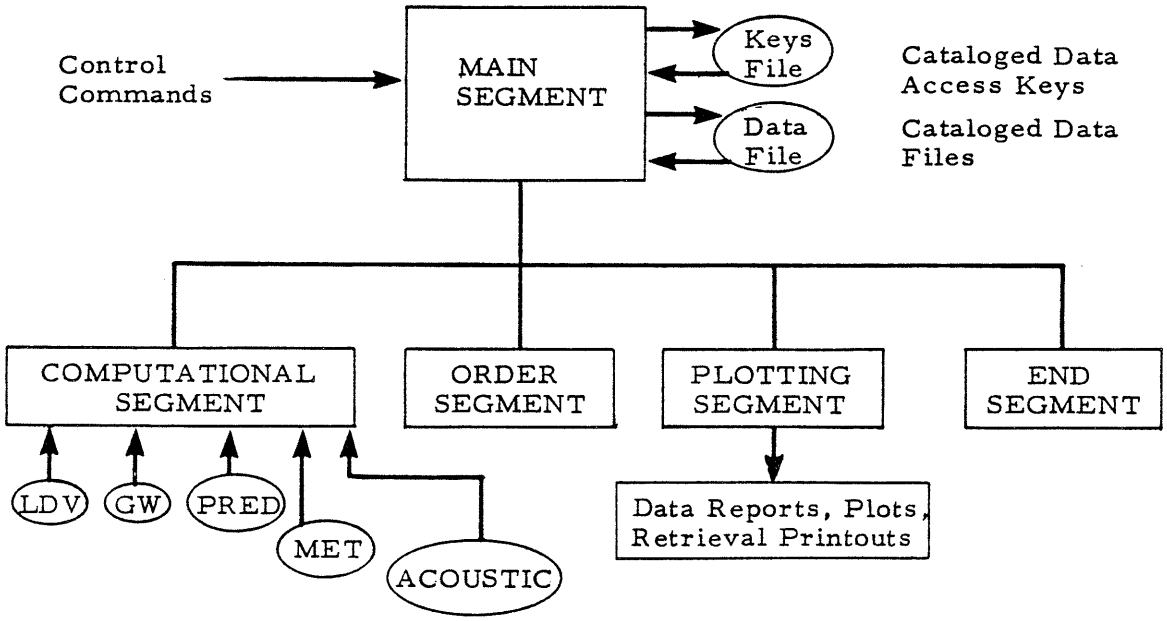

LDV is vortex trajectory data measured by laser Doppler velocimeters.

GW is data measured by ground wind anemometer systems.

PRED is vortex trajectories calculated from the analytic transport model using measured values of meteorological parameters and assumed values of aircraft parameters.

MET is measured meteorological data.

ACOUSTIC is vortex trajectory measured by acoustic systems.

FIGURE A-1. SCHEMATIC DIAGRAM OF VORTEX DATA MANAGEMENT SYSTEM

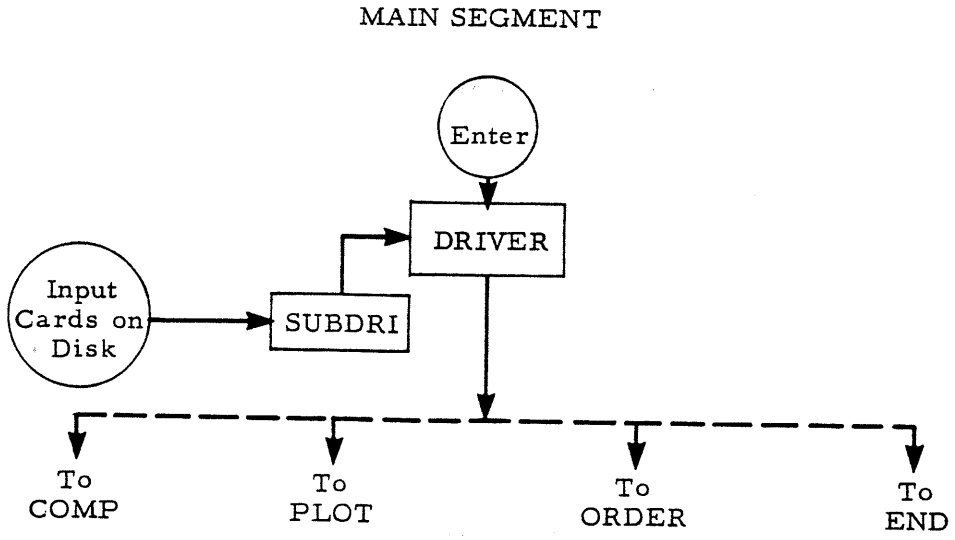

COMP performs the tape decode and performs the calculations necessary for the generation of calculated parameters.

PLOT generates plots and printouts of retrieval parameters and contains the logic for initiating searches from the data base.

ORDER arranges the input data and values of calculated parameters into the cataloged data files.

END closes the permanent data files after updates.

FIGURE A-2. ORGANIZATION OF DATA MANAGEMENT SYSTEM MAIN SEGMENT

COMPUTATIONAL SEGMENT

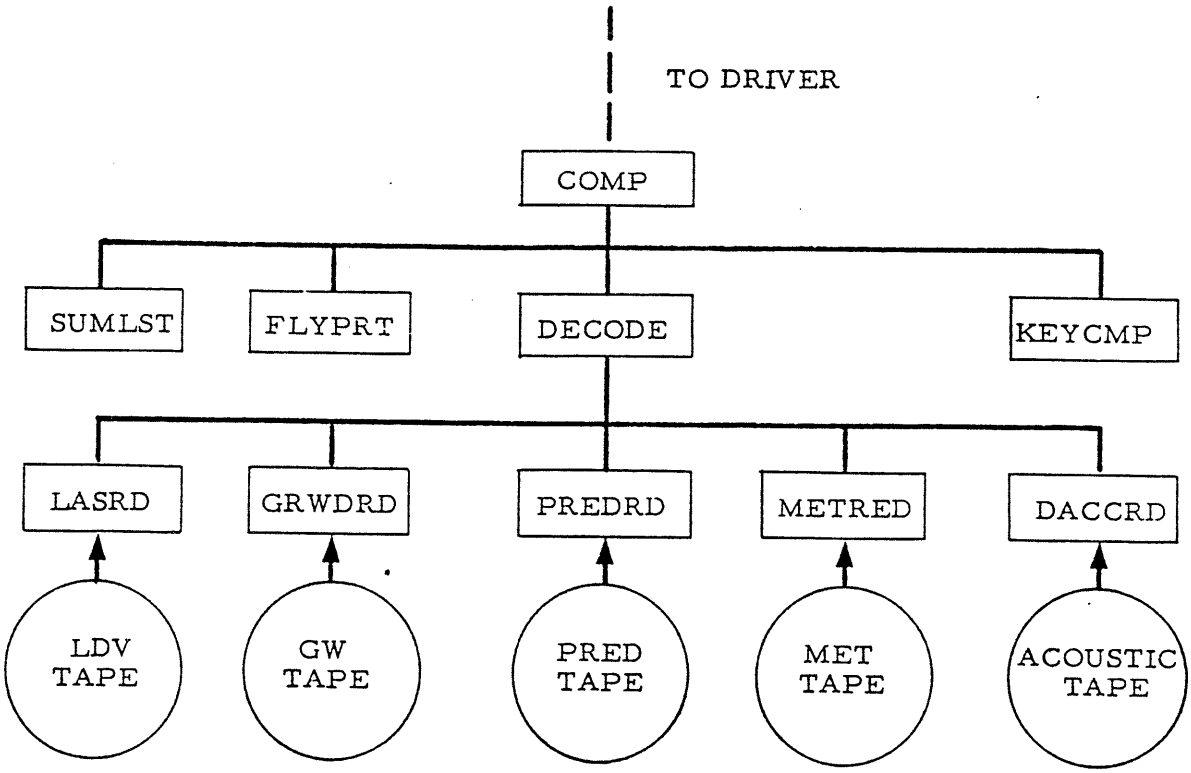

SUMLST	creates a summary listing of all cataloged flybys by flyby number. Values of significant data access keys are printed for each flyby.
FLYPRT	retrieves and prints all cataloged data for selected flyby(s).
DECODE	reads tapes in catalog mode.
KEYCMP	calculates values of data access keys in catalog mode.
LASRD	reads vortex trajectories recorded by LDV.
GRWDRD	reads vortex trajectories recorded by ground wind anemometers.
PREDRD	reads calculated vortex trajectories.
METRED	reads meteorological data.
DACCRD	reads vortex trajectories recorded by acoustic system.

FIGURE A-3. ORGANIZATION OF DATA MANAGEMENT SYSTEM COMPUTATIONAL SEGMENT

ORDER SEGMENT

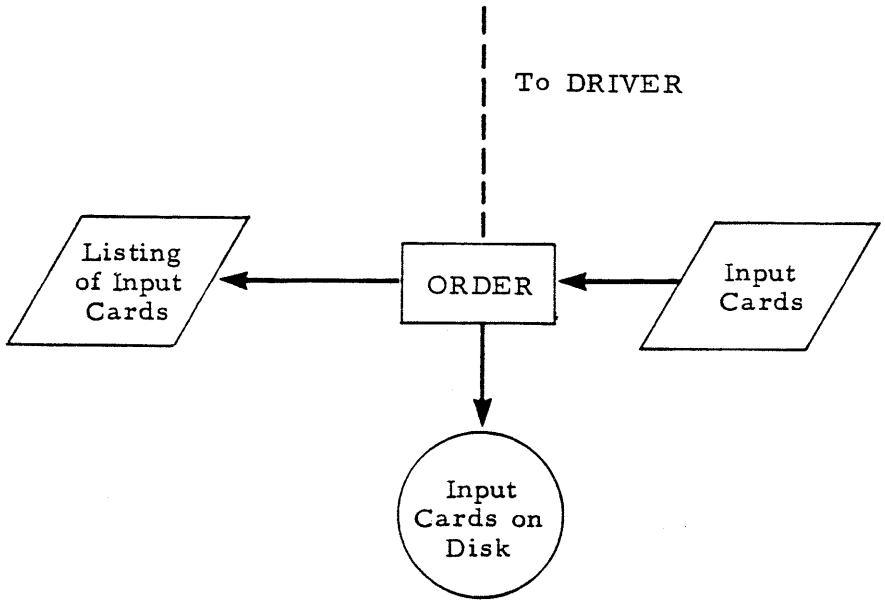

FIGURE A-4. ORGANIZATION OF DATA MANAGEMENT SYSTEM ORDER SEGMENT

PLOTTING SEGMENT

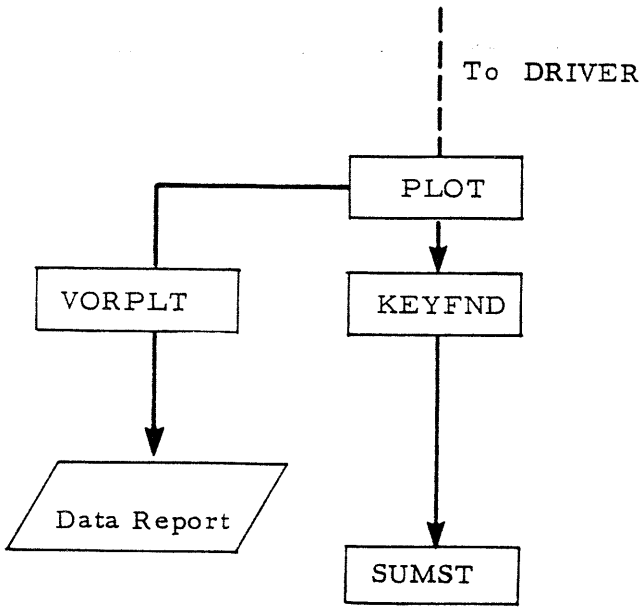

VORPLT	Creates data report (a complete set of all measured parameters, all calculated parameters, and all trajectories for each flyby).
KEYFND	Selects flybys for analysis on basis of user-defined values of data access keys.
SUMST	User-generated analysis subroutine (may include plots)

FIGURE A-5 ORGANIZATION OF DATA MANAGEMENT SYSTEM PLOTTING SEGMENT

contains the following modules; DRIVER, SUBDRIVER, SEARCH, INSERT, WRTDSK, and REDDSK. The DRIVER and SUBDRIVER modules monitor the program and transfer information to the segments. The SEARCH module locates and retrieves entries from the cataloged files when the DMS is operating in the retrieval mode. The INSERT module updates or extends the cataloged files when the DMS is operating in the catalog mode. The REDDSK and WRTDSK modules control the read and write from the disk.

The COMPUTATIONAL segment of the DMS software, illustrated in Fig. A-3, reads, decodes, and processes the information from the laser Doppler velocimeter (LDV), ground wind sensor (GW), calculated vortex track (PRED), meteorological data (MET), and Doppler acoustic tapes (ACOUSTIC). (While the DECODE module was written to accommodate all of the above types of vortex sensors, the processing of Doppler acoustic vortex tapes was not carried out during the contract due to a small number of available measurements and lack of concurrent meteorological measurements.) The COMP module consists of several programs (shown in Fig. A-3) for processing the information read in from tape.

Preprocessing (external to the DMS software) of all data occurs before the data are read into the DMS. The LDV tape contains vortex altitude and vortex lateral position as a function of time for both port and starboard vortices. Data are given for both Laser Van 1 and Laser Van 2. The GW tape contains vortex lateral position as a function of time for both port and starboard vortices for each of the three ground wind anemometer baselines. The PRED tape contains calculated values of vortex altitude and vortex lateral position as a function of time for both port and starboard vortices for each of four baselines. The MET tape contains a summary of meteorological parameters averaged over the 128-sec period following each flyby. A list of specific parameters measured is presented in Section 3.

The ORDER segment of the DMS software, illustrated in Fig. A-4, sorts the input control cards, lists them on the printer, and stores them on disk.

Plotting and display of retrieved files is carried out in the PLOT segment of the DMS, shown in Fig. A-5. The KEYFND routine converts the input search commands into logical sort and retrieve functions and then performs the retrieval of data, based on the specified values of selected data access keys. The SUMST routine is a user-defined routine which performs mathematical operations (such as correlation coefficients between parameters, calculation of additional parameters, flagging of flybys based on a user-defined criterion, etc.) and/or user-defined plotting operations on the the retrieved data.

The PLOT and VORPLT modules direct the retrieval, computation, and plotting of cataloged key parameters in a standardized data report which was generated for each flyby. A sample data report is given in Section 3. Pertinent flow charts for the DMS are given in Appendix B.

A.2 DMS OPERATING MODES

The DMS software operates in two basic modes: catalog and retrival, as described below.

A.2.1 Catalog Mode

In the catalog mode, the system reads tapes containing vortex measurements, corresponding meteorological measurements, and calculated vortex tracks. The system enters the information into discrete files. The data files consist of the list of key parameters computed or derived from the sensors as well as the arrays containing the measured and calculated vortex trajectories and the wind speed and direction measurements. The format of the catalog files is shown in Fig. A-6.

The cataloged data files contain the laser Doppler velocimeter wake vortex trajectories (vortex altitude, horizontal position versus time) for both

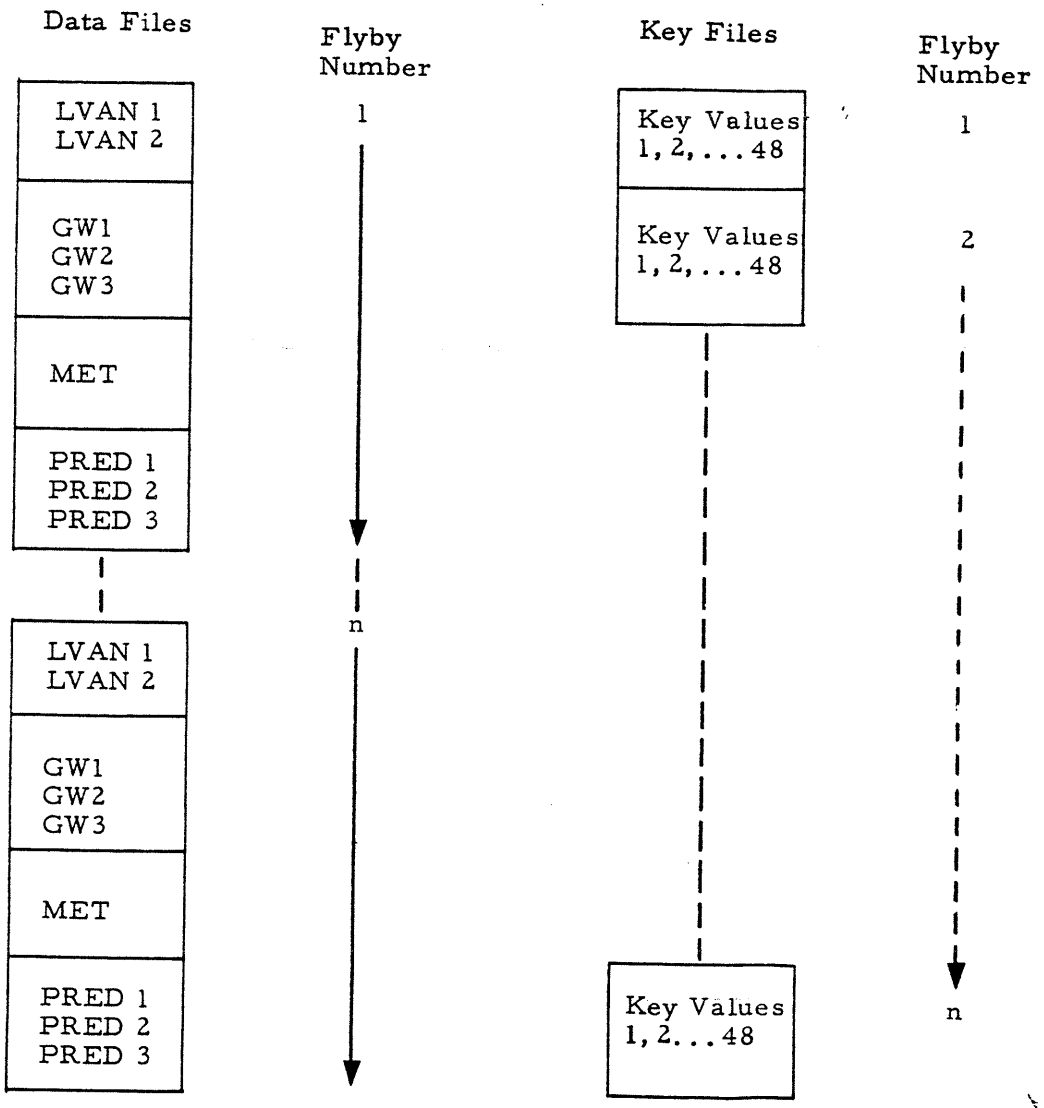

FIGURE A-6. FORMAT OF CATALOGED FILES

LDV vans (labeled LVAN1 and LVAN2), and the wake vortex trajectories measured by the ground wind anemometer array (vortex horizontal position versus time) at three baselines are stored in the data files (GW1, GW2, and GW3). The wind measurements (mean and standard deviation for the 128-second record associated with each flyby) from the sensors on each of the four meteorological towers are stored on the data files. The calculated wake vortex trajectories (vortex attitude, horizontal position versus time) for all three baselines are also stored in the data files.

The cataloged key files contain the values of the 48 data access keys computed for each flyby (discussed in Section 3.6). A description of the DMS catalog capabilities and a sample catalog run are given in Appendix C.

A.2.2 Retrieval Mode

Retrieval of access keys and cataloged data files is the second major function of the DMS. Retrieval may be conducted in the data-report mode or the key-retrieval mode. In the data-report mode, data reports which contain all measured parameters, all calculated parameters, and all vortex trajectories are created. The data report is discussed in Section 3.5. A sample DMS data-report run is presented in Appendix D.

In the key-retrieval mode, the system searches the cataloged data and recalls the data on a selective basis according to sort commands in the form of logical IF statements performed upon the values of the data access keys. A summary of the access keys available in the program is given in Table 8 (Section 3.6). The capabilities of the key compiler for retrieval of the vortex parameters is illustrated in Table A-1. By means of flexible IF-type sort commands, the DMS system can efficiently retrieve the cataloged vortex and meteorological key parameters to determine various correlations and functional relationships. A more detailed description of the DMS key retrieval process is given in the sample DMS retrieval run presented in Appendix E.

Table A-1

CAPABILITIES OF KEY COMPILER

1. Hierarchy of Operators

   (1) .EQ. .IS. .TO.

   (2) .NOT.

   (3) .AND.

   (4) .OR. .XOR.

2. A Maximum of Five Embedded Parentheses is Permitted

3. Example of Logical IF Statement for Retrieval of Vortex Parameters: Retrieval of all DC-10 or L-1011 Flybys Where the Crosswind at the 40-ft Level for Tower 1 Was Between -5 and 5 ft/sec:

   IF (V-40 .EQ. -5. .TO. 5. .AND. (AIRCFT .EQ. DC10 .OR. AIRCFT .EQ. L1011))

In addition to the search and retrieval of cataloged key parameters, the DMS has the capability to retrieve the complete data file for each flyby which contains the detailed vortex tracks and meteorological measurements. A discussion of the DMS data file retrieval capability is given in the sample DMS data file retrieval run presented in Appendix E.

Attachment B

FLOW CHARTS FOR DATA MANAGEMENT SYSTEM

This appendix contains flow charts for the major segments of the data management system shown in Figs. A-2 through A-4. Flow charts for segments for which the logic is simple or obvious are omitted. The segments in this appendix appear in the order in which they appear in Figs. A-2 through A-4.

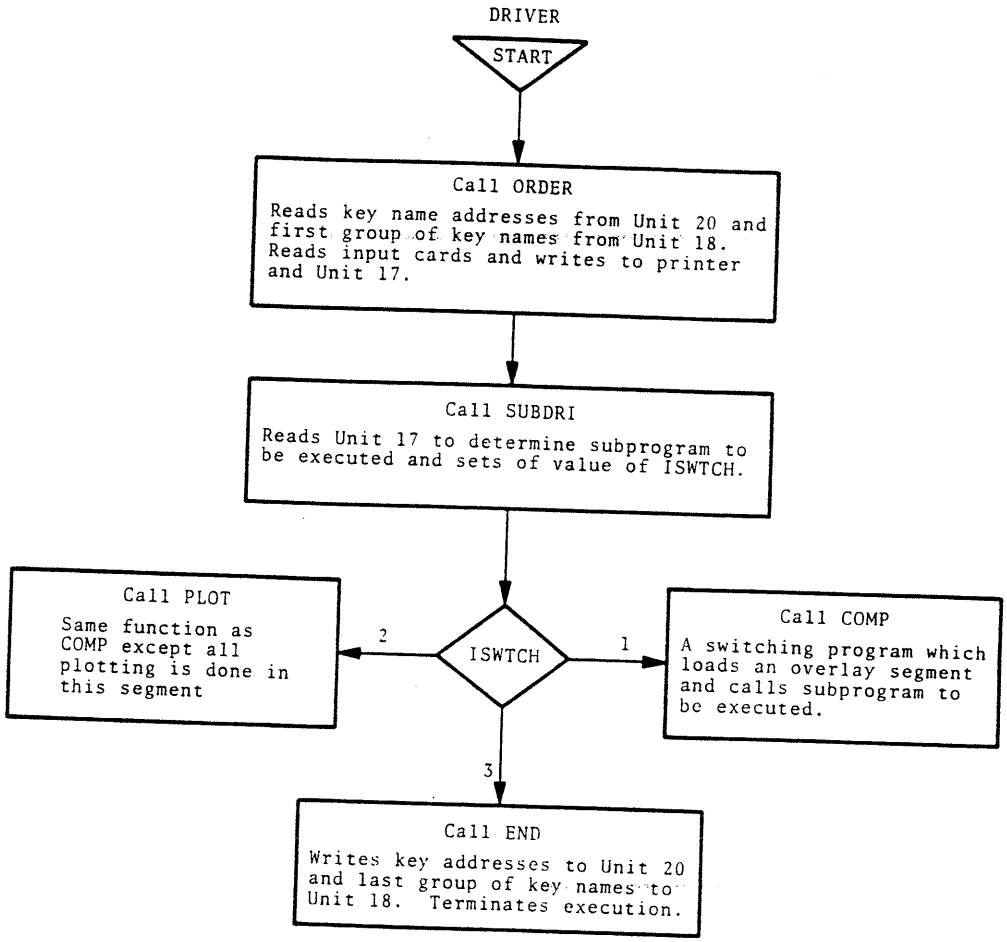

FIGURE B-1. DATA MANAGEMENT SYSTEM DRIVER PROGRAM

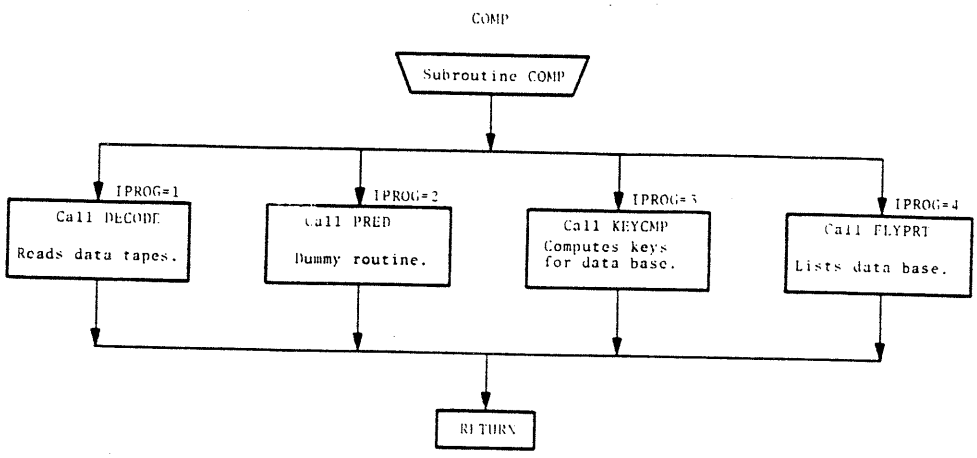

FIGURE B-2. SEGMENT FOR TAPE DECODE AND PARAMETER CALCULATION

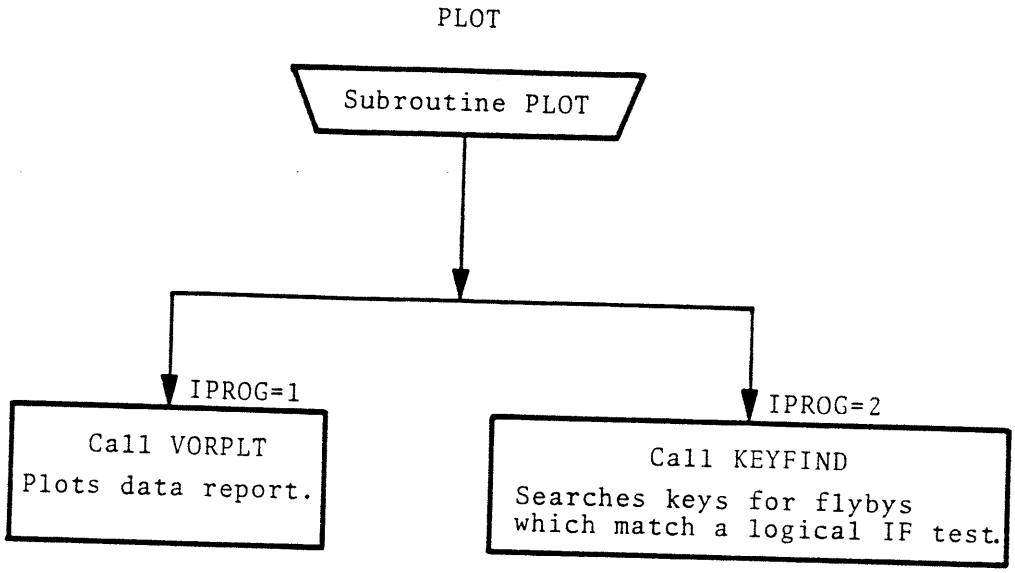

FIGURE B-3. PLOT SEGMENT

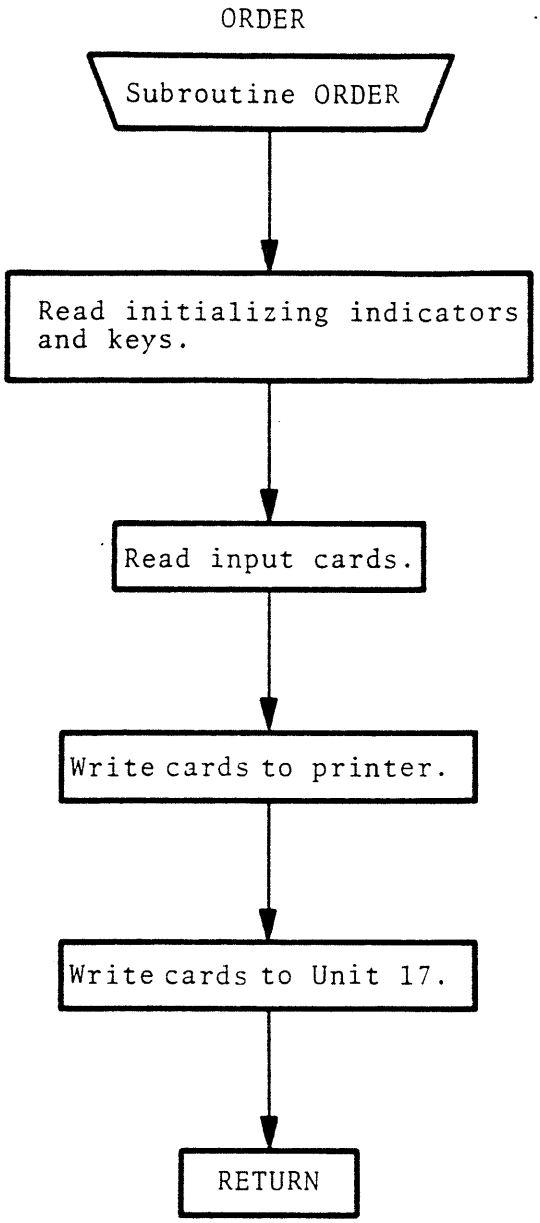

FIGURE B-4. SEGMENT FOR ARRANGING INPUT DATA

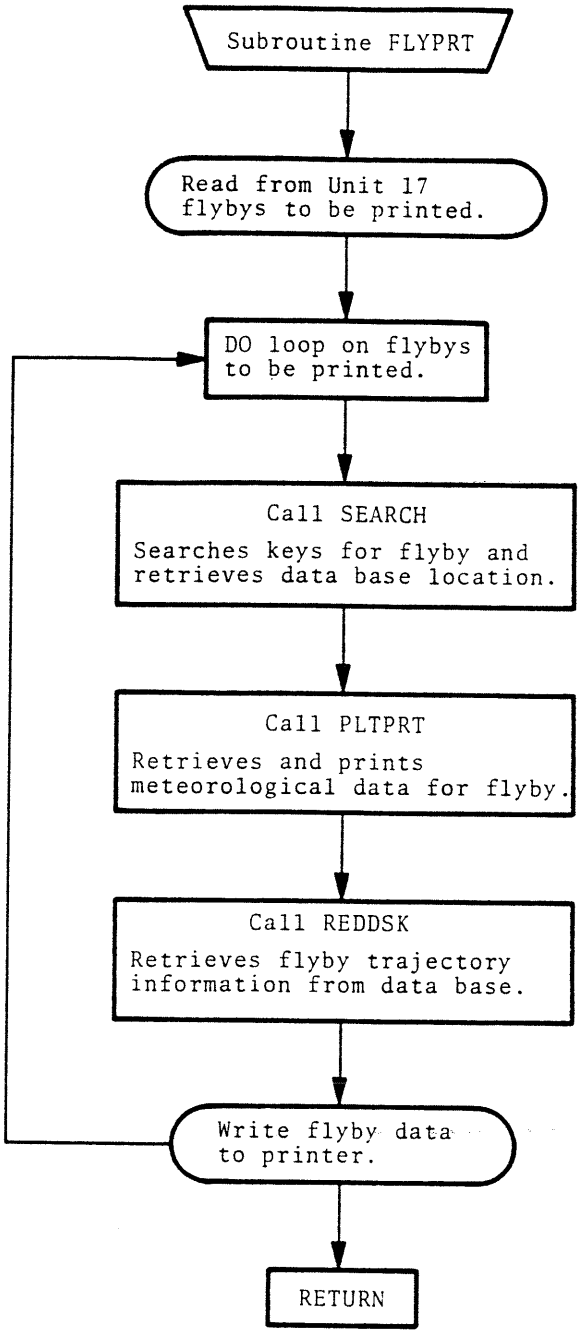

FIGURE B-5. SEGMENT FOR RETRIEVAL AND PRINTING DATA FOR SELECTED FLYBYS

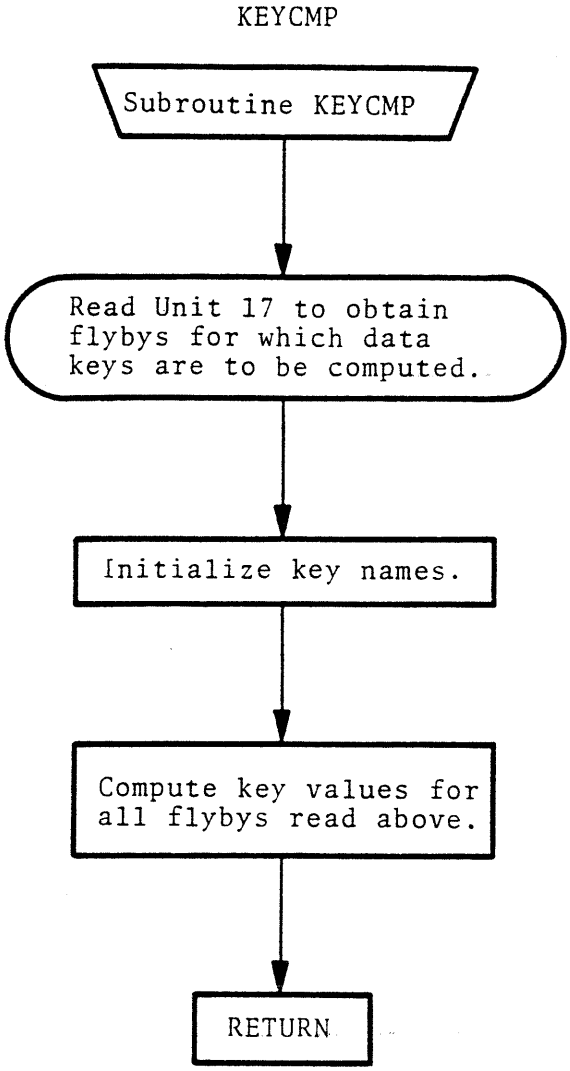

FIGURE B-6. SEGMENT FOR CALCULATING VALUES OF DATA ACCESS KEYS

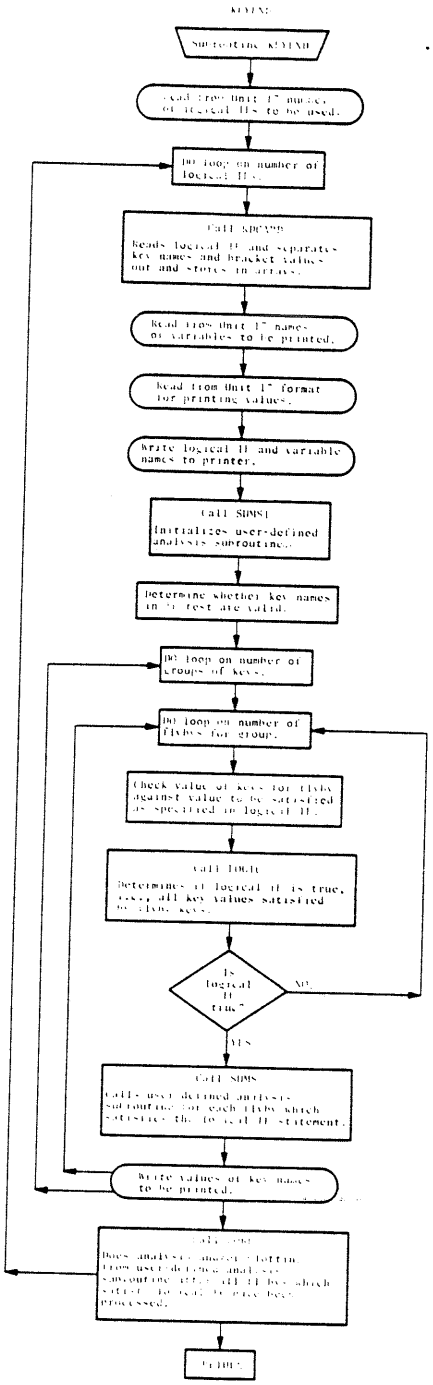

FIGURE B-7. SEGMENT FOR RETRIEVING DATA BASED ON LOGICAL IF STATEMENTS

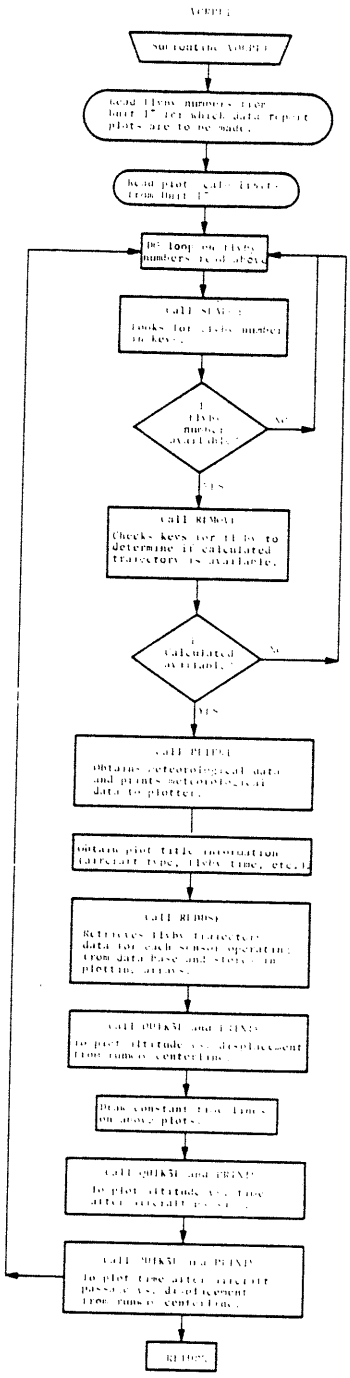

FIGURE B-8. SEGMENT FOR PRINTING DATA REPORTS

Appendix C

SAMPLE DATA MANAGEMENT SYSTEM CATALOG RUN

The procedure for cataloging vortex tracks and meteorological parameters into the data management system data base is illustrated in the following sample catalog run. Initially, the DMS program is loaded into core and the three tapes containing the ground wind vortex tracks (GW), meteorological measurements (MET) and calculated vortex tracks (PRED) are mounted. The input to the DECODE routine is read in and printed out. The catalog run output consists of printouts from the METRED, GRWDRD, and PREDRD programs (pages C-2 through C-4).

Table C-1

SAMPLE OUTPUT FROM CATALOG RUN

12 OCT 76 ENTERING OF GW, MET AND PRED CORRESPONDING TO MET TAPE J-41

INPUT CARDS

DECODE								
	MET	25184	9		7			
1								
	GRWD	3666	9		7			
1		3		0.0		-1500.	-2800.	
	PRED	25204	9		7			
1		4		0.0		-650.	-1500.	-2800.
END								

Data Input Cards

Line 1:

Program module to be executed (DECODE)

Line 2:

Data card for reading a MET data tape. Reading left to right: First word is type tape to be read (e.g., MET or GRWD); next number is tape reel number; next is logical unit to which tape is assigned; last number is number of tracks on tape.

Line 3:

Sensor information card: First number is airport code (1 for JFK); next number is the number of baselines on which sensor is active (not applicable for MET); remaining numbers are baseline locations (ft from baseline 1) (not applicable for MET).

Following Lines:

Repeat of cards 2 and 3 for each active sensor.

Table C-1 (Continued)

```
12 OCT 76          ENTERING OF GW, MET AND PRED CORRESPONDING TO MET TAPE J-41

                                   SUBROUTINE METRED

    0  500 1282MET   201400000000 211502000000 220455600000 207454000000 111071050505
FLYBY NUMBER = 1283, AIRCRAFT ID = DC9    DATE = 11/18/75 TIME = 10:43:44
    0  283 1283MET   201400000000 211502000000 220461220000 207454000000 076762670505
FLYBY NUMBER = 1284, AIRCRAFT ID = B727   DATE = 11/18/75 TIME = 10:51:16
    0  284 1284MET   201400000000 211502000000 220464044000 207454000000 111070050505
FLYBY NUMBER = 1285, AIRCRAFT ID = DC8    DATE = 11/18/75 TIME = 10:57:13
    0  285 1285MET   201400000000 211502000000 220465234000 207454000000 111070050505
FLYBY NUMBER = 1286, AIRCRAFT ID = DC8    DATE = 11/18/75 TIME = 10:59:51
    0  286 1286MET   201400000000 211502000000 220502124000 207454000000 111070050505
FLYBY NUMBER = 1287, AIRCRAFT ID = DC8    DATE = 11/18/75 TIME = 11:27:17
    0  287 1287MET   201400000000 211502000000 220504574000 207454000000 076762670505
FLYBY NUMBER = 1288, AIRCRAFT ID = B727   DATE = 11/18/75 TIME = 11:32:47
    0  288 1288MET   201400000000 211502000000 220506430000 207454000000 111071050505
FLYBY NUMBER = 1289, AIRCRAFT ID = DC9    DATE = 11/18/75 TIME = 11:36:38
    0  289 1289MET   201400000000 211502000000 220514100000 207454000000 111061600505
FLYBY NUMBER = 1290, AIRCRAFT ID = DC10   DATE = 11/18/75 TIME = 11:48:32
    0  290 1290MET   201400000000 211502000000 220515710000 207454000000 076760670505
FLYBY NUMBER = 1291, AIRCRAFT ID = B707   DATE = 11/18/75 TIME = 11:52:18
    0  291 1291MET   201400000000 211502000000 220521070000 207454000000 111070050505
FLYBY NUMBER = 1292, AIRCRAFT ID = DC8    DATE = 11/18/75 TIME = 11:59:10
    0  292 1292MET   201400000000 211502000000 220523674000 207454000000 076760670505
FLYBY NUMBER = 1293, AIRCRAFT ID = B707   DATE = 11/18/75 TIME = 12: 5: 3
    0  293 1293MET   201400000000 211502000000 220563430000 207454000000 111071050505
FLYBY NUMBER = 1294, AIRCRAFT ID = DC9    DATE = 11/18/75 TIME = 13:12:38
    0  294 1294MET   201400000000 211502000000 220564350000 207454000000 111071050505
FLYBY NUMBER = 1295, AIRCRAFT ID = DC9    DATE = 11/18/75 TIME = 13:14:34
    0  295 1295MET   201400000000 211502000000 220573224000 207454000000 076762670505
FLYBY NUMBER = 1296, AIRCRAFT ID = B727   DATE = 11/18/75 TIME = 13:29: 9
    0  296 1296MET   201400000000 211502000000 220576230000 207454000000 111071050505
FLYBY NUMBER = 1297, AIRCRAFT ID = DC9    DATE = 11/18/75 TIME = 13:35:34
    0  297 1297MET   201400000000 211502000000 220601700000 207454000000 076760670505
FLYBY NUMBER = 1298, AIRCRAFT ID = B707   DATE = 11/18/75 TIME = 13:43:12
    0  298 1298MET   201400000000 211502000000 220606600000 207454000000 076764670505
FLYBY NUMBER = 1299, AIRCRAFT ID = B747   DATE = 11/18/75 TIME = 13:53:36
    0  299 1299MET   201400000000 211502000000 220610750000 207454000000 076762670505
FLYBY NUMBER = 1300, AIRCRAFT ID = B727   DATE = 11/18/75 TIME = 13:58:18
    0  300 1300MET   201400000000 211502000000 220614404000 207454000000 076764670505
FLYBY NUMBER = 1301, AIRCRAFT ID = B747   DATE = 11/18/75 TIME = 14: 5:51
    0  301 1301MET   201400000000 211502000000 220615660000 207454000000 076762670505
FLYBY NUMBER = 1302, AIRCRAFT ID = B727   DATE = 11/18/75 TIME = 14: 8:44
    0  302 1302MET   201400000000 211502000000 220616600000 207454000000 111071050505
FLYBY NUMBER = 1303, AIRCRAFT ID = DC9    DATE = 11/18/75 TIME = 14:10:40
    0  303 1303MET   201400000000 211502000000 220617300000 207454000000 076760670505
FLYBY NUMBER = 1304, AIRCRAFT ID = B707   DATE = 11/18/75 TIME = 14:12: 0
    0  304 1304MET   201400000000 211502000000 220622344000 207454000000 111071050505
FLYBY NUMBER = 1305, AIRCRAFT ID = DC9    DATE = 11/18/75 TIME = 14:18:33
```

Sample output for cataloging meteorological data. There are two lines of output for each flyby.

Line 1:

Internal program information printed for debugging purposes.

Line 2:

Information on flyby being cataloged.

Table C-1 (Continued)

```
12 OCT 76                    ENTERING OF GW, MET AND PRED CORRESPONDING TO MET TAPE J=41

                                                SUBROUTINE GRWDRD

 119.0000  119.0000
  45.0000   45.0000
 119.0000  119.0000
  45.0000   45.0000
 119.0000  119.0000
  45.0000   45.0000
    1  283 1320GRWD  201400000000 211502000000 220455600000 207454000000 111071050505
  35.0000   35.0000
  70.0000   70.0000
  35.0000   35.0000
  70.0000   70.0000
  35.0000   35.0000
  70.0000   70.0000
    1  284 1320GRWD  201400000000 211502000000 220461220000 207454000000 074762670505
  56.0000   56.0000
  34.0000   34.0000
  56.0000   56.0000
  34.0000   34.0000
  56.0000   56.0000
  34.0000   34.0000
    1  285 1320GRWD  201400000000 211502000000 220464044000 207454000000 111070050505
  85.0000   85.0000
  11.0000   62.0000
  85.0000   85.0000
  10.0000   10.0000
  85.0000   85.0000
  10.0000   10.0000
    1  286 1320GRWD  201400000000 211502000000 220465234000 207454000000 111070050505
  23.0000   23.0000
 115.0000  115.0000
  23.0000   23.0000
 115.0000  115.0000
  23.0000   23.0000
 115.0000  115.0000
    1  287 1320GRWD  201400000000 211502000000 220502124000 207454000000 111070050505
 102.0000  102.0000
  23.0000   59.0000
 102.0000  102.0000
  37.0000   37.0000
 102.0000  102.0000
  37.0000   37.0000
    1  288 1320GRWD  201400000000 211502000000 220504574000 207454000000 074762670606
 119.0000  119.0000
  14.0000  112.0000
 119.0000  119.0000
  22.0000   22.0000
 119.0000  119.0000
  22.0000   22.0000
    1  289 1320GRWD  201400000000 211502000000 220506430000 207454000000 111071050505
  28.0000   28.0000
  59.0000   59.0000
  28.0000   28.0000
```

Sample output for cataloging ground wind anemometer data. All information is for debugging purposes.

Table C-1 (Concluded)

```
12 OCT 76                ENTERING OF GW, MET AND PRED CORRESPONDING TO MET TAPE J=41

                                                  SUBROUTINE PREDRD
   58.0000   94.0000
   50.0000   80.0000
   53.0300   91.0300
   47.0300   75.0300
   44.8400   82.8400
   38.8400   68.8400
   35.5600   71.5600
   29.5600   57.5600
     1  283 1320PRED   201400000000 211502000000 220455600000 207454000000 111071050505
   68.0000  128.0000
   24.0000  128.0000
   64.9800  128.9800
   22.9800  128.9800
   56.9700  128.9700
   24.9700  128.9700
   37.6500  129.6500
  125.6500  129.6500
     1  284 1320PRED   201400000000 211502000000 220461220000 207454000000 076762678505
   40.0000  128.0000
   68.0000  128.0000
   30.8600  128.8600
   64.8600  124.8600
   22.7000  128.7000
   54.7000  108.7000
   46.8200  112.8200
   28.8200   66.8200
     1  285 1320PRED   201400000000 211502000000 220464044000 207454000000 111070050505
   28.0000  128.0000
   84.0000  128.0000
   36.8800  128.8800
   72.8800  128.8800
   46.6900  128.6900
   58.6900  128.6900
   56.7500  128.7500
   36.7500  128.7500
     1  286 1320PRED   201400000000 211502000000 220465234000 207454000000 111070050505
   40.0000  128.0000
   94.0000  128.0000
   40.8700  128.8700
   82.8700  128.8700
   40.6700  128.6700
   68.6700  128.6700
   38.7100  128.7100
   44.7100  128.7100
     1  287 1320PRED   201400000000 211502000000 220502124000 207454000000 111070050505
   60.0000  118.0000
   44.0000   78.0000
   57.0400  113.0400
   41.0400   75.0400
   50.9100  102.9100
   36.9100   68.9100
   37.7700   81.7700
```

Sample output for cataloging calculated vortex trajectories. All information is for debugging purposes.

Appendix D

SAMPLE DATA MANAGEMENT SYSTEM RUN FOR GENERATING A DATA REPORT

The procedure for generating plots and summaries of the cataloged vortex tracks and meteorological parameters in the form of a data report is illustrated in the following sample run. Initially, the DMS program and data base is loaded into core and disk. The input to the VORPLT routine is read in and printed out. The output from the data report run consists of the individual data reports for each flyby, discussed earlier in Section 2, as well as the printout from the VORPLT routine showing the status of the plots.

Table D-1

SAMPLE OUTPUT FROM DATA REPORT RUN

30 OCT 76 PLOT OF FLYBYS 1240-1320

INPUT CARDS

```
VORPLT
          1240      1320
 -600.0   600.0     0.0      200.0     0.0      140.0
 -600.0   600.0     0.0      200.0     0.0      140.0
 -600.0   600.0     0.0      200.0     0.0      140.0
 -600.0   600.0     0.0      200.0     0.0      140.0
END
```

Input Data Cards

Line 1:

Program module to be executed (VORPLT)

Line 2:

Flyby number to begin plotting and flyby number to stop plotting.

Lines 3-6:

Parameter limits for plotting for baselines 1, 2, 3 and 4 (in that order). Reading from left to right: Minimum lateral position, maximum lateral position, minimum altitude, maximum altitude, minimum time, maximum time.

Table D-1 (Concluded)

```
                                        SUMMARY OF DATA PLOTTED FOR FLYBY NO.  1241
***ERROR*** INCORRECT SENSOR ID MACC1
***ERROR*** INCORRECT SENSOR ID MACC2
***ERROR*** INCORRECT SENSOR ID TMON
***ERROR*** INCORRECT SENSOR ID FSCAT
                              SENSOR TYPE PRED   XBASE =        .0
                              SENSOR TYPE GRWD   XBASE =        .0
NOW PLOTTING FRAME 1
NOW PLOTTING FRAME 2
NOW PLOTTING FRAME 3
***ERROR*** INCORRECT SENSOR ID MACC1
***ERROR*** INCORRECT SENSOR ID MACC2
***ERROR*** INCORRECT SENSOR ID TMON
***ERROR*** INCORRECT SENSOR ID FSCAT
                              SENSOR TYPE PRED   XBASE =    -650.0
NOW PLOTTING FRAME 1
NOW PLOTTING FRAME 2
NOW PLOTTING FRAME 3
***ERROR*** INCORRECT SENSOR ID MACC1
***ERROR*** INCORRECT SENSOR ID MACC2
***ERROR*** INCORRECT SENSOR ID TMON
***ERROR*** INCORRECT SENSOR ID FSCAT
                              SENSOR TYPE PRED   XBASE =   -1500.0
                              SENSOR TYPE GRWD   XBASE =   -1500.0
NOW PLOTTING FRAME 1
NOW PLOTTING FRAME 2
NOW PLOTTING FRAME 3
***ERROR*** INCORRECT SENSOR ID MACC1
***ERROR*** INCORRECT SENSOR ID MACC2
***ERROR*** INCORRECT SENSOR ID TMON
***ERROR*** INCORRECT SENSOR ID FSCAT
                              SENSOR TYPE PRED   XBASE =   -2800.0
                              SENSOR TYPE GRWD   XBASE =   -2800.0
NOW PLOTTING FRAME 1
NOW PLOTTING FRAME 2
NOW PLOTTING FRAME 3
```

Summary of printed output during data report generation. ERROR indicates no available data for sensor called. When a sensor type is successfully called, it is identified with the corresponding baseline locations.

Appendix E

SAMPLE DATA RETRIEVAL RUN FROM DATA MANAGEMENT SYSTEM

The procedure for retrieval and analysis of vortex trajectory and meteorological information from the DMS data base is illustrated in the following sample run. The sample shown is the retrieval used for generating the plots shown in Figs. 63 through 65. Calculated vortex trajectories based on measured values of initial vortex altitude, initial vortex vertical velocity, and initial vortex horizontal velocity are to be generated and compared with measured vortex trajectories.

The user must write an analysis subroutine (called SUMST) to perform the required analysis. The subroutine for the sample retrieval is shown as Table E-1. Comment cards with asterisks describe general information needed to perform retrievals and conduct analysis of the retrieved information. Comments without asterisks contain information related to the particular example shown in Table E-1. The input data cards are shown in Table E-2. The printed output is a list of the requested data access keys. A sample for the data access keys shown in Table E-2 is shown in Table E-3. Additional printed output may be specified in SUMST. Graphical output is specified in SUMST. All of the computer-generated plots in this report (except the data report plots) were generated by specification in SUMST.

Table E-1

ANALYSIS SUBROUTINE LISTING FOR EXAMPLE OF DATA RETRIEVAL USING THE DATA MANAGEMENT SYSTEM

```
      SUBROUTINE SUMST (NVALU)
C
C**   SUMST IS THE USER-DEFINED ANALYSIS SUBROUTINE.  SUMST IS CALLED AT
C**   THE BEGINNING OF EVERY RETRIEVAL SET.  NVALU IS THE NUMBER OF DATA
C**   ACCESS KEYS TO BE TRANSMITTED TO SUMST.
C
      COMMON/VDATA/NPMAX,NBASE,XARAY(4),REZTIM(4,2),LIFTIM(4,2),LN(4,2),
     1TIME(100,4,2),DDATA(100,4,4)
C
C**   VDATA IS THE COMMON BLOCK IN WHICH TRAJECTORY INFORMATION IS
C**   STORED WHEN A VORTEX TRAJECTORY DATA FILE IS CALLED.
C**     NPMAX = MAXIMUM NUMBER OF POINTS IN A TRAJECTORY.
C**     NBASE = NUMBER OF BASELINES FOR WHICH DATA ARE STORED.
C**     XARAY(I) = DISTANCE OF BASELINE I (IN A DIRECTION PARALLEL TO
C**       THE RUNWAY) MEASURED FROM BASELINE 1.
C**     REZTIM(I,J) = VORTEX RESIDENCE TIME FOR VORTEX ON BASELINE I.
C**       J=1 FOR STARBOARD VORTEX.  J=2 FOR PORT VORTEX.
C**     LIFTIM(I,J) = VORTEX LIFE TIME FOR VORTEX ON BASELINE I.  J=1
C**     FOR STARBOARD VORTEX.  J=2 FOR PORT VORTEX.
C**     LN(I,J) = NUMBER OF POINTS IN THE VORTEX TRAJECTORY ON BASELINE
C**       I.  J=1 FOR STARBOARD VORTEX.  J=2 FOR PORT VORTEX.
C**     TIME(I,J,K) = TIMES FOR WHICH VORTEX POSITION DATA ARE AVAILABLE
C**       FOR BASELINE J.  K=1 FOR STARBOARD VORTEX.  K=2 FOR PORT VORTEX.
C**     DDATA(I,J,K) = VORTEX POSITION CORRESPONDING TO TIMES IN
C**       TIME(I,J,K) FOR BASELINE J.  K=1 FOR STARBOARD LATERAL
C**       POSITION.  K=2 FOR STARBOARD VORTEX ALTITUDE.  K=3 FOR PORT
C**       VORTEX LATERAL POSITION.  K=4 FOR PORT VORTEX ALTITUDE.
C
      COMMON/MET/PLAW(3,4),NPOLY,COEFF(3),COEFV,USTAR1(14),USTAR2(12),
     1USTAR4(4),ROUGH1(14),ROUGH2(12),ROUGH4(4),VGRAD(4,14),HGRGR4(4),
     2TEMP(11),TEMPA2,TEMPA3,ATEMP,APTEMP,PRESH,HUMID,IPASQ(3,4),RICH(3)
     3,DISIP(13,4),BRUNT2,BRUNT3,STAB2,STAB3,VBAR(6,18),VVAR(6,18)
      DIMENSION TLP(50),YLP(50),ZLP(50),TLS(50),YLS(50),ZLS(50),TGP(50),
     1YGP(50),TGS(50),YGS(50)
C
C**     MET IS THE COMMON BLOCK IN WHICH METEOROLOGICAL INFORMATION IS
C**       STORED WHEN THE MET DATA FILE IS CALLED.  PARAMETERS ARE
C**       DEFINED IN TABLE 3.
C
      DIMENSION TMP(50),YMP(50),ZMP(50),TMS(50),YMS(50),ZMS(50)
      DIMENSION LABT(12),LABY(12),LABZ(12),VALU(20)
      DIMENSION ZB(15),YBP(15),YBS(15)
      DIMENSION LGR(21)
      DIMENSION ZI(100),VIN(100),ZOUT(100),ATYPE(8),YIN(8),YP(51),YS(51)
     1,Z(51),G(3),DG(3),TI(51),SUM(4,3)
      REAL LGR
C
C     INITIAL VORTEX ALTITUDES FOR FLYBYS 451-511.
C
      DATA ZI/160.,160.,140.,135.,190.,160.,200.,165.,155.,175.,170.,
     1165.,170.,130.,150.,200.,185.,135.,175.,190.,140.,170.,130.,150.,
     2165.,200.,185.,190.,160.,140.,140.,175.,60.,165.,150.,140.,110.,11
```

Table E-1 (Continued)

```
     30.,170.,160.,140.,140.,135.,180.,100.,160.,140.,200.,135.,160.,
     4200.,145.,160.,175.,145.,100.,100.,145.,200.,195.,170.,39*0./
C
C      INITIAL VERTICAL VELOCITIES FOR FLYBYS 451-511.
C
       DATAZDOT/-6.67,-4.86,-6.36,-9.,-6.33,-4.21,-5.71,-6.35,-5.34,-5.67
     1,-7.39,-5.69,-7.08,-1.50,-2.94,-6.67,-6.2,-7.3,-3.27,-5.43,
     2-7.00,-6.51,-4.64,-4.41,-3.43,-5.26,-8.4,-7.3,-2.76,-1.35,-7.,-4.6
     36,-.01,-3.93,-3.75,-5.,-6.11,-4.75,-6.1,-4.44,-7.65,-6.24,-3.64,
     4-3.,-6.7,-5.71,-11.67,-2.44,-1.41,-10.7,
     5       -6.45,-2.9,-4.21,-4.37,-4.39,-.1,-5.55,-4.39,-5.13,-6.5,-7.
     639,39*0./
C
C      INITIAL CROSSWIND FOR FLYBYS 451-511.
C
       DATA VIN/-11.,0.,-15.9,-7.9,-10.,-15.9,-8.8,-10.9,-8.6,-15.5,-16.7
     1,-8.1,-6.7,-4.1,-7.1,-8.4,-4.8,-16.6,-15.3,-16.9,-5.1,-5.75,-2.42,
     2-.86,-6.9,-6.2,-4.2,-3.2,-13.8,-2.1,-11.7,-11.3,0.,-9.7,4.2,6.3,
     3-2.1,-1.93,-1.64,-7.5,1.64,2.29,2.42,0.,-5.56,6.,2.29,2.14,4.9,6.2
     4,0.,-3.67,0.,-1.1,-4.1,1.3,0.,1.6,6.6,6.0,6.13,3.39*0./
C
C      DATA FOR PRINTING BOUNDARIES OF VORTEX CORRIDOR ON GRAPHS.
C
       DATA ZB/0.,10.,20.,30.,40.,50.,60.,70.,80.,90.,100.,110.,120.,130.
     1,140./
       DATA YBP/-150.,-150.,-150.,-150.,-150.,-150.,-150.,-150.,-150.,
     1-150.,-150.,-150.,-150.,-150.,-150.,-150./
       DATA YBS/150.,150.,150.,150.,150.,150.,150.,150.,150.,150.,150.,
     1150.,150.,150.,150./
C
C      GRAPH HEADING AND LABEL DATA.
C
       DATA LGR/6HDMS FL,6HYBY NO,6H      ,6H   DAY,6H      ,6H  TIME,3*6
     1H      ,6HAIRCRA,6HFT TYP,6HE     ,6H      ,6H  BASE,6HLINE ,6HIS
     2TANC,6HE     ,6H      ,6H FT   ,6HC WIND,6H      /
       DATA LABT/6HTIME A,6HFTER A,6HIRCRAF,6HT PASS,6HAGE   ,7*6H      /
       DATA LABY/6HDISPLA,6HCEMENT,6H FROM ,6HRUNWAY,6H CENTE,6HRLINE ,6*
     16H      /
       DATA LABZ/6HALTITU,6HDE    ,10*6H      /
       DATA ATYPE/6HL1011 ,6HB747  ,6HB707  ,6HB727  ,6HB737  ,6HDC10  ,6
     1HDC8   ,6HDC9   /
       DATA YIN/61.,76.9,56.9,42.4,36.6,64.9,56.3,35.1/
       RETURN
       ENTRY SUMS(VALU,NVALU)
C
C**    SUMS IS THE ENTRY POINT AFTER EACH FLYBY WHICH SATISFIES THE
C**    SELECTION CRITERIA IS FOUND.  VALU IS THE MATRIX OF VALUES FOR THE
C**    REQUESTED DATA ACCESS KEYS.  NVALU IS THE NUMBER OF DATA ACCESS
C**    KEYS.
C
       DO 21 I=1,NVALU
       IF (VALU(I).EQ.0.)VALU(I)=1.E30
    21 CONTINUE
C
C      ENCODE INFORMATION FOR HEADINGS ON GRAPHS.
C
       ENCODE (901,LGR(3))VALU(1)
   901 FORMAT (F5.0)
```

Table E-1 (Continued)

```
      IHR=VALU(3)/3600.
      IMIN=(VALU(3)-3600*IHR)/60.
      SEC=VALU(3)-3600*IHR-60*IMIN
      SEC=IMIN+.01*SEC
      ENCODE (902,LGR(8))SEC
  902 FORMAT (F6.2)
      ENCODE (904,LGR(7))IHR
  904 FORMAT (I4)
      LGR(13)=VALU(4)
      ENCODE (901,LGR(5))VALU(2)
      ENCODE (907,LGR(21))VALU(5)
  907 FORMAT (F6.2)
      BA=0.
      ENCODE (906,LGR(18))BA
  906 FORMAT (F6.0)
C
C     DETERMINE AIRCRAFT TYPE FOR VORTEX INITIAL LATERAL SEPARATION.
C
      DO 16 I=1,8
      IF (VALU(4).EQ.ATYPE(I)) GO TO 19
   16 CONTINUE
      RETURN
   19 YP(1)=-YIN(I)
      YS(1)=YIN(I)
      IFY=VALU(1)-449.5
      Z(1)=ZI(IFY)
      GAM=ZDOT(IFY)/(2.*YS(1)/((2.*Z(1))**2+(2.*YS(1))**2)-.5/YS(1))
      IS=1
      VI=VIN(IFY)
      T=0.
      Q(1)=YP(1)
      Q(2)=YS(1)
      Q(3)=Z(1)
      DO 120 I=1,51
      TI(I)=T
      YP(I)=Q(1)
      YS(I)=Q(2)
      Z(I)=Q(3)
C
C     CALCULATE VORTEX TRAJECTORIES.
C
  110 YD=GAM*((Q(2)-Q(1))**2/((2.*Q(3))**2+(Q(2)-Q(1))**2))/(2.*Q(3))
      DQ(1)=VI-YD
      DQ(2)=VI+YD
      DQ(3)=GAM*((Q(2)-Q(1))/((2.*Q(3))**2+(Q(2)-Q(1))**2) -1./(Q(2)-Q(1
     1)))
C
C     RUNGK IS A RUNGE-KUTTA INTEGRATION SUBROUTINE LISTED AFTER THIS
C     SUBROUTINE.
C
      CALL RUNGK(T,2.,Q,DQ,3,IS,DUM)
      IF (IS.GT.1) GO TO 110
  120 CONTINUE
C
C     RETRIEVAL OF TRAJECTORY DATA FOR LASER VAN 1.
C
      CALL READSK(5HLVAN1,IACT)
C
```

Table E-1 (Continued)

```
C**    REDDSK RETRIEVES DATA FROM DATA FILES.
C**      5HLVAN1 RETRIEVES DATA FOR LASER VAN 1.
C**      5HLVAN2 RETRIEVES DATA FOR LASER VAN 2.
C**      4HGRWD RETRIEVES GROUND WIND ANEMOMETER DATA.
C**      4HPRED RETRIEVES CALCULATED VORTEX TRAJECTORIES STORED IN DMS.
C**      3HMET RETRIEVES METEOROLOGICAL DATA.
C**      IACT=1 IF SENSOR IS ACTIVE.  IACT=0 IF SENSOR IS INACTIVE.
C
      IF (IACT.EQ.0) GO TO 25
      NLP=LN(1,2)
      DO 22 I=1,NLP
      TLP(I)=TIME(I,1,2)
      YLP(I)=DDATA(I,1,3)
      ZLP(I)=DDATA(I,1,4)
   22 WRITE (6,800) I,TLP(I),YLP(I),ZLP(I)
  800 FORMAT (I4,3F10.2)
      NLS=LN(1,1)
      DO 24 I=1,NLS
      TLS(I)=TIME(I,1,1)
      YLS(I)=DDATA(I,1,1)
      ZLS(I)=DDATA (I,1,2)
   24 WRITE (6,800)I,TLS(I),YLS(I),ZLS(I)
C
C     RETRIEVAL OF TRAJECTORY DATA FROM LASER VAN 2.
C
   25 CALL REDDSK (5HLVAN2,KACT)
      IF (KACT.EQ.0) GO TO 30
      NMP=LN(1,2)
      DO 26 I=1,NMP
      TMP(I)=TIME(I,1,2)
      YMP(I)=DDATA(I,1,3)
   26 ZMP(I)=DDATA(I,1,4)
      NMS=LN(1,1)
      DO 28 I=1,NMS
      TMS(I)=TIME(I,1,1)
      YMS(I)=DDATA(I,1,1)
   28 ZMS(I)=DDATA(I,1,2)
C
C     RETRIEVAL OF GROUND WIND ANEMOMETER DATA.
C
   30 CALL REDDSK(4HGRWD,JACT)
      IF (JACT.EQ.0) GO TO 50
      NGP=LN(1,2)
      DO 32 I=1,NGP
      TGP(I)=TIME(I,1,2)
      YGP(I)=DDATA(I,1,3)
   32 WRITE (6,800)I,TGP(I),YGP(I)
      NGS=LN(1,1)
      DO 34 I=1,NGS
      TGS(I)=TIME(I,1,1)
      YGS(I)=DDATA(I,1,1)
   34 WRITE (6,800)I,TGS(I),YGS(I)
C
C     PLOT VORTEX ALTITUDE VERSUS TIME FOR CALCULATED AND MEASURED
C     TRAJECTORIES.
C
   50 L=-1
      IF (IACT.EQ.0) GO TO 60
```

Table E-1 (Concluded)

```
      CALL QUIK3L(-1,0.,140.,0.,200.,51,LABT,LABZ,NLP,TLP,ZLP)
      CALL QUIK3L(0,0.,140.,0.,200.,50,LABT,LABZ,NLS,TLS,ZLS)
      CALL QUIK3L(0,0.,140.,0.,200.,20,LABT,LABZ,-51,TI,Z)
      IF (KACT.NE.0) CALL QUIK3L(0,0.,140.,0.,200.,54,LABT,LABZ,NMP,TMP,
     1ZMP)
      IF (KACT.NE.0) CALL QUIK3L(0,0.,140.,0.,200.,53,LABT,LABZ,NMS,TMS,
     1ZMS)
      CALL PRINTV (126,LGR,5,1007)
      CALL QUIK3L (-1,-600.,600.,0.,140.,51,LABY,LABT,NLP,YLP,TLP)
      CALL QUIK3L ( 0,-600.,600.,0.,140.,50,LABY,LABT,NLS,YLS,TLS)
      CALL QUIK3L(0,-600.,600.,0.,140.,20,LABY,LABT,-51,YP,TI)
      CALL QUIK3L(0,-600.,600.,0.,140.,40,LABY,LABT,-51,YS,TI)
      IF(KACT.NE.0.) CALL QUIK3L(0,-600.,600.,0.,140.,54,LABY,LABT,NMP,Y
     1MP,TMP)
      IF(KACT.NE.0.) CALL QUIK3L(0,-600.,600.,0.,140.,54,LABY,LABT,NMP,Y
     1MS,TMS)
      L=0
 60   IF (JACT.EQ.0) GO TO 80
      CALL QUIK3L(L,-600.,600.,0.,140.,21,LABY,LABT,NGP,YGP,TGP)
      CALL QUIK3L(0,-600.,600.,0.,140.,24,LABY,LABT,NGS,YGS,TGS)
      CALL QUIK3L (0,-600.,600.,0.,140.,14,LABY,LABT,15,YBP,ZB)
      CALL QUIK3L (0,-600.,600.,0.,140.,14,LABY,LABT,15,YBS,ZB)
      CALL PRINTV (126,LGR,5,1007)
 80   CALL QUIK3L (0,-600.,600.,0.,140.,14,LABY,LABT,15,YBP,ZB)
      CALL QUIK3L (0,-600.,600.,0.,140.,14,LABY,LABT,15,YBS,ZB)
      CALL PRINTV (126,LGR,5,1007)
      RETURN
      ENTRY CORR (NVALU)
C
C**   CORR IS THE ENTRY POINT AT THE END OF THE RETRIEVAL (WHEN ALL
C**   FLYBYS WHICH MEET THE SPECIFIED SELECTION CRITERIA HAVE BEEN
C**   FOUND).
C
      RETURN
      END
*FOR,IS RUNG1,RUNG1                                                    RUNG0000
      SUBROUTINE RUNGK(X,DX,Y,DY,N,IS,DUM)                             RUNG0010
C   RUNGE-KUTTA METHOD FOR SOLVING DIFFERENTIAL EQUATIONS              RUNG0020
C   ARGUMENTS                                                          RUNG0030
C        X     INDEPENDENT VARIABLE
C        DX    STEP SIZE FOR X                                        RUNG0050
C        Y     DEPENDENT VARIABLE
C        DY    RATE OF CHANGE OF Y WITH RESPECT TO A CHANGE IN X      RUNG0070
C        N     NUMBER OF DEPENDENT VARIABLES
C        DUM   WORKING STORAGE                                        RUNG0090
C        IS  INDICATES PASS (=1 FIRST  =2 SECOND  =3 THIRD =4 FOURTH) RUNG0100
      DIMENSION Y(N),DY(N),DUM(4,N),DTWO(3)                          RUNG0110
      DATA DTWO /.5,.5,1. /                                          RUNG0120
C     ENTRY RUNG                                                     RUNG0130
      IF(IS-1) 20,2,6                                                RUNG0140
    2 DO 5 I=1,N                                                     RUNG0150
    5 DUM(4,I)=Y(I)                                                  RUNG0160
    6 GO TO (6,15,6,19),IS                                           RUNG0170
    6 X=X+.5*DX                                                      RUNG0180
   15 DO 10 I=1,N                                                    RUNG0190
      IF(IS-3) 16,16,17                                              RUNG0200
   16 DUM(IS,I)=DX*DY(I)                                             RUNG0210
      Y(I)=DUM(4,I)+DUM(IS,I)*DTWO(IS)                               RUNG0220
      GO TO 10                                                       RUNG0230
   17 Y(I)=DUM(4,I)+.166666667*(DUM(1,I)+2.*DUM(2,I)+2.*DUM(3,I)+DX*  RUNG0240
     $ DY(I))                                                        RUNG0250
   10 CONTINUE                                                       RUNG0260
   20 IS=IS+1                                                        RUNG0270
      IF(IS.GT.4) IS=1                                               RUNG0280
      RETURN                                                         RUNG0290
      END                                                            RUNG0300
```

Table E-2

SAMPLE INPUT CARDS FOR EXAMPLE OF DATA RETRIEVAL USING THE DATA MANAGEMENT SYSTEM

```
                    1
  IF (RUNNO.EQ.491..TO.511.)
5      RUNNO        DAY          TIMEDA      AIRCFT      V-40
(3F10.2,A6,2X,F10.2)
```

Card 1

Number of Retrievals to be Conducted (Col. 16)

Card 2

Logical IF Statement by Which Flybys to be Included in the Analysis are Selected.

Card 3

Number of Data Access Keys to be Printed (Col. 5) and List of Data Access Keys to be Printed (Cols. 11, 21, 31, 41, . . .). List of Data Access Keys May be Continued on a Second Card, if Necessary.

Card 4

Format in Which the Values of the Data Access Keys are to be Printed.

Table E-3

DATA OUTPUT FOR EXAMPLE OF DATA RETRIEVAL
USING THE DATA MANAGEMENT SYSTEM

A SEARCH IS BEING PERFORMED BASED ON THE FOLLOWING LOGIC STATEMENT
IF (RUNNO.EQ.451..TO.511.)

RUNNO	DAY	TIMEDA	AIRCFT	V-40
451.00	136.00	49266.	DC9	**********
452.00	136.00	49885.	B707	**********
453.00	136.00	50219.	B727	**********
454.00	136.00	50316.	DC9	-13.78
455.00	136.00	50862.	B727	**********
456.00	136.00	50995.	DC8	-15.09
457.00	136.00	52235.	B747	-9.40
458.00	136.00	52382.	B727	-13.39
459.00	136.00	52501.	B707	-10.68
460.00	136.00	52776.	B747	**********
461.00	136.00	52990.	DC9	-14.52
462.00	136.00	53790.	VC10	**********
463.00	136.00	53919.	B747	-7.11
464.00	136.00	54087.	DC8	-6.47
465.00	136.00	54211.	B707	-4.34
466.00	136.00	54345.	B707	-3.47
467.00	136.00	54646.	B727	-10.38
468.00	136.00	54791.	B727	-13.62
469.00	136.00	54902.	L1011	-9.79
470.00	136.00	55115.	B727	-15.49
471.00	136.00	56379.	DC8	-5.48
472.00	136.00	56475.	B747	-5.88
473.00	136.00	56602.	B727	-6.32
474.00	136.00	56750.	VC10	**********
475.00	136.00	56821.	B747	-8.46
476.00	136.00	57000.	B747	-6.89
477.00	136.00	57228.	B707	-6.15
478.00	136.00	57367.	B727	-4.69
479.00	136.00	57444.	DC8	**********
480.00	136.00	57581.	DC8	-7.49
481.00	136.00	58016.	B707	-5.43
482.00	136.00	58230.	B727	-9.44
483.00	136.00	58396.	B747	-8.26
484.00	136.00	58635.	B747	-9.60
485.00	136.00	58877.	B727	**********
486.00	136.00	59019.	B727	**********
487.00	136.00	59117.	B727	**********
488.00	136.00	59214.	DC8	**********

Appendix F

REPORT OF INVENTIONS

The purpose of the work performed under this contract and reported herein was an analysis of aircraft wake vortex data measured at Kennedy International Airport in Jamaica, New York. The work included the formulation of a computerized data management system for effective retrieval of data and the analysis which used the data management system for selective retrieval of data. Because the purpose of the work was analysis of existing data, no innovation, discovery, improvement, or invention was made.

200 copies